



Norwegian University of
Science and Technology

The Unstable Rock Slope Kassen

A Hazard, Consequence and Stability

Assessment of the Rock Slope

Kaja Krogh

Geotechnology

Submission date: January 2017

Supervisor: Reginald Hermanns, IGP

Co-supervisor: Bjørn Nilsen, IGB

Norwegian University of Science and Technology
Department of Geoscience and Petroleum

MASTERKONTRAKT

- uttak av masteroppgave

1. Studentens personalia

Etternavn, fornavn Krogh, Kaja	Fødselsdato 14. feb 1991
E-post kajakr@stud.ntnu.no	Telefon 99250584

2. Studieopplysninger

Fakultet Fakultet for ingeniørvitenskap og teknologi	
Institutt Institutt for geologi og bergteknikk	
Studieprogram Tekniske geofag	Studieretning Ingeniørgeologi og bergmekanikk

3. Masteroppgave

Oppstartsdato 22. aug 2016	Innleveringsfrist 15. jan 2017
Oppgavens (foreløpige) tittel The unstable rock slope Kassen, Telemark	
Oppgavetekst/Problembeskrivelse Based on regional mapping by NGU, a potential unstable rock slope, "Kassen", is identified South of Bandak lake in Telemark county. The students specialization project included geomorphic and structural geological mapping of the area which resulted in kinematic models for different sliding scenarios. This master thesis will build on the results from the specialization project finished December 2015, and include the following points; <ul style="list-style-type: none">- Hazard assessment, volume estimation and run-out analysis of potential failure scenarios, following the NGU system.- Back analysis of a historic slope failure at Kassen by using numerical methods. Input parameters are obtained through laboratory tests on a rock sample from Kassen and geotechnical measurements on joint surfaces from fieldwork summer 2016.- Stability analysis of two unstable blocks in the Kassen slope, observed during fieldwork.	
Hovedveileder ved institutt Reginald Hermanns	Medveileder(e) ved institutt Bjørn Nilsen
Merknader 1 uke ekstra p.g.a jul.	

4. Underskrift

Student: Jeg erklærer herved at jeg har satt meg inn i gjeldende bestemmelser for mastergradsstudiet og at jeg oppfyller kravene for adgang til å påbegynne oppgaven, herunder eventuelle praksiskrav.

Partene er gjort kjent med avtalens vilkår, samt kapitlene i studiehåndboken om generelle regler og aktuell studieplan for masterstudiet.

Trondheim 25.08.2016
Sted og dato

Kaja Krogh
Student

[Signature]
Hovedveileder

Abstract

NGU is currently in the process of identifying, mapping and classifying all potential, unstable rock slopes in Norway. In this context, a hazard and preliminary consequence assessment is performed in this master thesis for the unstable rock slope Kassen, located in Kviteseid municipality in Telemark county. The study site is located at a north facing slope in the south-eastern end of the 27 km long Bandak lake orientated WNW-ESE. This master thesis is a continuation of the authors specialization project, completed December 2015.

Based on delimiting cracks observed in the field and on high resolution digital terrain models, seven smaller potential failure scenario (A-G) are defined within the Kassen unstable area. NGUs hazard assessment is applied to all these scenarios, resulting in four medium hazard class scenarios and three low hazard class scenarios. The preliminary consequence assessment involves a volume estimation and run-out analysis for all scenarios, where the resulting volumes range from 0.11 – 2.09 million m³. All medium hazard class scenarios have computed run-out lengths which can reach Bandak Lake, and the susceptibility for this is especially high for scenario A, B and G due to steep terrain downslopes with average dip angles of 30-40°. Run-up heights from potential displacement waves for the medium hazard class scenarios are roughly estimated based on empirical relations developed by NGU. Only displacement waves from scenario G (the biggest scenario) can cause devastating effects for smaller communities located at the shoreline at Bandak Lake. Based on a preliminary risk matrix, it is suggested that the Kassen site shall be periodically monitored in the future, continuing with annual dGNSS measurements.

Stability analyses are performed at two sites at Kassen which differ in rock mass quality, assumed failure mode and size. Input parameters for the analyses are obtained through geotechnical field measurements and laboratory tests. Both analyses are motivated by historic events.

The first event is a rock avalanche of uncertain age, identified by deposits seen on bathymetric maps in Bandak Lake beneath the Kassen slope. The volume of the deposits are estimated to be 3.37 million m³, which is 21% greater than the volume of the reconstructed terrain before the failure. Such a volume increase is reasonable due to disintegration and fragmentation of the rock mass. A back-analysis is performed using the software RS² with the shear strength reduction technique for a detailed study of the parameters and trigger factors that affected the slope stability. It is demonstrated that this post-glacial rock avalanche occurred due to high groundwater pressure and some amount of strain softening of the rock mass. The debuttressing effect after the ice- retreat can have reactivated the slope and also contributed to the failure. For todays topography, with present geological and hydrogeological conditions the slope is stable with an Factor of Safety (FS) of 1.78.

The second event is of relatively newer time and is registered in the National landslide database provided by NVE as a rockslide. The slide occurred from Skipet, a prominent cliff situated in the lower, western part of Kassen, in 1985. In the field, two potential unstable blocks were detected at Skipet, and the Limit Equilibrium Method is applied to find the Factor of Safety against planar sliding for these blocks. For dry conditions, the calculated FS for the upper and lower block are respectively 1.57 and 1.74. The lower block was still stable even when incorporating a full water pressure over the entire length of an open tension crack at the back of the block. The block shape test show that the blocks also are stable against toppling.

Sammendrag

NGU identifiserer, kartlegger og klassifiserer alle potensielle, ustabile fjellparti i Norge. Som en del av dette arbeidet, er det i denne masteroppgaven utført en fare- og konsekvensvurdering av fjellpartiet Kassen i Kviteseid kommune, Telemark. Området som er blitt studert ligger i en nordvendt skråning i sør-øst enden av den 27 km lange innsjøen Bandak, orientert VNV-ØSØ. Masteroppgaven er en fortsettelse av prosjektoppgaven av samme forfatter, ferdigstilt i desember 2015.

Syv mindre potensielle skredscenarioer (A-G) er blitt definert basert på avgrensede sprekker som er observert i felt og på høytoppløselige, digitale terrengmodeller. Fire av disse faller innenfor klassen med medium faregrad og tre innenfor lav faregrad. Den foreløpige konsekvensvurderingen består av volumestimering og utløpsanalyser for alle scenarioene. Resultatet viser at skredvolumene spenner fra 0.11-2.09 millioner m³. Potensielle skred fra scenarioene med medium faregrad har beregnet utløpslengde som alle kan nå Bandak. Det er ekstra høy sannsynlighet for dette i scenarioene A, B og G fordi terrenget nedenfor er jevnt bratt med en helning på 30-40°. Oppskyllingshøyder fra potensielle flodbølger fra scenarioene med medium faregrad er omtrentlig estimert ved å bruke empiriske sammenhenger utviklet av NGU. Kun en flodbølge fra scenario G (som er det største scenarioet) kan ha ødeleggende konsekvenser for mindre bebyggelser lokalisert ved strandlinjen rundt Bandak. Kassen området bør overvåkes periodisk basert på resultatene fra den foreløpig risikomatriksen og de årlige dGNSS målingene opprettholdes.

Det har blitt utført stabilitetsanalyser ved to lokasjoner i den ustabile fjellsiden, som er forskjellig med hensyn til bergmassekvalitet, antatt skredtype og størrelse. Inngangsparameterne brukt i analysene er samlet inn ved geotekniske målinger i felt og ved laboratoriearbeid. Begge stabilitetsanalysene er gjennomført med bakgrunn i to historiske skredhendelser fra Kassen.

Den første historiske hendelsen er et fjellskred av ukjent alder, identifisert ved skredavsetninger på bunnen av Bandak, svært tydelige på batymetriske kart. Volumet av avsetningene er estimert til å være omtrent 3.37 millioner m³, en økning på 21 % i forhold til volumet av det rekonstruerte terrenget i fjellsida før skredet gikk. En slik volumøkning er rimelig grunnet fragmentering og nedbrytning av bergmassen. «Shear strength reduction» teknikken i den todimensjonale programvaren RS² er benyttet til å utføre en tilbakeanalyse av fjellskredet. Hensikten har vært å utføre detaljerte studier av parametere og utløsende faktorer som kan ha påvirket skråningsstabiliteten. Resultatene viser at det post-glasiale fjellskredet skyldtes et høyt grunnvannsspeil og en viss mengde tøyningssavherding av bergmassen. Da breen trakk seg tilbake, kan det ustabile fjellpartiet ha blitt reaktivert og i så fall også vært en av de utløsende faktorene. Under dagens geologiske og hydrogeologiske forhold er skråningen derimot stabil med en sikkerhetsfaktor på 1.78.

Den andre historisk hendelsen er av nyere tid, og er registrert i NVEs skreddatabase som et mindre fjellskred. Skredet gikk fra Skipet i 1985 som er en markant klippe i den nedre, vestre delen av den ustabile Kassen området. Under feltarbeidet ble det observert to mindre, potensielle ustabile blokker øverst på Skipet. Sikkerhetsfaktoren for disse blokkene er funnet ved å bruke likevektsmetoden som viser at under tørre forhold er blokkene stabile mot planær utglidning med sikkerhetsfaktorer på 1.57 og 1.74. Den nedre blokka er stabil selv når fullt

vanntrykk i den åpne tensjonssprekken bak blokka er medregnet. Blokk-form testen viser at blokkene også er stabile mot utveltning.

Acknowledgements

This master thesis is the last step in completing my master degree in engineering geology and rock mechanics at the Department of Geology and Mineral Resource Engineering, Norwegian University of Science and Technology (NTNU). It is written in collaboration with the Geological survey of Norway (NGU). My supervisors have been Reginald Hermanns (head of the Geohazard and Earth Observation team at NGU and professor at NTNU) and Bjørn Nilsen (professor at NTNU).

First of all, a huge thanks goes to Reginald Hermanns for all discussions, meetings, reviews and guidance with this master thesis. I really appreciate the honest and valuable feedback you have given and for showing a genuine interest for my work. I am also very grateful for the summer jobs I have had with NGU the two last summers, I have learnt a lot!

Secondly I would like to thank my supervisor Nilsen. Our meetings and discussions have been very useful for me, especially concerning all challenges related to the stability analyses. You have challenged me to think in new ways, but also supported my ideas and helped to improve them. Thanks also to Quoc Nghia Trinh (professor at NTNU) for giving valuable tips regarding technical details in applied software.

A special thanks also goes to Thierry Oppikofer and Martina Böhme at NGU for answering all questions I have had, and helping me with software details.

I would also like to thank my student friend Odd Andre Morken (also master student at NTNU) for assisting me in field, your knowledge was of great importance for successive field mapping. Without your strength, the rock sample from field would never have arrived at the laboratory in Trondheim.

My mom also deserves a sentence here, as she reviewed this thesis, your comments were of great importance.

Last but not least, thanks to all my classmates at NTNU. Because of you, I have looked forward to go to the “lesesal” almost every day!

Stavanger, 02.01.17

Kaja Krogh

Contents

1	Introduction.....	1
1.1	Unstable rock slopes in Norway.....	1
1.2	Available data and site specific literature.....	2
1.3	Location and geological conditions.....	3
1.4	Aim and structure of the study.....	8
2	Completed investigations and findings.....	9
2.1	Joint sets.....	9
2.2	Structural domains.....	10
2.3	Kinematics.....	12
2.4	Profiles.....	12
2.5	Gemorphological feauters.....	14
3	General theory of landslides.....	15
4	Hazard and preliminary consequence assessment applied to Kassen.....	19
4.1	NGU Mapping Approach.....	19
4.2	Hazard assessment.....	21
4.3	Preliminary consequence assessment.....	29
4.4	Results.....	34
5	Stability analyses performed at Amfiteateret and Skipet.....	46
5.1	Stability analyses of rock slopes.....	46
5.2	Material Models.....	50
5.3	Classes of rock strength.....	51
5.4	Input parameters from field work and laboratory testing.....	56
5.5	Numerical modeling applied to Amfiteateret.....	60
5.6	Stability assessment of Skipet.....	81
5.7	Results from numerical analysis of Amfiteateret.....	86
5.8	Results from stability assessment of Skipet.....	102
6	Discussion.....	105
6.1	Hazard and future risk at Kassen.....	105
6.2	Evaluation of the numerical modeling.....	107
6.3	Stability of blocks at Skipet.....	121
7	Conclusions and further investigations.....	122
8	Appendix.....	129
8.1	Hazard assessments scenarios A-G.....	129

8.2	dGNSS movement	136
8.3	Laboratory results	139
8.4	JRC and JCS calculations	140
8.5	Determination of JCS based on Schmidt hardness	141
8.6	Calculation of Joint Stiffness	142
8.7	RocLab conversions	143
8.8	Centroid of Block 2	144

1 Introduction

1.1 Unstable rock slopes in Norway

Rock slope failures is a major natural hazard in mountainous areas all over the world (Turner & Schuster, 1996). In Norway, the tectonic and glaciological history has formed a country rich with steep slopes and deep fjords, a landscape susceptible for landslides. These potential landslides can cause catastrophic consequences for settlement and infrastructure located in the run-out area. In addition, secondary effects such as displacement waves in fjords and lakes, river damming and outburst floods can cause huge hazard to society (Oppikofer et al., 2015)

Many rock slope failures have occurred in the past which is well documented by boulder rock-avalanche deposits found in most regions of Norway (Blikra et al., 2006). Today there are registered 33 000 landslides in Norway which have claimed 4475 lives (Hermanns, Blikra, et al., 2013). Rapid rock falls and rockslides contribute to 13 500 of these events, causing 932 fatalities. Together, this makes rock slope failures one of the biggest natural hazards in Norway.

In order to address this hazard, the Geological Survey of Norway (NGU) has carried out a national mapping program of potential unstable rock slopes since 2005, financed and supervised by the Norwegian Water Resources and Energy Directorate (NVE). The goal of this project is to detect all rock slopes that could fail catastrophically and define the affected areas of these potential failures in order to communicate possible consequences to the societies in danger (Hermanns, Oppikofer, Molina, Dehls, & Böhme, 2014). The mapping is relevant in 17 counties in Norway, and the last years work have identified more than 300 potentially unstable rock slopes that show signs of post-glacial deformation (Hermanns, Oppikofer, et al., 2013).

Systematic mapping is completed in three counties where most historical events have occurred (Troms, Møre og Romsdal and Sogn og Fjordane) and started in a fourth county (Rogaland) (Figure 1). For the remaining relevant counties, punctual slopes are selected to be included in the mapping program. The latter is the case for the study site of this master thesis, Kassen unstable slope located in Telemark.

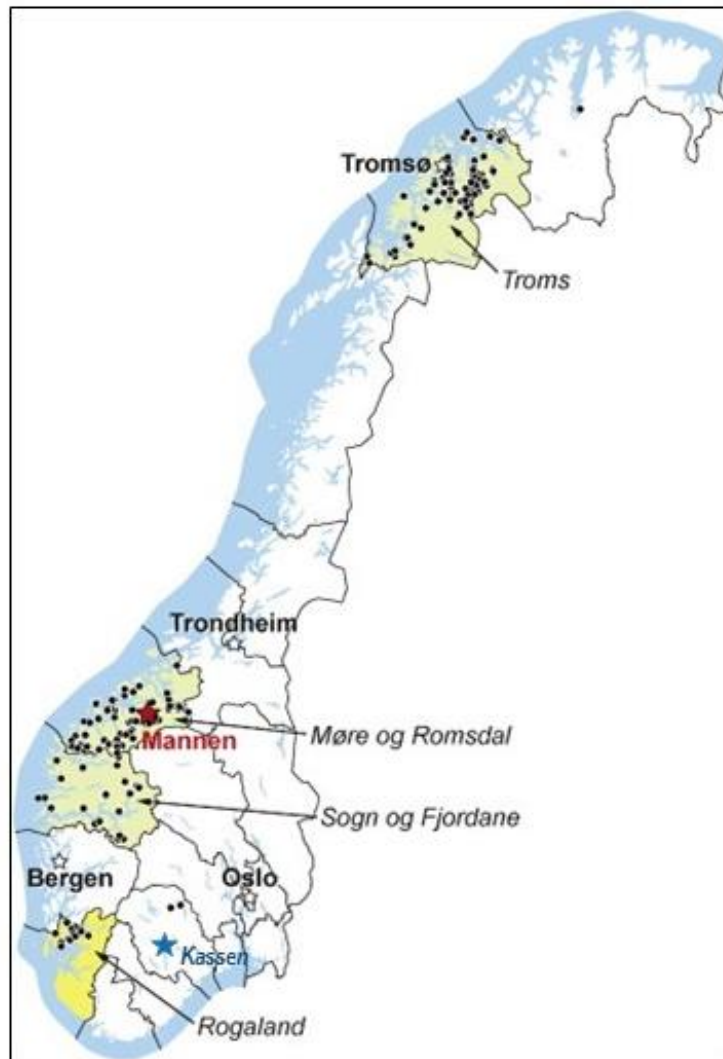


Figure 1: Map showing detected unstable rock slopes in Norway. Figure after Oppikofer et al. (2015).

1.2 Available data and site specific literature

The following list shows the available data concerning the instability at Kassen:

- Geological data obtained from detailed mapping through three weeks of fieldwork in June 2015 and June 2016. This work was done by the author together with Martine L. Andresen and Odd Andre Morken, all master students at The Norwegian University of Technology and Science (NTNU).
- LiDAR data provided by NGU. Two scans of the slope is done in 2011 and 2013. The first from the back scarp of Kassen, and the second from the opposite slope at the south shore of Bandak Lake.
- Geological maps (1:250 000 and 1: 50 000) provided by NGU.
- Bathymetric data obtained by NGU in 2011.
- Deformation measurements from 2012 to 2016 collected with differential Global Navigation Satellite System (dGNSS) in collaboration with Trond Eiken representing the University in Oslo (UiO), Department of Geoscience.

- Literature concerning the geology in central parts of Telemark County; “Litt om geologien i det sentrale Telemark” (Dahlgren, 1993).
- National landslide incident database accessed from Norwegian Water Resources and Energy Directorate (2016).
- Specialization project from the same site, written by the author in 2015.

1.3 Location and geological conditions

Regional settings

Several pronounced fracture and fault zones exist in the county of Telemark. The bedrock is in large scale mainly dominated by two structures orientated SW-E and NW-SE, originating from several different deformation processes through the geological history. These include folding of the sedimentary and volcanic rocks in Precambrian together with high volcanic activity later in Perm in connection with the formation of “Oslofeltet” (Jansen, 1986). Later on, erosion by glaciers and water have worked intensely in existing zones of weakness. This process has in turn led to a high relief in many valleys in Telemark, creating potential unstable slopes.

Kassen unstable area

The Kassen site is defined as a potential unstable slope due to very high rock mass deformation within the domain compared to the adjacent slopes. The site is located at the North shore, in the southeastern part of the 27 km long Bandak Lake (72 masl), shown in Figure 2. Bandak lake is orientated WNW-ESE, parallel to several other distinct structures in the region. A major fault zone is identified underneath the lake (Nilsen, Dons J.A., & Gyøry, 2013).



Figure 2: Kassen unstable slope is located in Kviteseid municipality in Telemark county.

The unstable slope is dipping towards north with an average dip angle of 34° and the total area of the instability is estimated to be approximately $3,2 \text{ km}^2$ (calculated in ArcGIS 10.4 by using the area measuring tool). The instability is limited in the upper part by a depression parallel to the back scarp, evident in field and on the High-Resolution Digital Elevation Model (HRDEM). The lateral limits differ in the western and eastern part of the instability; a high contrast in degree of deformation in the west makes the limit easy to locate while degree of deformation

in the east varies over a greater area (up to 900 meters). The top of Kassen represents the highest point of the slope, rising 884 masl.

Figure 3 shows an ortophoto and hillshade over the area, where two important features are marked out; Amfiteateret which is the most deformed part within the instability, and Skipet which is an isolated, steep cliff. The stability analyses in this thesis are conducted at these two locations.

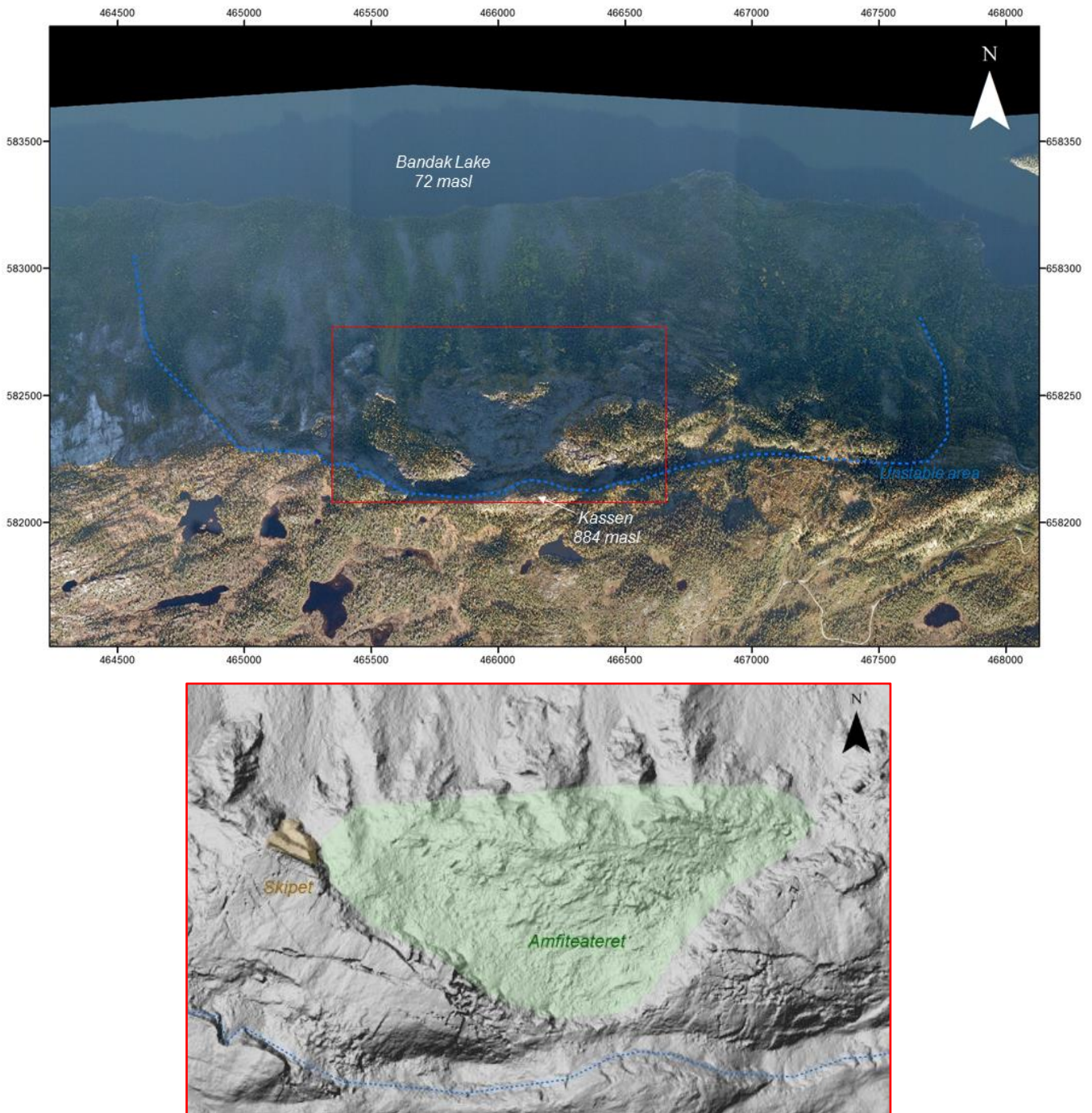


Figure 3: An overview of the unstable area (limits marked with blue) is given in the upper Orto photo. Notice the difference in degree of deformation and activity between the western and eastern part. The lower figure shows the DEM of the area marked with red, where the locations of Amfiteateret and Skipet are highlighted.

Geological framework

The geology in the central parts of Telemark is characterized by low to medium grade metamorphic supracrustal rocks (rocks deposited on existing basement)(Nilsen et al., 2013). These are divided into four groups; Rjukan group, Seljord group, Heddal group and Bandak group where the Rjukan group is the oldest, assumed to be of Mesoproterozoic age (1500 Ma). Two generations of granites are also represented in the geology of central Telemark. The oldest is formed about 1190 million years ago, and the youngest 930 million years ago. Together with the Bandak group, the granites formed under the Sveconorwegian orogenic event (Dahlgren, 1993).

Figure 4 shows the distribution of rock types in the area, provided by NGU (2016). All rock types presented in this bedrock map were recognized in field. The amphibolite (belonging to the Rjukan group), is described by Nilsen et al. (2013) as a greenish to grey coloured rock with medium to fine grains. It is assumed to originate from basic to intermediate volcanites. In field, the rock was mostly grey to dark grey with medium grain size. Due to low-grade metamorphism of the Rjukan group, the foliation was poorly defined in the amphibolite.

The older generation of granites is found in the western part of the unstable slope. This granite is named after the lake, Bandak, and is estimated to have an age of 1240 ± 140 Ma (Nilsen et al., 2013). The rock has a pale red colour with small reddish and dark grey spots, and a fine to medium fine grain size. The foliation in the Bandak Granite is easier to recognize than in the amphibolite, by clearly elongated biotite minerals (Figure 5).

Acidic vulcanite (found in the eastern part of the area) also belongs to the Rjukan group, but shows a more clear foliation than the amphibolite. The rock was reddish and grey in colour, thin banded, with a medium grain size. In some outcrops, darker micas and greenish epidote was observed together with chloride-bearing layers (Figure 5).

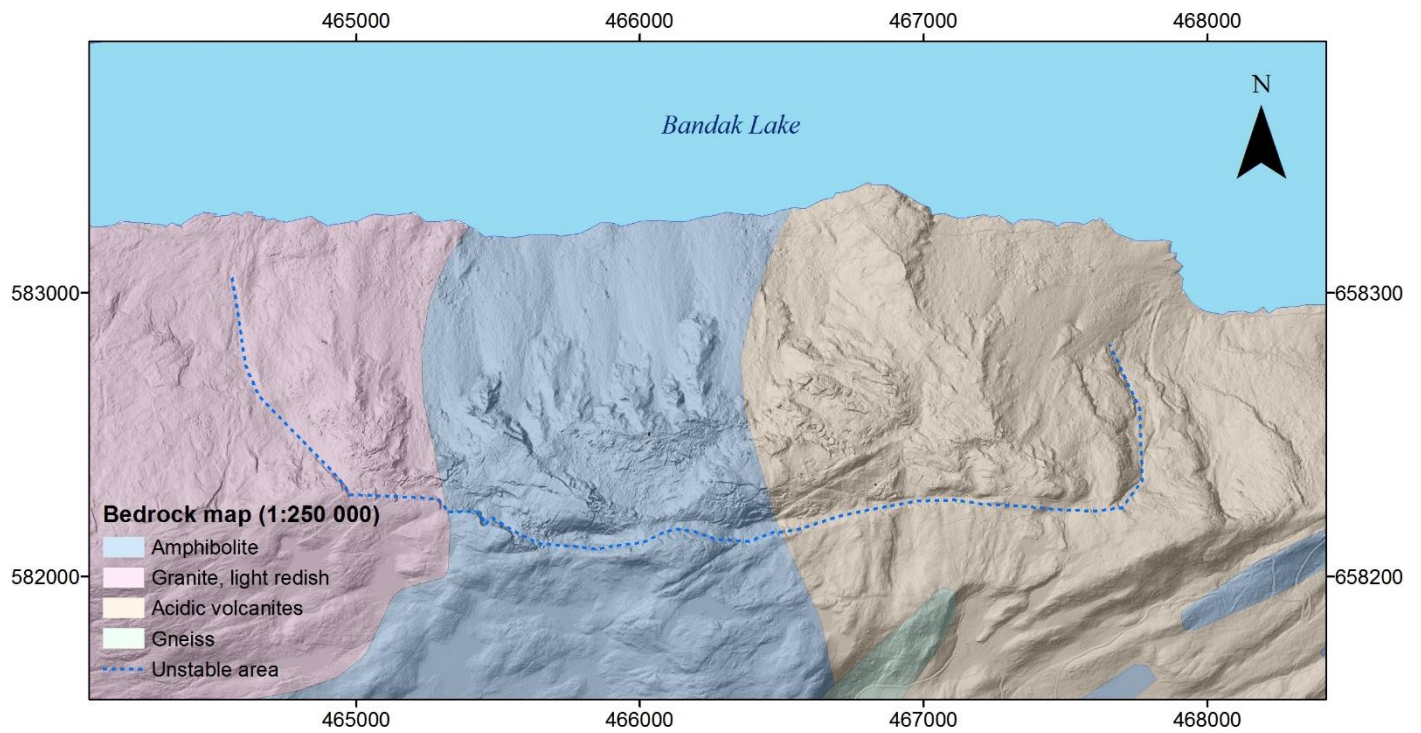


Figure 4: Bedrock map (1:250 000) from NGU.

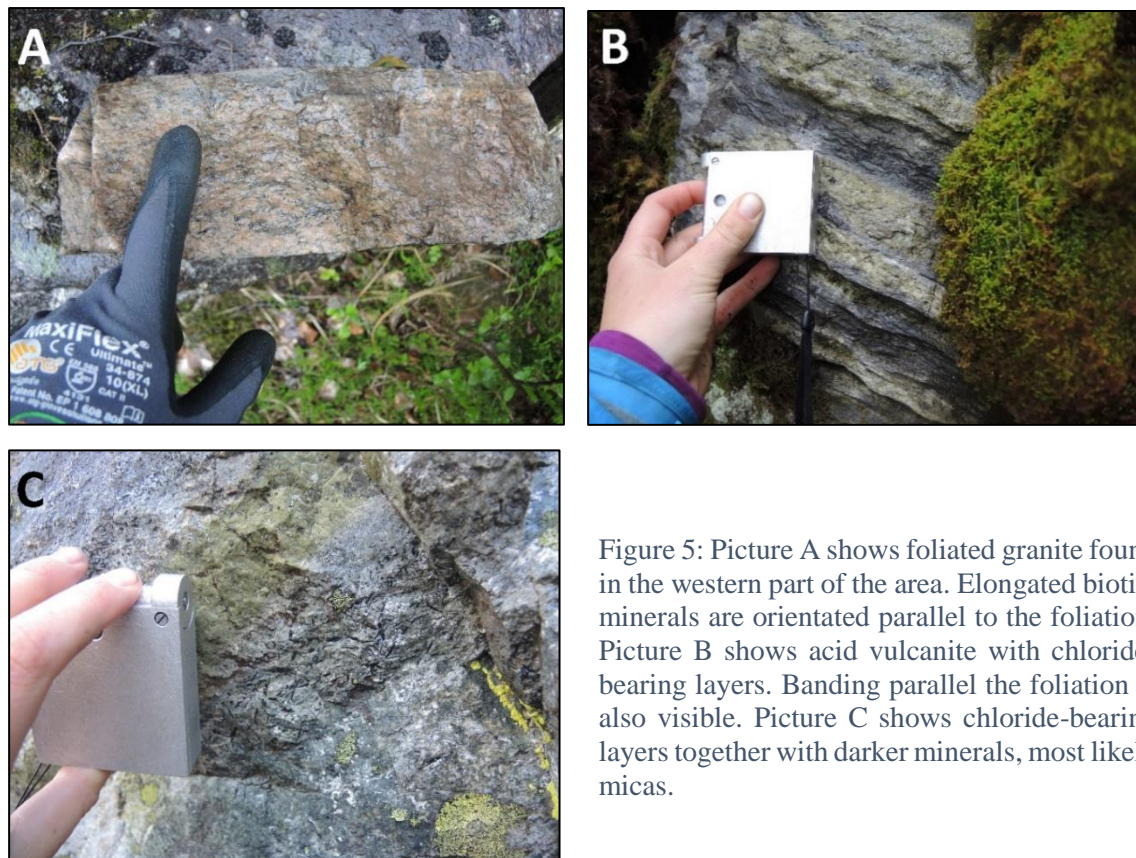


Figure 5: Picture A shows foliated granite found in the western part of the area. Elongated biotite minerals are orientated parallel to the foliation. Picture B shows acid vulcanite with chloride-bearing layers. Banding parallel the foliation is also visible. Picture C shows chloride-bearing layers together with darker minerals, most likely micas.

Glacial history

Glaciers have retreated and advanced numerous times in Norway through the last 2-3 million years. During this time they formed the present-day landscape, with most profound effect in the formation of large U-shaped valleys, fjords and alpine relief (Fredin et al., 2013).

Figure 6 shows main glacial movement direction at the last glacier maximum, 25 000 – 18 000 years ago (Ramberg, Bryhni, & Nøttvedt, 2007). The ice movement direction at Kassen and the surrounding area was towards southeast, parallel to the orientation of Bandak Lake. In Telemark, U-shaped valleys like the one at Bandak Lake characterize the topography with an increasing relief from east to west.

The deglaciation of the Scandinavian Ice Sheet began in Old Dryas, approximately 18 000 years ago. Figure 6 shows that the Kassen site was located at the ice margin about 10 600 years ago (after Younger Dryas). At this time, melting of ice was accelerating, and on the lower altitudes of the glacier surface it could melt away 10-15 meters ice each summer which is equivalent to 10 000 – 15 000 mm of rain (Ramberg et al., 2007).

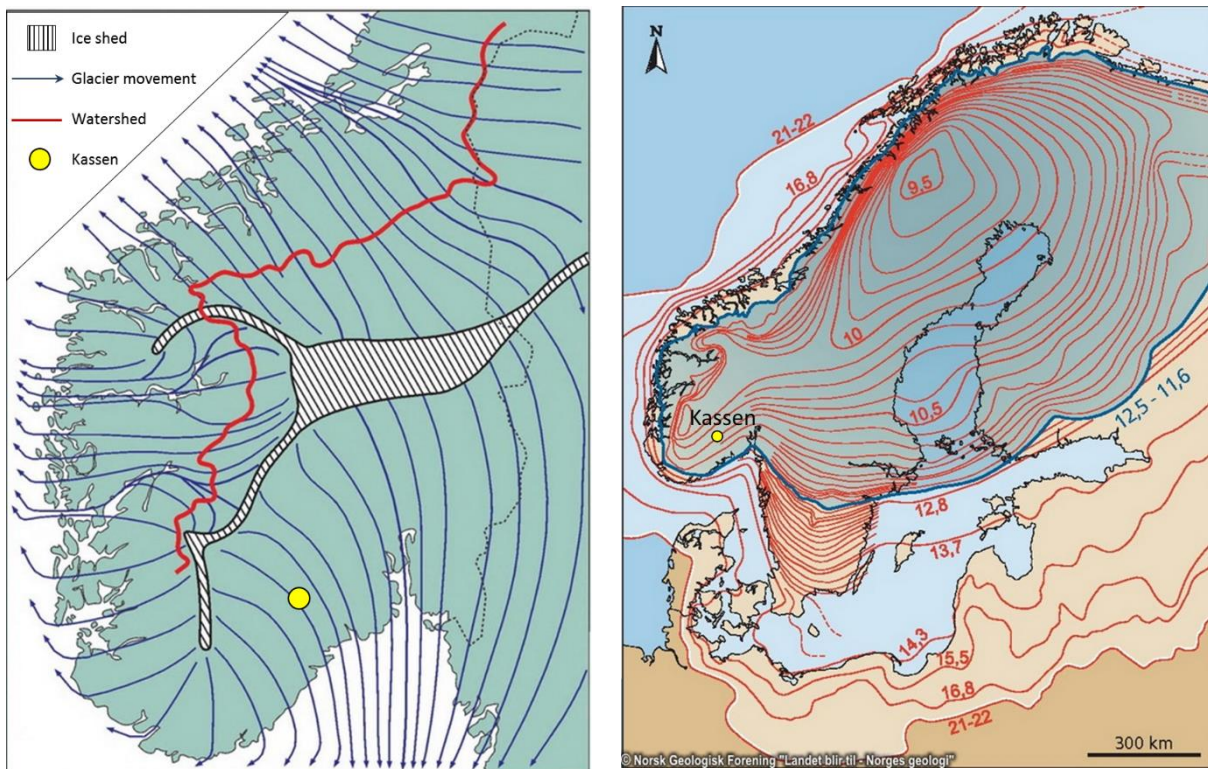


Figure 6: The left figure shows glacial movement direction under the last glacial maximum. The deglaciation of the Scandinavian Ice Sheet is shown in the right figure. Numbers are ages in 1000 years and the respective lines show where the ice margin was located. Figures modified from Ramberg et al. (2007).

Historical events

One rockslide event is registered for the Kassen unstable area in the National landslide database provided by NVE. This slide occurred around 1985, and originated from Skipet located 700 masl. The slide is subjectively described as “very big” and run out to the lake,

creating flood waves of minor size. During field work summer 2015, this event was confirmed by a local. This rockslide will be noted the “1985-event” in this thesis.

Bathymetric data of Bandak Lake show rock avalanche deposits located at the lake bottom, which have run out to the opposite shoreline. These deposits are located beneath the central parts of Amfiteateret which means that another, greater post-glacial slope failure event have occurred from the Kassen slope. Based upon bathymetric data this event is estimated to a volume of 3.37 million m³. Based on the run-out length and size of the deposits it is believed that this prehistoric slope failure was a rock avalanche. This event will be noted “the Bandak rock avalanche” in this thesis.

1.4 Aim and structure of the study

The aim of this master thesis is to investigate the instability at Kassen by using several different tools. The main objectives are summarized below;

1. Perform and preliminary consequence assessment of seven potential failure scenarios in the slope, following guidelines developed by NGU. The consequence assessment includes volume estimation, run-out analysis and empirically estimated run-up heights from potential displacement waves.
2. Perform a detailed stability analysis at Amfiteateret using the software RS² (Phase 2, 9.0) from Rocscience. This analysis is a back-analysis of the Bandak rock avalanche where the main goal is to investigate which geological and climatic settings lead to the slide. The last step in the modeling is a forward analysis at the same location in order to determine a Factor of Safety for the slope today.
3. Perform a stability analysis of two unstable blocks detected at Skipet. This analysis will be performed by using limit equilibrium methods. The analysis is motivated by the 1985 event.

This master thesis is a continuation of the author’s specialization project, completed in December 2015. A summary of this project will be presented in the next chapter. Chapter three presents general theory of unstable rock slopes before theory, methodology and results from the hazard and preliminary consequence assessment is presented in chapter four. Chapter five involves theory, methodology and results of the two stability analyses at Amfiteateret and Skipet. A discussion of the applied methods and results is given in chapter six, and finally a conclusion of the study in chapter seven.

2 Completed investigations and findings

A detailed study of the Kassen unstable area was done in 2015 as the authors specialization project. The work in this study is listed below;

- Detailed mapping of the structural geology and geomorphology
- Description and location of the lateral and rear limits of the instability
- Defining structural domains
- Kinematic feasibility test
- Structural profiles for simple stability assessment
- Defining possible failure scenarios

This work will serve as a basis for further stability analyses and hazard assessment performed in this master thesis. Main observations and results from the specialization project are presented in the following.

2.1 Joint sets

Detailed discontinuity mapping was performed summer 2015 where 1788 measurements of dip direction/dip was performed. Through field recognition and stereographic projection, four main joint sets (J1, J2, J3, J4) are identified (Table 1). The stereographic projection was performed in DIPS (Rocscience, 2016a).

The foliation in the area was hard to determine due to weathering and rock types showing no clear foliation, especially in the amphibolite which covers the central and most deformed parts of the unstable area. However, J2 structures were in some observation points mapped as the foliation, especially in the acidic volcanites in the eastern domain. Here, the foliation were recognized at six observation points dipping towards NW with a dip angle of 30-40°. In the granitic gneiss in the western parts of the area it was recognized in four observations points showing less consistent orientation, but the general trend is that the foliation dips steeper (up to 80°) and more towards north.

Table 1: Description and properties for joint sets at Kassen. The orientation is given in dip direction/dip and the variance in degrees are found by a 1σ variability cone around the mean orientation in DIPS 6.0.

Joint set	Description	Orientation \pm Variance [°]	Spacing [m]	Persistence [m]
J1	J1 dips steeply towards NNE and is parallel to the back scarp in the southwestern part of the unstable area. In several observation points, the structure is measured directly on minor scarps following the back scarp. J1 is the most consistent in terms of orientation and is also the most persistent. The surface is rough and planar, and exfoliation joints have developed parallel to this structure.	025/87 \pm 22°	0.3 - 3	1.5 - 12
J2	J2 has a mean dip direction NW, with a high variability through the area; in the east it dips towards ENE while the dip direction is directly north in the western parts. However, it was easy recognized in field being the only shallow dipping structure. The joint set was mostly interlocked with a smoother surface relative to the other joint sets.	313/19 \pm 24°	0.2 - 1	0.3 - 5
J3	J3 is orientated orthogonally to J1, dipping steeply towards southeast. The surface is stepped and planar to rough. Together, J1, J2 and J3 creates a cubic fracture pattern.	127/79 \pm 24°	0.1 - 2	2 - 5
J4	J4 was identified in field in the western part of the area, but is only significant represented in the stereographic projection for the eastern part. The joint set appears planar with a rough surface.	243/68 \pm 19°	0.6 - 8	-

2.2 Structural domains

Based on variation in orientation of the four joint sets, the Kassen unstable area was divided into three structural domains; Lower West (LW), Upper West (UW) and East. The rock mass in the LW domain is most dissected, including Amfiteateret. The East domain is less deformed than the two western domains, and the back scarp in this area is in general 10-20 meters lower and has a more circular curvature than further west. The boundaries of the domains are shown in Figure 7, and stereographic projections of the joint sets for each domain in Figure 8.

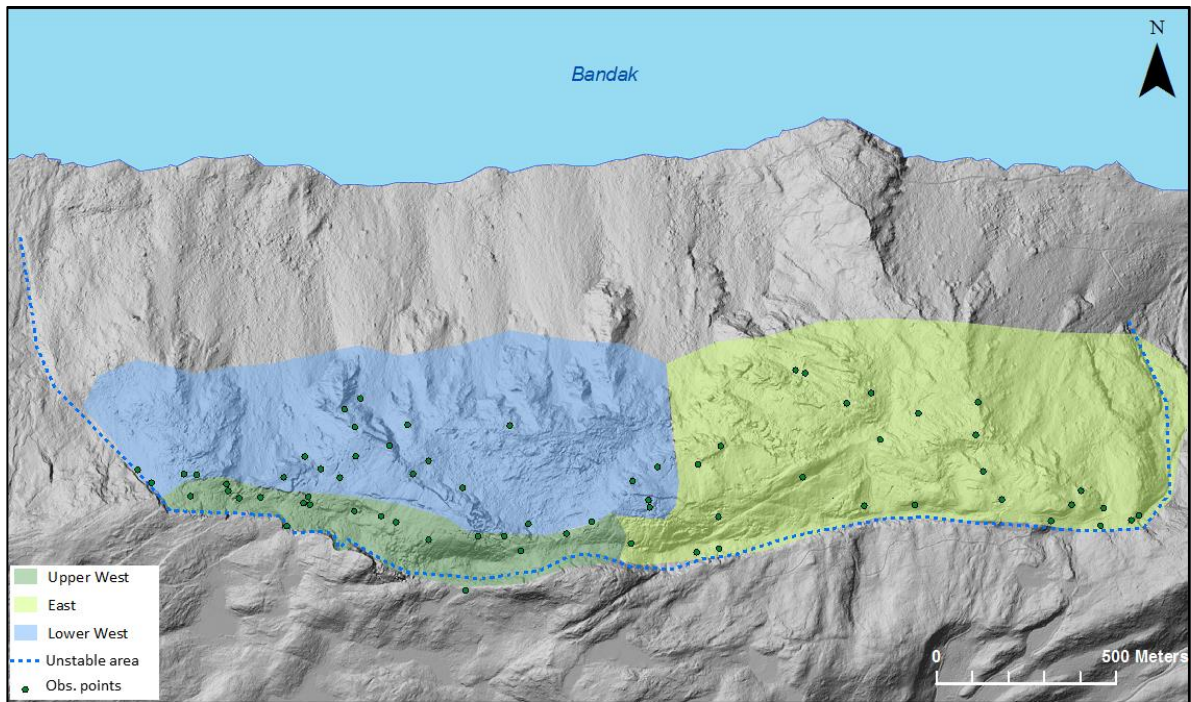


Figure 7: Subdivision of the three structural domains of the unstable area. The joint set J2 has the highest influence of the location of domain boundaries due to its high variance in both dip and dip direction.

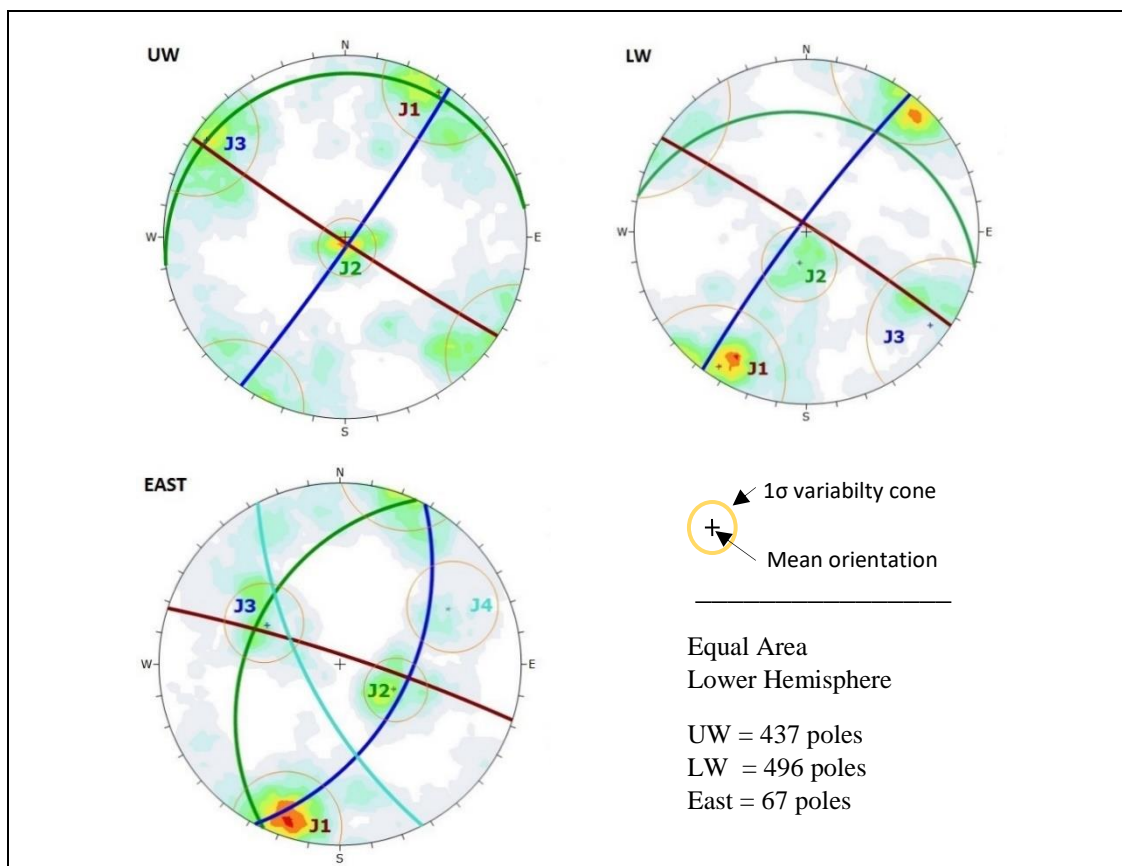


Figure 8: Stereographic projection of joint sets in the subdomains. The projection is performed in DIPS 6.0 (Rocscience). J2 is the structure varying the most from domain to domain.

2.3 Kinematics

For each structural domain, a kinematic feasibility test was performed using DIPS 6.0 for planar failure, wedge failure and toppling. The aim of this work was to assess possible failure modes as a first stability approach. The main findings from the kinematic analysis is listed in Table 2.

Table 2: Results from kinematic feasibility test.

Domain	Planar Sliding	Wedge Sliding	Toppling
UW	Only possible for the steepest part of the slope along steepest parts of J2.	No critical intersections of planes for wedge sliding.	Possible along J3 and partly possible along J1.
LW	Possible along J2.	Partly possible along the intersection of J2 and J3.	Possible along J1 and partly possible along J3.
East	Possible along J2 and shallow parts of J1.	Partly possible along the intersection of J2 and J4.	Possible along J1 and partly possible along J4.

2.4 Profiles

In order to obtain a more throughout understanding of the possible failure modes, profiles showing critical structures, were created for each structural domain. This method especially points out the possibility for biplanar failure which kinematics do not show. The profiles for the lower west domain is shown in Figure 9.

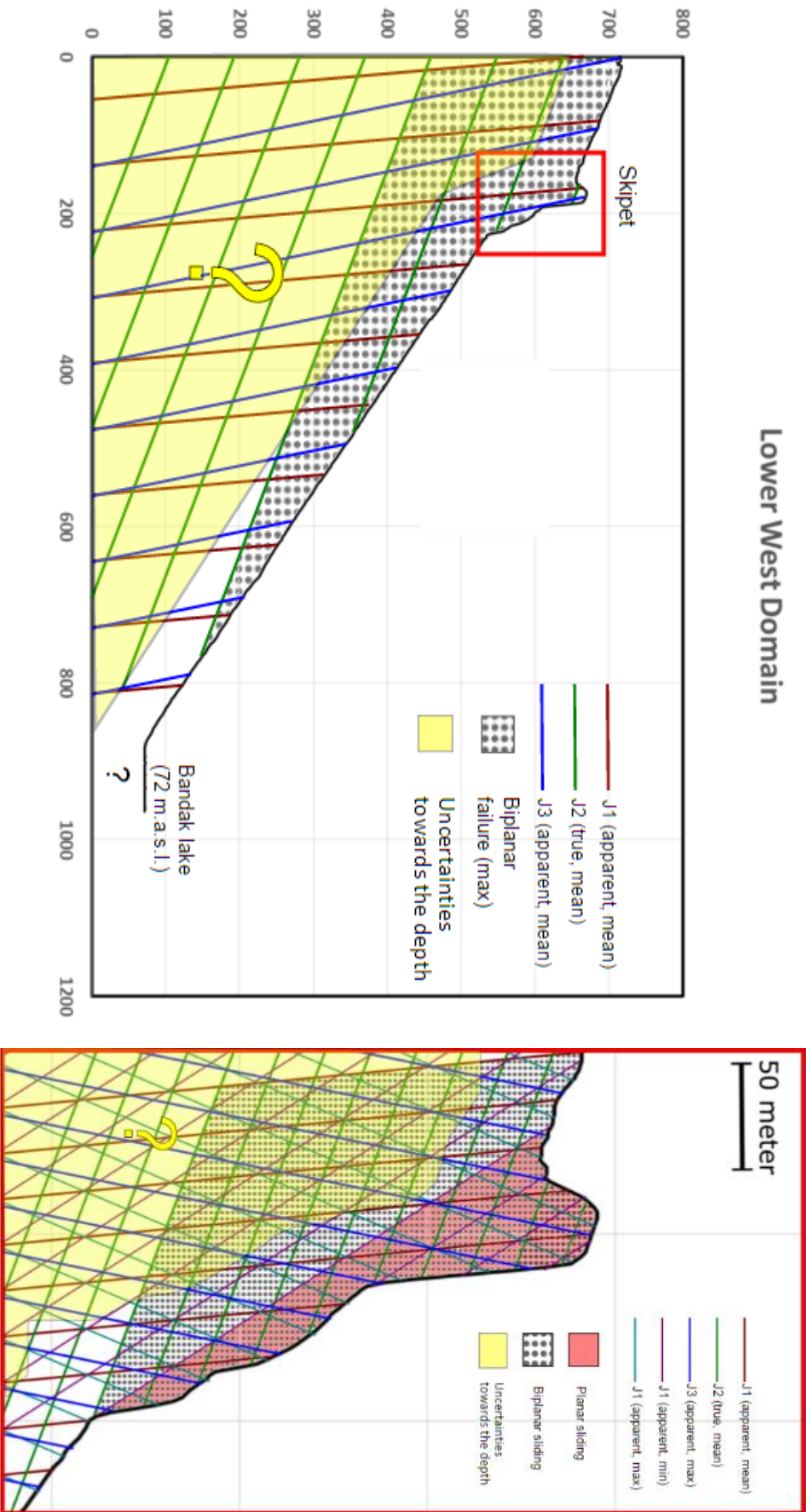


Figure 9: Profile created for the LW domain. An more detailed investigation of potential failure modes were conducted for Skipet, shown in the right figure.

2.5 Geomorphological features

Collected geomorphological data was used to create the geomorphological map shown in Figure 10. The main uncertainty in this work was the location of the eastern lateral limit. Opposite to the western flank, the eastern flank shows less contrast in deformation between the assumed unstable and stable area. This aspect was investigated in more detail during fieldwork 2016, and it was decided to keep the eastern boundary at its original location, but to emphasize that the degree of deformation is increasing towards the central parts of the instability. A pronounced contrast in deformation occurs after the morphological lineament striking NW in Figure 10. This feature continues far outside the instability and is interpreted as a zone of weakness. The mean orientation of this zone was measured in field to have a dip direction/dip of $342/74^\circ$, which is too steep to daylight the slope. In addition, no clear sliding plane structures were recognized in the field. The role of this structure to the overall stability of the slope is therefore considered to be of minimal importance, and not included in any further stability analyses.

Typical morpho-structures for Deep Seated Gravitational Slope Deformation (DSGSD) are recognized for the unstable slope such as counterscarps, minor scarps and tension cracks. The size of the instability is comparable to the entire slope and the present day displacement is very low which are typical characteristics for DSGSD. A throughout definition and description of DSGSD is presented by Agliardi, Crosta, and Zanchi (2001).

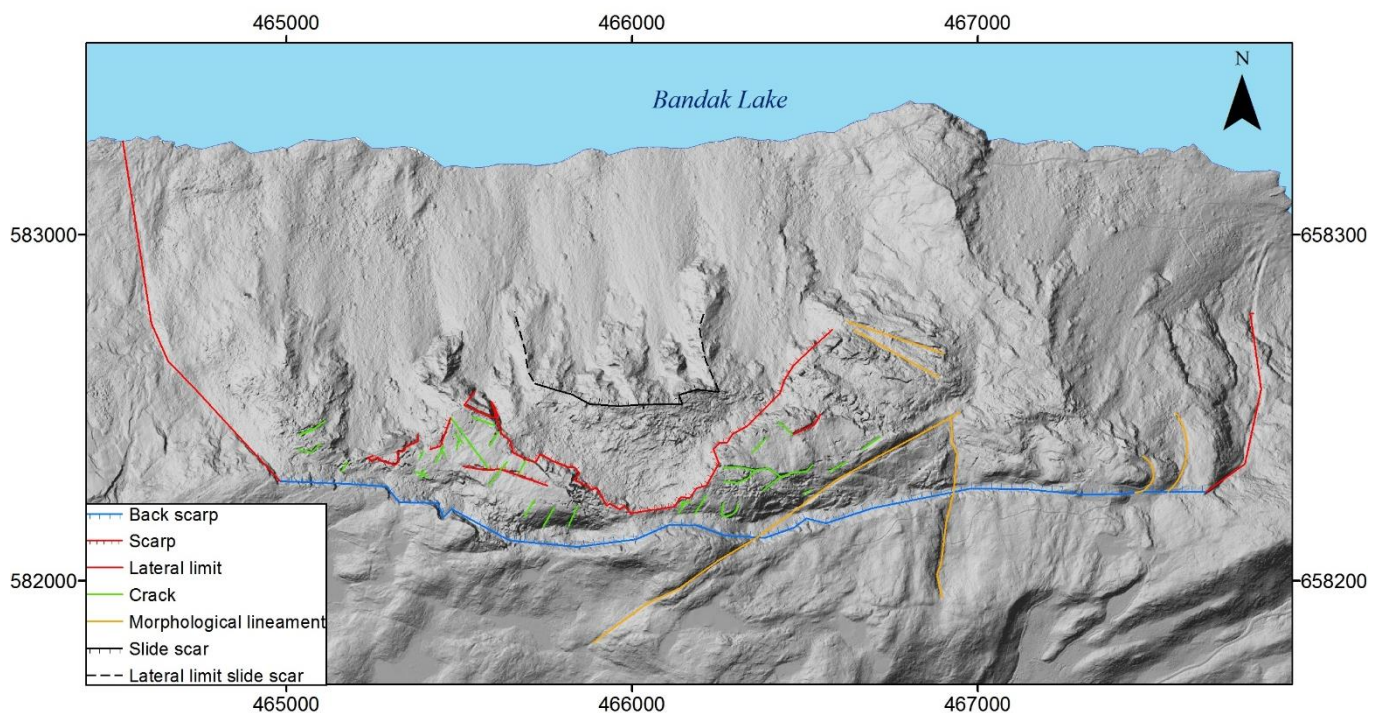


Figure 10: Geomorphological map created after investigations performed in the specialization project.

3 General theory of landslides

Landslides exist almost anywhere in the world, and most countries have to some degree been affected by landslides (Highland & Bobrowsky, 2008). This widespread geographic coverage is connected to the wide spectrum of behaviour which depends on the material content and movement type but also on the geological, geotechnical and geomorphic environments where they occur (Hermanns, 2016a). Even though they vary, all landslides can be destructive when impacting settlement or infrastructure. Through time, landslides and their secondary effects have caused numerous casualties and huge economic losses (Turner & Schuster, 1996). Landslide activity and the subsequent hazardous consequences are expected to increase in the 21st century. The reasons for this development is described by Turner and Schuster (1996):

1. Increasing human population leads to urbanization and development into unstable hillside areas.
2. Deforestation is rapidly increasing in landslide-prone areas. This point does however not count in the Norwegian context as vegetation is increasing due to less mountain farming.
3. Changing climate is causing increased regional precipitation.

Even though landslide mitigation, warning systems and prediction have developed over the past years, these topics are still important for future research, highlighted by the listed points above. Prerequisite for all mitigation and preventative work is an appropriate understanding of landslide hazards and their consequences, which is the aim of NGUs mapping program of unstable rock slopes in Norway.

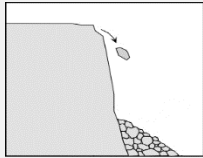
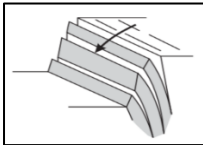
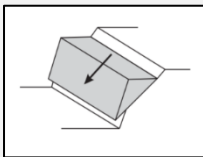
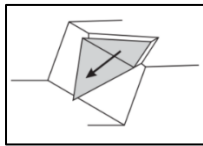
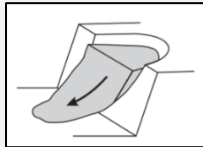
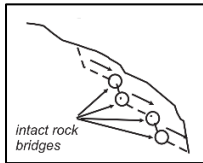
Terminology

Landslides vary a lot concerning the type of movement, velocity, material involved and triggering factors. It is a complex phenomena, studied by many disciplines, which is reflected in the diversity of definitions of a landslide. Hermanns (2016a) suggest the following general definition of a landslide:

“A landslide is the gravitational downslope movement of solids on natural or artificial slopes. The solids are geotechnical materials that can contain water, ice, and air; however the solids are volumetrically dominant over the transport medium (water, ice and air).”

Varnes (1978) developed the first classification of landslide types based on movement type and the material in motion. The latest update was published by Hungr, Leroueil, and Picarelli (2014) in order to adapt the classification to the newest research on the topic, especially concerning the geotechnical and geological properties of rock and soils. Table 3 shows parts of this classification for landslides involving movement of rock.

Table 3: Overview of some landslide types classified by Varnes (1978). Figures are modified from Wyllie and Mah (2004) and (Stead, Eberhardt, & Coggan, 2006).

Name	Description	Figure
Rock fall	<i>Detachment, fall, rolling and bouncing of rock fragments.</i>	
Rock topple	<i>Forward rotation and overturning of blocks, caused by steeply dipping joints into the slope.</i>	
Rock planar slide	<i>Failure where rock masses slide on a single discontinuity forming a planar rupture surface.</i>	
Rock wedge slide	<i>Failure where rock masses slide along two intersecting discontinuities, forming a wedge-shaped block.</i>	
Rock rotational slide	<i>Sliding of weak rock mass following a cylindrical rupture surface which is not structurally controlled.</i>	
Rock irregular slide	<i>Sliding occurs on an irregular rupture surface due to failure of rock bridges (intact rock) between randomly orientated joints. Occurs in strong rocks.</i>	
Rock avalanche	<i>Extremely rapid, massive flow-like motion of fragmented rock from a large rockslide or rock fall.</i>	

It is useful to introduce landslide terminology dealing with morphometry and dimensions to allow for precise communication on landslides. Varnes (1978) defined landslide terminology describing the unique parts of a landslide which is frequently used in literature, including this master thesis (Figure 11).

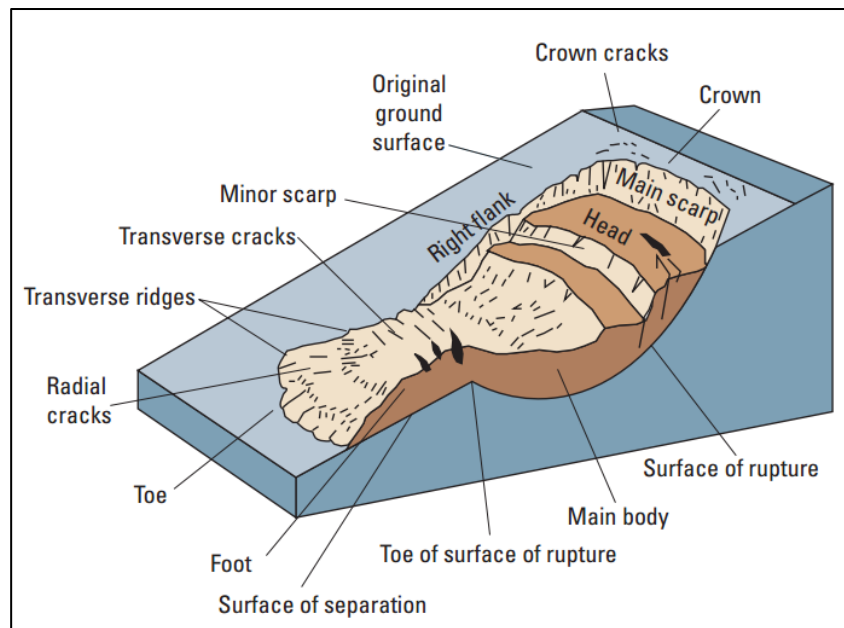


Figure 11: Common labels for different parts of a landslide. From Highland and Bobrowsky (2008)

Controlling factors of large scale rock slopes

The stability of large, unstable rock slopes are in general difficult to analyze due to complex and varying geological settings. The controlling factors influencing the stability and rate of movement for a rock slope under past and present Norwegian conditions are summarized by Grøneng (2010) as follows;

- Slope topography
- Orientation of discontinuities
- Shear strength of discontinuities and intact rock
- Groundwater pressure
- In situ stress conditions
- Seismic activity
- Freezing/thawing effects
- Glacial and deglacial processes

The importance of each factor varies from setting to setting. However, it is suggested by Wyllie and Mah (2004) that the role of discontinuities and groundwater conditions are the main governing factors concerning the stability of a rock slope.

In most cases the properties of the discontinuities govern the stability more than the intact rock itself (Norrish & Wyllie, 1996). Such properties are orientation, persistence, spacing, surface roughness and shear strength. The latter works as the resistant force against failure. Unfavourable orientated discontinuities with low shear strength values increases the likelihood for failure.

Studies by Sandersen, Bakkehøi, Hestnes, and Lied (1997) of four large historic rockslides in Norway (Modalen 1953, Tafjord 1934 and Loen 1095 and 1936) show that the influence of

increased water pressure in the slope was one of the main causes for the failures. The presence of groundwater in a slope can affect the stability for several reasons (Wyllie & Mah, 2004);

- Water pressure reduces the shear strength of potential failure planes and acts as a driving force in tension cracks. This is by far the most important effect of groundwater.
- Changes in moisture content can for some materials reduce the internal friction (e.g. joint infilling).
- Water expands when freezing, causing displacements and increased driving forces. Frozen water can block drainage paths resulting in increased water pressure.
- Erosion by surface- and ground water decreases the stability.

For past glaciated areas, the glacial history is of importance for the slope stability. One of the major consequences of deglaciation in mountainous areas is the exposure of rockwalls, steepened by glacial erosion (Ballantyne, 2002). The steepening of rock slopes increases the shear stresses acting in the rock mass due to the increased overburden, which in turn can promote rock-slope failure along planes of weakness (e.g. pre-existing joint sets) after ice retreat (Augustinus, 1996).

Another effect of deglaciation is through debuttrressing which is the removal of support provided by the glacier ice. The weight of the overlying ice induces internal stress levels in the rock mass that is much higher than what the rock overburden would induce alone. Consequently, unloading of glacial stressed rock, leads to a rebound or stress-release within the rock which generally results in propagation of the internal joint network, loss of cohesion along joint surfaces and a reduction of internal locking stresses (Braathen, Blikra, Berg, & Karlsen, 2004; Wyrwoll, 1977). These processes can lead to catastrophic rock slope failures right after deglaciation or a delayed failure due to large-scale rock mass deformation, in the form of progressive slow movements. In Norway, there are very few of the mapped rock avalanches that show evidence of being deposited on top of glaciers (Schleier, Hermanns, Rohn, & Gosse, 2015). This leads to the assumption, that failure connected to stress release due to debuttrressing are delayed failures conditioned by time-dependent dissipation of residual stresses within the rock mass (Wyrwoll, 1977).

The complexity and variety of slope failures demonstrates that seldom can a landslide be attributed by a single process (Popescu, 2002). The processes discussed and listed above will result in fatigue and accumulation of damage in the rock mass, which can eventually bring a rock slope to a critical damage threshold where failure occurs (Stead & Eberhardt, 2013).

4 Hazard and preliminary consequence assessment applied to Kassen

This chapter presents the theory, methodology and results of the hazard, and preliminary consequence assessment applied to Kassen. This work is performed by following the NGU approach.

4.1 NGU Mapping Approach

In 2012, a team of Norwegian and international experts developed a standardized hazard and risk classification system for large unstable rock slopes. The system follows a standard approach for the analyzed sites which is iterative, starting with simple assessments (Hermanns et al., 2014). A higher hazard/risk level of a site requires a larger amount of geological information, and more detailed run-out models and consequence analysis. This approach allows resources and follow-up activities to be focused on the sites of highest risk and discard low risk sites early in the mapping process. Follow-up activities include detailed geological mapping, periodic displacement measurements, continuous monitoring and early-warning or other mitigation measures (Hermanns, Oppikofer, et al., 2013; Oppikofer et al., 2015). Every site (except sites showing no sign of instability) is recorded in a national database of unstable rock slopes in Norway. The iterative steps in the mapping approach is summarized in Figure 12. Due to temporal restrictions, all steps are not completed for Kassen in this master thesis. A hazard assessment, volume estimation, run-out analysis and empirical determination of run-up heights have been performed, but the site is missing a detailed displacement wave analysis. When this work is completed, potential loss of life can be determined and the site can be risk-classified which will help to decide on follow-up activities.

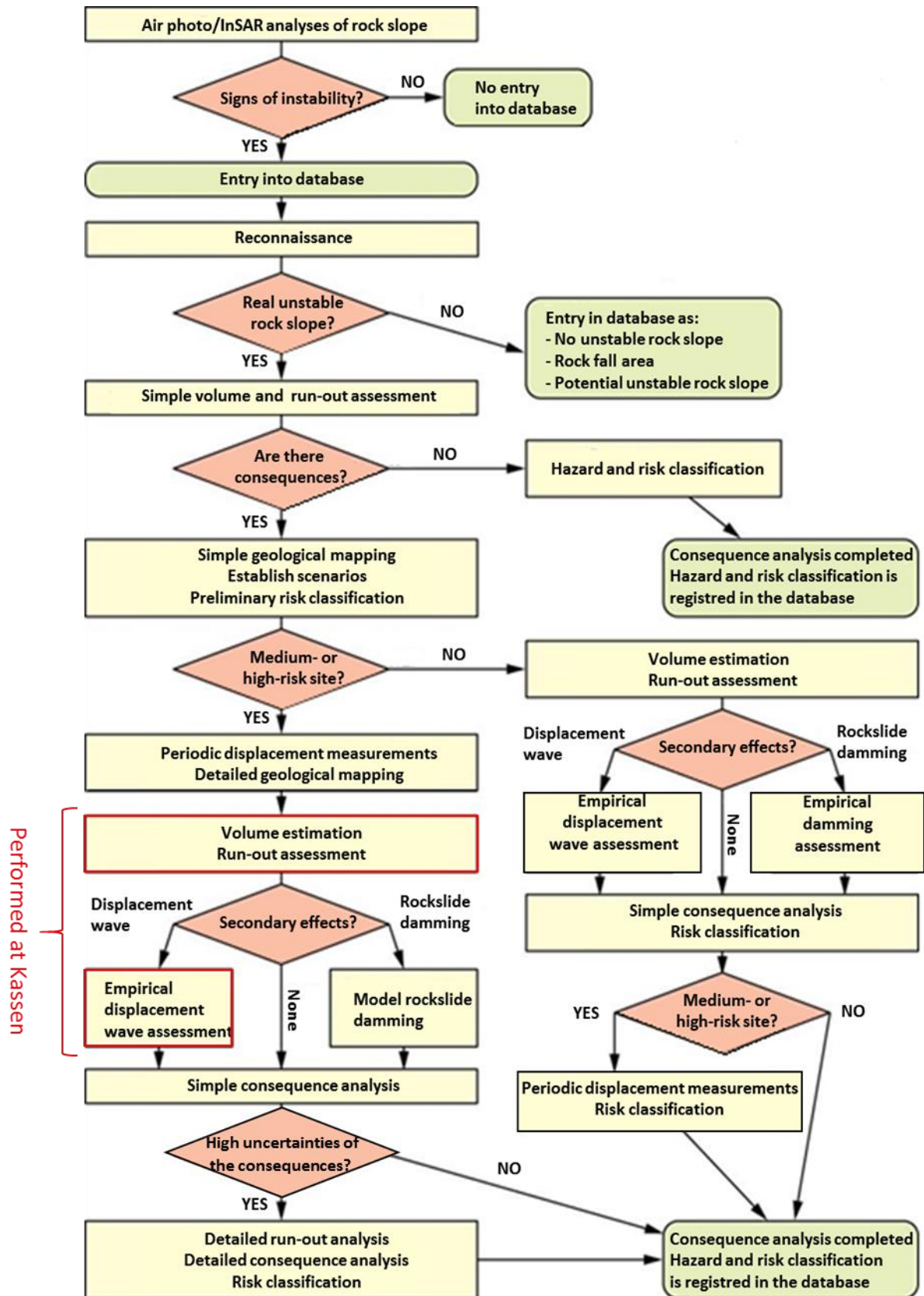


Figure 12: Flowchart showing the mapping approach for unstable rock slopes in Norway. The step marked in red is performed in this master thesis in addition to the hazard assessment. Modified from Oppikofer, Böhme, Nicolet, Penna, and Hermanns (2016).

4.2 Hazard assessment

By analyzing historical slope failures in Norway, it is suggested that deformation can occur uniformly over the entire slope or locally. This is evident in geological records showing slopes which have collapsed repeatedly where others have failed in one single event (Longva, Blikra, & Dehls, 2009). Following these observations, the hazard classification is scenario-based, where each defined failure scenario will have an independent hazard classification. Different scenarios are defined on slopes that show a combination of the following features (Hermanns, Oppikofer, et al., 2012);

- Different deformation rates
- Varying structural conditions
- Internal scarps, cracks and depression which dissect the unstable rock slope

Based on the listed features, the preliminary hazard assessment was applied to 7 minor scenarios at Kassen using the methods described in Hermanns, Oppikofer, et al. (2012) and Hermanns, Oppikofer, et al. (2013). The minor scenarios were defined in the specialization project based on field observations and studies of hillshade maps, and are shown in Figure 13. Failure of the entire slope in one compartment is of a very low likelihood due to varying structural conditions and degree of deformation, and will therefore not be studied any further through a hazard and consequence assessment.

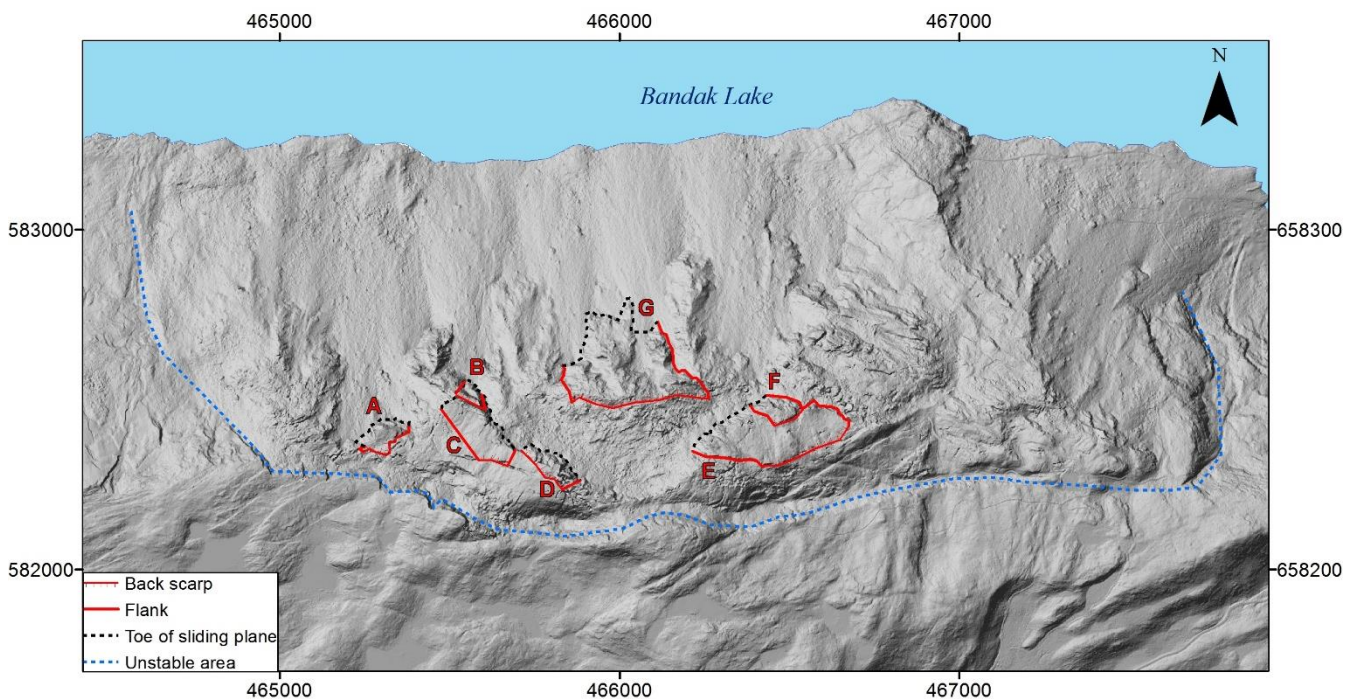


Figure 13: Overview of the seven minor scenarios defined in the unstable slope. The hazard and preliminary consequence assessment are performed for each scenario.

The hazard classification has nine criteria to describe the present state of the instability (Figure 14). Several outcomes are possible for each of the nine criteria, assigned with different scores. Adding the scores together gives the total score for the scenario, the hazard score. This number can range from 0-12, and the likelihood of failure increases with increasing number.

Due to complexities related with landslide phenomena, it may be difficult to be certain of one outcome for each criterion. Therefore, probabilities for each outcome can be given and is included when assigning the hazard score to a failure scenario. A decision tree is used to account for the uncertainties of each individual criterion (including the chosen conditions) by computing the entire range of possible outcomes. In addition, the probability for the actual path of the decision tree is included in the calculations. A throughout description of this system is found in Hermanns, Oppikofer, et al. (2012).

1. Back-scarp	Score
Not developed	0
Partly open over width of slide body (few cm to m)	0.5
Fully open over width of slide body (few cm to m)	1
2. Potential sliding structures	Score
No penetrative structures dip out of the slope	0
Penetrative structures dip on average < 20 degree or steeper than the slope	0.5
Penetrative structures dip on average > 20 degree and daylight with the slope	1
3. Lateral release surfaces	Score
Not developed	0
Partly developed on 1 side	0.25
Fully developed or free slope on 1 side or partly developed on 2 sides	0.5
Fully developed or free slope on 1 side and partly developed on 1 side	0.75
Fully developed or free slope on 2 sides	1
4. Kinematic feasibility test	Score
Kinematic feasibility test does not allow for planar sliding, wedge sliding or toppling	0
Failure is partly kinematically possible (movement direction is more than $\pm 30^\circ$ to slope orientation)	0.5
Failure is kinematically possible (movement direction is less than $\pm 30^\circ$ to slope orientation)	0.75
Failure is partly kinematically possible on persistent discontinuities (movement direction is more than $\pm 30^\circ$ to slope orientation)	0.75
Failure is kinematically possible on persistent discontinuities (movement direction is less than $\pm 30^\circ$ to slope orientation)	1
5. Morphologic expression of the rupture surface	Score
No indication on slope morphology	0
Slope morphology suggests formation of a rupture surface (bulging, concavity-convexity, springs)	0.5
Continuous rupture surface is suggested by slope morphology and can be mapped out	1
6. Displacement rates	Score
No significant movement	0
0.2 - 0.5 cm/year	1
0.5 - 1 cm/year	2
1 - 4 cm/year	3
4 - 10 cm/year	4
> 10 cm/year	5
7. Acceleration (if velocity is >0.5 cm/yr and <10 cm/yr)	Score
No acceleration or change in displacement rates	0
Increase in displacement rates	1
8. Increase of rock fall activity	Score
No increase of rock fall activity	0
Increase of rock fall activity	1
9. Past events	Score
No post-glacial events of similar size	0
One or several events older than 5000 years of similar size	0.5
One or several events younger than 5000 years of similar size	1

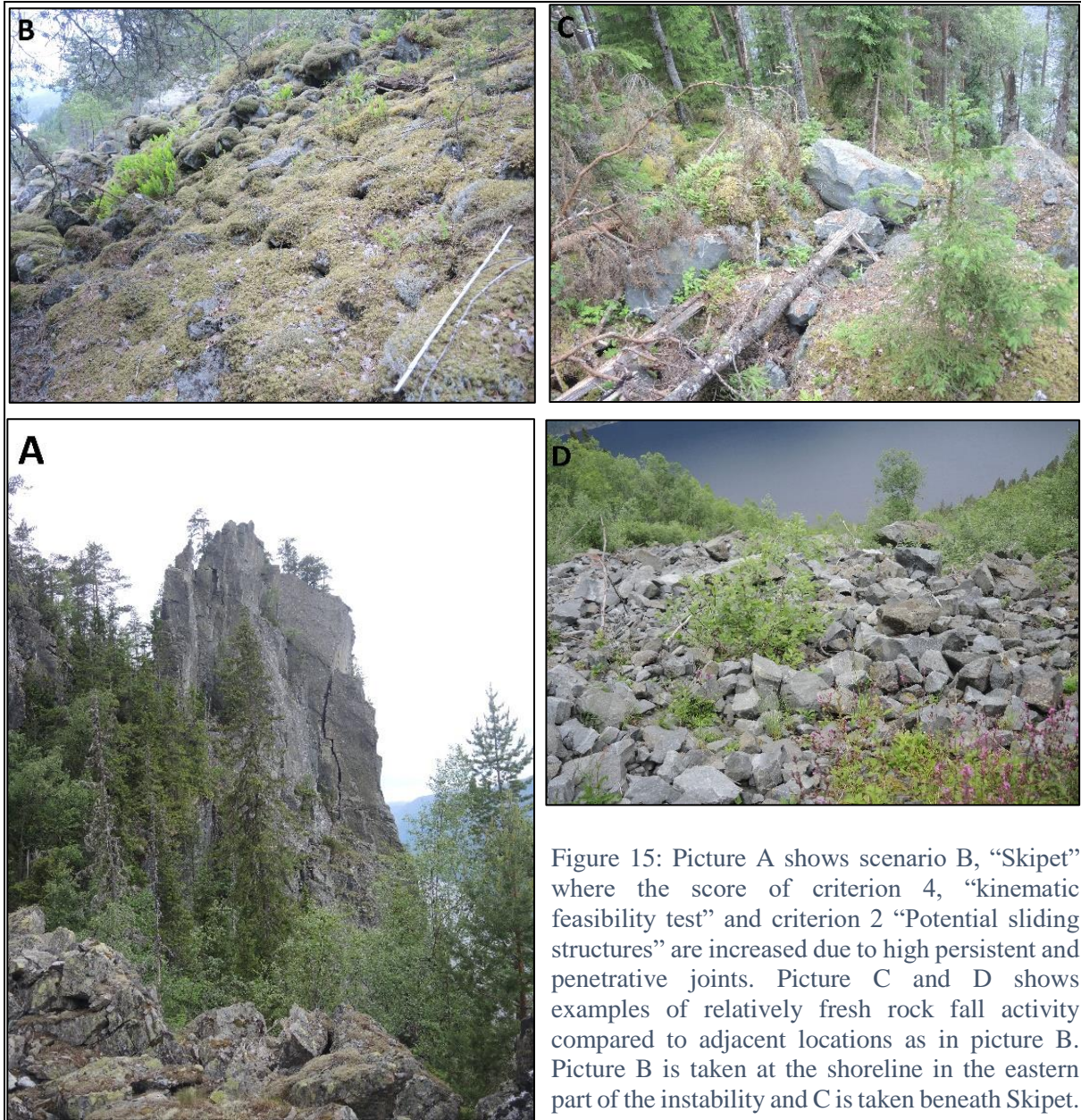
Figure 14: Criteria for hazard classification after Hermanns, Oppikofer, et al. (2013). The probability for each condition will be included when the system is applied.

In order to communicate the hazard to society in a simple way, the hazard score is divided into five hazard classes with equal intervals. Equal intervals is chosen because there is not sufficient amount of information on past catastrophic rock failures to define knowledge-based class limits (Hermanns, Oppikofer, et al., 2012). The probability of each hazard class is found by summation of all hazard score probabilities in the same class, or computed using the fitted normal distribution.

Table 4 summarizes the methods used to determine the hazard score for each criterion applied to the seven scenarios at Kassen. Figure 15 shows examples of how the criteria were applied. Methods used for criteria 4 and 6 will be described more throughout, as these require additional analyses and measurements.

Table 4: Methods used to evaluate the hazard score for the nine criteria describing the state of the instability.

Criterion	Method
1: Back scarp	<ul style="list-style-type: none"> - Hillshade maps over the area - Geomorphological observations from fieldwork
2: Potential sliding structures	<ul style="list-style-type: none"> - Structural measurements from observation points in close vicinity to the current scenario
3: Lateral release surfaces	<ul style="list-style-type: none"> - Hillshade maps over the area - Geomorphological observations from fieldwork
4: Kinematic feasibility test	<ul style="list-style-type: none"> - Kinematic analysis performed in the specialization project for three structural domains
5: Morphologic expression of the rupture surface	<ul style="list-style-type: none"> - Hillshade maps over the area - Field observations
6: Displacement rates	<ul style="list-style-type: none"> - dGNNS measurements performed at Kassen from 2012 – 2016
7: Acceleration	<ul style="list-style-type: none"> - dGNNS measurements performed at Kassen from 2012 – 2016
8: Increase of rock fall activity	<ul style="list-style-type: none"> - Field observations - Ortophoto
9: Past events	<ul style="list-style-type: none"> - National landslide database (NVE) - Results from bathymetric mapping



Criterion 4: Kinematic feasibility test

Criterion 4 in the hazard assessment is to evaluate the results of a kinematic feasibility test for the instability. This has been performed in the authors’ specialization project for the three structural domains.

Kinematic methods investigate if translational failure is *kinematic* possible given the geometry of existing discontinuities in the rock mass. Consequently, these methods depend on detailed investigation of rock mass structure, where orientation and geometry of existing joint sets is crucial for obtaining a reliable result (Eberhardt, 2003). The influence of joint orientation related to slope stability has been documented in several major rock slope failures such as Vaiont, Italy; Madison Canyon, Montana; Libby Dam, Montana; and Frank, Alberta (Johnson & DeGraff, 1988).

Standard criteria from rock mechanics for the different failure modes (planar failure, wedge failure and toppling) and for stereographic projection is applied following among others Wyllie and Mah (2004) and Hoek and Bray (1981). Some exceptions from these standards are recommended by Hermanns, Oppikofer, et al. (2012) to better fit the analysis for the purpose of failure of large rock slopes (Figure 16). Generally, there are more complex structures involved in large rockslides and more variable orientations of the slope than for instance a man-made road cut. The following modifications have been applied (described in detail in Hermanns, Oppikofer, et al. (2012));

- For planar and wedge sliding a lateral tolerance of 30° is applied between the discontinuity dip direction and the slope aspect.
- For toppling failure, a lateral tolerance of 45° is applied between the dip direction of discontinuities dipping into the face and the dip direction of the slope.

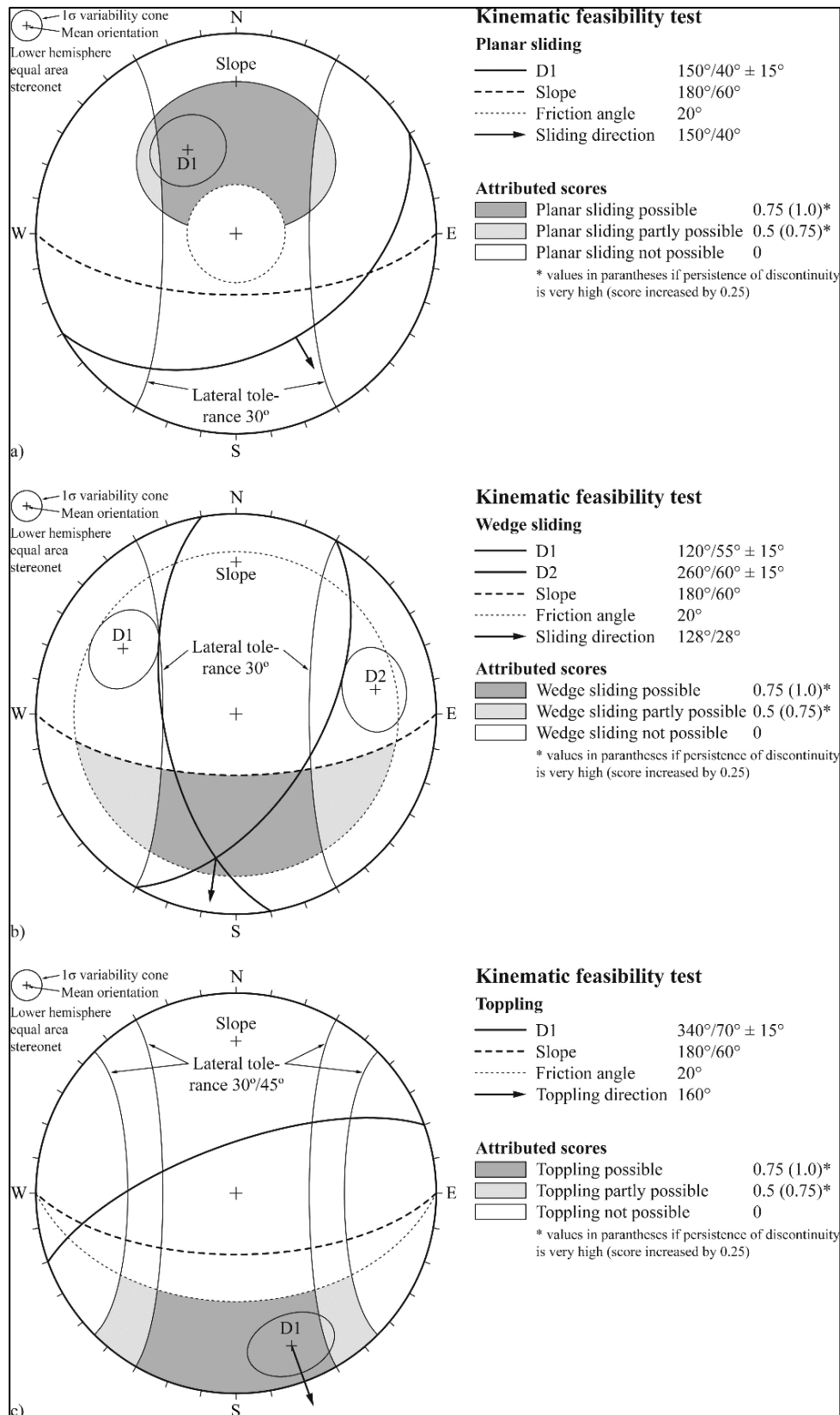


Figure 16: Kinematic feasibility test for planar sliding, wedge sliding and toppling. Lateral tolerance limits are recommended by NGU and determine if the attributed scores are partly possible or possible. If the sliding structures are highly persistent relative to the size of the instability, the score is increased with values in brackets (Hermanns, Oppikofer, et al., 2012).

Criterion 6: Displacement rates and acceleration

Displacement rates for the Kassen site are found with dGNSS (Differential Global Navigation Satellite System). This method is used to monitor surface displacements of potential unstable slopes by identifying movement between fixed points and rover points. The fixed point (FP) is placed outside the assumed instability, while several rover points are placed at locations which are expected to move. NGU cooperates with the University of Oslo (UiO) to perform dGNSS measurements using Topcon two-frequency GNSS receivers (Eiken, 2013). The measuring method is based on static, relative phase measurements which calculates the position of rover points using a network of vectors. By measuring the same points over time, displacement can be identified and quantified.

Five rover points (BAN 1 – BAN 5) have been measured yearly at Kassen from 2012 to 2016. In 2016, two additional rover points were installed (BAN 6 and BAN 7), displacement results from these points are therefore not available.

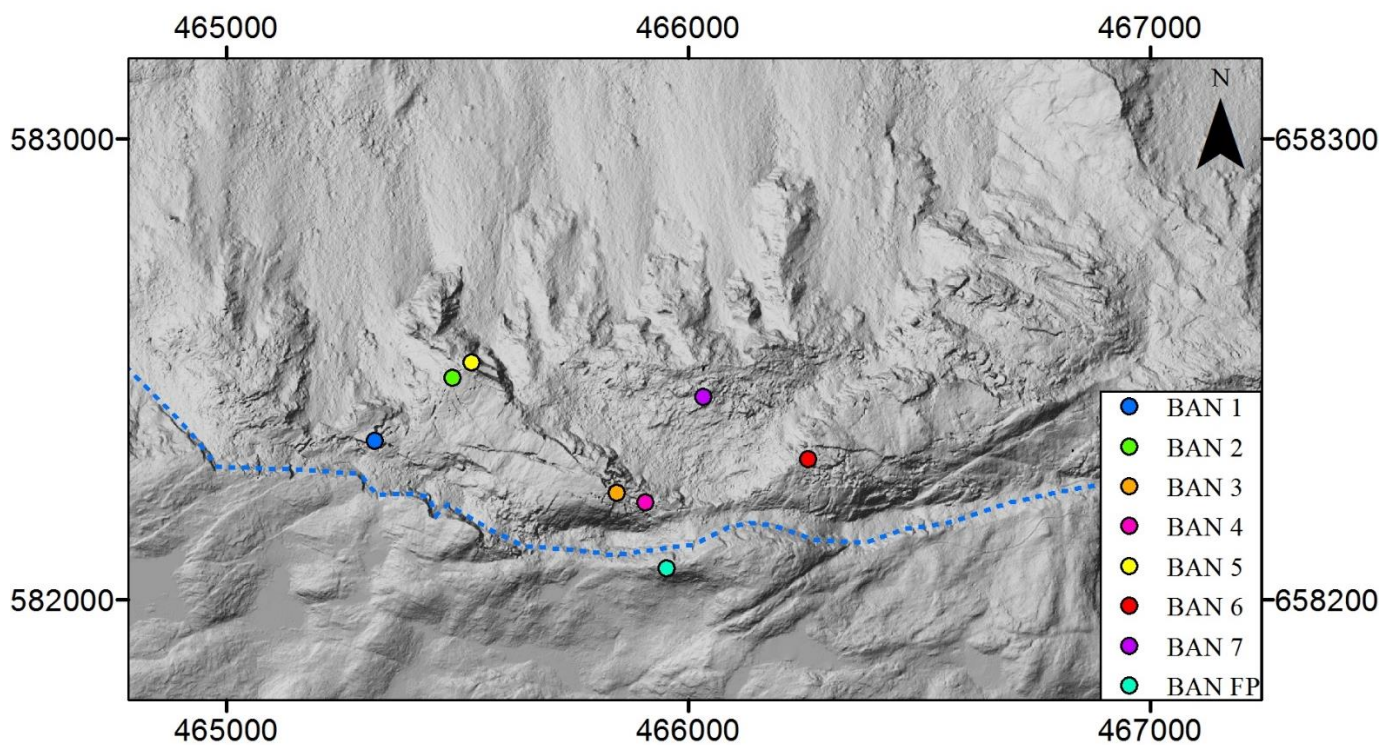


Figure 17: Locations of the dGNSS rover points (BAN 1 – BAN 7). The fixed point (BAN FP) is located outside the unstable area.

4.3 Preliminary consequence assessment

The workflow for the consequence assessment developed by NGU consists of four steps; volume estimation, run-out analysis, displacement wave analysis and consequences, where the last step focuses on loss of life only (Hermanns, Oppikofer, et al., 2012).

Only the two first steps and partly the third step are performed in this master thesis due to temporal restrictions (Figure 18). The third step, displacement wave run-up heights will only provide a first, rough estimated of possible consequences triggered by rock slope failures at Kassen. A final quantification of risk will not be determined, due to the limited consequence assessment. However, some indications of future risk will be discussed based on the results from the preliminary consequence assessment.

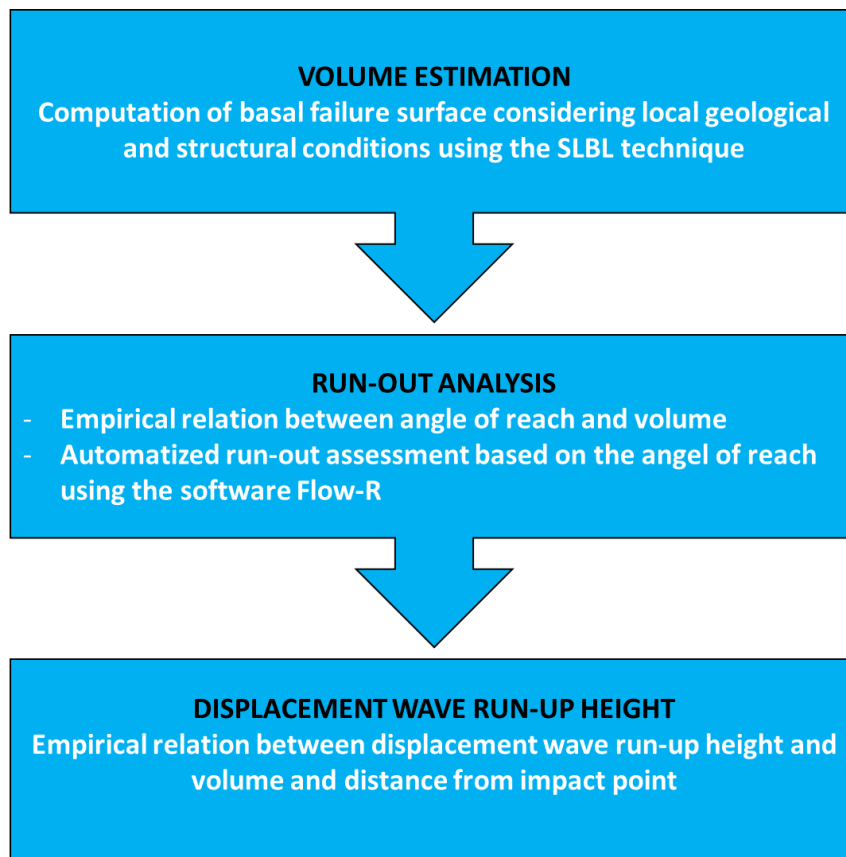


Figure 18: Workflow for the consequence assessment applied to the Kassen instability. Modified from T. Oppikofer et al. (2016).

To implement the volume estimation and the run-out analysis, an ArcGIS Toolbox developed by NGU was used to prepare all input files suitable for the different methods discussed in the next sections.

Volume estimation using the Sloping Local Base Level (SLBL) technique

The idea of geomorphological “base levels” was first introduced by Strahler and Strahler (2000) as the lowest level that can be eroded by stream. At regional and local scale this means respectively the sea or lake level. This definition is not very applicable in the landslide context

where the base level is sloping (not horizontal), and the time scale for the erosional processes is shorter (Jaboyedoff, Baillifard, Couture, Locat, & Locat, 2004). The SLBL is a generalization of the concept of “base levels”, and allows the calculation of the potential geometry of failure surfaces for landslides (Travelletti, Demand, Jaboyedoff, & Marillier, 2010). The basic idea is to find the volumes that are liable to slide by gravitational movement for a given relief at a given time (Jaboyedoff et al., 2004).

Calculations of the SLBL surfaces are performed in this master thesis following the guidelines in NGUs workflow for the consequence assessment for unstable rock slopes (T. Oppikofer et al., 2016) The first step in this calculation is to find the appropriate curvature parameters for the SLBL surface for each scenario by using an excel-spreadsheet developed by NGU. Long unstable areas with a relatively short height difference will for instance have a lower curvature parameter than unstable areas with shorter length and greater height difference. Three possible curvatures were calculated as shown in Table 5. The height difference was found directly by the ArcGis ToolBox, based on polygons delimitating the scenarios and the DEM of the whole area. The length of each scenario was measured directly in the GIS software ArcGIS 10.4.

Table 5: Curvature parameters for estimating the SLBL surfaces (T. Oppikofer et al., 2016)

Curvature parameter	Description	Input files
C_{min}	Creates the shallowest sliding surface from the back scarp to the toe-line of the instability. C _{min} is always zero as this is a plane surface.	Height difference of the scenario Length of the scenario Resolution of the DEM
C_{max}	Creates the deepest sliding surface. An ellipse that is vertically aligned with the back scarp and horizontally aligned with the toe-line defines C _{max} . Dependent on the height and length of the unstable area.	Height difference of the scenario Length of the scenario Resolution of the DEM
C_{inter}	Creates the most realistic sliding surface since it accounts for local geological structures. C _{inter} is found by adjusting an ellipse to the angle of the back scarp and the basal angel at the toe. The resulting geometry of the sliding surface fits the scar curvature defined by the user.	Height difference of the scenario Length of the scenario Resolution of the DEM Angle at backscarp Basal angle at the toe

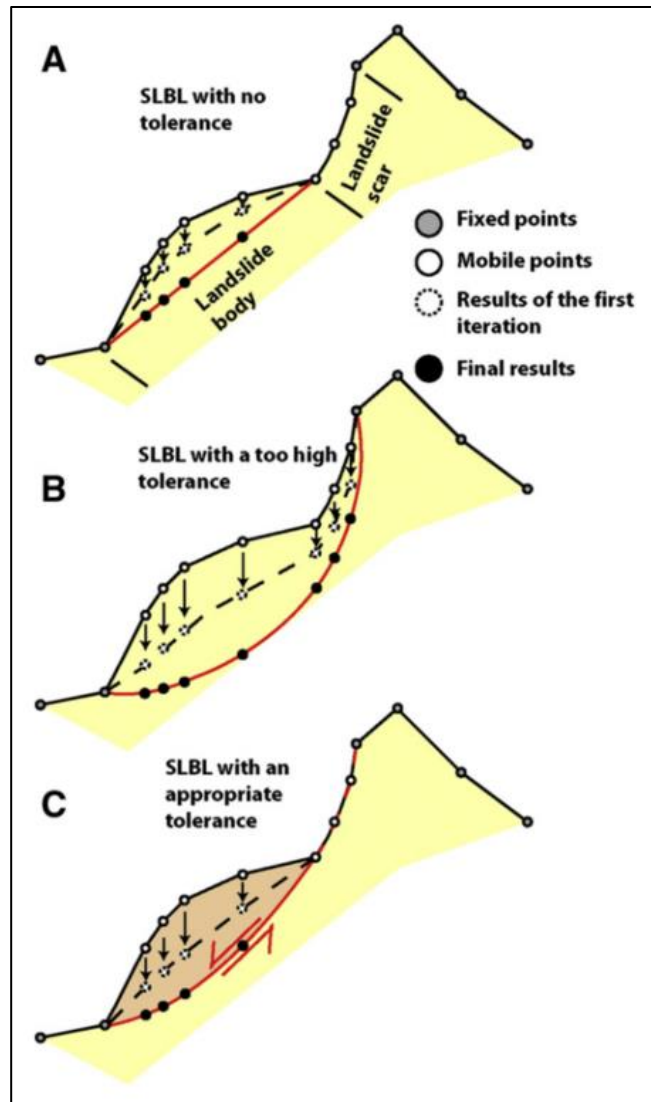


Figure 19: Example of an unstable slope with three sliding structures of different depth. A, B and C corresponds to C_{min} , C_{max} and C_{inter} . Modified from (Travelletti et al., 2010).

The actual construction of the SLBL surface was done using the software CONEFALL developed by Jaboyedoff and Labiouse (2011) which is based on a simple Coulomb frictional model. The input parameters for each scenario in this software is the DEM, a raster file delimitating the failure scenario, length and height of the scenario and the curvature parameters. The output raster file contains residuals which represents the height difference between the SLBL surface and the current topography. The ArcGIS tool “Stack Profile” was used in order to check if the constructed residuals matched the topography. For some scenarios, the curvature parameter had to be changed manually to achieve the best fit with the terrain. The volume was finally calculated by multiplying the area of the instability with the average residuals from the SLBL calculation.

Run-out modeling

As a first step in the run-out modelling, the run-out length (L) is calculated based on the empirical relationship between the volume of the sliding mass (V) and the potential drop height (H) suggested by Scheidegger (1973);

$$\tan \alpha = \frac{H}{L} = 10^{0.62419} \times V^{-0.15666} \quad (1)$$

Equation 1 gives the run-out length, and is measured manually downslope in ArcGIS 10.4 for the given scenario to check whether there are any possibility for loss of life or infrastructure. This is however a conservative approach in the Norwegian context where more than 90 % of Norwegian events have shorter run-out length than given by equation 1 (T Oppikofer et al., 2016).

The angle α in Equation 1 is referred to as “the angle of reach”, and usually decreases with increasing volume for rock avalanches (Corominas, 1996; Scheidegger, 1973). For volumes less than 0.25 Mm³ the angle of reach is fixed to 31° as proposed by Corominas (1996), and also applied in this master thesis.

The software Flow-R (Flow path assessment of gravitational hazards at Regional scale) was applied as a second and more detailed step in the run-out assessment. Flow-R is an empirical model for regional susceptibility assessments of debris flows developed by Horton, Jaboyedoff, Rudaz, and Zimmermann (2013). The software has also been found relevant for other natural hazards such as rock fall or snow avalanches, and has been adapted by T Oppikofer et al. (2016) for rock avalanches. The propagation extent in the model is based on various spreading algorithms and simple frictional laws. The spreading algorithms defines the path and spreading, while frictional laws control the run-out length (Horton et al., 2013).

The software is easy to apply due to few input data. In order to assess the run-out of potential failure scenarios at Kassen, the following input data was required;

- DEM (5x5m resolution)
- Angle of reach (α) (dependent on volume for each failure scenario)
- Source area delineation

The resulting file is a ASCII raster file, readable in ArcGIS 10.4, which shows the computed run-out area with susceptibility limits for different paths. The last step in the run-out modeling is to check if the computed run-out area is reasonable in relation to the terrain beneath the scenario. If needed, the run-out area is manually modified based on expert-judgement.

Empirical run-up heights

T. Oppikofer et al. (2016) present an empirical relation between run-up height, volume, and distance from the impact area of the event based on collected data from displacement waves caused by landslides (Equation 2). This relation is only applied as a first approach for the run-up-height in NGUs system, but works as a first, quick tool to assess consequences from rock-slope triggered displacement waves before applying other methods such as numerical

simulations. The developed empirical relation show expected behaviour of displacement waves, i.e. an increase in run-up height with increasing volume and a decrease in run-up height for increasing distance away from the event.

$$R = 18.093 * V^{0.57110} * x^{-0.74189} \quad (2)$$

Where: R = run-up height in *meters*
 V = Volume of landslide in Mm^3
 x = distance from the impact area in the fjord, lake or river in *km*

Figure 20 shows Kassen and the surrounding infrastructure and buildings. Buildings in the nearest vicinity are cabins, while residences are found in Lårdal and Roeid located respectively 12.5 and 2.5 km away from the toe of Kassen. Dalen is located 23 km away from the shoreline, and is a smaller community with 265 residents (Statistics Norway, 2016). There are no roads or other infrastructure at the slope toe or at the opposite shoreline, and the community Tveitgrendi is located approximately 400 masl; a safe elevation from potential displacement waves. Bandak Lake is a part of the “Telemark canal” connecting the interior of Telemark to the coast, and consist of several locks. The nearest lock from the study site is located at Hogga, approximately 45 km SW from Kassen.

Equation 2 will be applied as a rough estimate of run-up heights caused by displacement waves from slope failures at Kassen at Dalen, Lårdal, Roeid and Hogga.

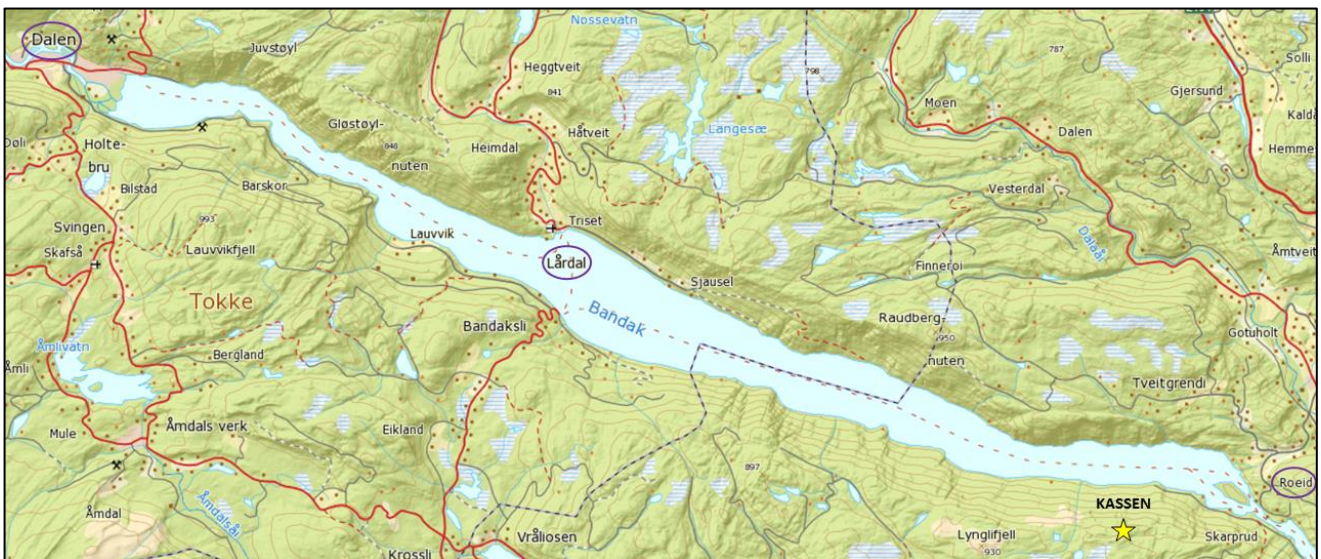


Figure 20: Overview of Kassen, and the populated areas around Bandak lake. The distance to respectively Dalen, Lårdal and Roeid is 23, 12.5 and 2.5 km.

4.4 Results

4.4.1 Hazard assessment

Structural data, geomorphological observations, map studies, kinematic feasibility tests and dGNSS measurements have served as a basis for the results of this hazard assessment. The assessment have been performed for scenarios A-F by following the hazard classification described in Hermanns, Oppikofer, et al. (2012). The full resulting hazard assessments for each scenario is given in Appendix 8.1.

Scenario A, B, F and G resulted in the medium hazard class, while the remaining scenarios got a low hazard class as shown in Table 6.

Table 6: Main results from the hazard assessment for scenarios A-F. Hazard classes are chosen after the one with the highest probability.

Scenario	Max hazard score	Mean hazard score	Min hazard score	Hazard class
A	6.0	4.9	3.8	Medium
B	7.5	7.0	6.5	Medium
C	4.5	3.7	2.0	Low
D	5.3	4.0	2.0	Low
E	8.0	4.7	2.0	Low
F	9.8	5.9	2.5	Medium
G	10.0	6.5	4.3	Medium

Results for determination of criterion 4: Kinematic feasibility test

Applied scores in criterion 4 is based on the results of the kinematic feasibility tests for the different structural domains. Figure 21 show the test results for the LW domain where scenario A, B, C, D and G is located. Scenario E and F are partly located in the East and partly in the LW domain. In the East domain, the kinematic feasibility test results show that planar sliding and toppling is possible. Consequently, failure is kinematically possible for all scenarios and score 0.75 in the hazard assessment. This score is increased for scenario A, B and F as the potential sliding structures are highly persistent relative to the scenario size. See Appendix 8.1 for details.

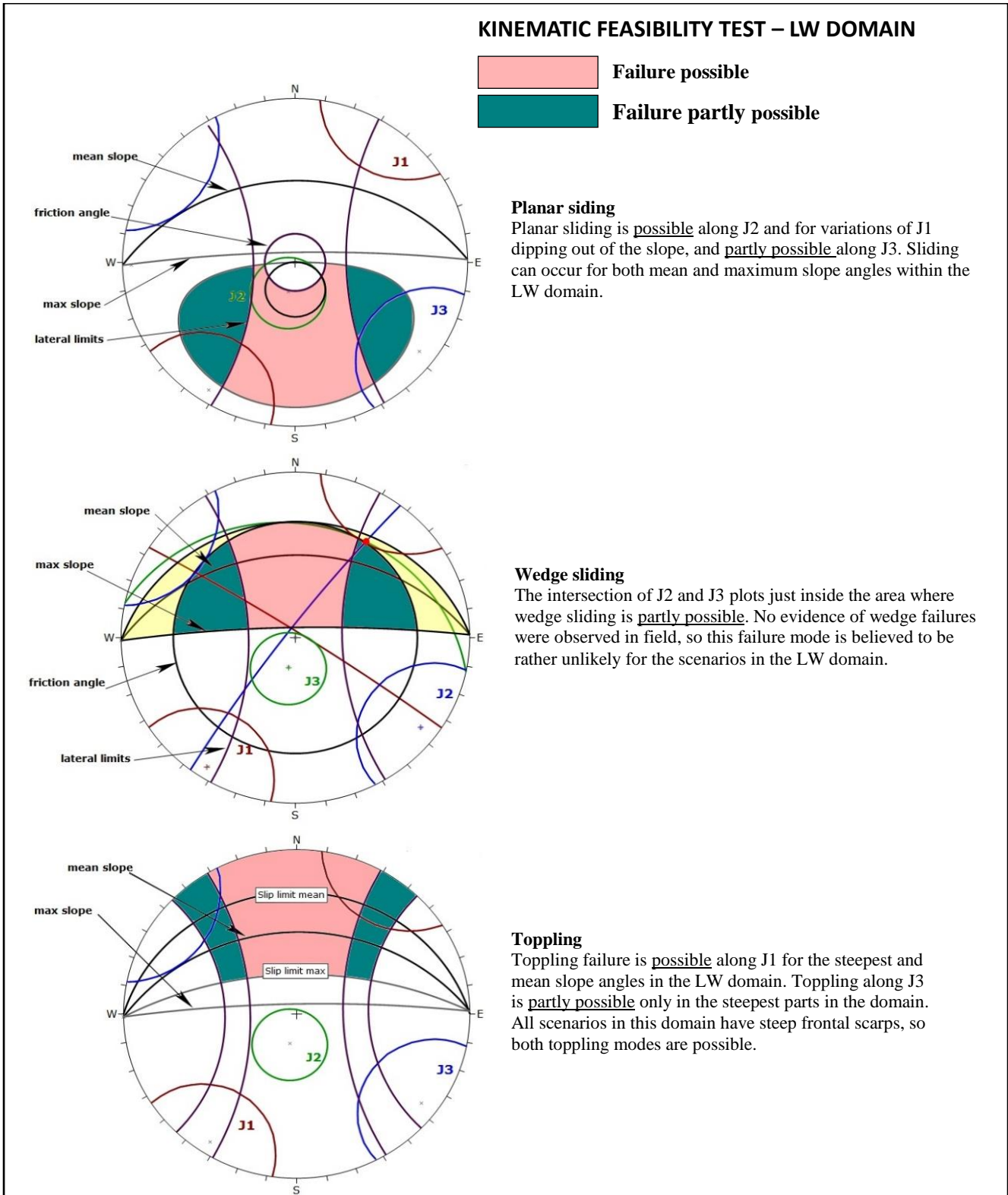


Figure 21: Kinematic feasibility test for the LW domain. Planar sliding and toppling is possible.

Results for determination of criterion 6: Displacement rates

Criterion 6 requires information regarding measured displacement rates. None of the displacement rates are statistically significant, as they are lower than three times the standard deviation as recommended by Eiken (2013). From 2014 to 2015, a significant southeastern movement were observed at BAN 1 – BAN 5, but this trend did not continue in 2016. The metrological conditions on the measuring day in 2015 were very different from the conditions the other years; snowstorm and very cold weather is unusual for Telemark in June. This might have affected the data since the method does not correct for metrological variations. In total, the displacements do not show a consistent moving trend.

Measured displacements less than 2 mm/year are *not significant* in the hazard assessment as they are below the significance limit of the monitoring system. Acceleration (criterion 7) is only evaluated in the hazard assessment if the average displacement is more than 5mm/year, which is not the case for any of the measured dGNSS points.

Table 7 shows the calculated average displacements and errors for the rover dGNSS points BAN 1 – BAN 5. See Appendix 8.2 for details. Table 8 relates the average displacement to the different scenarios and the resulting hazard score for criterion 6.

Table 7: Displacement in mm/y for the rover points installed at Kassen. Average movement and trend/plunge of the 3D vector are calculated by robust linear regression. The uncertainties are given as three standard deviations (3σ).

dGNSS point	Average horizontal movement [mm/y]	3σ	Average vertical movement [mm/y]	3σ	Average 3D movement [mm/y]	3σ	Trend/plunge [°]
BAN 1	0.27	2.18	0.78	6.54	0.83	4.48	93/67
BAN 2	1.02	5.07	0.18	8.52	1.04	5.93	105/50
BAN 3	0.80	0.74	-1.08	5.29	1.34	4.36	87/59
BAN 4	0.59	1.60	-0.20	1.51	0.62	1.64	348/(-2)
BAN 5	1.66	1.50	2.06	6.13	2.65	3.05	302/(-56)

Table 8: Measured displacement rates associated with the different scenarios.

Scenario	Average 3D movement [mm/year]	Rover point	Comments
A	0.83	BAN 1	Not significant
B	2.65	BAN 5	Significant in the hazard assessment, but not statistically significant ($< 3\sigma$). Still, score 1 is given as a conservative approach.
C	1.04 / 1.34	BAN 2 / 3	Not significant
D	1.34 / 0.65	BAN 3 / 4	Not significant
E	No results, installed 2016	BAN 6	To account for uncertainties several outcomes are weighted, with an upper boundary of 4 cm/year.
F	No results, installed 2016	BAN 6	Same situation as for Scenario E.
G	No results, installed 2016	BAN 7	Same situation as for Scenario E.

4.4.2 Volume estimation and run-out analysis

The consequence assessment involves estimation of volumes and run-out for the seven minor scenarios A-G. The assessment is performed by using CONEFALL, FLOW-R and the ArcGIS ToolBox (developed by NGU) and have resulted in the following key data and run-out for each scenario presented in the following pages.

Scenario A

Scenario A is a fully isolated frontal block. Hence, the back scarp and lateral limits are fully developed as seen in the photo in Table 9. The horizontal joint set J2 penetrates the potential sliding block, but dips in slope direction with a low angle of only 6 °. The area beneath the toe-line is dominated by rock fall debris, which was mapped as relatively active compared to other deposits in adjacent slopes – both inside and outside the whole unstable area. The rock fall debris runs out all the way to the shoreline of Bandak Lake.

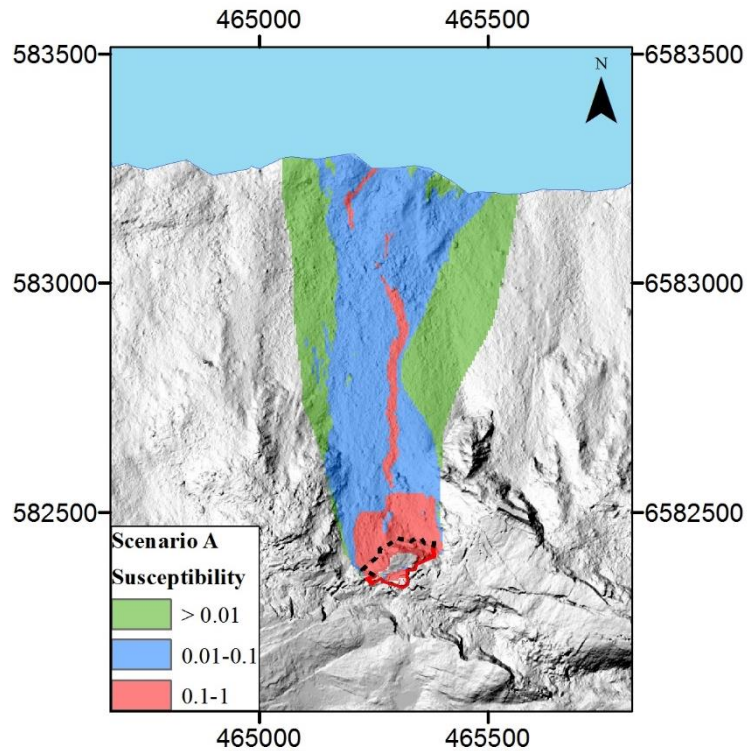


Figure 22: Computed runout area for scenario A (Flow-R). The intermediate Scheidegger length is 1045 m, which indicates runout reaching the lake. This is confirmed in the Flow-R analysis, however the susceptibility is low for such an event.

Table 9: Key data for scenario A. The photo is viewing the back scarp of the potential sliding block.

Scenario A			
Area [m ²]		9525	
Angle at backscarp [°]		85	
Basal angle at toe [°]		17	
H _{max} (m.a.s.l)		699	
H _{min} (m.a.s.l)		589	
Volume Min [Mm ³]	Runout Min [m]	0.16	1045
Volume Mean [Mm ³]	Runout Mean [m]	0.21	1045
Volume Max [Mm ³]	Runout Max [m]	0.24	1045

Scenario B

Scenario B, Skipet, is a pronounced cliff located in the LW domain which rises 140 m from the toe line to the highest point at 677 masl. Skipet was clearly recognized in field, appearing to be potential unstable. The frontal scarp dips 83 °, and is the steepest feature in the LW domain. The back scarp is fully developed, as Skipet is fully isolated with lateral limits being free surfaces. Several structures penetrates the cliff with dip angles above 20° making both planar, biplanar and toppling feasible. Very fresh rock fall activity located beneath the toe of Skipet indicates that this is one of the most active parts of the entire unstable slope. The rock slide event from 1985 supports this indication.

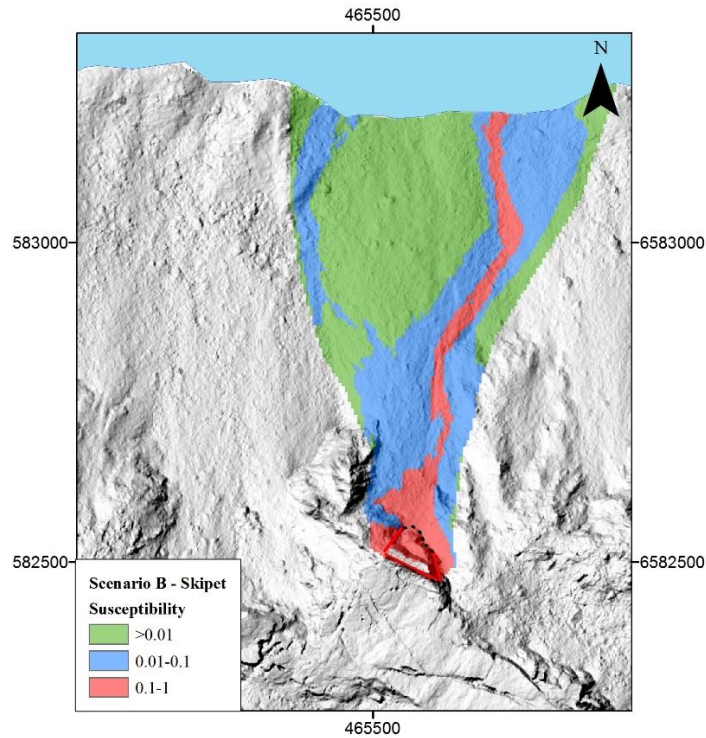


Figure 23: Computed runout area for scenario B (Flow-R). Runout lengths reaching the lake is possible, and corresponds with the rockslide from 1985, reporting small tsunami waves in the lake.

Table 10: Key data for scenario B.

Scenario B			
Area [m ²]	4100		
Angle at backscarp [°]	90		
Basal angle at toe [°]	30		
H _{max} (m.a.s.l)	677		
H _{min} (m.a.s.l)	534		
Volume Min [Mm ³]	Runout Min [m] /	0.07	1045
Volume Mean [Mm ³]	Runout Mean [m]	0.11	1045
Volume Max [Mm ³]	Runout Max [m]	0.15	1045
<p>Left photo: Skipet is clearly visible as a prominent cliff. The light coloured vegetation indicates that the area is relatively active concerning rock fall activity.</p>			



Scenario C

Scenario C includes Skipet as the foremost part of the potential sliding block, located in the LW domain. The scenario was identified due to a prominent crack, dipping vertically and striking W-NW. The depth of this crack is estimated from field observations to be at least 10 meters long with a width varying from 7-10 m. This crack is the back scarp of the instability which is fully developed. The lateral limits are partly developed, following cracks with openings of less than 50 cm. The sliding direction of the instability can either be NE, towards the interior of Amfiteateret, or North directly towards Bandak lake. There are no observed structures penetrating through the whole potential instability.

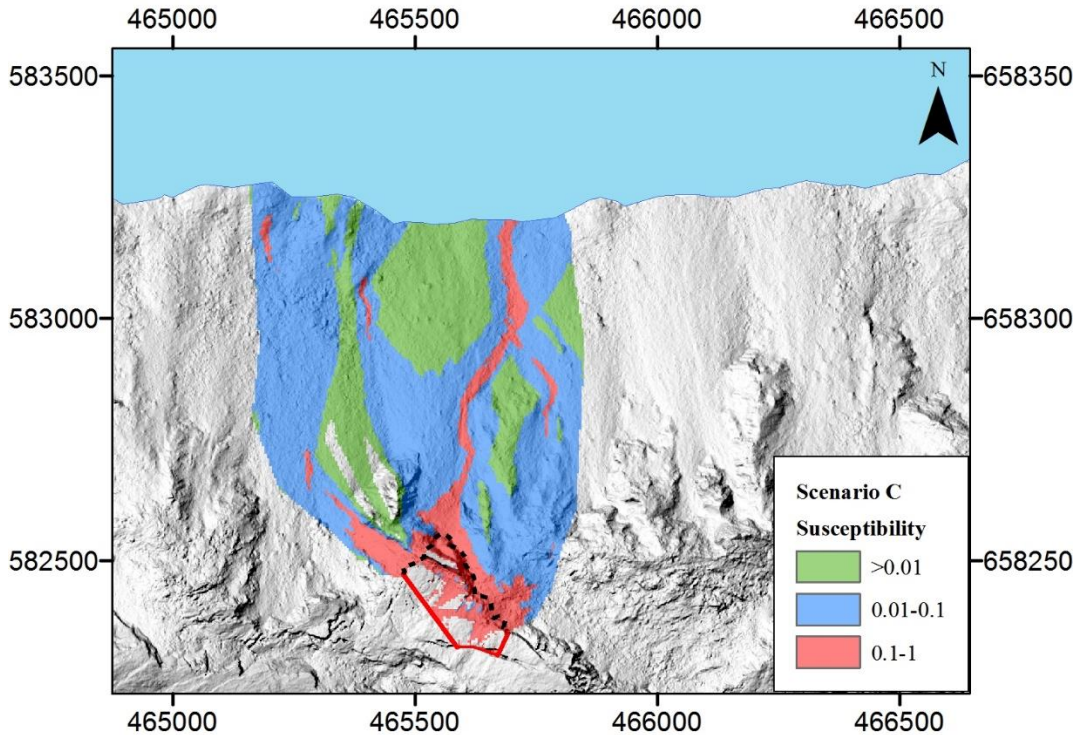


Figure 24: Computed runout area for scenario C (Flow-R). Runout reaching the lake is possible since Skipet is included in this scenario.

Table 11: Key data for Scenario C.

Scenario C			
Area [m ²]		26150	
Angle at backscarp [°]		86	
Basal angle at toe [°]		21	
H _{max} (m.a.s.l)		736	
H _{min} (m.a.s.l)		531	
Volume Min [Mm ³]	Runout Min [m] /	0.67	1290
Volume Mean [Mm ³]	Runout Mean [m]	0.87	1344
Volume Max [Mm ³]	Runout Max [m]	1.06	1386

Scenario D

Scenario D is located in the LW domain, delimited by a free face at the north western lateral limit, a back scarp showing varying degree of displacement and a partly developed south eastern lateral limit. The back scarp is fully developed towards NW, but shows more juvenile displacement towards the east end. J2 dips is measured in the area with dip angles from 14 - 23° out of the slope. The persistence of potential sliding surfaces is however uncertain. The area beneath the toe line is composed of bigger blocks and highly deformed rock mass, relatively fresh rock fall activity is not observed.

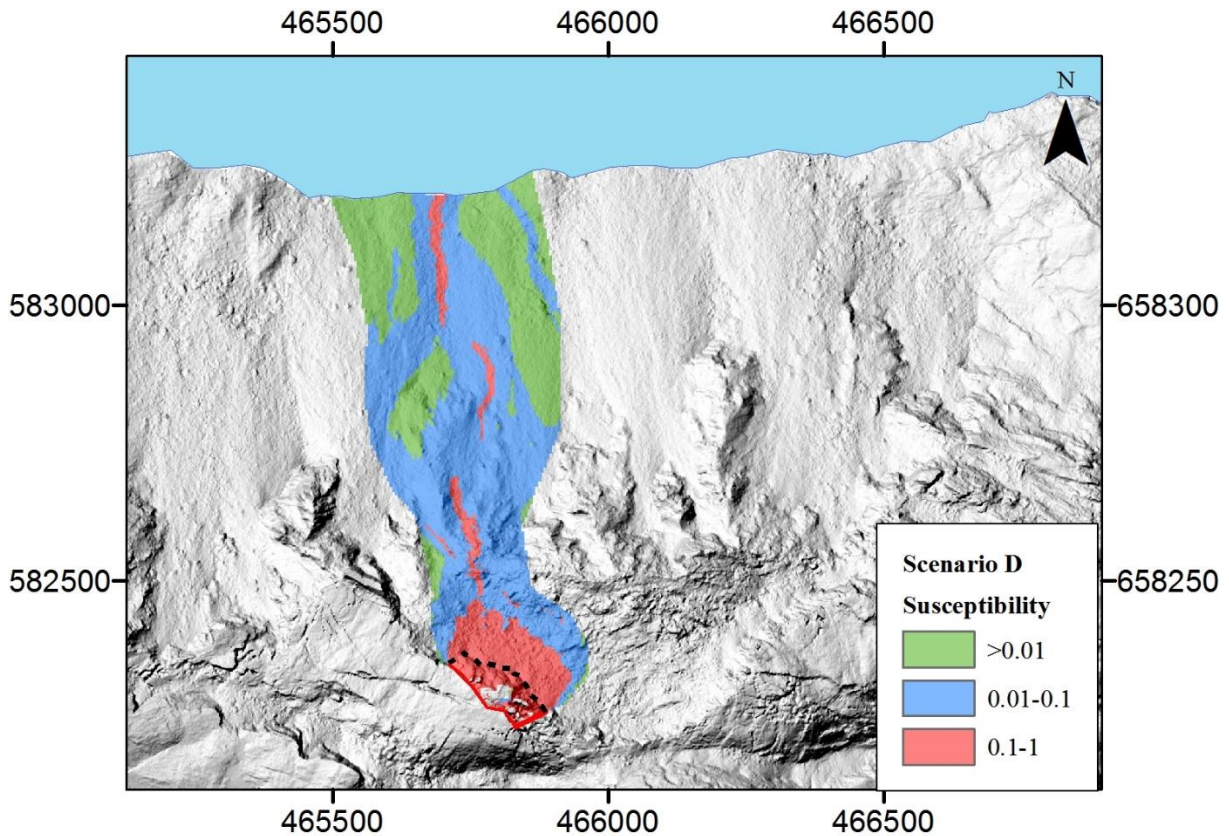


Figure 25: Computed runout for scenario D. The susceptibility for runout reaching the lake is low.

Table 12: Key data for scenario D.

Scenario D			
Area [m ²]		9975	
Angle at backscarp [°]		81	
Basal angle at toe [°]		21	
H _{max} (m.a.s.l)		787	
H _{min} (m.a.s.l)		680	
Volume Min [Mm ³]	Runout Min [m] /	0.12	1192
Volume Mean [Mm ³]	Runout Mean [m]	0.26	1199
Volume Max [Mm ³]	Runout Max [m]	0.33	1242

Scenario E

Scenario E is the second largest scenario, located partly in the East, partly in the LW Domain. The height from the toe-line to the highest point (763 masl) is 134 m. The back scarp consists of disconnected cracks, which makes it partly developed. The western lateral limit is a major continuous crack, with opening up to 10 meters and depth of 5-10 meters (field estimations). Hence this lateral limit is fully developed. The eastern lateral limit is composed of disconnected cracks, and therefore partly developed. No structures are penetrative relative to the size of the potential sliding body.

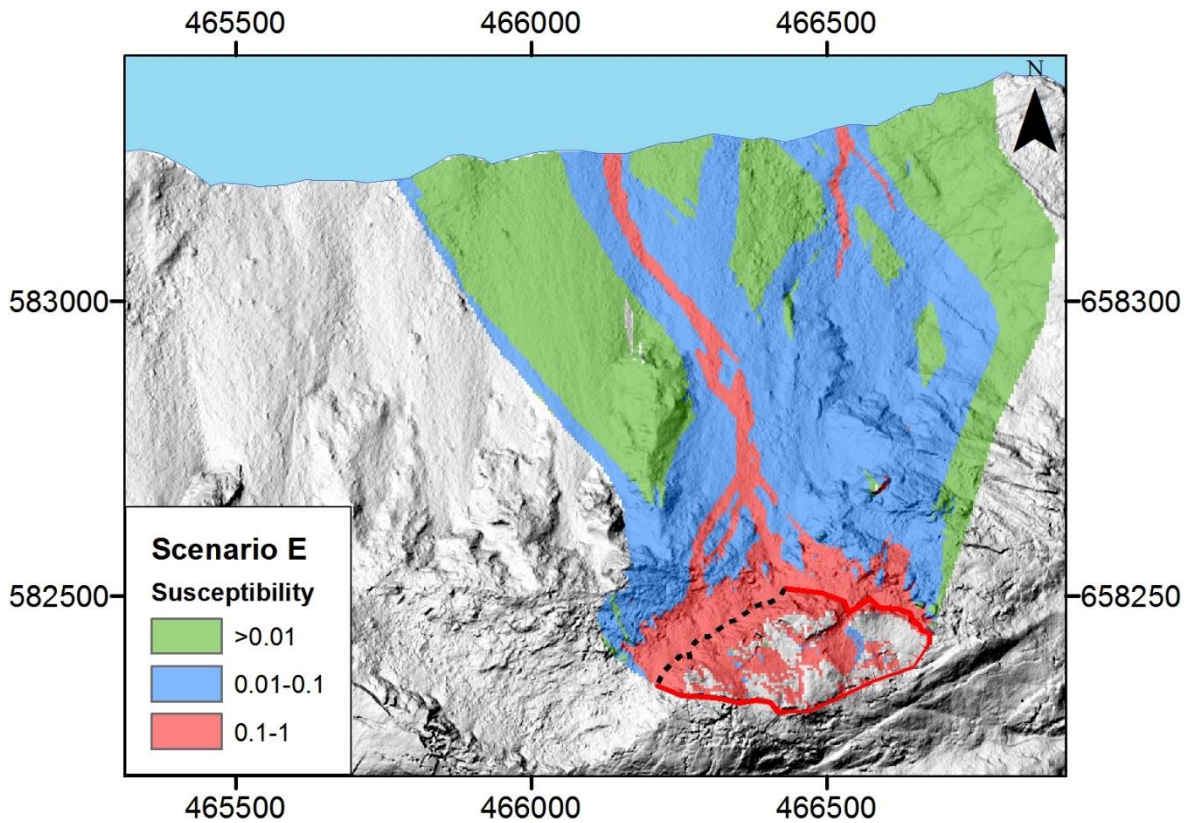


Figure 26: Computed runout area of scenario E. Parts of the sliding material have high susceptibility for reaching the lake, confirmed by an intermediate Scheidegger length of 1546 m. However there are terrain constraints downslopes, which can limit the travel length of the entire sliding body.

Table 13: Key properties for scenario E.

Scenario E			
Area [m ²]		59975	
Angle at backscarp [°]		85	
Basal angle at toe [°]		32	
H _{max} (m.a.s.l)		763	
H _{min} (m.a.s.l)		629	
Volume Min [Mm ³]	Runout Min [m] /	1.23	1477
Volume Mean [Mm ³]	Runout Mean [m]	1.65	1546
Volume Max [Mm ³]	Runout Max [m]	2.12	1609

Scenario F

Scenario F is the second smallest scenario, located in the interior of scenario E, partly in East and partly in the LW domain. The back scarp is fully developed over the entire width of the block. The eastern lateral limit is a crack with dip direction/dip of 200/85, continuous length of 15 meters, depth of 5-7 meters and an opening around one meter. These measurements are done in field and the crack is shown in Table 14. The crack transitions into a free surface, which defines the eastern lateral limit as fully developed. The western lateral limit is partly developed, due to discontinuous cracks. J2 dips from 15 – 35°, penetrating the sliding body. Some rock fall deposits are located beneath the toe of the instability, but these are not relatively fresh compared to more active adjacent sites. Computed runout and key properties are shown in Figure 27 and Table 14.

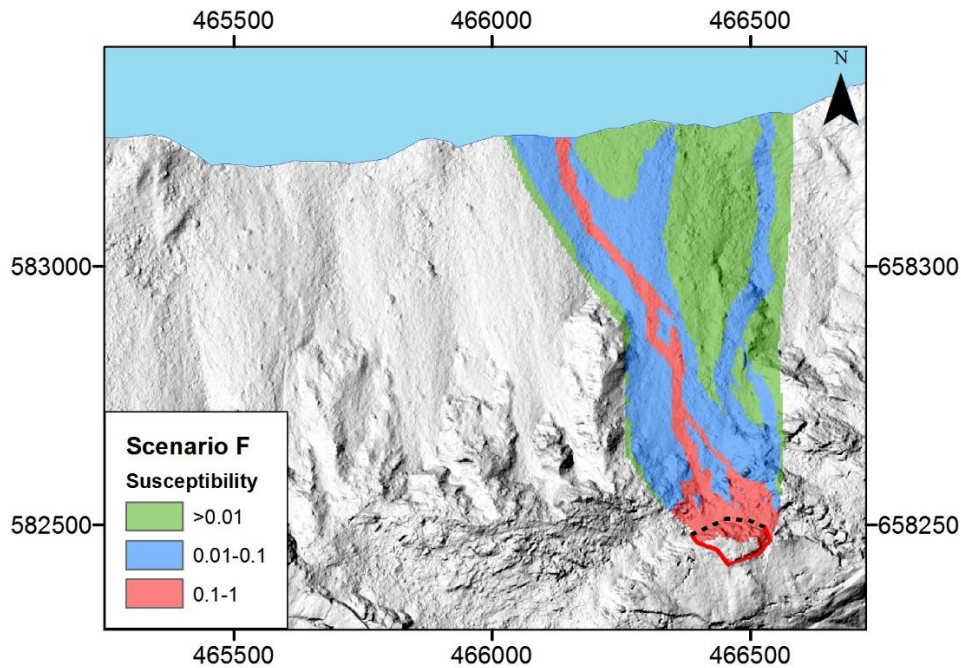


Figure 27: Computed runout area for scenario F. Only parts of the assumed sliding material have a high susceptibility to reach the lake due to terrain constraints and flat terrain at the toe.

Table 14: Key data for scenario F. The photo shows the crack which defines the eastern lateral limit.

Scenario F			
Area [m ²]		7975	
Angle at backscarp [°]		78	
Basal angle at toe [°]		36	
H _{max} (m.a.s.l.)		726	
H _{min} (m.a.s.l.)		628	
Volume Min [Mm ³]	Runout Min [m]	0.12	1090
Volume Mean [Mm ³]	Runout Mean [m]	0.17	1090
Volume Max [Mm ³]	Runout Max [m]	0.21	1090

Scenario G

Scenario G is located at the lowest altitude of all scenarios (663 masl) in the LW domain, right above the assumed location of the slide scar of the Bandak rock avalanche. The back scarp was hard to examine in field due to very blocky terrain in the area, with blocks up to approximately 200 m³. Due to the character of the rock mass, there is no continuous bedrock left and the back scarp and lateral release surfaces are believed to be fully developed. The structure J2 is dipping steeply with 50°, but the persistence of this structure in the area is unknown. Downslopes of the instability there are three transverse rock ridges with lengths of about 200 meters. The area beneath and between these ridges is covered by rock fall debris, where relatively fresh rock falls have been observed. Computed runout and key parameters are shown in Figure 28 and Table 15.

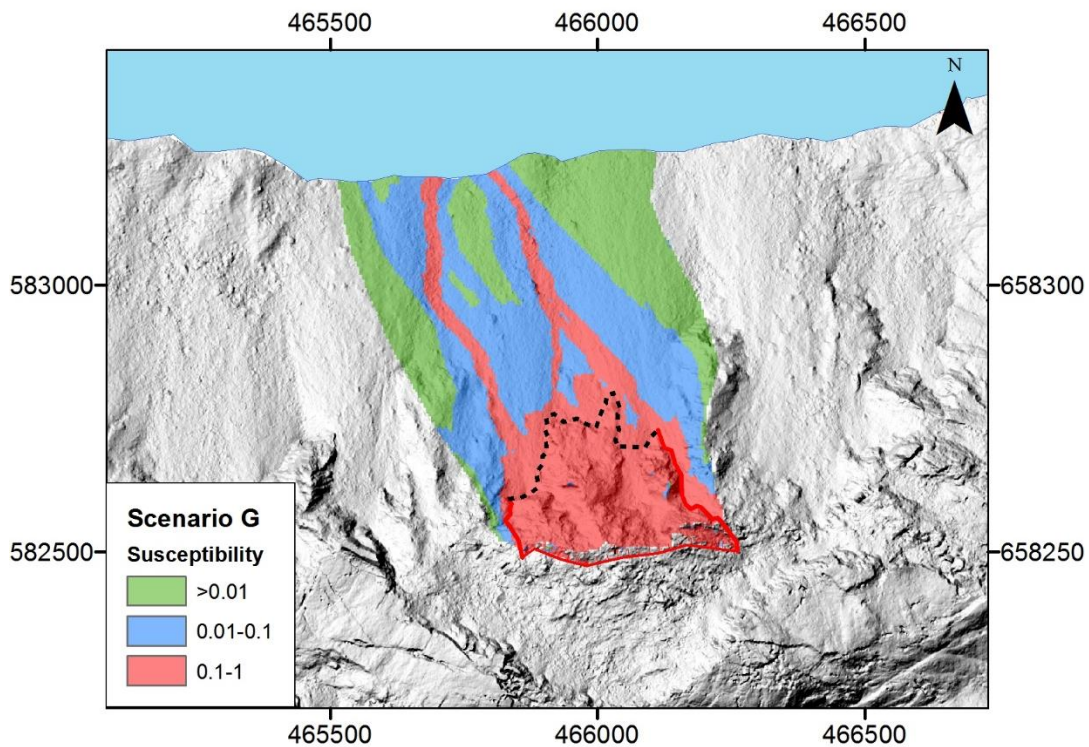


Figure 28: Computed runout area of scenario G (Flow-R). If failure occurs, the sliding mass is expected to reach the lake, with a Scheidegger length of 1396 m. This seems reasonable considering the Bandak rock avalanche run out to the opposite side of the lake

Table 15: Key parameters for scenario G.

Scenario G			
Area [m ²]		74300	
Angle at backscarp [°]		84	
Basal angle at toe [°]		50	
H _{max} (m.a.s.l)		673	
H _{min} (m.a.s.l)		378	
Volume Min [Mm ³]	Runout Min [m] /	1.07	1256
Volume Mean [Mm ³]	Runout Mean [m]	2.09	1396
Volume Max [Mm ³]	Runout Max [m]	3.35	1503

4.4.3 Empirical run-up heights

In order to get a first, rough indication of possible run-up heights, equation 2 was applied for the estimated volumes of the four medium hazard class scenarios A, B, F and G. The resulting run-up heights in Roeid, Lårdal, Dalen and the canal lock at Hogga are presented in Table 16

Table 16: Calculated run-up heights for scenario A, B and G at the three locations Roeid, Lårdal and Dalen based on the empirical relationship presented by (T. Oppikofer et al., 2016).

Scenario	Estimated mean volume [Mm ³]	R [m]			
		Roeid x = 2.5 km	Lårdal x = 12.5 km	Dalen x = 23 km	Hogga Lock x = 45
A	0.11	2.6	0.8	0.5	0.3
B	0.21	3.8	1.1	0.7	0.4
F	0.17	3.3	1.0	0.6	0.4
G	2.09	14.0	4.2	2.7	1.6

5 Stability analyses performed at Amfiteateret and Skipet

This chapter will describe theory, methodology and results from the numerical modeling of the Bandak rock avalanche at Amfiteateret and the stability assessment using the Limit Equilibrium Method of two unstable blocks at Skipet.

5.1 Stability analyses of rock slopes

The aim of a rock slope stability analysis is to achieve safe and functional design of excavated slopes and/or assess the equilibrium conditions of natural slopes. Eberhardt (2003) suggests the following primary objectives for rock slope stability in the landslide context:

- To determine the rock slope stability conditions
- To investigate potential failure modes
- To determine the slopes sensitivity/susceptibility to different triggering mechanisms

All stability analysis shall start with a site investigation study including geological and discontinuity mapping to provide the necessary input data for the analysis. Rock mass characterization and collecting rock samples for laboratory testing is also preferred for obtaining valuable input data.

Today, several methods are available for slope stability analysis. Following the advances in computing power, advanced software for numerical modelling is accessible for everyone owning a computer. However, it is crucial for the user to fully understand the varying strengths and limitations for each methodology. Depending on the site conditions and potential failure mode, different analyse techniques are appropriate for different sites (Eberhardt, 2003). Stead et al. (2006) suggests that rock slope analyses shall be undertaken using three levels of sophistication which apply to different failure modes (Figure 29).

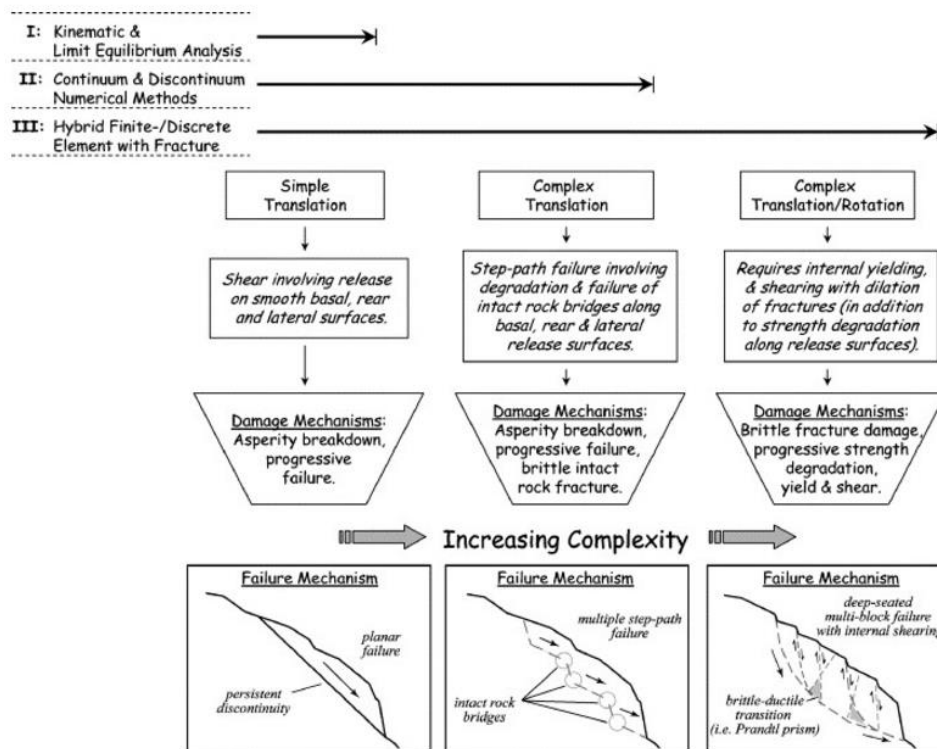


Figure 29: Increasing level of complexity of the failure mode requires different levels of landslide analysis. After Stead et al. (2006)

Limit Equilibrium Method (LEM)

The Limit Equilibrium Method (LEM) investigates the stability based on static forces and moment equilibrium for both translational and rotational failures. The method is the backbone for stability analysis of rock slopes, and has been in widespread use since the early 20th century (Ureel & Momayez, 2014). LEM are highly relevant to simple block failures along known discontinuities or to highly fractured or strongly weathered rock mass which than acts as soil. LEM compares the driving forces/moments against the resisting forces/moments, which act on a predefined sliding plane in order to compute a Factor of Safety (FS). The LEM method is applied for the stability analysis of the two observed blocks at the northeastern side of Skipet, as the potential sliding structures are known, and the failure mode is assumed to be either toppling or planar sliding. Further details about the applied method and results from the stability assessment is presented in respectively chapter 5.6 and 5.8.

Numerical analysis

Rock slope stability problems often involves complexity related to geometry, material anisotropy, non-linear behaviour, internal deformation, structural fabric, pore pressures, seismic loading and other factors (Eberhardt, 2003). For such instabilities, involving all or some of these factors, simple LEM methods come too short. Numerical modelling techniques are capable of addressing these challenges, by providing approximate solution to problems that are unsolvable by conventional techniques. Numerical models are more general than LEM and can be used to address a wide variety of instability problems. These methods consist of computer

programs that try to simulate the mechanical response of a rock mass subjected to a set of initial conditions like *in situ* stresses, water pressure and boundary conditions. Consequently, they are much slower than LEM.

The basic principle of numerical methods is division of the rock mass into zones, and each zone is assigned a material model and properties. The zones can either be connected together or separated by discontinuities, and the rock mass will then be modelled as a continuum or a discontinuum. It is also possible to use hybrid modelling, which is a combination between continuum and discontinuum modelling in order to maximize the advantages from both methods. Figure 30 provides an overview of the different numerical models.

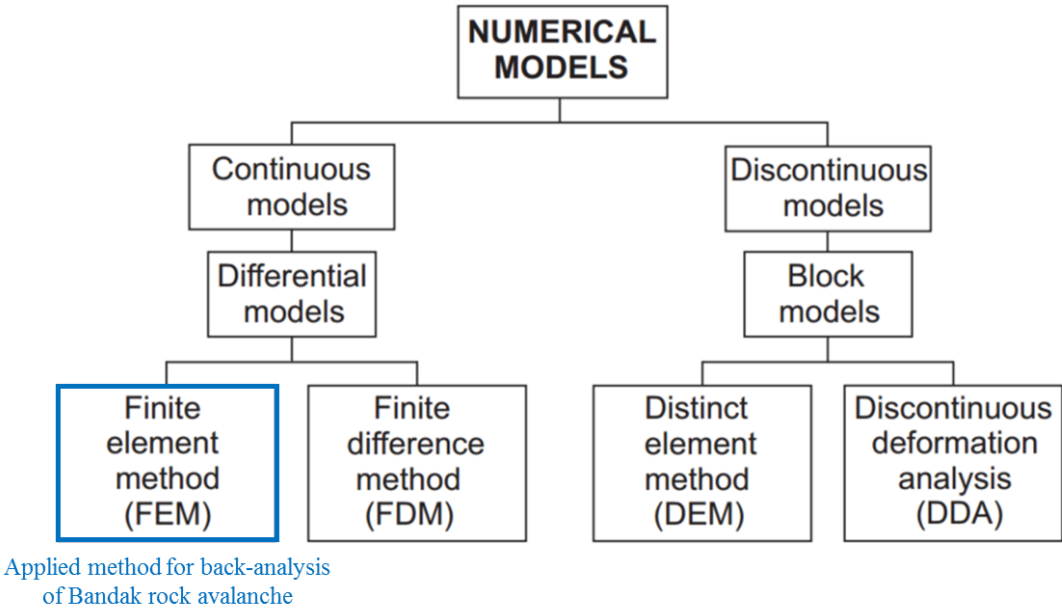


Figure 30: Overview of different numerical models (Grøneng, 2010). The finite element method is suitable for the back-analysis of the Bandak rock avalanche.

Discontinuum modelling

Discontinuum methods (also called discrete-element method) models the rock mass as an assemblage of separate, interacting blocks. The discontinuities are represented explicitly with assigned properties such as orientation and location. The blocks separated by the discontinuities in the model can be either rigid or deformable, depending on the rock mass in question (Wyllie & Mah, 2004). The blocks are subjected to external loads and can experience significant motion with time. The methods also allows for sliding along and opening/closure between the blocks (Eberhardt, 2003). Discontinuum methods are very well suited for rock slopes where multiple joint sets control the mechanism of failure.

Continuum modelling

In continuum modelling the material is assumed continuous throughout the domain and discontinuities are represented implicitly (Wyllie & Mah, 2004). The method calculates approximations to the connectivity of elements, and continuity of displacements and stresses

between elements (Eberhardt, 2006) by using either Finite Element Codes or Finite Difference Codes. The differential equations for these two codes are the same, but the methods used to derive them differ. Continuum methods works best for rock slopes that have a homogenous character; either massive, intact rock, weak rock or highly fractured rock masses. The latter is the case for the rock mass in Amfiteateret where the Bandak rock avalanche occurred.

A numerous of commercial software codes are available for continuum modelling, both in 2D and 3D. As always, analyzing a 3D problem in 2D will lead to some limitations; the 2D codes assume plane strain conditions, which in most cases differ from reality where rock slopes have varying structure, lithology and topography (Eberhardt, 2003).

Finite Element Methods

The finite element method (used in continuum models), divides the problem domain in to an assembly of discrete, interacting elements of various geometrical shapes like triangles (

Figure 31). Displacement components at any point within an element is given by the nodal displacement (u), which ensures continuity of the displacement. From the displacement field, the induced strain can be found by applying established strain-displacement relations. The induced stress in an element is determined by the induced strain and the elastic properties of the material. Transmission of internal forces (q) are represented by interactions of the nodes of the elements. A throughout description of the FEM method including the governing equations for displacement variation, stresses and nodal forces can be found in Brady and Brown (2013).

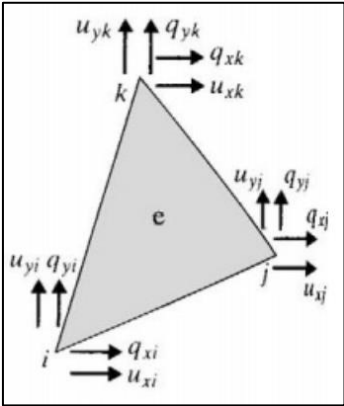


Figure 31: Example of element (e) used in FEM. The nodes are defined by the letters i, j and k. Displacement and forces at the nodes are given by the vectors u and q (Brady & Brown, 2013).

Shear Strength Reduction (SSR)

The SSR technique is commonly used in FEM codes to find the factor of safety (FS) for the slope, which can be done without a pre-defined sliding plane. The idea behind this method is to perform a systematic search for a stress reduction factor (SRF) that brings a slope to the very limit of failure (Hammah, Curran, Yacoub, & Corkum, 2004). The resulting SRF is the ratio of the actual shear strength of the rock to the reduced shear strength (Wyllie & Mah, 2004). This is done by iteratively decreasing the strength properties of the material, expressed by the Mohr-

Coulomb failure criterion, until a Critical Strength Reduction Factor (CSRF) is reached where the model becomes unstable. Mohr-Coulomb is the most widely applied failure criterion in geotechnical engineering. The criterion is a linear relationship (Equation 3) that involves shear stress (τ) and normal stress (σ_n) acting along the failure plane, cohesion of the material (c), and the friction angle (φ) (Johnson & DeGraff, 1988);

$$\tau = c + \sigma_n \tan \varphi \quad (3)$$

The final reduced shear strength (expressed with c and φ) can be determined from the Equation 4 (Hammah et al., 2004);

$$\frac{\tau}{CSRF} = c^* + \tan \varphi^* \quad (4)$$

Where: CSRF = Critical Strength Reduction Factor
 $c^* = c/CSRF$ = factored Mohr-Coulomb cohesion
 $\varphi^* = \varphi/CSRF$ = factored Mohr-Coulomb friction

5.2 Material Models

Type of material model is an essential input parameter in the numerical modeling, and theory behind the different models will therefore be presented in the following.

Material models are stress/strain relations that describe how the material behaves under variable stress conditions. The simplest model is the linear elastic model which only accounts for the elastic properties Young's Modulus and Poisson's ratio for the rock. These properties were determined through laboratory work, which will be described in chapter 5.4. Linear elastic materials obeys Hooke's law, which states that normal stress is proportional extensional or axial strain (Johnson & DeGraff, 1988). If the deforming stress is removed, the material will return to its initial state.

If a material strains after the yield point without rupture or failure, the deformation is not elastic, but plastic. The yield point is defined as the stress level which is greater than that can be tolerated elastically (Johnson & DeGraff, 1988). Plastic deformation results in non-recoverable strain, meaning that the material has obtained a permanent deformation. In other words, the shear strength at failure is independent of shear strain for ideally plastic materials, as shown in Figure 32.

Most earth material exhibit both elastic and plastic behaviour. Linear elastic-perfectly plastic stress-strain relations are most commonly used in numerical modeling of rock masses (Wyllie & Mah, 2004). However, brittle rock masses often fails in a progressive manner, meaning that failure appears to develop over time (Wyllie & Mah, 2004).

The physical processes related to progressive failure of brittle rock specimens can be explained through different phases of typical stress-strain relationship curves. These phases are described by Aubertin, Gill, and Simon (1994). The first phase involves closure of microcracks in the

rock, which is almost non-existing for dense rocks with low porosity. In the second phase the rock behaves linearly elastic which extends up to the point where stable crack propagation replaces microfracturing. Approaching the peak strength, the size and density of stable cracks increase until some unstable crack propagation initiates. Under a certain normal stress, the peak strength value is reached and progressively decreases to the residual strength value as the inelastic shear strain increases. The latter is a result of strain localization in the material due to damage accumulation (Aubertin et al., 1994; Manfredini, Martinetti, & Ribacchi, 1975). This causes a softening of the material, a phenomena that can be handled by defining characteristics of the post-peak or post-failure behaviour through a strain-softening model. For this case, residual strength values for the rock mass and discontinuities are applied.

Progressive failure leads to difficulties in design and evaluation of slope stability in strain softening materials. In limit equilibrium methods, either the peak strength or the residual strength of the material can be selected as input in the method. Depending on the chosen strength, the apparent safety factor could in fact be quite different from the real safety conditions (Manfredini et al., 1975). A solution of the problem requires a complete stress analysis where stress-strain properties of the rock mass and joints are accounted for. This is only possible with numerical methods.

For the numerical modeling at Amfiteateret, all material models shown in Figure 32 have been applied in different steps of the modeling.

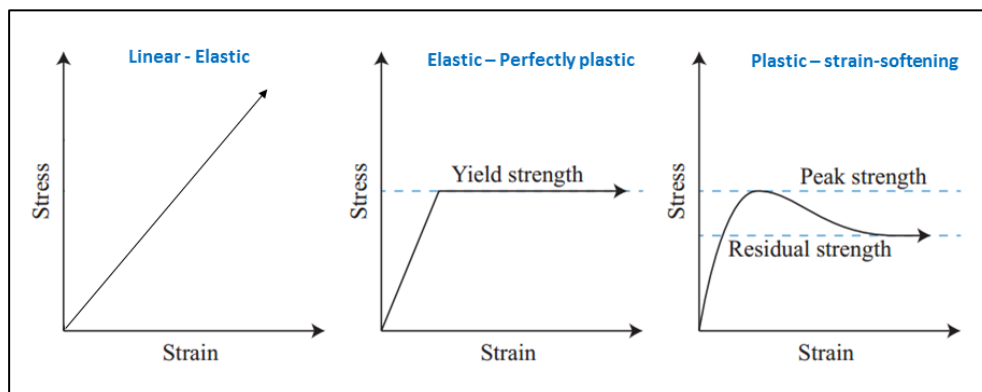


Figure 32: Idealized Stress-strain relationships for rock masses. Brittle rock masses commonly exhibits a plastic – strain softening model, defined by the materials residual strength.

5.3 Classes of rock strength

Reliable input parameters concerning the rock strength properties in both LEM methods and numerical methods are crucial in order to obtain reliable results. This chapter will therefore present the most suitable rock mass and discontinuity shear strength criteria which will be applied in the stability analyses of the Bandak rock avalanche and the two unstable blocks at Skipet.

Sliding surfaces can form either along pre-existing discontinuities or through the rock mass, depending on the scale of the event and the geological conditions on the site. Consequently in slope stability analyses, it is important to apply either the discontinuity strength or the rock mass strength after the assumed failure mode of the slope as shown in Figure 33.

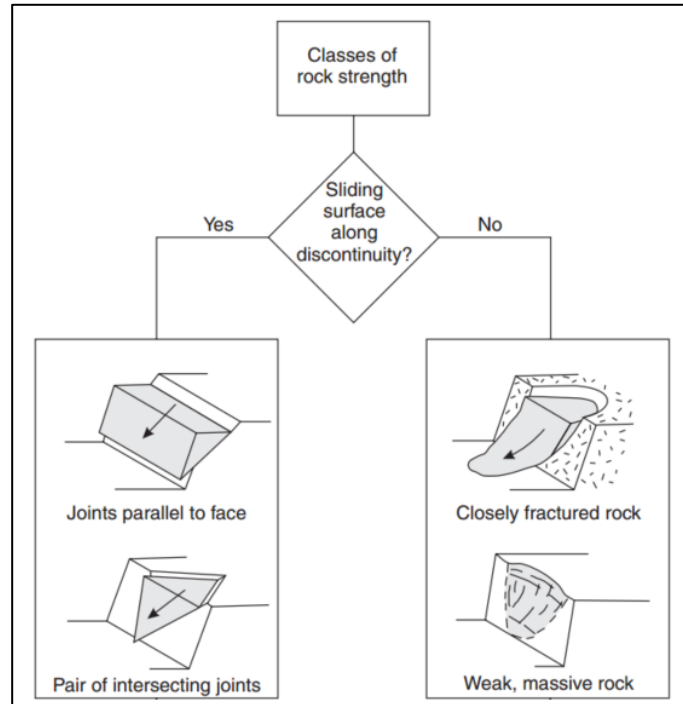


Figure 33: Classes of rock strength can be either discontinuity shear strength or rock mass shear strength depending on the character of the rock mass. Figure modified from Wyllie and Mah (2004).

Rock mass shear strength

Fractured rock masses are composed of intact pieces of hard brittle material separated by joints that may be covered by layers of weaker materials (infilling). The strength of such rock masses is therefore dependent on the strength of the intact pieces and on their freedom to move. The latter is determined by number, orientation, spacing and shear strength of discontinuities (Hoek, 1983).

Hoek (1983) proposed an empirical failure criterion for estimating the strength of jointed rock mass. This relationship have been modified and revised over the years to meet new challenges concerning rock engineering such as engineering weak rocks and adapting to the new classification system “Geological Strength Index (GSI)” (Hoek, 2000). The most recent version, the Generalised Hoek-Brown failure criterion, (Hoek, Carranza-Torres, & Corkum, 2002) is applied in the numerical analysis of the Bandak rock avalanche.

The Generalised Hoek-Brown failure criterion for jointed rock masses is defined by Hoek (2007):

$$\sigma'_1 = \sigma'_3 + \sigma_{ci} \left(m_b \frac{\sigma'_3}{\sigma_{ci}} + s \right)^a \quad (5)$$

Where: σ'_1 and σ'_3 = maximum and minimum effective principle stresses at failure
 σ_{ci} = uniaxial compressive strength of intact rock mass

m_b = value of the Hoek-Brown constant m for the rock mass
 s and a = constants which depend on the rock mass characteristics

Equation (5) should only be applied for rock masses suited for the Generalized Hoek-Brown criterion. The criterion assumes isotropic rock mass behaviour, which is attained for rock masses having a sufficient number of closely spaced discontinuities with similar properties. If the area being analyzed is large, with relatively small block sizes, the criterion is reasonable to apply. Figure 34 shows how Equation 5 is dependent on sample size.

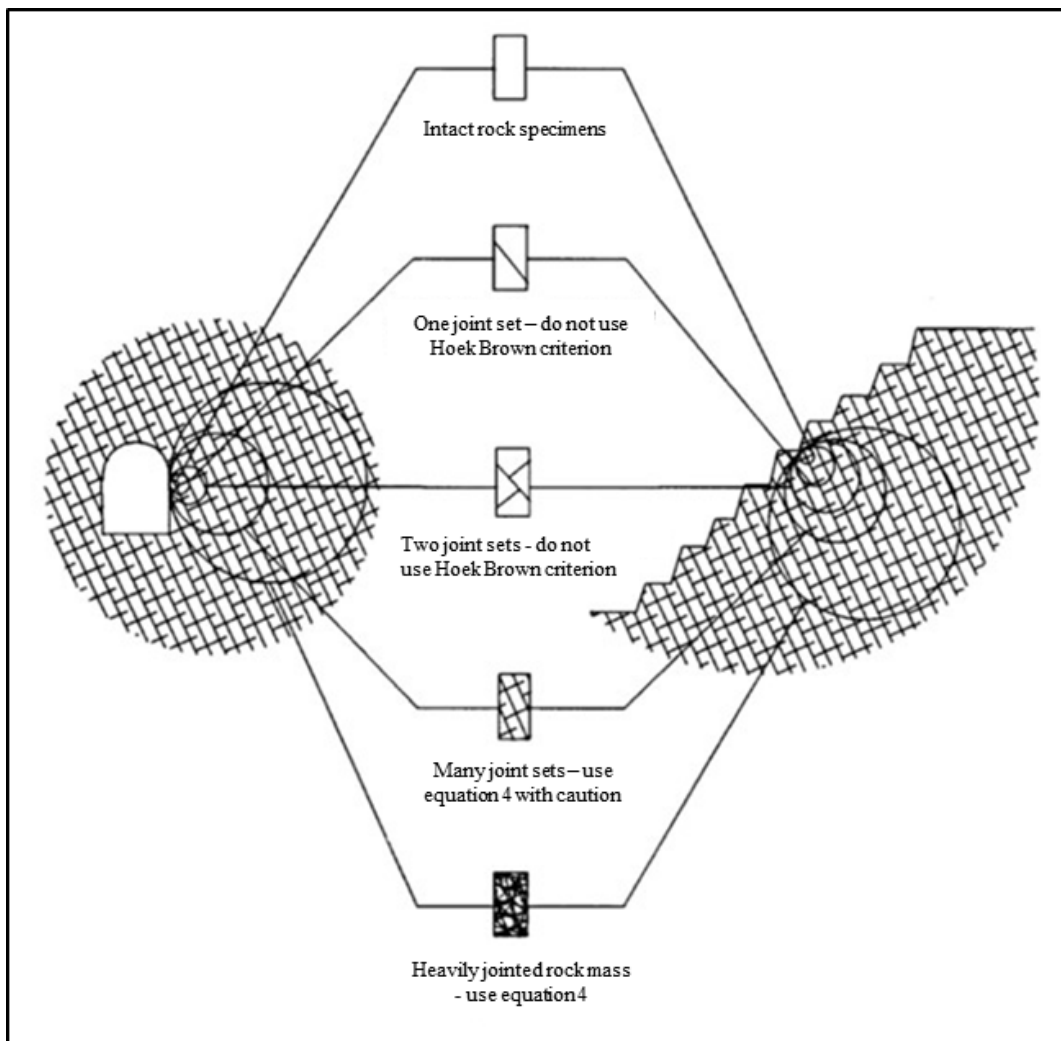


Figure 34: Diagram showing transition from intact rock to heavily jointed rock mass dependent on sample size. Modified from Hoek (2007).

Geological Strength Index (GSI)

The GSI classification system is one way of quantifying the rock mass quality in field, and was introduced in relation to the upgrade of the Hoek-Brown criteria in 1994 (Hoek, 1994). The system is used “*specifically for estimation of rock mass properties rather than tunnel reinforcement and support*” (Marinos, Marinos, & Hoek, 2005), and differs therefore from other classification systems mainly developed for use in underground excavation projects.

The GSI system is composed by two factors; the degree of fracturing and the condition of the fracture surfaces (Figure 35). The GSI value for the rock mass is included in the Generalized Hoek-Brown criterion through the following constants:

$$m_b = m_i e^{\left(\frac{GSI-100}{28-14D}\right)} \quad (6)$$

$$s = e^{\left(\frac{GSI-100}{9-3D}\right)} \quad (7)$$

$$a = \frac{1}{2} + \frac{1}{6} \left(e^{-GSI/15} - e^{-20/3} \right) \quad (8)$$

D is the disturbance factor which depends on the degree of disturbance due to blast damage and stress relaxation (Hoek, 2007).

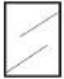



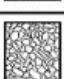

GEOLOGICAL STRENGTH INDEX FOR JOINTED ROCKS (Hoek and Marinos, 2000) From the lithology, structure and surface conditions of the discontinuities, estimate the average value of GSI. Do not try to be too precise. Quoting a range from 33 to 37 is more realistic than stating that GSI = 35. Note that the table does not apply to structurally controlled failures. Where weak planar structural planes are present in an unfavourable orientation with respect to the excavation face, these will dominate the rock mass behaviour. The shear strength of surfaces in rocks that are prone to deterioration as a result of changes in moisture content will be reduced if water is present. When working with rocks in the fair to very poor categories, a shift to the right may be made for wet conditions. Water pressure is dealt with by effective stress analysis.		SURFACE CONDITIONS				
STRUCTURE		SURFACE QUALITY				
		VERY GOOD Very rough, fresh unweathered surfaces	GOOD Rough, slightly weathered, iron stained surfaces	FAIR Smooth, moderately weathered and altered surfaces	POOR Slackensided, highly weathered surfaces with compact coatings or fillings or angular fragments	VERY POOR Slackensided, highly weathered surfaces with soft clay coatings or fillings
	INTACT OR MASSIVE - intact rock specimens or massive in situ rock with few widely spaced discontinuities	90			N/A	N/A
	BLOCKY - well interlocked undisturbed rock mass consisting of cubical blocks formed by three intersecting discontinuity sets	80				
	VERY BLOCKY - interlocked, partially disturbed mass with multi-faceted angular blocks formed by 4 or more joint sets		70			
	BLOCKY/DISTURBED/SEAMY - folded with angular blocks formed by many intersecting discontinuity sets. Persistence of bedding planes or schistosity		60			
	DISINTEGRATED - poorly interlocked, heavily broken rock mass with mixture of angular and rounded rock pieces		50			
	LAMINATED/SHEARED - Lack of blockiness due to close spacing of weak schistosity or shear planes		40			
			30			
			20			
		N/A	N/A			10

Figure 35: Chart for determining the GSI value (Hoek, 2007).

Shear strength of discontinuities

For rock slope analysis where the stability is governed by discontinuities, it becomes necessary to understand the factors controlling the strength of the discontinuities. Shear tests for smooth, planar surfaces where a constant normal stress and an increasing shear stress is applied, will show stress-displacement curves as in Figure 36 (left). By testing specimens at different normal stress levels, a relationship described by the linear Mohr-Coulomb curve is obtained which shows that the material has an elastic behaviour until the peak strength is reached. The residual strength is determined when the stress level required to obtain displacement reaches a constant value (Wyllie & Mah, 2004).

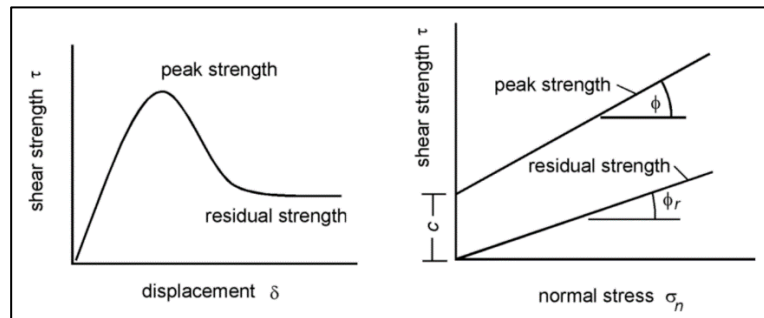


Figure 36: Peak strength and residual strength plotted after shear testing of planar surfaces. Figure to the right shows the Mohr plot. After Wyllie and Mah (2004).

The relationship shown in Figure 36 (right) can be represented by the linear Mohr-Coulomb shear strength, given by the friction angle and cohesion (see Equation 3, chapter 5.1). However, most natural joints are not smooth, planar surfaces, and determining strengths of such joints with the Mohr-Coulomb criteria is unsuitable.

Several modifications of the Mohr-Coulomb criteria have been presented through the years, such as Patton (1966) who studied bedding plane traces in limestone and found that the friction angle increases with higher degree of roughness. Through studies of the behaviour of natural rock joints, the first non-linear strength criterion for rock joints were developed by Barton (1973, 1976) and is now known as the Barton-Bandis criterion for rock joint strength and deformability (Barton & Bandis, 1991):

$$\tau = \sigma_n \tan \left(\varphi_r + JRC \log_{10} \left(\frac{JCS}{\sigma_n} \right) \right) \quad (9)$$

Where:

- τ = shear strength
- σ_n = normal stress
- φ_r = residual friction angle
- JRC = joint roughness coefficient
- JCS = joint wall compressive strength

For natural, unweathered surfaces the residual friction is approximately equal to the basic friction angle, ϕ_b (Bandis, 1993). The basic friction angle is valid for smooth, planar surfaces while the residual friction angle refers to joint surfaces after shear displacement. Additionally, the criterion considerate the relationship between the friction angle and normal stress acting on the plane, as high levels of normal stress will reduce the friction angle due to shearing of asperities (Wyllie & Mah, 2004)

Methods for determining the parameters in Equation 9 is described in the next chapter.

5.4 Input parameters from field work and laboratory testing

Geotechnical data of joints was collected during fieldwork 2016, and have been applied for determination of discontinuity shear strength. One rock sample was collected in field for laboratory analysis, in order to obtain input parameters related to the strength and deformability of the rock mass. Figure 37 shows locations of where the geotechnical measurements and the rock sample was taken. This chapter will describe the methods used in field and laboratory for determination of input parameters used in the stability analyses.

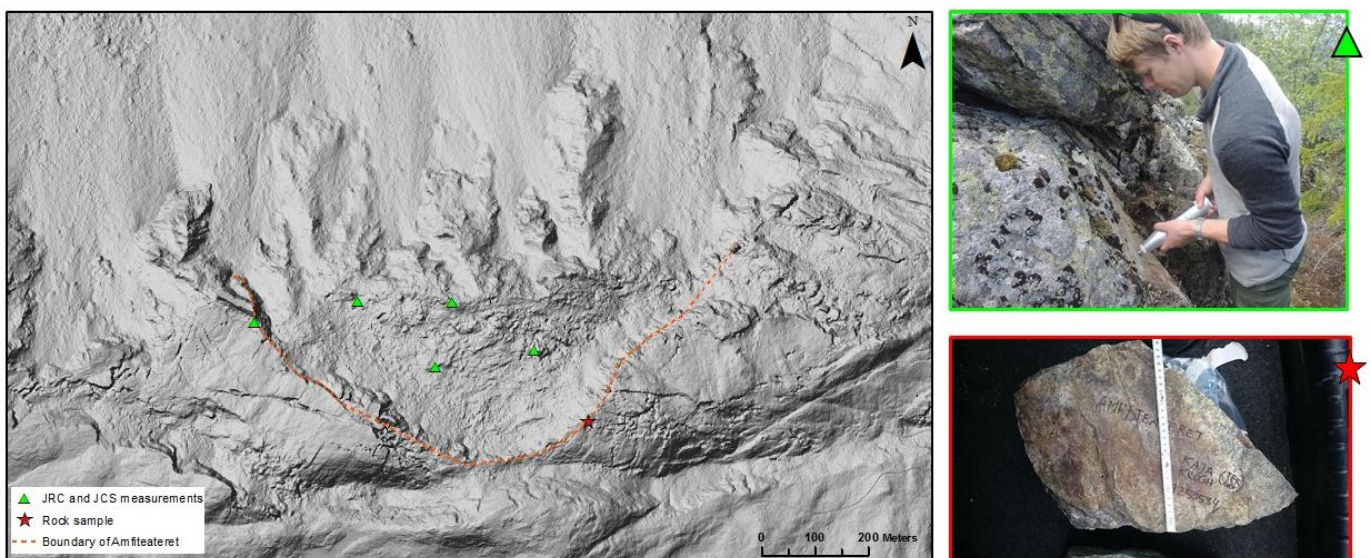


Figure 37: Map showing the locations of JRC and JCS measurements. Picture marked in green shows the Schmidt hammer used to determine the compressive strength of joint walls. The rock sample used for laboratory analysis was taken from the location marked by a red star.

Joint Roughness Coefficient (JRC)

The Joint Roughness Coefficient, JRC, is an empirical index used to characterize surface roughness and is included in the Barton Bandis criterion (Grøneng & Nilsen, 2008). There are several ways to measure this parameter, both in field and in laboratory. In relation to this master thesis, JRC was found in field by directly measuring the largest surface roughness amplitude from a one-meter long straight ruler. The measurements were carried out in four directions; along the dip direction, along the strike and $\pm 45^\circ$ relatively to the dip direction. The final JRC value was found by using the chart shown in Figure 38.

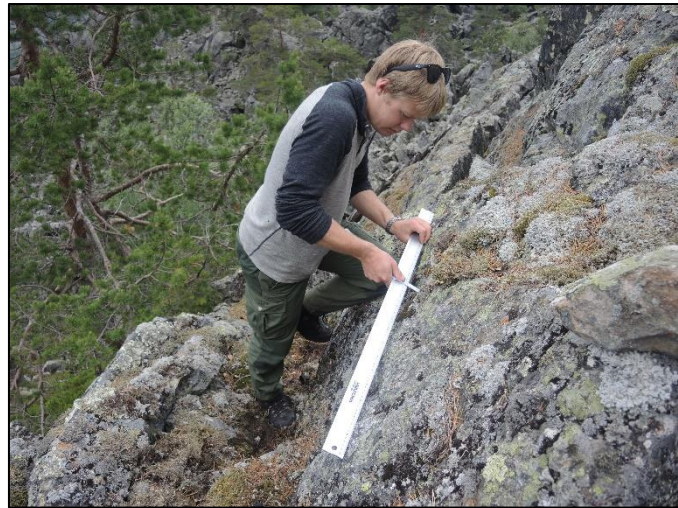
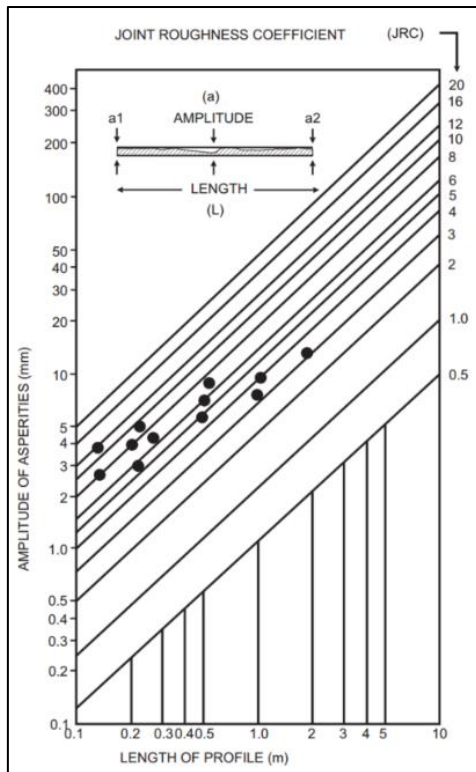


Figure 38: Chart to the left shows how to find the JRC value (Deere & Miller, 1966). The practical method in field is demonstrated in the upper right picture. At Kassen, a one-meter straight ruler was used.

Joint Compressive Strength (JCS)

The Joint Compressive Strength, JCS, is also a part of the Barton Bandis criterion. The JCS value will equal the Unconfined Compressive Strength (UCS) if the surface of the discontinuities are completely unweathered (Grøneng & Nilsen, 2008). This is not the case in practice since rock walls generally are weathered to a certain degree. JCS was found following the methodology described in ISRM (1978) by using a Schmidt hammer (L-type) on exposed rock joints, shown in Figure 37. The Schmidt hammer records the rebound of a spring loaded plunger after its impact with the rock surface. 20 measurements were taken at each joint surface, and the mean value calculated from the 10 highest values. Finally the rebound value was converted to an estimate of compressive joint strength by using a diagram developed by Deere and Miller (1966) (Appendix 8.5). This conversion accounts for hammer orientation and the unit weight of the rock.

Laboratory testing

The laboratory testing have been conducted on a rock sample of Amphibolite collected from Amfiteateret. The block measures 30 x 60 x 20 cm and was taken from the location shown in Figure 37. This rock sample is assumed to be representative for the area where the stability analyses will be carried out, as the bedrock at Skipet and in Amfiteateret consists of Amphibolite (see bedrock map, Figure 4). All laboratory tests have been carried out by the author at the NTNU/SINTEF Engineering Geology and Rock Mechanics Laboratory during autumn 2016.

Tilt test

The tilt test is a laboratory shear test where the basic friction angle (φ_b) is determined. There are no international standard for this test, and therefore NTNU's own procedure is followed. A

throughout description of this method is given by Grøneng and Nilsen (2008). Three samples were sawn out from the block with a diameter of 34.5 mm and a length/diameter relation of 2.5 – 2.6. The cores were cut axially before the test was carried out in order to force the upper half of the core to slide under its own weight in the testing apparatus (see Figure 39). Each core was tested in four different sliding configurations, and repeated three times for each configuration. Based on these results, a mean basic friction angle were calculated.

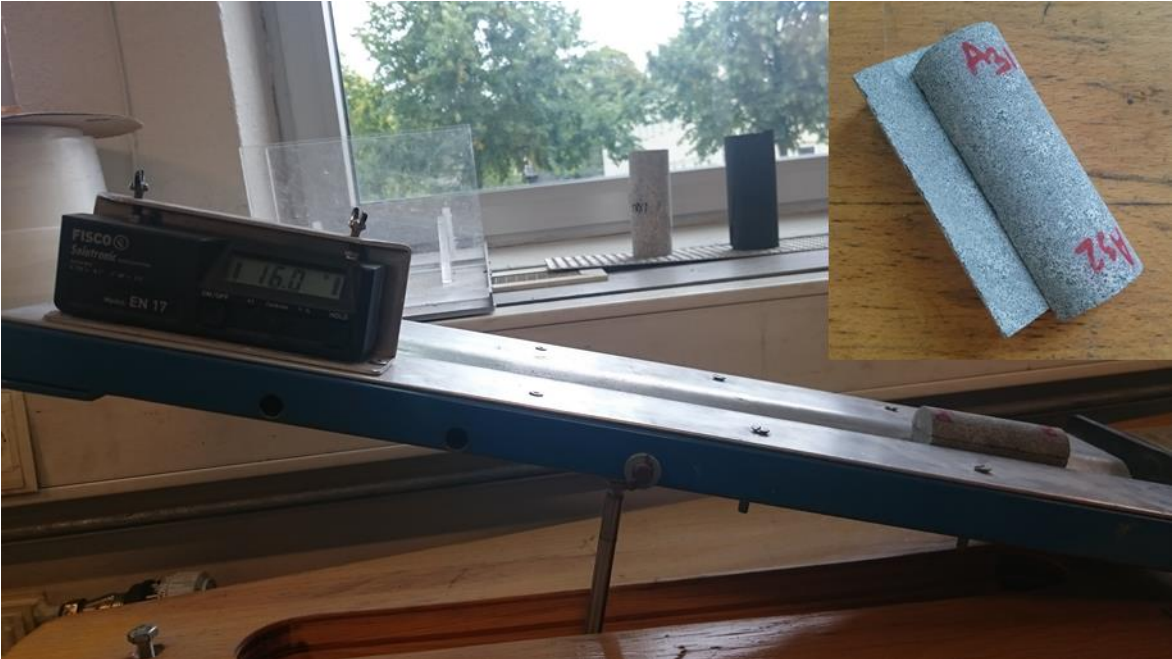


Figure 39: Apparatus for determining the basic friction angle after NTNUs procedure. The cores are sawn axially before tested, shown in the upper right photo.

Uniaxial Compressive Strength (UCS)

The test was performed following the standards of ISRM (1979). The standards recommends to carry out the test for at least five specimens with diameter 50 mm. Only four cores from the site had satisfying quality to be tested, each having a diameter of approximately 34.3 mm (See Appendix 8.3 for detailed measurements). The test procedure consists of applying a continuous load on the samples until failure. The UCS value is then found by dividing the maximum load carried by the specimen during the test, by the original cross-sectional area (ISRM, 1979). Hoek, Brown, Institution of, and Metallurgy (1980) reviewed the relationship between sample diameter and the measured material strength, and found that the sample strength increases as the sample diameter decreases. To find the equivalent uniaxial compressive strength for standard cores with 50 mm diameter, equation 10 was used for the 34.3 mm cores.

$$\sigma_{c50} = \frac{\sigma_c}{\left(\frac{50}{d}\right)^{0.18}} \tag{10}$$

Where: σ_{c50} = the calculated uniaxial compressive strength of a 50-mm diameter sample
 σ_c = the uniaxial compressive strength measured on the specimen
 d = the diameter of the specimen in mm

Deformability in uniaxial compression

The intention of this laboratory test is to determine stress-strain curves for the rock material, and the elasticity parameters Young’s modulus (E) and Poisson’s ratio (ν). The test was done simultaneously as the UCS test by measuring the radial and axial strain of the rock specimen in uniaxial compression. The test was performed after the ISRM standards using electrical resistance strain gauges. Young’s modulus and Poisson’s ratio were found by the tangent method (Figure 40), and are given by the following equations;

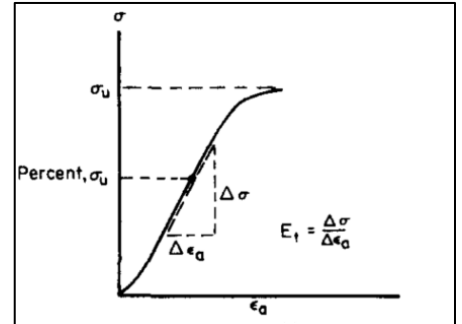


Figure 40: Tangent modulus measured at a fixed percentage of maximum strength. The fixed percentage is set to 50.

$$E = \frac{\Delta\sigma_c}{\Delta\epsilon_a} \tag{11}$$

Where: $\Delta\sigma_c$ = UCS interval defined by a tangent set at 50% of σ_c max.
 $\Delta\epsilon_a$ = axial strain interval defined by a tangent set at 50% of σ_c max.

$$\nu = - \frac{\epsilon_a}{\epsilon_d} \tag{12}$$

Where: ϵ_a = axial strain at the point where UCS = 50% of σ_c max
 ϵ_d = diametrical strain at the point where UCS = 50% of σ_c max

5.5 Numerical modeling applied to Amfiteateret

5.5.1 Background of the analysis

In order to reconstruct the ground surface before the Bandak rock avalanche, the location of the slide scar had to be recognized in the slope. It was suggested in the specialization project that this slide scar was the scarp bounding Amfiteateret. During fieldwork summer 2016, glacial deposits were observed below the scarp of Amfiteateret, meaning that the post-glacial rockslide deposits must have originated from another location than first assumed. A new possible location for the slide scar is shown in Figure 41 which is used to reconstruct the slope before failure.

However, the scarp of Amfiteateret has a height of 60-80 meters and is limiting an area of highly deformed rock mass. This geomorphology indicates that some kind of displacement has taken place. One possible theory is that sliding along the scarp of Amfiteateret has occurred at low velocities, not leading to any dramatic collapse of the slope. This process would however change the stability situation in the entire slope, which lead to a collapse of the frontal part causing a rapid rock avalanche which run out all the way across Bandak Lake. This theory concerning the deformation history of Amfiteateret will be investigated through the second step of the numerical analysis.

As the numerical modeling is performed in 2D, a profile through the instability is defined as shown in Figure 41. The profile is striking directly towards North, and is located in the central part of Amfiteateret, including the scar of the rockslide event. The grey area lacks bathymetric data due to limited boat access close to the shoreline. An interpolation of the lake bottom relief is conducted on the combined DEM (onshore and offshore terrain data) for this area.

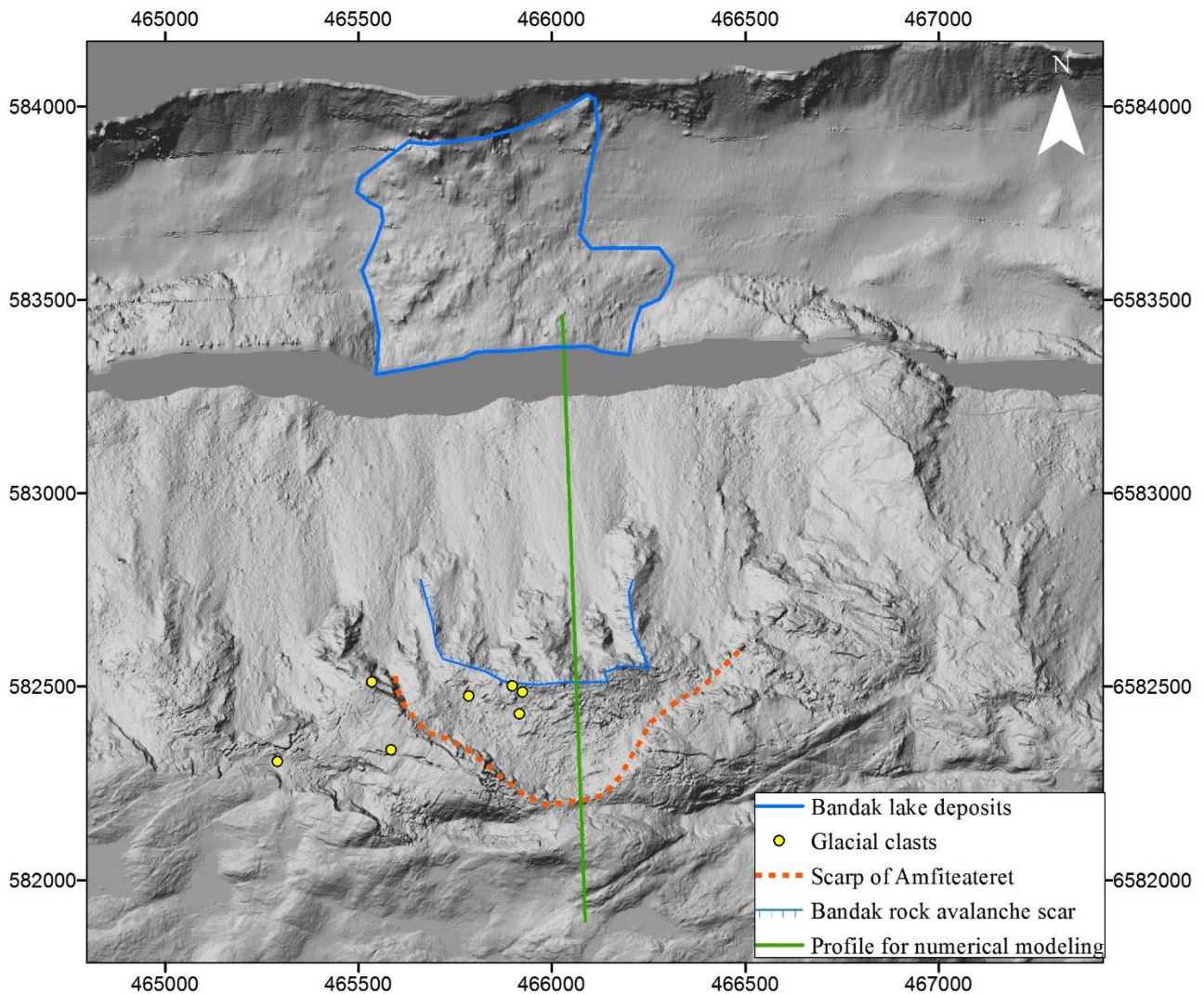


Figure 41: Observations of glacial clasts in the area of Amfiteateret lead to a new suggestion for the location of the scar from the Bandak rock avalanche. The deposits of this event is clearly visible on the bathymetric data, outlined with green. The long run-out indicates that the Bandak rock avalanche had a high velocity.

5.5.2 Reconstruction of topography and volume estimations

The reconstruction of the surface before the Bandak rock avalanche is done by analyzing adjacent topography close to the failed slope, which gave an impression of how the relief of the slope might have been before failure. The tool *Stack Profile* in ArcGis is applied for this task in order to compare topography at different profiles inside and outside of the defined instability (Figure 42). The procedure is of a relatively simple kind, but is believed to give accurate enough results for the purpose of the analysis.

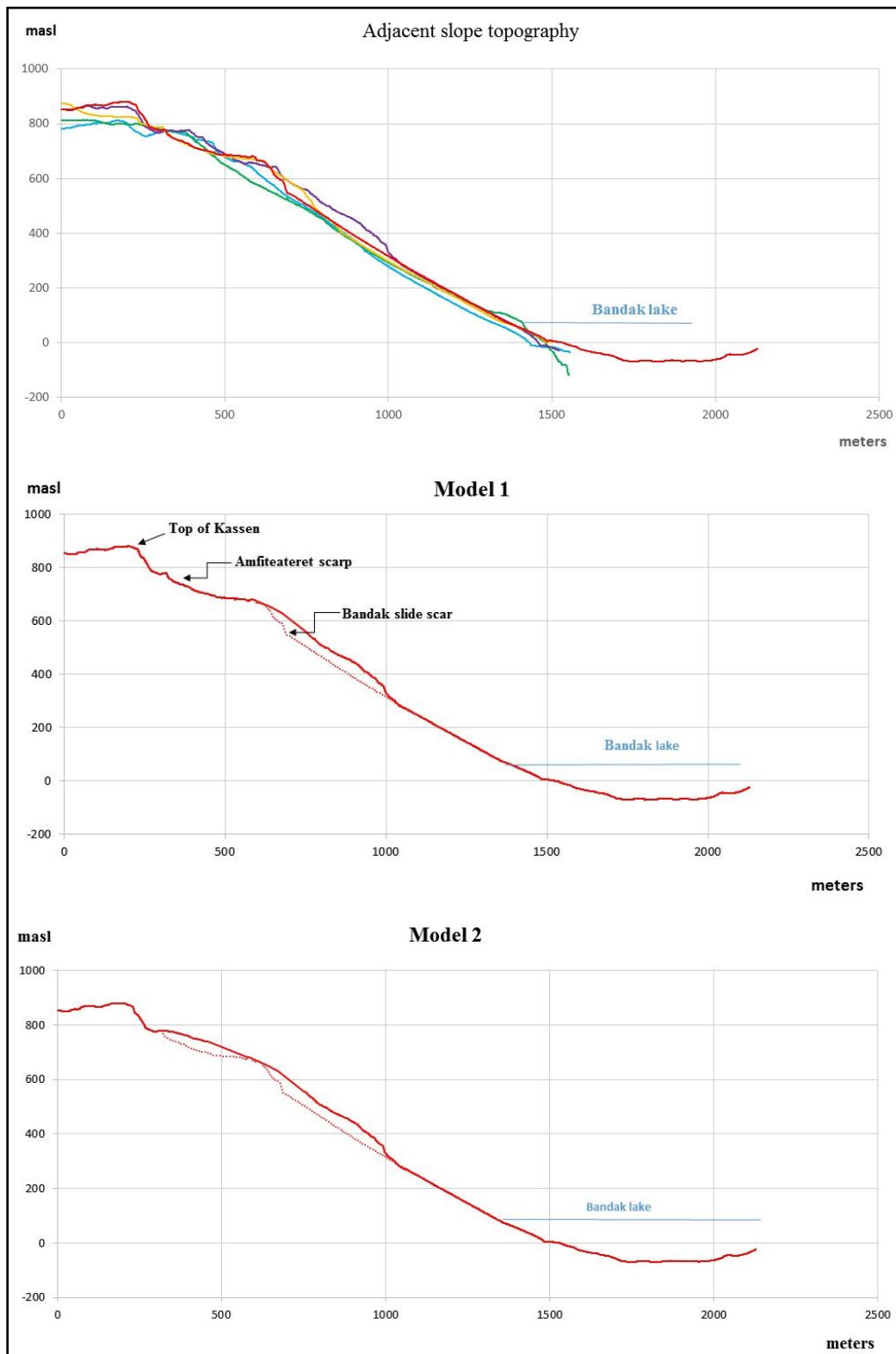


Figure 42: The uppermost figure shows all profiles at adjacent slopes that was used to construct the most likely surfaces before failure. Model 1 shows reconstruction of the lower part of the slope before the Bandak rock avalanche occurred. Notice that the shape of Amfiteateret is the topography of today. Model 2 is the assumed ground surface before any displacement in the slope, neither along the scarp of Amfiteateret or in the lower part. Present topography is shown with dashed lines.

To verify the reconstruction of the topography, the volume of the rock deposits from the Bandak rock avalanche is compared to the volume of the reconstructed surface. The latter is estimated from Model 1 by multiplying the reconstructed cross sectional area by the width of the assumed rock avalanche scar which resulted in a volume of 11.06 million m³ (Table 17).

Table 17: Volume of the reconstructed surface at Model 1.

Parameter	Value	Method
Area of reconstructed surface at cross-section	20867 m ²	Measured on Model 1, by applying measuring tool in the software RS ² , presented in chapter 5.5.4.
Width of rock avalanche scar	530 m	Measured using measuring tools in ArcGIS 10.4
VOLUME	11.06 million m ³	Calculated

The volume of the deposits in Bandak Lake are calculated by applying the 3D Analyst Tool *Polygon Volume* in ArcGIS 10.4. This tool calculates the volume between a terrain surface and a chosen reference plane. The input files applied for calculating the Bandak rock avalanche deposits are;

- Triangulated irregular network (TIN) surface, converted from the DEM of the area.
- Polygon which delimits the TIN surface
- Reference plane, given by a chosen reference height.

Calculations are only made for portions of the TIN surface that overlap with the input polygon, marked in blue in Figure 43. The reference plane is set to -80 meters below sea level (MBSL) which is the depth of the lake bottom adjacent to the rock avalanche deposits at point A and B. The volume is then calculated between the reference plane and the underside of the polygon-cut TIN surface.

The average inclination of the slope in the black area without bathymetric data is estimated to be 25 – 30 °. This slope angle is based on the width of the area and heights on the two opposite sides where surface data exist. It is believed that this slope angle is too steep for rock avalanche to deposit, and therefore the calculations of the volume are restricted to the deposits within the polygon in Figure 43.

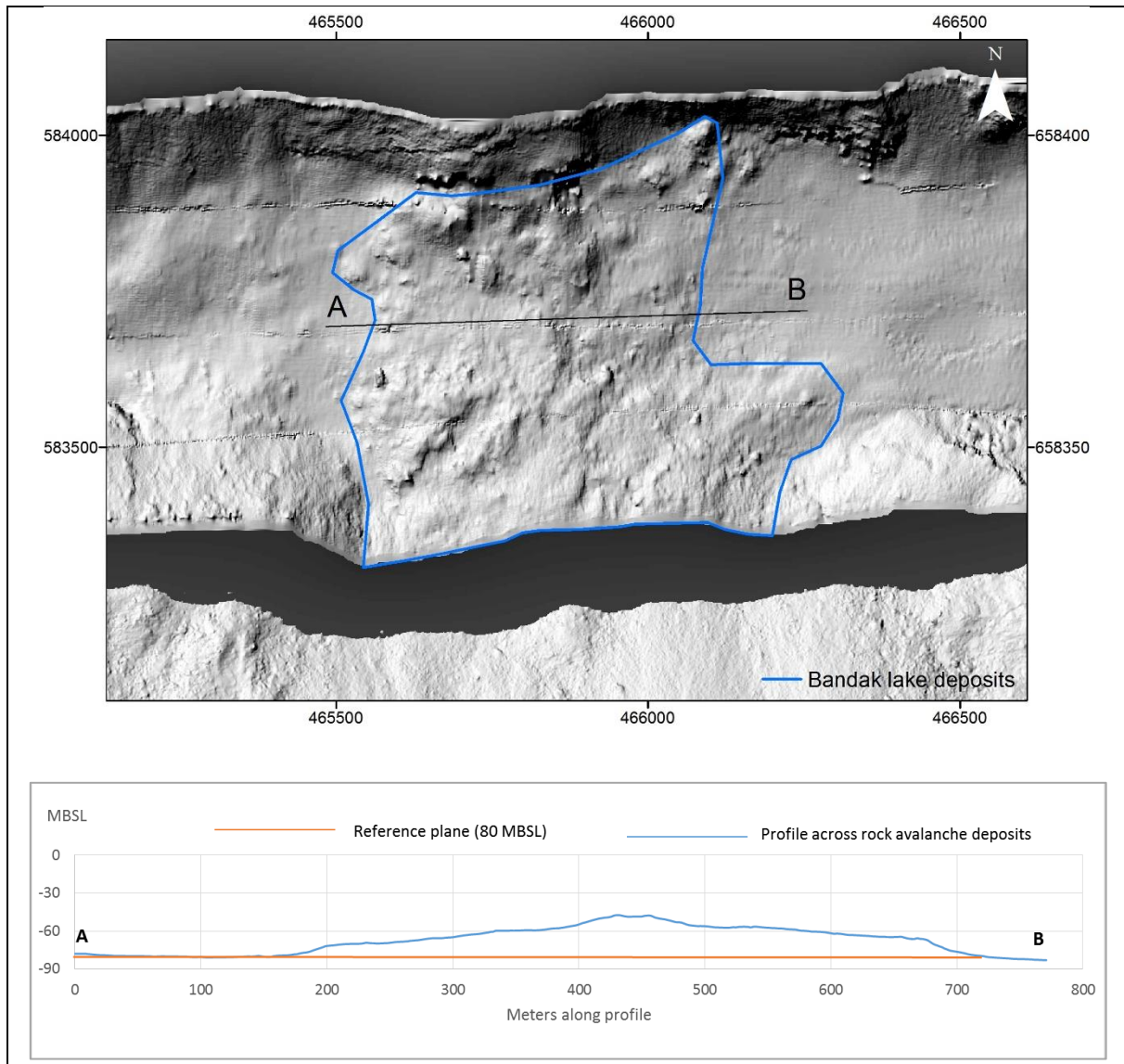


Figure 43: Upper figure shows the polygon applied for delimiting the TIN surface in order to calculate the volume of the rock avalanche deposits. The volume is calculated between the TIN surface and the reference plane shown in the lower figure.

The resulting volume of the rock avalanche deposits are 13.4 million m^3 , a volume increase of 21 % compared to the volume of the reconstructed surface. Such a volume increase, also termed bulking factor, is reasonable as the rock mass disintegrates and fragments from a coherent mass into a rock avalanche. Hungr and Evans (2004) presents a typical range of bulking factors of 18 – 35 %, which shows that the reconstructed volume is reasonable.

5.5.3 Structure of the analysis

The most appropriate methodology during modelling is to start with a simple model and gradually build up its complexity as the problem dictates. Sensitivity analyses of key parameters should be incorporated as a part of the modelling. These suggestions by Eberhardt (2003) are used as guidelines for the structure of the numerical modeling which consists of the following five steps:

Step 1

Step 1 of the analysis is done in order to evaluate the Model 1 concerning the in situ stress situation, groundwater level and mesh set-up.

Step 2

Step 2 involves an analysis of the stress distribution in the rock mass before (Model 2) and after the displacement along the scarp of Amfiteateret (Model 1) to check if the presented deformation theory can be confirmed by numerical modeling. By analyzing and comparing the stress distribution in the two models, it can be discussed to which extent the low-velocity displacement along the scarp of Amfiteateret effected the stability of the slope, and consequently the Bandak rock avalanche. The analysis is run with an elastic material model since the aim is to investigate stresses.

Step 3-5

The three next steps in the analysis are a back-analysis of the Bandak rock avalanche using Model 1. The main goal of these steps is to analyze how different controlling factors influence the Critical Strength Reduction Factor (CSRF). Special attention is drawn to the role of the discontinuities and the water conditions, as these often are the main factors governing rock slope stability (Wyllie & Mah, 2004). The analyses is run with the SSR technique, and with plastic material models with either residual strengths equal peak strengths, or lower residual values to simulate progressive failure.

Step 6

The final step in the numerical analysis is run as a forward analysis with todays topography and input parameters set to reflect present conditions as accurate as possible with the available data. The purpose of the last step is to evaluate the stability of scenario G defined in the hazard and consequence assessment, which corresponds to the location of this forward analysis.

5.5.4 Applied software RS²

RS² (Phase2 9.0) is a two dimensional elastoplastic finite element program for soil and rock applications, which can be used for many different geotechnical projects including rock slope stability (Rocscience, 2016b). The program offers a wide range of material models making it applicable for many cases. The program can perform a finite element slope stability analysis by using the Shear Strength Reduction (SSR) method discussed in chapter 5.1. This method is well accepted for determining the Factor of Safety of a slope based on FEM (Grøneng, 2010). The FS is expressed with the Critical Strength Reduction Factor (CSRF) in RS², which is the maximum value of Strength Reduction Factor (SRF) for which the model remains stable (Rocscience, 2016c).

RS² is chosen for the numerical modeling at the study site primary due to the highly fractured rock mass in Amfiteateret which can be modeled as a continuum material with the FEM method. Secondly, the software is easy available and free for all NTNU students.

5.5.5 Model set up

Boundary conditions

Boundaries in a model are either real or artificial. The surface of the model corresponds to the natural (or reconstructed) surface, while the vertical sides and the lower boundary are artificial and do not exist in reality. Therefore, slope stability problems require far-field artificial

boundaries to avoid boundary effects (Wyllie & Mah, 2004). The slope model needs to extend past the likely location of slope failure for a continuum-mechanics-based solution to be meaningful (Chugh, 2003).

The boundary conditions are defined in the models by prescribed displacement. Dimensions and boundary conditions used for the models are described respectively in Figure 44 and Table 18.

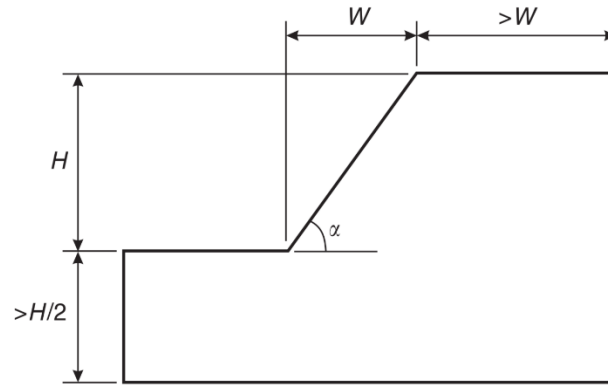


Figure 44: Recommended model size after Wyllie and Mah (2004). Dimensions for W and H are set to avoid effects of artificial boundaries.

Table 18: Boundary conditions applied to the models at Amfiteateret.

Boundary	Type	Description	Recommendations
Surface	Free	The ground surface is free to move in all directions.	Rocscience (2016c)
Left/right sides	Restrain X	The left and right boundaries are free to move in the vertical direction, which allows for deformation and prevents stress concentrations at the boundaries.	Chugh (2003) Sandøy (2012)
Bottom	Restrain X,Y	The lower boundary is restrained in all directions to inhibit rotation of the model.	Chugh (2003) Wyllie and Mah (2004)
Lower corners	Restrain X,Y	The lower corners are restrained in all directions.	Chugh (2003). No displacement in x-direction

Mesh

The analyses are conducted with a graded mesh consisting of 6-noded triangles. This mesh type was used successfully by Hammah (2005) for finite element slope stability analysis. Hammah (2005) showed that the number of elements had minimal impact on computed factor of safety, and for the analysis at Amfiteateret this number is set to 500.

Completed Models

Figure 45 show the three completed models used in numerical analyses. Models with joints and groundwater tables will be presented in the results of the numerical modeling.

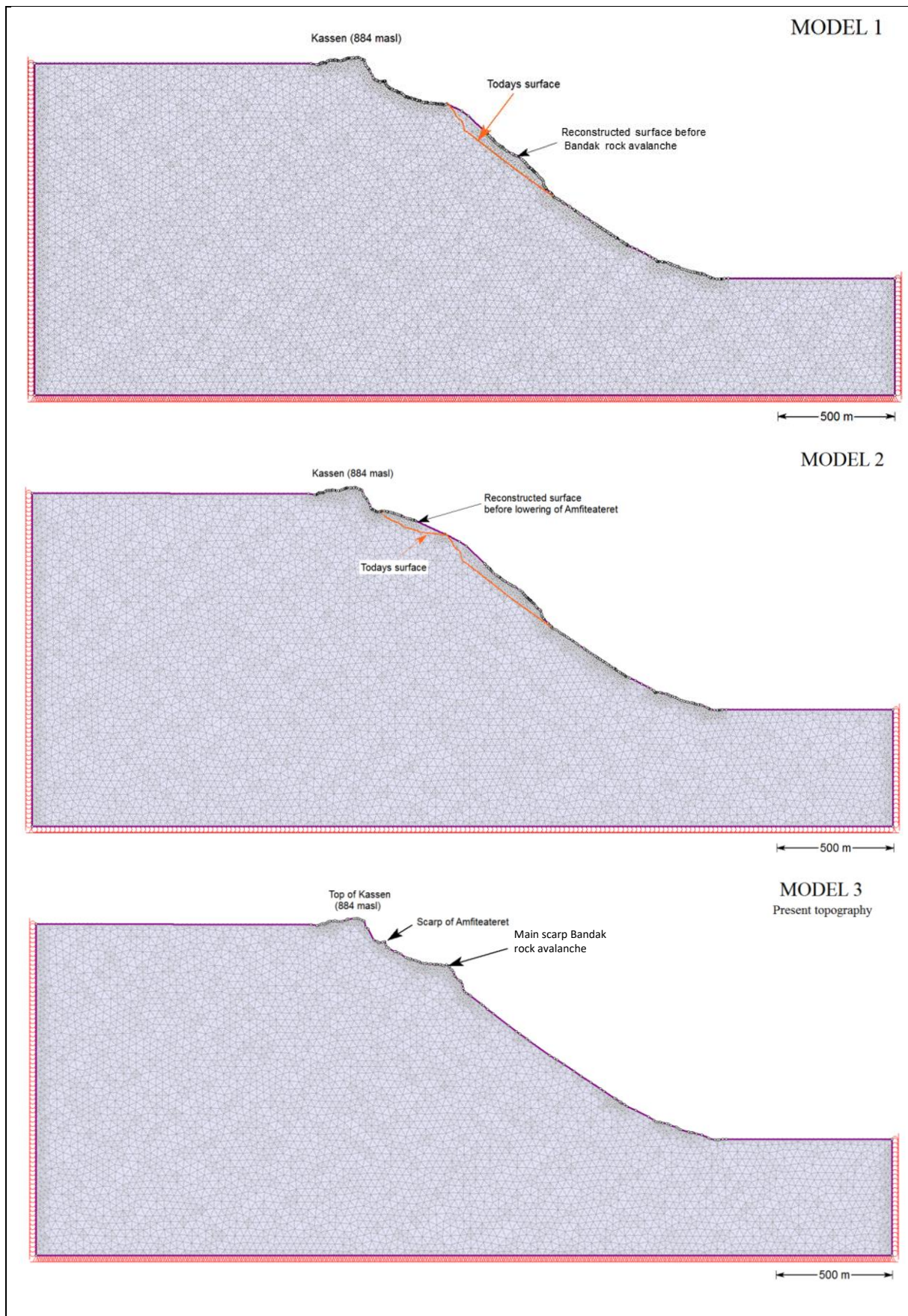


Figure 45: Completed models with mesh and boundary conditions.

5.5.6 Analysis Setup

Field stress setup

The changing topography in mountain regions has a major effect on the field stress in the rock mass (Nilsen & Broch, 2013). In a valley, fjord or lake bottom the horizontal stress component will increase since it cannot be transferred out in the slope. The principle stresses (σ_H , σ_h and σ_v) will therefore vary from place to place in a mountainous area (Nilsen and Broch, 2013). This means that stress measurements are necessary for obtaining correct values.

No stress measurements exist for the Kassen slope, so the input numeric values for the principle stresses are found in a database presented by Hanssen (1998). This database have gathered all available information on three-dimensional rock stress measurements from both NTH (NTNU) and SINTEF archives, and is known as the newest collection of field stress measurements in Norway. The nearest borehole is *Borehole Dalen01 Tokke*, located in a north-facing slope at the western end of Bandak lake, 21 km away from the Kassen site (Figure 46). The stress regime at this point is assumed to be similar to the study site since the measurements were taken in a slope with the same orientation as Kassen and is adjacent to the same regional structures (such as Bandak lake).



Figure 46: Location of Borehole Dalen01 Tokke where numeric values for the principle stresses are found.

The values obtained for the measured three dimensional stress field (magnitude and orientation) at the borehole *Dalen01 Tokke* is shown in Table 19.

	Overburden [m]	σ_v [Mpa]	σ_H [Mpa]	σ_H [°]	σ_h [Mpa]	σ_h [°]
Dalen01	260	3.8	5.9	62	2.7	152

Table 19: Measured three-dimensional stress field for Borehole Dalen01. Modified from Hanssen (1998).

The final *Field Stress Properties* used in the RS2 model is shown and justified in Table 20.

Table 20: Input parameters in RS2 for the Field Stress Properties

Input parameter	Relevant formulas	Values	Justification
<i>Gravity Field Stress</i>	$\sigma_v = \gamma * h$	$\gamma = 29 \text{ kN/m}^3$	The depth and the unit weight of the material determines the vertical stress distribution. The horizontal stress components are given by the Total Stress Ratio. Recommended by Rocscience (2016c) for near surface excavations.
	$\gamma = \text{Unit weight}$ $h = \text{depth}$		
<i>Ground Surface Elevation – Use Actual Ground Surface</i>	-	-	Defines the depth (h) measured from the actual ground surface of the model.
<i>Total Stress Ratio (TSR) In Plane</i>	$\frac{\sigma_{\text{horizontal in plane}}}{\sigma_v}$	$\frac{2.7 \text{ Mpa}}{3.8 \text{ Mpa}} \sim 0.71$	The model profile is trending with 175 °, making σ_h the in plane component. Magnitude of the stresses are given in Table 19.
<i>Total Stress Ratio (TSR) Out-of-Plane</i>	$\frac{\sigma_{\text{horizontal out-of-plane}}}{\sigma_v}$	$\frac{5.9 \text{ Mpa}}{3.8 \text{ Mpa}} \sim 1.55$	σ_H is the out-of-plane component. Magnitude of the stresses are given in Table 19.
<i>Locked in horizontal stresses (in and out-of-plane)</i>	-	0	Norwegian stress regimes often have locked in horizontal stresses such as tectonic stresses (Hanssen, 1998). However, stress relief is assumed at the Kassen site due to the heavily dissected character of the rock mass. Therefore this parameter is set to zero.

Groundwater setup

As mentioned earlier, water is one of the main controlling factors for slope stability. The groundwater is therefore set at different levels in the model to determine how the water pressure influences the stability. Three configurations are analyzed;

- High groundwater table
- Present groundwater table
- Dry slope

In order to determine the present groundwater table at Kassen, some assumptions had to be made due to limited hydrological data. No direct measurements of the groundwater level exists at the Kassen site. There are no observed springs in the slope from either field observations or air photo studies, and the fractured rock mass appears to be dry. Marsh and lakes characterize the area above the crown, extending away from the unstable site. To give a best estimate of the present groundwater conditions for the slope, given the limited knowledge, the conditions at the unstable rock slopes Åknes and Mannen is investigated in order to compare.

At Åknes the depth to the groundwater have been measured in three boreholes located in the upper, middle and lower part of the slope. They give groundwater depths of respectively 53, 40 and 40 meters (Kveldsvik, Einstein, Nilsen, & Blikra, 2009). Several springs is observed in the slope, most of them in the lower part of the slope (about 100 m.a.s.l.). The groundwater depth was consequently set by Kveldsvik et al. (2009) to linearly rise downslopes following the borehole measurements and reaching ground surface at 100 m.a.s.l.

No water is observed in a 136 m deep borehole located at the crown of Mannen according to Farsund (2011). The same author states that there are no rivers, lakes or other observations indicating a high groundwater table at Mannen. Dry slope conditions are supported through two-dimensional resistivity measurements performed by NGU in 2012 (Dalsegg & Rønning, 2012). This report reveals zones with high to extremely high resistivity (20-60 kΩm) which is suggested in the report to indicate excellent drainage of the slope. The zones showing moderate resistivity can be water-saturated rock in a drained environment.

The highly fractured rock mass in the area of interest (Amfiteateret) shows most similarities to the conditions at Mannen (Hermanns, 2016b). This can indicate a higher drainage in the rock mass than for the situation at Åknes, where the rock mass exhibits relatively less fractures. Additionally, no springs exist in the slope at either Kassen and Mannen, while several springs are observed at Åknes. Based on these observations, the maximum depth to groundwater at Kassen is set to approximately 60-80 meters below ground surface, a lower level than for Åknes. The groundwater table is set to ground surface behind the crown, corresponding to the observed marsh areas. As for Åknes, the groundwater depth rises linearly downslopes, reaching ground surface at 72 m.a.sl, the height of Bandak Lake.

5.5.7 Rock mass input parameters

Input parameters for the rock mass consisting of amphibolite have been obtained through fieldwork and laboratory tests on cores from the rock sample, discussed in chapter 5.4. Table 21 in the end of this chapter provides an overview of all input parameters related to the rock mass.

Hoek-Brown conversion

The strength of the rock mass in the numerical modeling is assigned by the Generalized Hoek Brown criterion, since it is the most suitable strength model for predicting failure of fractured rock masses (Hammah et al., 2004). However, applying this failure criterion in the SSR-FEM analysis is not straightforward. The computation time increases and finding closed form equations for the Hoek-Brown parameters is difficult (Hammah et al., 2004).

This problem was solved by Hoek et al. (2002) by introducing equivalent Mohr-Coulomb friction angles and cohesive strengths for the rock mass at different stress levels. This is done by calculating an equivalent Mohr-Coulomb envelope to the Hoek-Brown model. Since the Mohr-Coulomb criterion is linear and the Hoek-Brown criterion is non-linear, the former needs to be defined for a certain value of normal stress (σ_n) (Figure 47). According to Nilsen (2000), it is crucial to adjust the friction parameters to the actual normal stress level, otherwise serious calculation errors can occur.

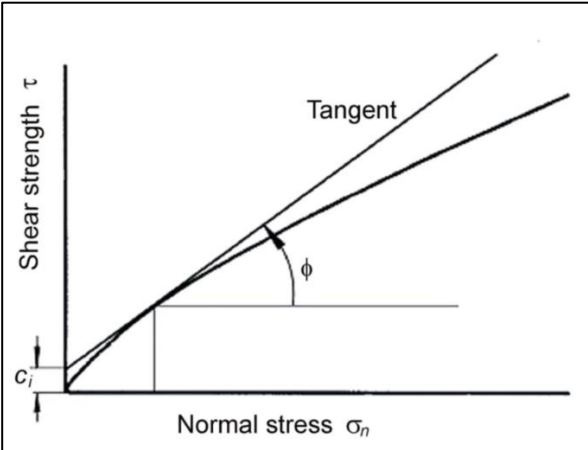


Figure 47: Equivalent Mohr-Coulomb envelope fitted to a non-linear Hoek-Brown envelope. Instantaneous friction and cohesion values are defined by the actual normal stress level (σ_n). Figure from Hoek (2000).

In RS², the conversion from Hoek-Brown input parameters to equivalent Mohr-Coulomb parameters is done in the software RocData by using the function *Instantaneous MC Sampler*, cohesion and friction values can be found for a specific normal stress level. The latter is given by Equation 13;

$$\sigma_n = \gamma H \tag{13}$$

- Where:
- σ_n = normal stress at a certain depth
 - γ = Unit weight of overlying material
 - H = depth, perpendicular to the slope surface

A normal stress level at Kassen is defined at a level corresponding to the rupture surface of the Bandak rock avalanche. This is considered as a reasonable, as the history has showed that failure can occur at such normal stress levels. The depth to the slope surface, was measured (using measuring tools in Excel) from the historic sliding surface to the reconstructed surface shown in Model 1. With $\gamma = 29 \text{ kN/m}^3$ and $H = 56 \text{ m}$ gives $\sigma_n = 1.6 \text{ Mpa}$. This normal stress level is therefore used to find the corresponding cohesion and friction angle in RocLab.

Table 21: Overview of all input parameters used for the rock mass in the numerical modeling.

Description	Symbol	Unit	Value	Remarks
Laboratory tested				
Uniaxial Compressive Strength	σ_c	Mpa	241	Laboratory
Young's Modulus	E	Gpa	74.5	Laboratory
Poisson's ratio	ν	-	0.27	Laboratory
Unit weight	γ	kN/m ³	29	Laboratory
Estimated for rock mass based on Hoek-Brown Failure criterion				
Geological Strength Index	GSI	-	55	Field estimation
Disturbance factor	D	-	0	Discussed with supervisor
Constant (s)	s	-	0.007	See chapter 0. Calculated by RocLab.
Constant (a)	a	-	0.504	See chapter 0. Calculated by RocLab.
Material Constant (m _i)	m _i	-	26	Evaluated based on inbuilt RocData values for amphibolites (Rocscience)
Equivalent Mohr Coulomb parameters obtained in RocLab (for $\sigma_n = 1.6$ Mpa)				
Peak cohesion	c_p	Mpa	2.2	Instantaneous MC sampler
Residual cohesion	c_r	Mpa	1.5	2/3 of peak value. Recommended by Trinh (2016).
Peak friction angle	α_p	°	65.9	Instantaneous MC sampler
Residual friction angle	α_r	°	43.9	2/3 of peak value
Deformation modulus	E_m	Mpa	30416.9	Calculated in RocData
Peak tensile strength	σ_t	Mpa	-0.312	Calculated in RocData
Residual tensile strength	σ_{tr}	Mpa	-0.208	2/3 of peak value
Dilation Angle	-	-	0	Discussed with supervisor Bjørn Nilsen.

5.5.8 Discontinuity parameters

The discontinuities (J2 and J3) in the model are assigned with Barton-Bandis strength parameters, and implemented in the model through a joint network model. The joints are also assigned with stiffness parameters, describing joint deformability. Table 23 at the end of this chapter summarizes all input parameters in the model related to the discontinuities.

Barton Bandis input parameters

Additional 161 measurements of dip and dip direction were taken in the area of Amfiteateret during fieldwork 2016. The joint network in Amfiteateret show a high degree of variance considering orientation compared to the discontinuity mapping outside the area (see results from the specialization project). The defined joint sets J1, J2 and J3 were recognized in the area of Amfiteateret. Especially joints parallel with J3 has a high concentration in the stereographic analysis (Figure 48).

Results from the kinematic analysis in the specialization project showed that planar sliding along J2 is most critical concerning stability in the LW domain (where the numerical analysis takes place). It is also feasible with biplanar sliding along J2, with either J1 or J3 as rear release surfaces, shown in the profile in chapter 2.4. To keep the models simple, only J2 and J3 are included in the model.

JRC and JCS measurements have been performed on 24 surfaces, where 7 surfaces are recognized as J2 and 5 surfaces are recognized as J3. The remaining 12 surfaces are randomly distributed in space as shown in Figure 48. All measurements of JRC and JCS are given in Appendix 8.4.

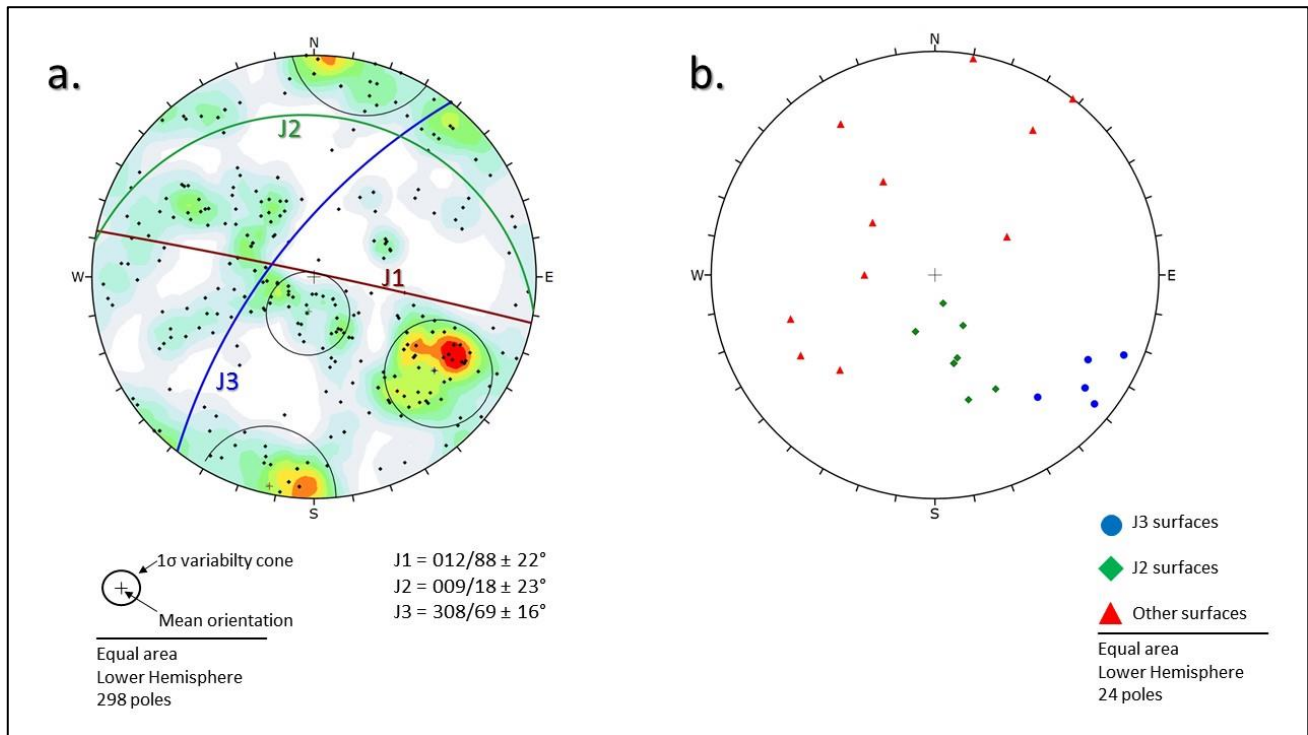


Figure 48: (a) shows all 298 orientation measurements taken in the area of Amfiteateret where J1, J2 and J3 were recognized. 24 structures Amfiteateret were mapped with JRC and JCS measurements, shown in (b). These are divided into J2, J3 and other surfaces.

Since relatively few measurements of JRC and JCS exist for J2 and J3, the standard deviation for JCS and JRC values is compared for samples within the respective joint sets and a sample for all measured surfaces. The standard deviation (std) is found by formula 14:

$$std = \sqrt{\frac{\sum(x - \bar{x})^2}{(n - 1)}} \quad (14)$$

Where: x = value in the sample
 \bar{x} = mean value of the sample
 n = number of values in the sample

JRC is statistically evaluated in the three measured directions; strike, dip and oblique. A combination of the oblique and dip direction is also plotted. The following main observations can be drawn from Figure 49:

- The roughness of J2 is higher in the dip and oblique than in the strike direction.
- The roughness of J3 is highest in the strike direction.
- The difference in JRC values among the measuring directions are highest for J2, where the maximum difference is 2.4 between the strike and oblique direction.
- J3 shows the highest variation in JRC values, represented by the standard deviation.

Since sliding is unlikely to occur in the strike direction (see kinematic analysis in chapter 2), input values for JRC for the two joint sets are chosen from the combined oblique and dip direction. The input JRC value for J2 is taken as the mean value of records on this surface since the standard deviation for this joint set is less than the standard deviation in total for all surfaces. For J3, the standard deviation for the joint set is higher than the total value. Therefore, the JRC value for this joint set is taken as a mean of all measurements. The final JRC input for J2 and J3 is respectively 13.7 and 12.0.

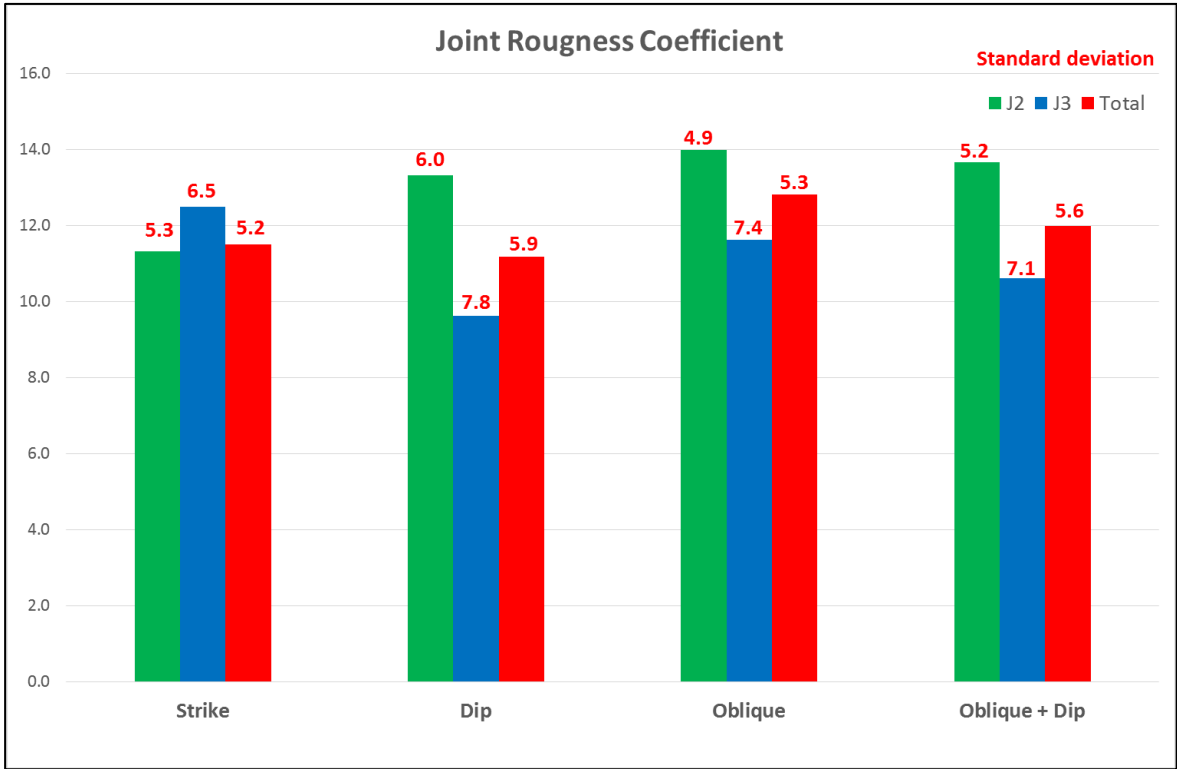


Figure 49: JRC values shown for the strike, dip and oblique measuring directions. Red numbers on top of each bar is the standard deviation for the sample. The JRC values are dimensionless and ranges from 0-20.

Figure 50 shows the calculated JCS values and standard deviations for J2, J3 and a total of all measured surfaces, leading to the following main observations:

- The difference in JCS value for J2 and J3 is relatively small (3.1 Mpa).
- All measurements combined (total) gave the highest JCS value and also the highest standard deviation.

The input values for JCS for the two joint sets J2 and J3, are taken from measurements on the respective surfaces, since the standard deviation is highest for the whole sample. The final JCS input values for J2 and J3 are respectively 149.7 and 152.8 Mpa.

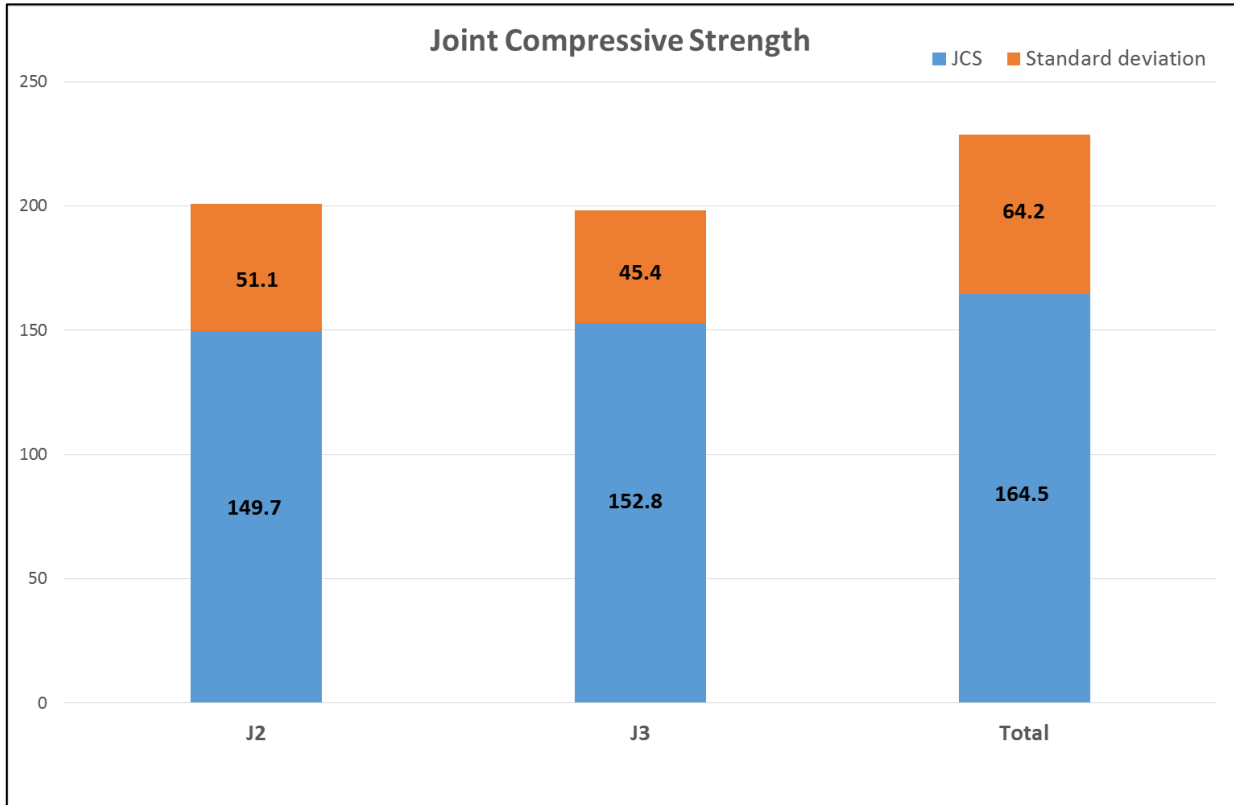


Figure 50: Mean JCS values and the standard deviation each joint set is graphically represented. The mean JCS value and standard deviation for all 26 measured surfaces (total) is also shown. All values are in Mpa.

The residual friction angle, φ_r , of weathered joints can be found empirically after equation 15, from Barton and Choubey (1977);

$$\varphi_r = (\varphi_b - 20) + 20 \frac{r}{R} \quad (15)$$

Where:

φ_r = Residual friction angle

φ_b = Basic friction angle

r = Schmidt hammer rebound value for wet, weathered joint surfaces

R = Schmidt hammer rebound value for dry, fresh joint surfaces

Fresh joint surfaces were not often represented in field, and the joint surfaces measured as R might have contained some degree of moisture. Based on the limited geological data, the residual friction angle is calculated from only one measurement of R , not corresponding to the orientation of either J_2 or J_3 . Values for r is taken from the same surface of weathered rock mass (Figure 51). The basic friction angle was determined by the tilt test in laboratory, discussed in chapter 5.4(Laboratory methods). Parameters for calculating the residual friction angle are shown in Table 22.

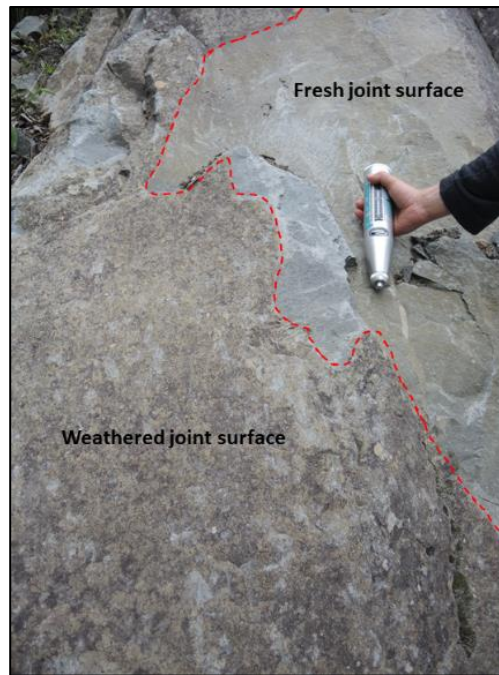


Figure 51: Surface showing both fresh unweathered rock where R is recorded and weathered rock where r is recorded.

Table 22: Parameters for calculating the residual friction angle

Parameter	Value	Comments	
φ_b	28.8 °	Determined from the tilt test performed in laboratory, following the ISRM standards. Mean of 36 measurements performed on three cylindrical samples of amphibolite from Amfiteateret (See Appendix 8.3 for details).	
R	58.2	Mean of the 10 highest of totally 20 records for one surface with hammer orientation 45° downwards. Taken at a dry, fresh surface with orientation 045/60. See Appendix 8.4 for details.	
r	J2 45.2	J3 45.9	Mean of the 10 highest of totally 20 records for each joint set. All records are converted to the same hammer orientation (45° downwards). See Appendix 8.4 for details.

Conversion from Barton-Bandis to Mohr-Coulomb parameters

Similar to the conversion of Hoek-Brown parameters of the rock mass, the discontinuity parameters have to be converted to equivalent Mohr-Coulomb parameters in order to apply the SSR-technique in RS². The procedure is similar by fitting a tangent to the non-linear Barton-Bandis criterion between shear strength and normal stress (Figure 47). The normal stress level (1.6 Mpa) is used to define the instantaneous cohesion and the instantaneous friction angle (see chapter 5.5.7 for details). The conversion is performed in the software RocData 5.0, where input parameters are JRC, JCS and residual friction angle for the Barton-Bandis criterion. By using the tool *Instantaneous MC Sampler*, the Mohr-Coulomb parameters used as input in the RS² model is determined.

Joint Stiffness

Before the advancement of finite-element and finite-difference computer methods, discontinuity properties were limited to friction parameters. With numerical methods available, stiffness properties of joints can be included in models containing discontinuities. The joint stiffness is defined by the shear stiffness (K_s) and normal stiffness (K_n), which describe the stress-deformation response before sliding occurs (Rosso, 1976).

For the numerical model at Kassen, K_n and K_s , are estimated as suggested by Rocscience (2016c). This calculation involves the normal and shear deformation modulus for the rock mass and intact rock, derived from the laboratory testing and relations given by Myrvang (2001). Calculation and resulting values for the joint stiffness parameters are shown in Appendix 8.6.

Joint Network Model

The joint sets are implemented in the model by using the Joint Network Model, which makes it possible to construct the joints with dip angle, spacing and persistence. By inserting orientation values for the trace plane (modeled cross section of the slope), true dip and dip direction can be directly inserted as input parameters. The joint spacing is exaggerated in the model in order to reduce computation time. This exaggeration is justified since the surrounding rock mass is modeled with Generalized Hoek Brown parameters, where true joint spacing is implemented indirectly through the GSI value. The persistence in the joint network model is defined differently than in structural geology, see Figure 52 for details.

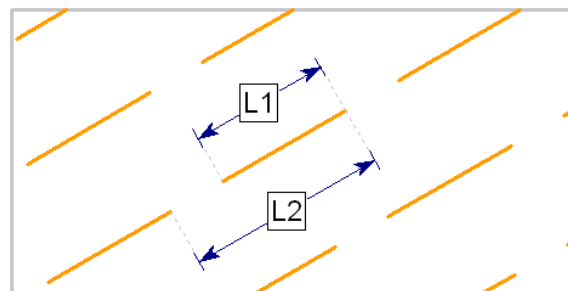


Figure 52: Persistence = $L1/L2$ in the RS^2 software. Figure from Rocscience (2016c).

Discontinuity input parameters in RS^2

Table 23, summarizes all input parameters related to the discontinuities J2 and J3 for the numerical modeling.

Table 23: Summary of input parameters for the joint sets J2 and J3 used for the numerical modeling.

Description	Symbol	Unit	Input		Remarks
			J2	J3	
Estimated for discontinuities based on Barton-Bandis shear strength criterion					
JRC (mean/min)	JRC	Mpa	13.7/5.5	12	Obtained through fieldwork. Mean/min refers to the mean value and lowest recorded value. The lowest values will give
JCS (mean/min)	JCS	Mpa	149.7/90	152.8	
Residual friction angle	ϕ_r	°	24.3	24.6	Fieldwork and laboratory
Equivalent Mohr-Coulomb parameters for $\sigma_n = 1.6$ Mpa					
Cohesion	c		0.43	0.33	Converted in RocData
Friction angle	ϕ	°	44.5	42.6	Converted in RocData
Joint stiffness					
Normal Stiffness	K_n	Mpa/m	102808.5	51404.3	Calculations recommended by Rocscience (2016c), and given in Appendix 8.6.
Shear Stiffness	K_s	Mpa/m	40476.0	20238.0	
Joint Network Model					
Joint Model	-	-	Parallel Statistical		The statistical model is chosen due to uncertainties regarding joint properties.
Joint end condition	-	-	Open at surface contact.		Field mapping of joints revealed that many were open at the surface (Table 1), and consequently the joint end is set as “open”. Open joint ends means that relative movement can occur at the joint end. Joint ends are defined as “closed” where the joints terminate into the rock mass.
Trace plane dip direction	-	°	270		The modeled cross-section through the slope is trending directly towards north, equal to a dip direction of 270°.
Dip	-	°	18	69	Based on 298 orientation measurements in Amfiteateret. See Figure 48.
Dip direction	-	°	009	308	
Spacing	-	m	10	40	Spacing and length are exaggerated values in order to reduce computation time. Generally, J2 showed denser spacing and shorter lengths than J3, which is reflected in the model. Real values are listed in Table 1.
Length	-	m	20	60	
Persistence	-	-	0.7	0.7	A persistence value of 0.7 is chosen for the rock mass in Amfiteateret to reflect its highly dissected character. See discussion above for definition of persistence in RS ² .

5.6 Stability assessment of Skipet

During field work 2016, two potential unstable blocks were observed at the eastern, upper corner of Skipet (see Figure 53 and Figure 54). Motivated by the historic event from 1985, a stability analysis of these two blocks is performed by using Limit Equilibrium Methods (LEM) as this technique is highly relevant to simple block failures along known discontinuities (Eberhardt, 2003).

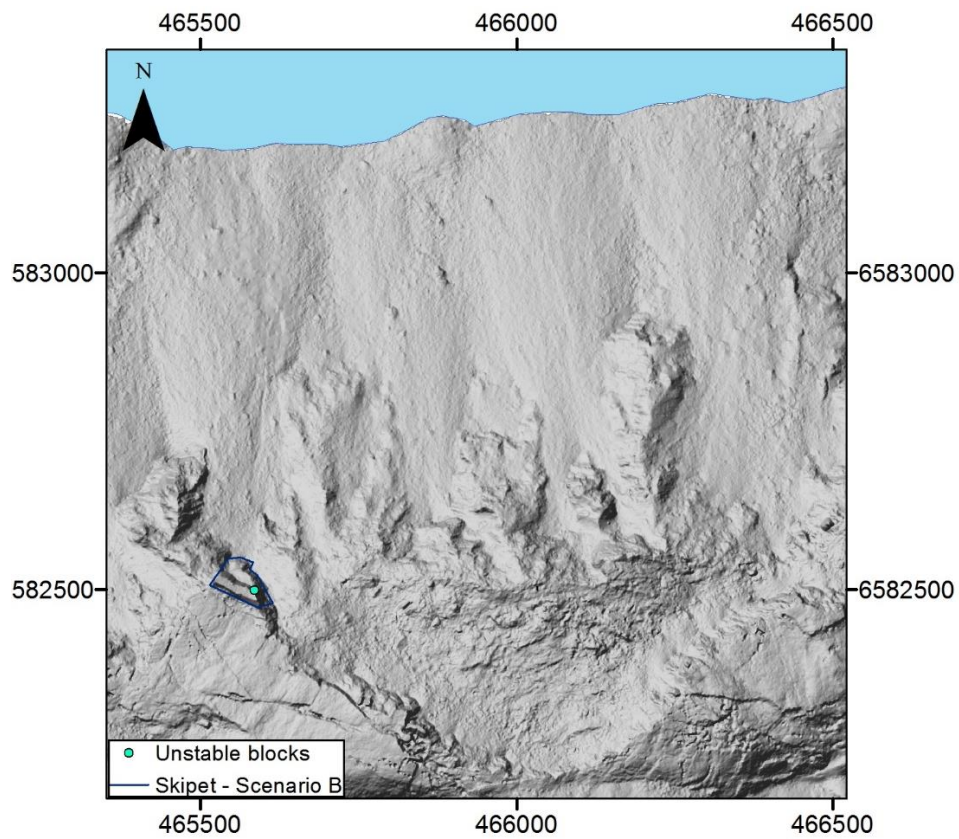


Figure 53: Location of the unstable blocks at the upper eastern side of Skipet.

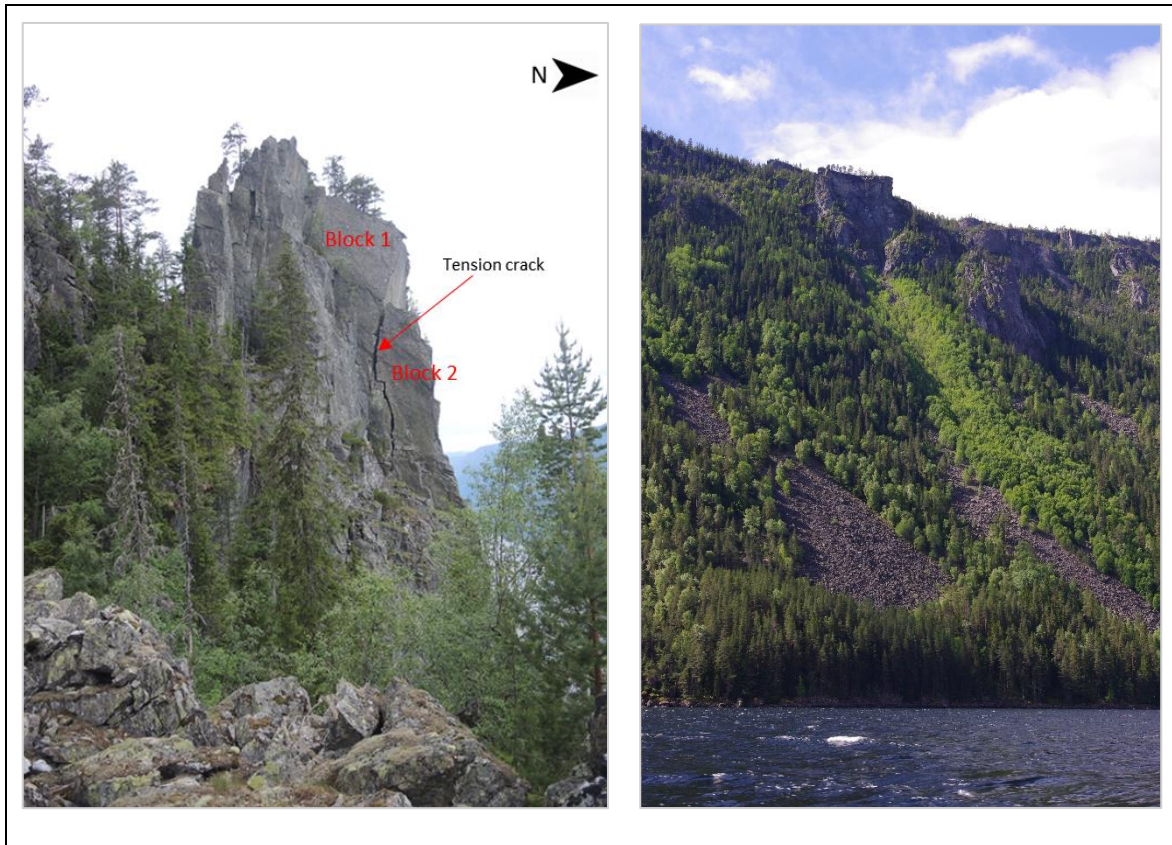


Figure 54: The left photo shows the two unstable blocks at Skipet. The light vegetation below Skipet in the right photo indicates that rock fall from Skipet has occurred in the past, and is believed to show the track from the 1985 event.

The two blocks have been tested for the possibility for toppling and planar failure. The blocks can topple if the center of gravity lies outside the base, given by Equation 16 (Wyllie & Mah, 2004), which from now is referred to as the block shape test. Figure 55 shows an example of a block that will topple.

$$\frac{\Delta x}{y} < \tan \psi_p \quad (16)$$

Where: Δx = width of the block
 y = height of the block
 ψ_p = inclination of the sliding surface

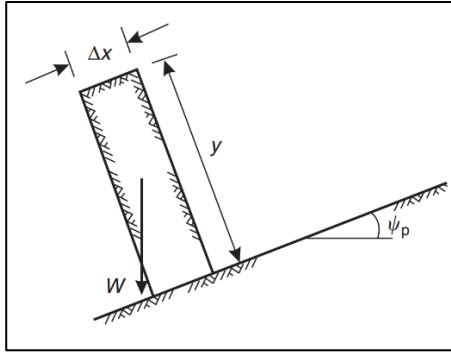


Figure 55: The height/width ratio of a block at an inclined surface will determine if the block will slide or topple.
Figure modified from (Wyllie & Mah, 2004)

The possibility for planar failure of the blocks is investigated through a LEM analysis, where the FS is determined by the ratio of resisting to driving forces, given by Equation 17 (Wyllie & Mah, 2004):

$$FS = \frac{\text{resisting forces}}{\text{driving forces}} \quad (17)$$

The resting forces acting on a plane for dry conditions is the shear strength (τ), and the driving forces is the weight of the block (W):

$$FS = \frac{\tau A}{W \sin \psi_p} \quad (18)$$

The shear strength of the sliding planes for the blocks at Skipet are best described with the Barton-Bandis criterion as they are rough surfaces. Inserting the Barton-Bandis shear strength criterion (presented in chapter 5.3) in Equation 18, gives:

$$FS = \frac{A * \sigma_n * \tan \left(\varphi_r + JRC \log_{10} \left(\frac{JCS}{\sigma_n} \right) \right)}{w \sin \psi_p} \quad (19)$$

The normal stress level (σ_n) in Equation 19 is the sum of normal forces acting on the plane ($\sum N$) divided by the area of the plane (A). For the case of dry slope conditions, the normal forces are the weight of the block (W) acting perpendicular to the sliding plane (Figure 56). σ_n for these conditions are given by Equation 20:

$$\sigma_n = \frac{\sum N}{A} = \frac{W \cos \psi_p}{A} \quad (20)$$

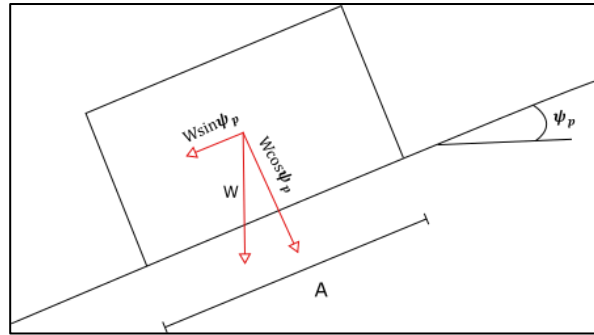


Figure 56: Under dry slope conditions, the vector components of the weight of the block control the driving and resisting forces as shown in the above equations.

Inserting Equation 20 into Equation 19 gives Equation 21, and finally Equation 22:

$$FS = \frac{W \cos \psi_p * \tan \left(\varphi_r + JRC \log_{10} \left(\frac{JCS}{\sigma_n} \right) \right)}{w \sin \psi_p} \quad (21)$$

$$FS = \frac{\tan \left(\varphi_r + JRC \log_{10} \left(\frac{JCS}{\sigma_n} \right) \right)}{\tan \psi_p} \quad (22)$$

Until now, all presented equations have represented dry slope conditions. If groundwater is present in the slope, the forces U and V will increase the driving forces and decrease the resisting forces. A conceptual model is shown in Figure 57.

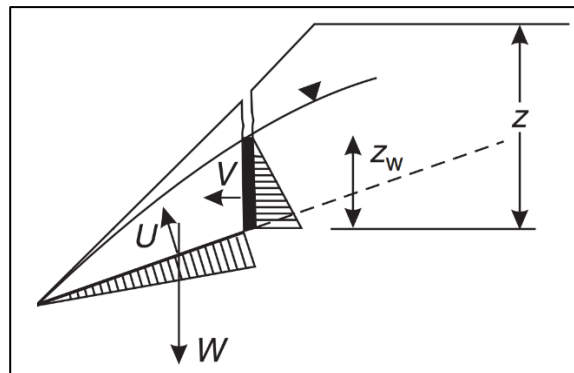


Figure 57: Slope with groundwater. The forces U and V will decrease the stability. Modified from Wyllie and Mah (2004).

The assumed present groundwater level is located beneath Skipet, however if a heavy rainstorm event occurred in the area, some amount of water pressure could build up in the cracks delimiting the blocks. The tension crack at Block 2, is the only open crack, and it is believed that surface water from a rainstorm would flow directly into this crack. The analysis including water pressure is therefore limited to the tension crack of Block 2, as the remainder of the rock mass is relatively impermeable. Adding the water pressure from the tension crack

(V) to equation 21 gives Equation 23, where the tension crack is assumed to be close to vertical.

$$FS = \frac{(W \cos \psi_p - V \sin \psi_p) * \tan \left(\varphi_r + JRC \log_{10} \left(\frac{JCS}{\sigma_n} \right) \right)}{W \sin \psi_p + V \cos \psi_p} \quad (23)$$

The distribution of water pressure, V, will occur as a triangular shape due to impermeable conditions at the bottom of the tension crack. V is in such a case given by the specific weight of water (γ_w) and the water height in the tension crack (z_w), after Wyllie and Mah (2004):

$$V = \frac{1}{2} \gamma_w z_w^2 \quad (24)$$

The FS for the two blocks were found by applying Equation 22, for dry slope conditions. Equation 23 was applied to investigate the effect of increased water pressure in the tension crack at Block 2.

The Barton-Bandis parameters JRC and JCS were measured in field, and calculated as described in 5.4. The measurements were taken at the southeastern side of Skipet, at a J2 surface with orientation 019/30, which is believed to have the same characteristics as the sliding surfaces for the two blocks with dip angles of 30 and 37°. As for the calculations of JRC in Amfiteateret, only the measurements in the fall and oblique directions are included, as sliding is unlikely to occur in the strike direction. The residual friction angle is calculated by using the same Schmidt hammer rebound value (R) as in Amfiteateret, since only one fresh rock surface was found during fieldwork. Rock density and basic friction angle is taken from laboratory work of the rock sample collected from Amfiteateret.

5.7 Results from numerical analysis of Amfiteateret

Step 1 – Stress, groundwater and mesh set up

The initial stress set-up for the model is based on the in-situ measurements from a borehole located in the lower part of a 900 meter high slope, 21 km away from Kassen. It became clear when analyzing maximum shear strain plots of the computed model, that the selected field stress properties were not representable for the situation at Kassen. Maximum shear strain plots should give an indication of where the most likely failure surface is located. Determination of appropriate field stress was therefore performed through a number of trial and error cycles. Different values of the in plane and out of plane total stress ratio were varied, until the resulting shear strain plot seemed reasonable for the slope at Amfiteateret (Table 24). All analyses of the field stress properties were done with a *Gravity Field* using the *actual ground surface*.

Table 24: Overview of the different field stress configurations applied for the model.

Analysis #	Total stress ratio (horiz/vert)		CSRF	Remarks
	<i>In Plane</i>	<i>Out of Plane</i>		
Stress configurations				
1	0.71	1.55	4.60	Stress measured in borehole <i>Dalen Tokke01</i>
2	0.5	0.5	4.56	Recommended by Eberhardt (2003).
3	1	1	4.60	
4	2	3	4.64	Gave most reasonable shear strain plot in the slope.
5	3	2	4.63	
6	0.37	0.37	4.57	Horizontal stress components are pure gravitational, equation after Myrvang (2001) based on the gravitational vertical stress (σ_v) and Poisson's ratio (ν): $\sigma_h = \frac{\nu}{1 - \nu} \sigma_v$

The SSR Search area were applied to all analyses and performed for dry slope conditions. Material properties for the rock mass are converted Mohr-Coulomb parameters in order to apply the SSR method. Analysis 4, with an *in plane* and *out-of-plane* stress ratio of respectively 2 and 3 gave the most reasonable shear strain plot (Figure 58). The figure show the situation for SRF higher than the CSRF, in order to highlight the failure surface better.

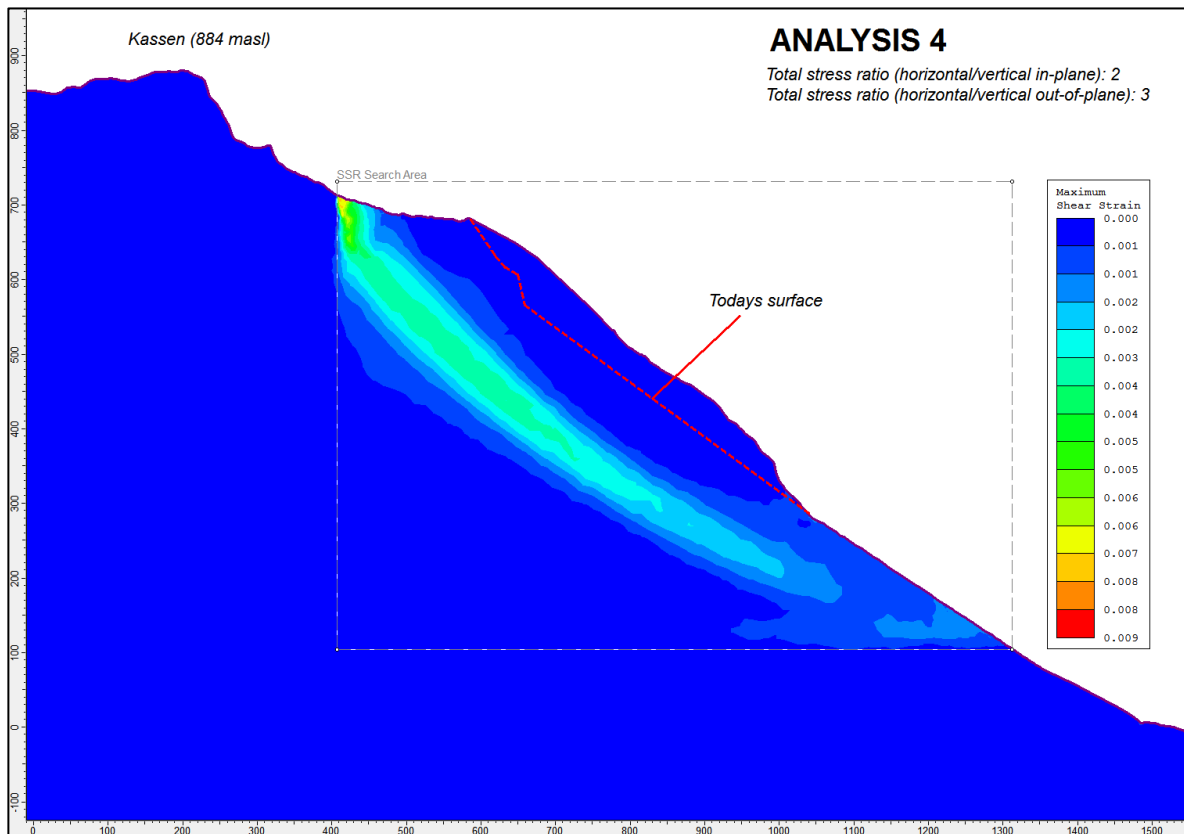


Figure 58: Maximum shear strain plot of analysis 4. The surface for the given stress field is located deeper than the historic slide surface, which is the present ground surface today (indicated by a red dotted line in the figure). A possible reason for the deep failure surface in the model can be the lack of discontinuities in the model, and therefore the rupture surface appears as a circular failure through the rock mass. Note that the figure represents the situation at a SRF of 4.65 while the CSRFS is 4.64.

With the field stress set up of analysis 4, two groundwater tables were added to the model; the assumed present groundwater (discussed in chapter 5.5.6) and a high groundwater table. The high groundwater table coincides with the slope surface, reflecting totally saturated slope conditions. To verify the chosen field stress set-up, a high groundwater table was also added to the stress set up of analysis 1 (stresses taken from the borehole at Tokke) which supports that a change of field stresses were necessary (Figure 59).

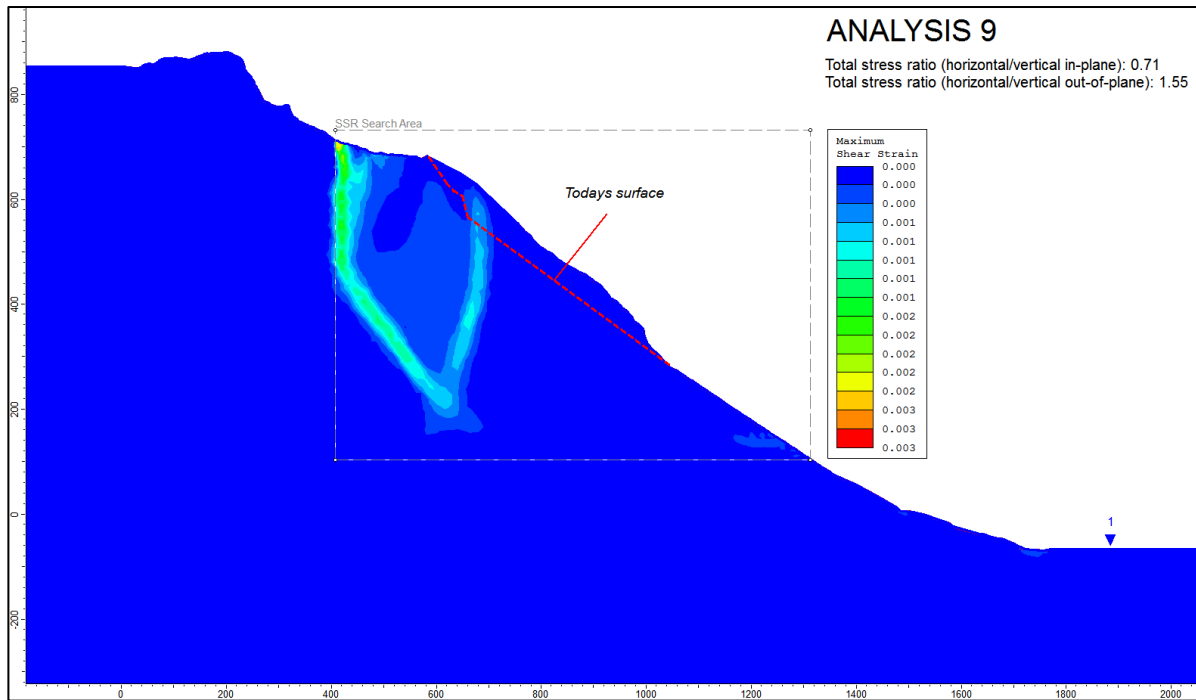


Figure 59: Shear strain plot for the model with field stress equal to the measurements from the borehole Dalen Tokke 01. Based on this plot it was decided to change the field stress to achieve a maximum shear strain plot representing a more likely failure surface.

Two different mesh set-ups were applied to the high ground water model in order to investigate the resulting effects;

1. *Graded mesh type with 6 Noded Triangles* element type. This set up resulted in a meshed model of 23210 nodes and 11241 elements. This mesh set-up is noted “Normal” in the further discussions.
2. *Advanced Mesh Regions* by adding a region corresponding to the SSR search area, where element lengths of 61 m. This set up resulted in a meshed model of 4604 nodes and 2127 elements. This mesh set-up is noted “Advanced” in the further discussions.

As Table 25 shows, the CSRF is reduced with 31 % when lowering the groundwater table from high to present for the normal mesh set up. The difference in CSRF between dry and totally saturated slope conditions is 1.85. These observations indicate that water pressure in the slope is a controlling factor for the stability.

The effect of changing the mesh set up from normal to advanced gave an marginally increased CSRF of 0.06. The advantage of the advanced mesh is less computation time for each analysis. However, the change in mesh set up from normal to advanced, effected the resulting maximum shear strain plot as seen in Figure 60. The interpreted potential failure surface indicated by the maximum shear strain is not realistic for the slope. Additionally, maximum shear strain contours cluster around the upper right corner of the SSR Search Area, indicating that the current combination of mesh and SSR Search Area is not ideal. Based on these observations, all further analyses are performed with the normal mesh set up.

Table 25: Overview of the analyses concerning the mesh and groundwater set up.

Analysis #	Mesh	Groundwater	Field stress (In plane/out of plane)	CSRF
6	Normal	Present	2/3	3.66
7	Normal	High	2/3	2.79
8	Advanced	High	2/3	2.85
9	Normal	High	0.71/1.55	2.79

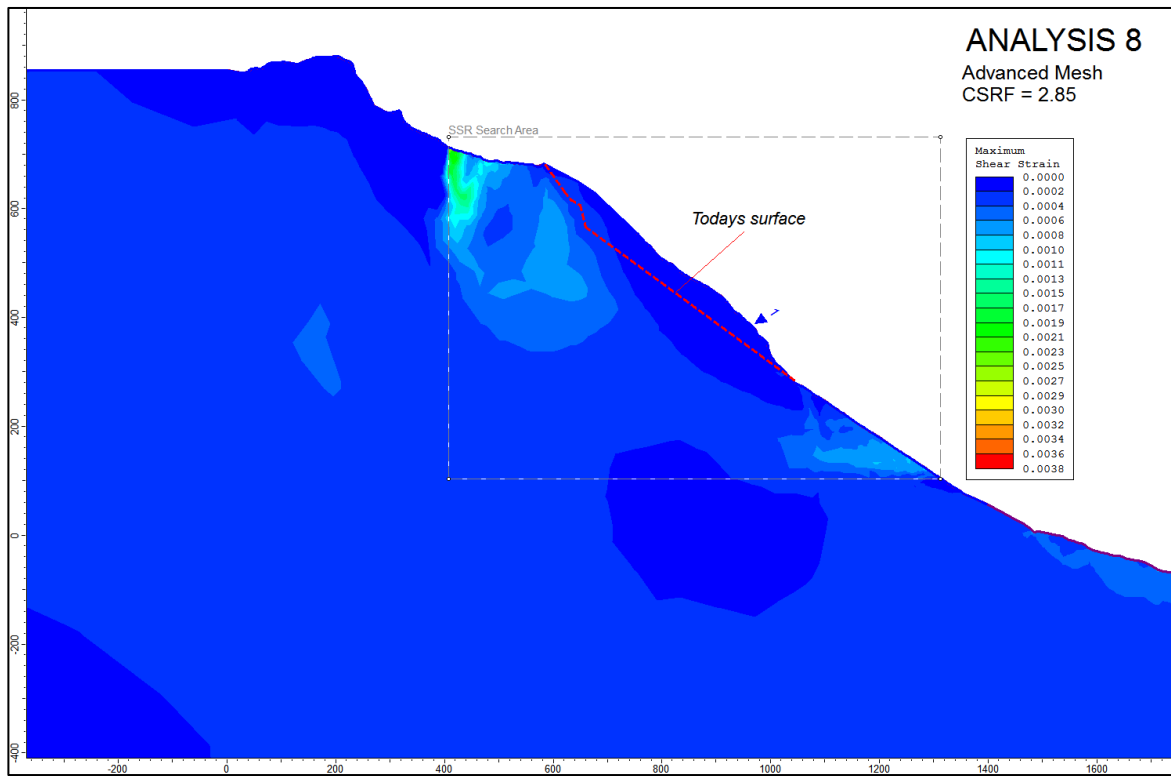


Figure 60: Maximum shear strain plot of the advanced mesh model giving a CSRF of 1.85.

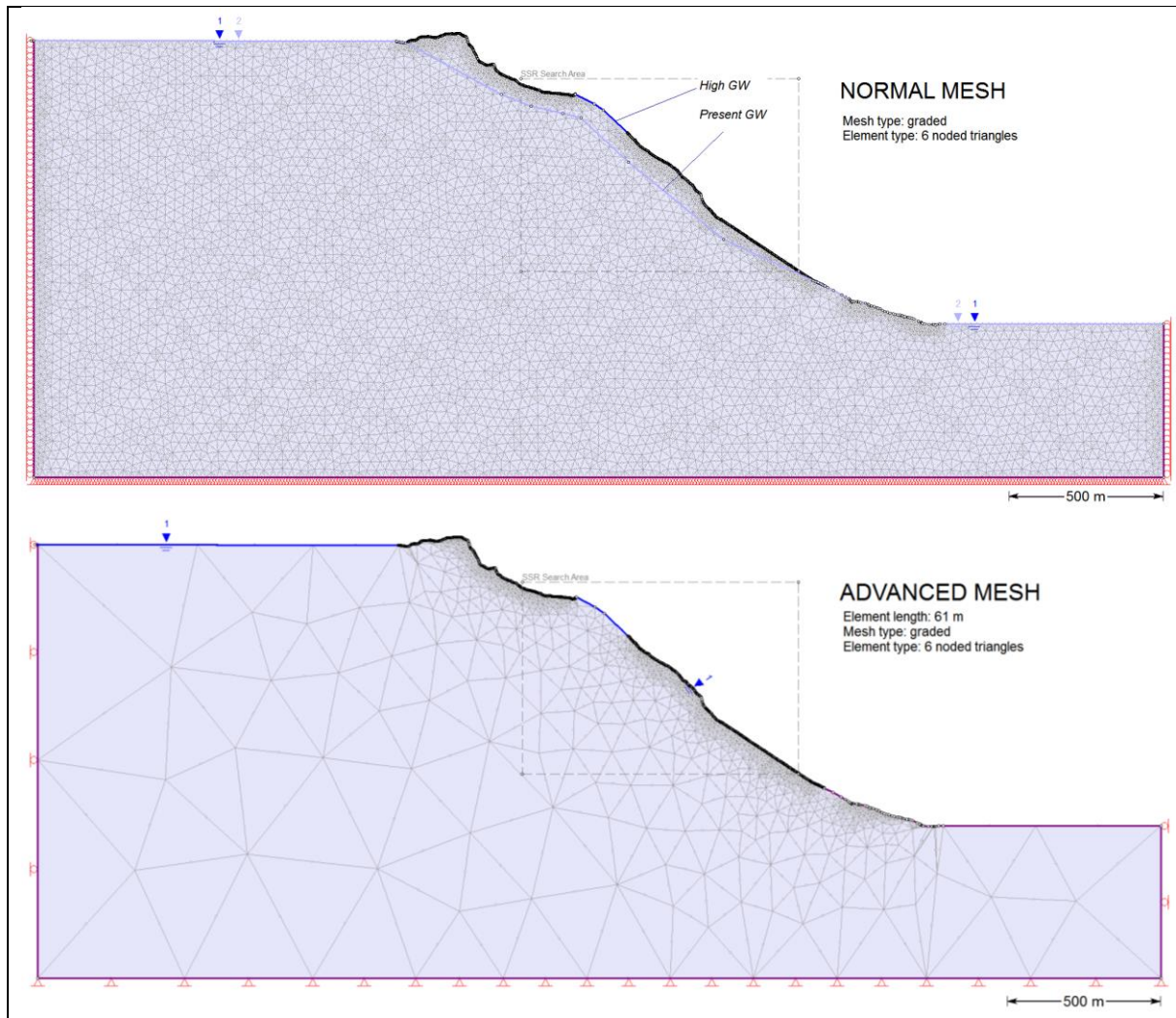


Figure 61: Normal and advanced mesh set up. The amount of nodes and elements are significantly decreased for the advanced mesh resulting in faster computation time.

Step 2 – Failure sequence

This step is performed in order to analyse if the presented deformation theory (chapter 5.5.1) can be confirmed by numerical analyses. In situ stresses from analysis 4 in the previous step is applied, with an elastic material model since the aim is to analyse stress distribution.

Comparing the stress ratio between the major and minor principle stress can indicate if the stress anisotropy increased after the assumed low-velocity deformation in Amfiteateret. Stress anisotropy can cause displacement, and hence formation of tension cracks and reduction of shear strength (Panthi & Nilsen, 2006). These processes could in turn be an influencing factor for the collapse in the frontal part of Amfiteateret.

Computed differential stress plots (Figure 62) show an unexpected result; the stress anisotropy in the rock mass actually decreases significantly after the deformation in Amfiteateret. The performed numerical modeling can therefore not support the proposed deformation theory.

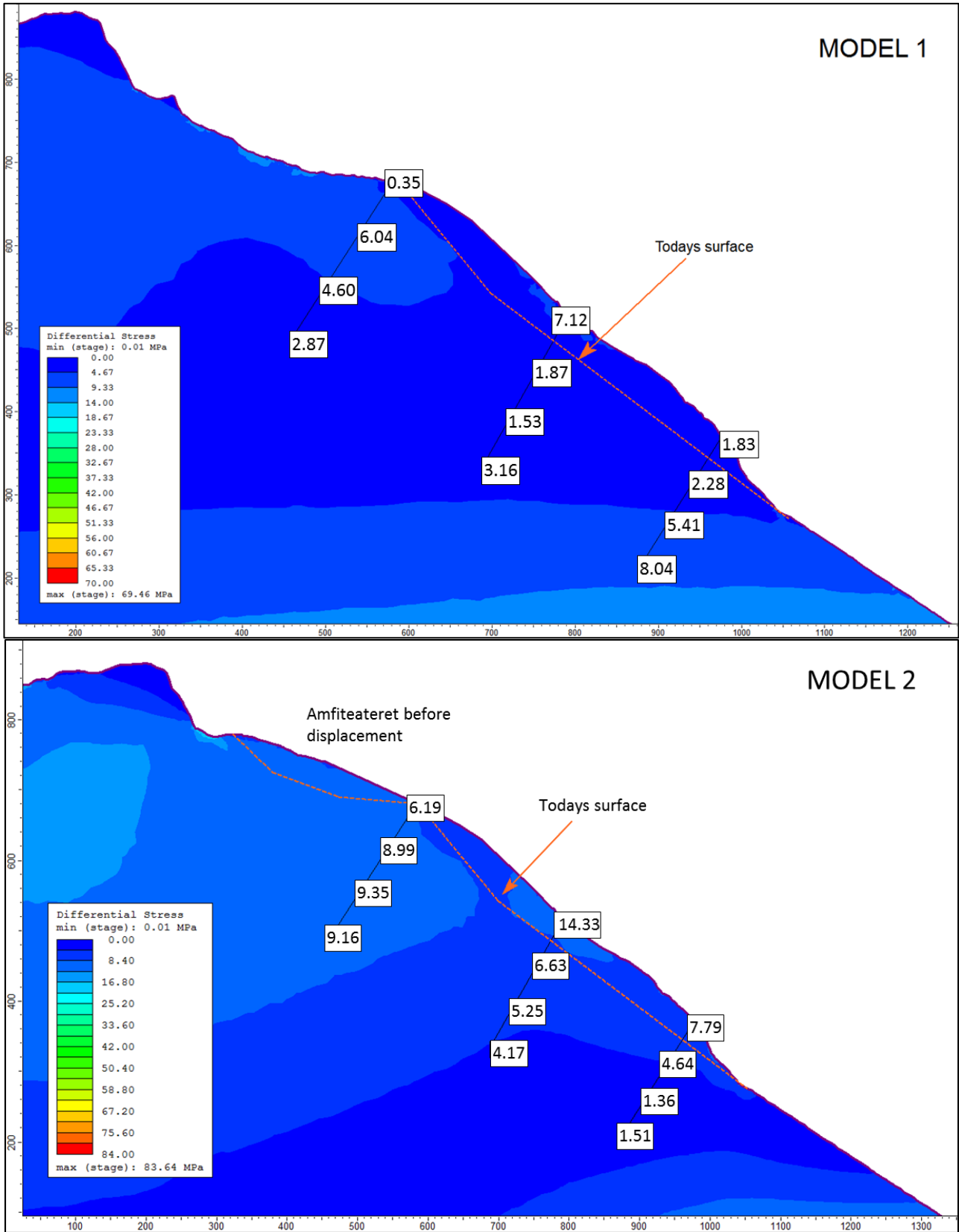


Figure 62: Differential stress plot before (Model 1) and after (Model 2) the deformation of Amfiteateret. Numerical values of the differential stresses are shown for equal locations in the two models in Mpa. Horizontal and vertical axes are in meters.

Step 3 - Effect of joints

In the third step of the numerical analysis, the joints were added in a joint network model. The boundaries of the network model is set inside the SSR-search area and extending inwards in the slope (Figure 63). Both mean and lowest joint strength properties are evaluated with Mohr-Coulomb criterion (Table 23). All analyses are performed with a linear elastic – perfectly plastic material and joint model, meaning that peak values equal residual values. Several different joint configurations are tested as shown in Table 26, and the resulting CSR_F is plotted against the factored peak friction angle for the rock mass in Figure 64. The groundwater table is varied from present to high.

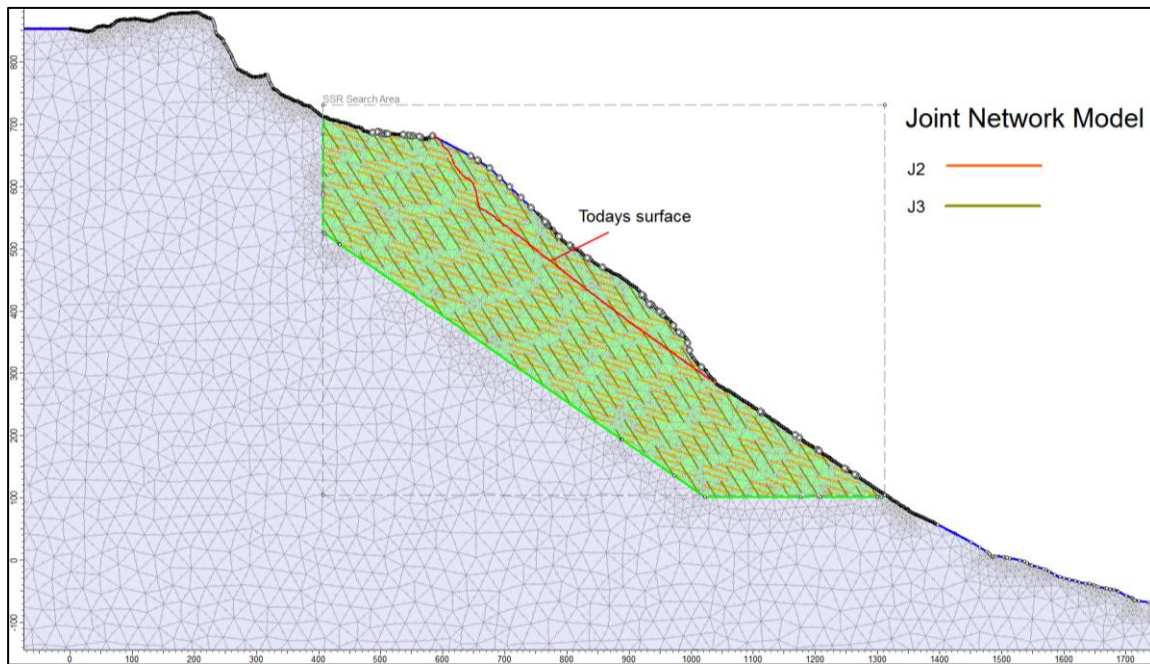


Figure 63: Set up of the joint network model.

Table 26: Overview of the analyses performed in Step 3. Reference analyses are from Step 1.

Analysis #	Included joints	Groundwater	Strength properties of joints
Reference 1	No joints	high	-
Reference 2	No joints	present	-
1	J2	high	mean
2	J2	high	lowest
3	J3	high	mean
4	J2, J3	high	mean
5	J2, J3	high	lowest
6	J2	present	lowest
7	J2, J3	present	lowest

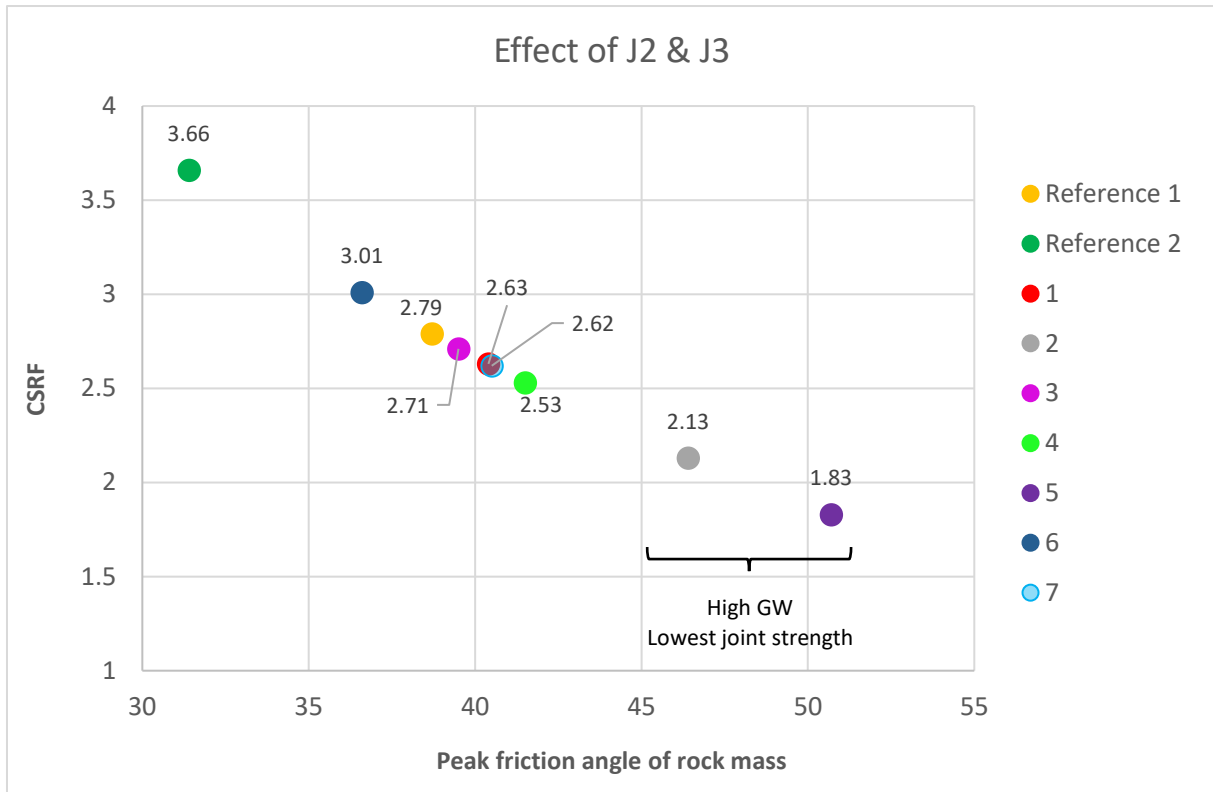


Figure 64: CSRf plotted against factored peak friction angle for the rock mass for analysis 1-7.

The following main results can be drawn from Step 3 of the numerical modeling:

- The joint set J2 has a marginally higher influence on the slope stability than J3. Adding the joint sets one at the time to the model decreased the CSRf with respectively 6 % and 3 % for J2 and J3. The lowest CSRf is obtained when both joint sets are added to the model, which is in correspondence with previous stability assessments where biplanar failure including these joint sets are highlighted as a possible failure mechanism (results from specialization project, chapter 2.4).
- Critical Strength Reduction Factors (CSRf) reveal that the stability of the slope is more sensitive to changes in groundwater levels for models with joints than the reference models without joints. For models where only the location of the groundwater table differs from present to high, the CSRf is reduced by approximately 0.9.
- Analyses with constant groundwater table and reduced peak strength properties of the joints from mean values to the lowest recorded values gives a reduction in CSRf of 0.5-0.7.
- The two above points show that the models are more sensitive to changes in groundwater level than changes in joint strength for the input values used in this numerical modeling.
- The lowest CSRf was obtained in analysis 5, where the computed plots of total displacement show that displacement in the slope partly follow the joint surfaces (Figure 65).

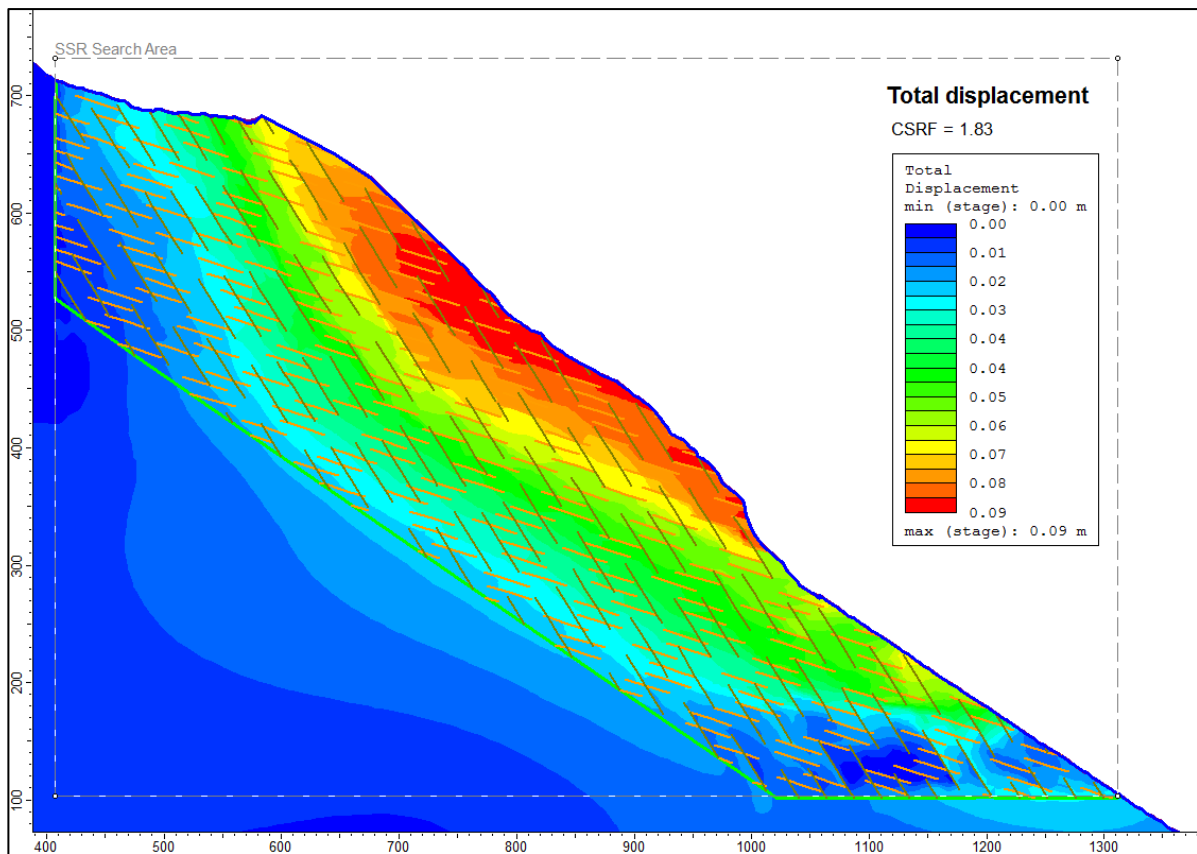


Figure 65: Zoom in of total displacement for analysis 5. Displacement contours partly align with joint orientation, indicating that displacement follow the joints. Irregular contours may indicate the failure of rock bridges, as the joints are modeled as discontinuous. Maximum displacement is 9 cm.

Step 4 – Parameter study on J2 properties

As the previous step in the numerical analysis showed, J2 is the joint set influencing the stability the most. This is also confirmed through the kinematic feasibility test performed in the specialization project. Therefore, a parameter study of the joint strength properties (cohesion and friction angle) and stiffness parameters for J2 are carried out in this step of the analysis. The parameter study is conducted as described in Table 27 and Table 28 for respectively the strength and stiffness parameters. Results are shown in Figure 66. The rock mass and joints are modeled as linear elastic – perfectly plastic.

Table 27: Overview of how the parameter study of the strength properties cohesion and friction angle is conducted. The parameters are decreased one at the time with 30, 50 and 80 % while keeping all other input values constant.

Analysis #	Friction angle	Cohesion
Reference	44.5	0.43
1	Peak value	30 % reduced
2	Peak value	50 % reduced
3	Peak value	80 % reduced
4	30 % reduced	Peak value
5	50 % reduced	Peak value
6	80 % reduced	Peak value

Table 28: Overview of the parameter study of the stiffness parameters for J2. The parameters are only reduced since the initial values are quite high.

Analysis #	Reduction [%]	Normal Stiffness [Mpa/m]	Shear Stiffness [Mpa/m]
Reference	0	102808.5	40476.0
7	30	71966.3	28333.2
8	50	51404.5	20238.0
9	80	20561.8	8095.2

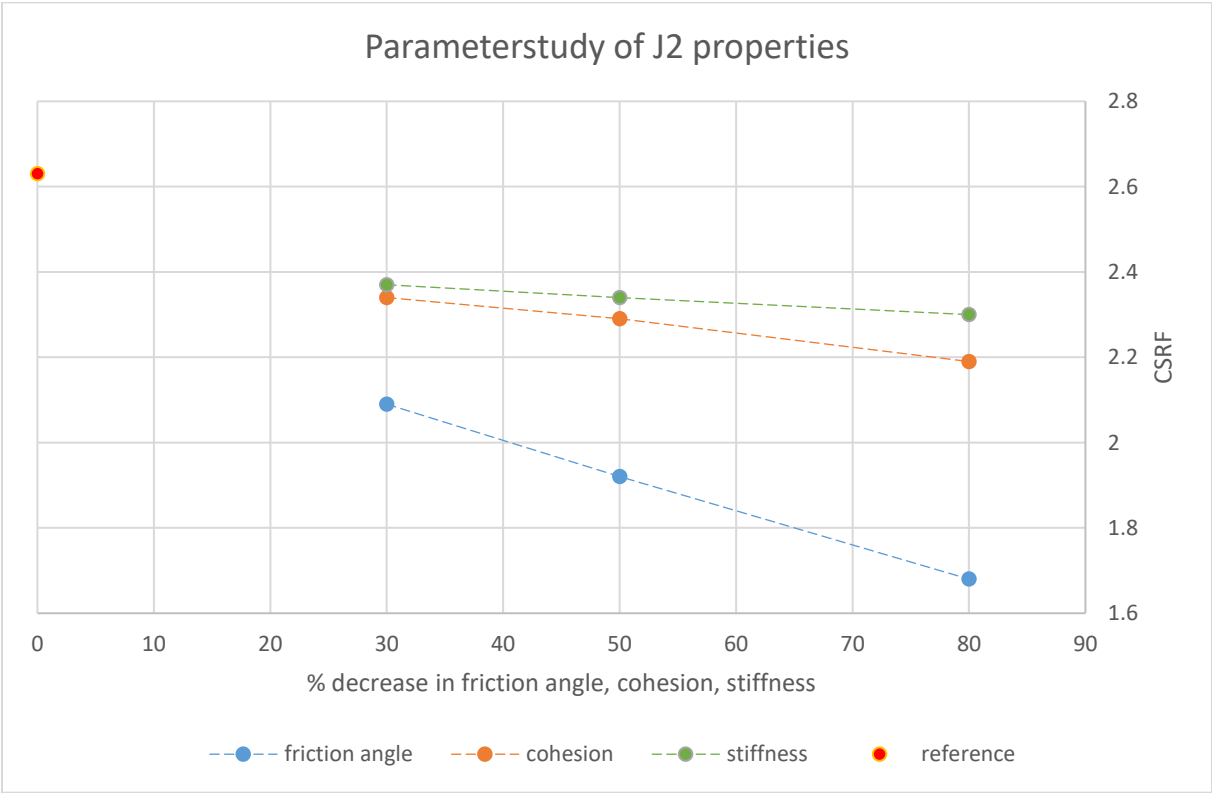


Figure 66: CSRf is plotted for analysis 1-9 where the friction angle, cohesion and joint stiffness is reduced one at a time.

The stability of the slope, evaluated by CSR values, is most sensitive to a decrease in the friction angle. Reducing the friction angle with 30, 50 and 80 % gave a reduction in CSR from 20.5 to 36.1 %. The similar range when reducing the other tested parameters gave 11.0 to 16.7 % reduction for the cohesion and 9.9 to 15.2 % reduction for the stiffness. It is also notable that the CSR decreases linearly when reducing the friction angle. This is expected due to the linear relationship between shear strength and friction angle in the Mohr-Coulomb strength criteria (Equation 3, chapter 5.1).

Step 5 – Strain softening, 2 layered model

Until now, the joints J2 and J3 have been modeled as discontinuous joints, meaning that rock bridges are included in the model. However, the rock mass in the area of Amfiteateret is highly dissected and therefore an approximately 50 m deep layer of continuous joint sets is added as a new joint network to reflect these conditions (Figure 67). The depth of continuous joints are uncertain, as joint persistence towards the depth is an unknown parameter due to infill of blocks in open cracks in the area.

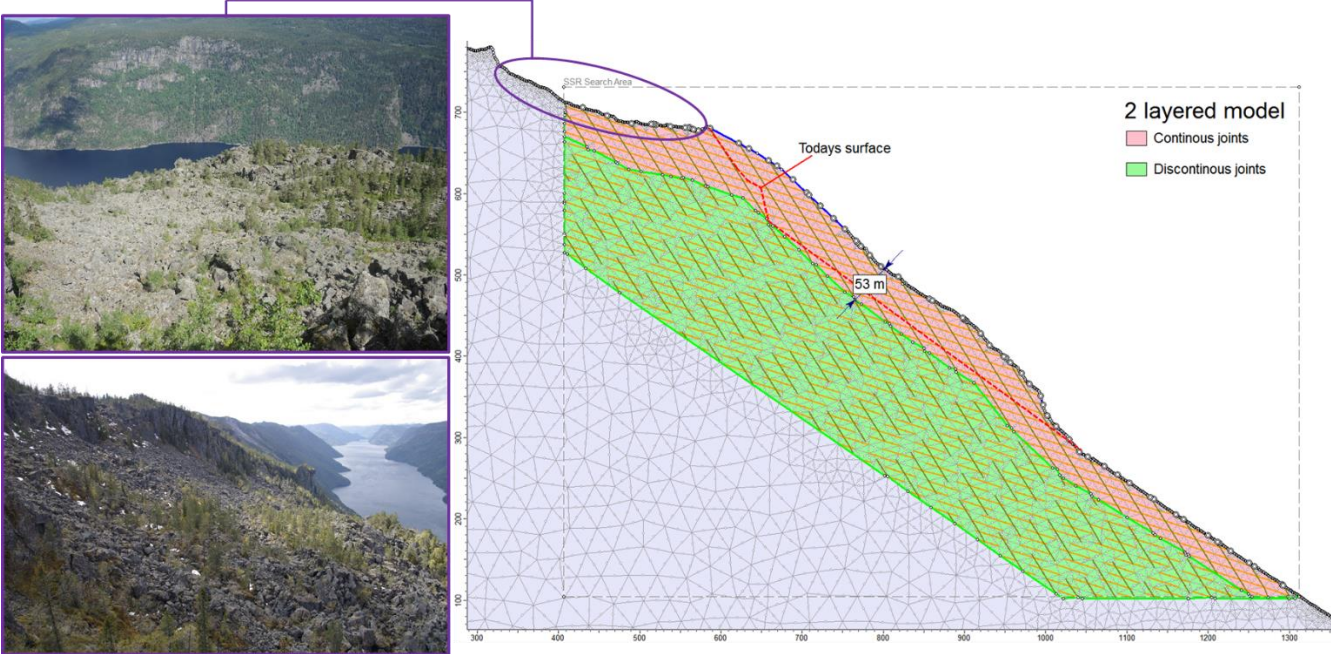


Figure 67: Set up of the two layered model, where J2 and J3 are modeled as continuous joints in the upper layer (marked with pink). The pictures to the left show the dissected rock mass in Amfiteateret in the area outlined with purple. The lower picture is taken from the eastern side and the upper picture is taken from the western side of Amfiteateret.

All analysis in the previous steps are conducted with a linear elastic – perfectly plastic material model for both joints and rock mass. As discussed in chapter 5.2, brittle rocks often fail progressively, which can be modeled with a plastic – strain softening model. The effect of strain softening on the CSR is therefore analyzed in this step of the numerical analysis for the two layered joint model. Different set ups are tried through six analysis, where the groundwater level, joint strength and material model are varied (Table 29). Residual values for the softening models are 2/3 of peak values as recommended by Trinh (2016). The peak material strength is constant for all analysis for both joints and the surrounding rock mass.

Table 29: Overview of analyses performed in step 4. Analyses 1-4 is done systematically to investigate the effect of strain softening material models. Analyses 5-7 are performed with different set-ups in order to reach unstable slope conditions.

Analysis #	GW table	Joint strength	Joint model	Material model
1	High	Mean	Linear elastic – perfectly plastic	Linear elastic – perfectly plastic
2	High	Mean	Plastic – strain softening	Plastic – strain softening
3	Present	Mean	Linear elastic – perfectly plastic	Linear elastic – perfectly plastic
4	Present	Mean	Plastic – strain softening	Plastic – strain softening
5	Present	Low	Plastic – strain softening	Plastic – strain softening
6	High	Low	Linear elastic – perfectly plastic	Linear elastic – perfectly plastic
7	Dry	Low	Plastic – strain softening	Plastic – strain softening

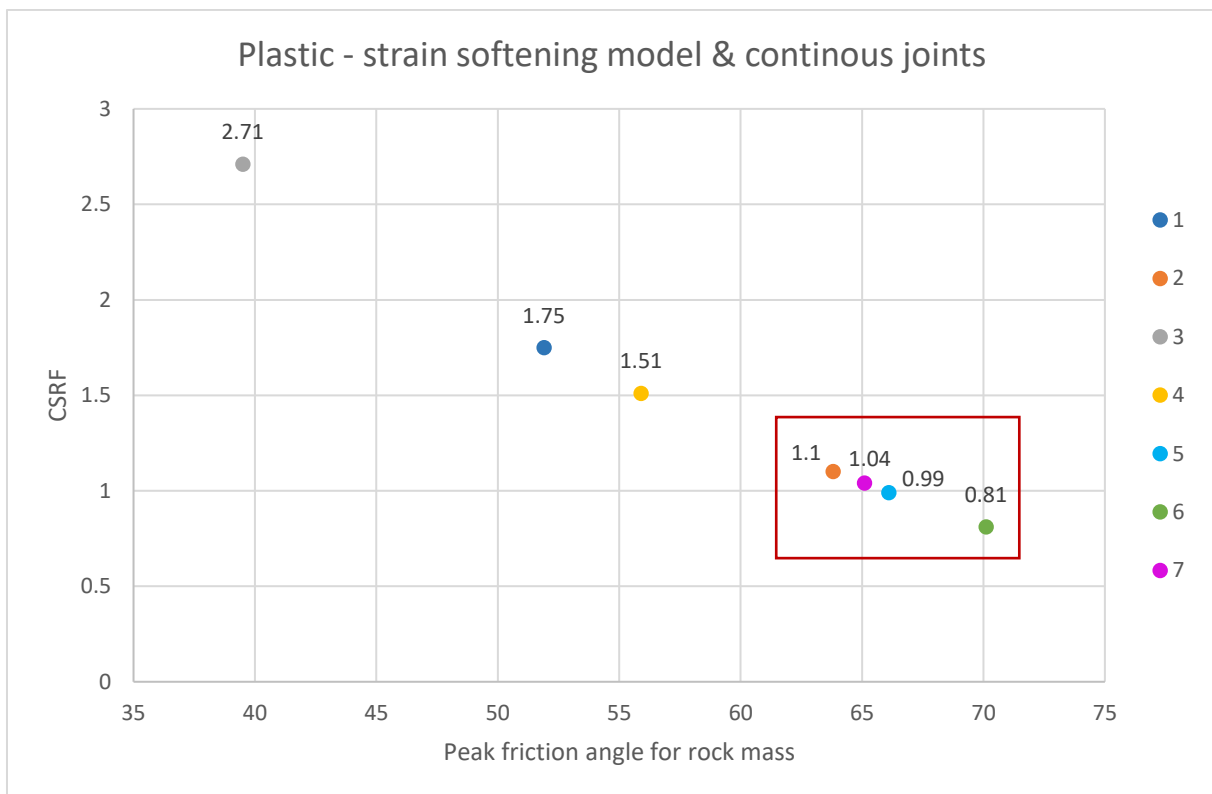


Figure 68: CSRF plotted against the factored peak friction angle for the rock mass. CSRF lower than one is per definition unstable, the analyses close or below this value are outlined with red.

In analyses 1-4 the effect of strain softening models for the joints and the rock mass is tested systematically by comparing linear elastic – perfectly plastic models to plastic – strain softening models for respectively a high groundwater table and present groundwater table. Analysis 2 show slope conditions close to failure (CSRF = 1.1). The three last analyses (5-7) show unstable

slope conditions ($CSR_F < 1$) for dry slope, present groundwater and high groundwater. The following main observations can be drawn from Step 5 of the numerical analysis:

- Modeling the joints as continuous instead of discontinuous (as in step 3) decreases the CSR_F by 4.4 %.
- The effect of lowering the groundwater table from high to present in the two-layered model (all other parameters constant) reduced the CSR_F by 35.4 % and 27.2 % for respectively elastic-perfectly plastic models and plastic-strain softening models. All other parameters were kept constant.
- The greatest effect on the CSR_F were achieved when changing the material model from linear elastic – perfectly plastic to plastic – strain softening. For analyses with high groundwater table (1 and 2), the CSR_F decreased with 37.1 %. For analyses with present groundwater table (3 and 4) the CSR_F decreased with 44.3%. The CSR_F for analysis 2 (high groundwater table and strain softening model) is 1.1, close to unstable conditions.
- Analysis 7 show that for dry slope conditions and present groundwater level, unstable conditions are reached for the lowest joint strength values with strain softening material and joint models where the residual strength value equal to $2/3$ of peak strength. The CSR_F for respectively no groundwater and present groundwater are 1.04 and 0.99.
- Analysis 2 and 6 both show unstable conditions for a high groundwater table. For the strain softening model (analysis 2), the slope becomes close to unstable ($CSR_F = 1.1$) when using the mean joint strength values. For the linear elastic – perfectly plastic model, unstable conditions are reached when applying the lowest strength of the joints. The resulting CSR_F of 0.81 indicates that even with slightly higher strength of the joints, the slope would fail.

Figure 69 shows total displacement and deformation vectors for analysis 3. Maximum displacement coincides fairly good with the Bandak rock avalanche scar (today's surface). Displacement follows the continuous joints indicating translational sliding for the given set up. Shear strain plots of the same situation shows no visible shear strain, which could indicate that slip occurs only at the joint interfaces, supporting the theory of translational sliding (Figure 70).

One interesting observation is the difference in deformation vectors for the upper and lower part of the slope. In the upper part, deformation vectors are parallel with J3, while they align with J2 in the lower part. This can be interpreted as an indication of a bi-linear failure where J3 surfaces act as the rear release plane and J2 as the sliding plane.

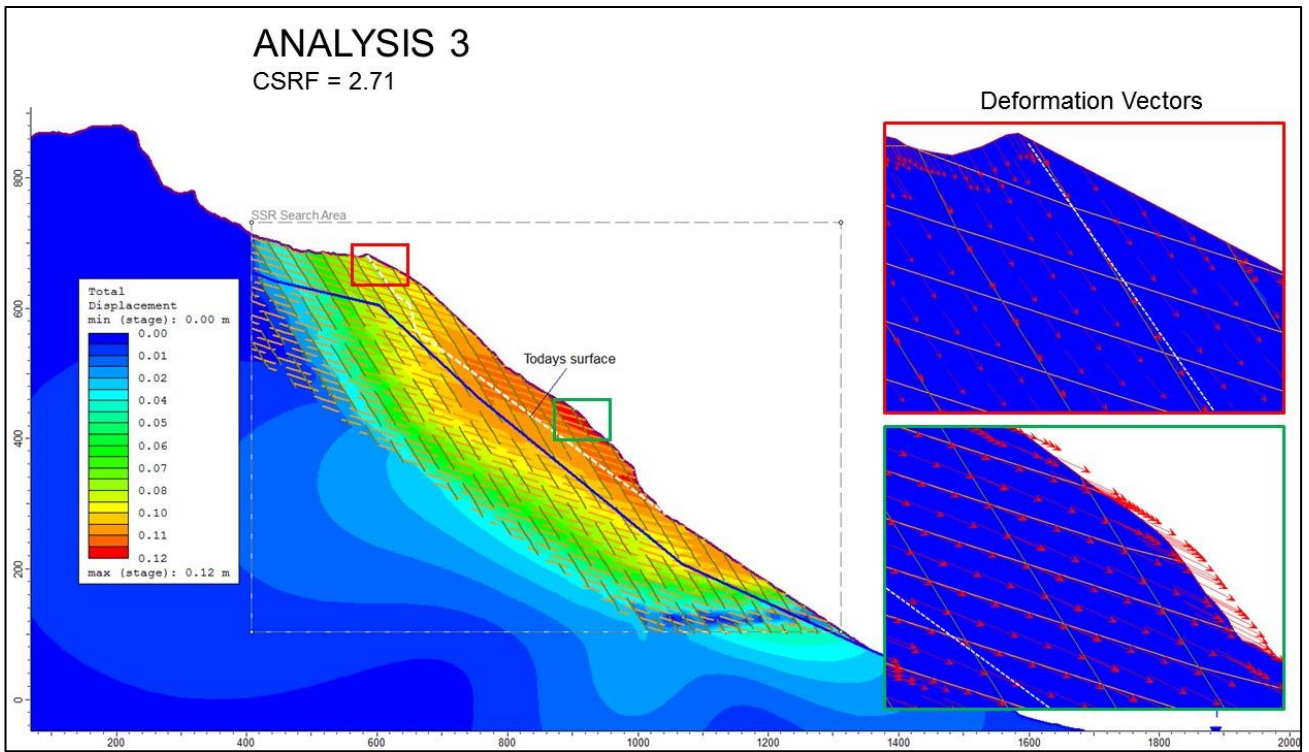


Figure 69: Total displacement and highlighted deformation vectors for the upper and lower part of the slope.

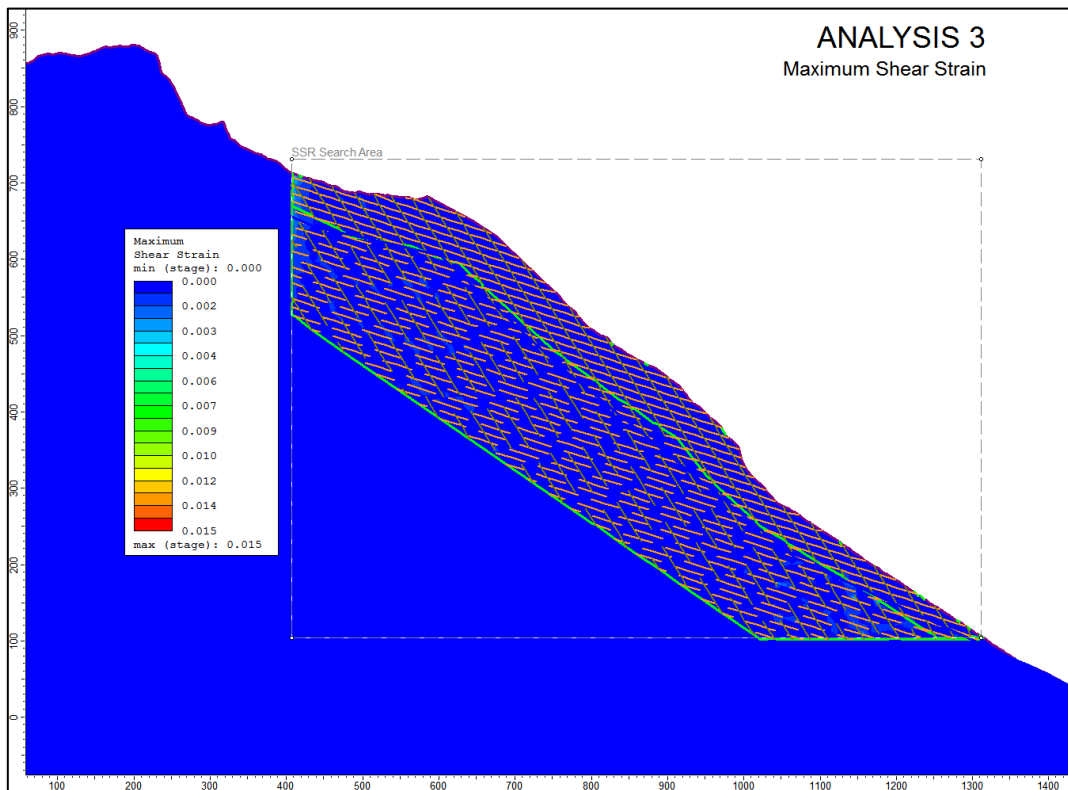


Figure 70: Maximum shear strain plot of Analysis 3 shows no visible shear strain and consequently no indication of the most likely failure surface. The reason for no visible shear strain is assumed to be that slip occurs only at the joint interfaces.

Step 6 – present condition

The last step of the modeling is run as a forward analysis of Model 3, corresponding to the present ground surface at the location of scenario G. The input parameters are based on the results from the previous steps, and are set to reflect today's conditions as exact as possible with the available data. The chosen parameters and final model set up are shown in Table 30 and Figure 71 below.

Table 30: Overview of chosen values for the input parameters used in the forward analysis in Step 6.

Parameter in Model 3	Description	Evaluation
Field stress	In plane component = 2 Out-of-plane component = 3	Based on the field stress evaluation in Step 1.
Groundwater table	Present	The location is based on comparison with other fractured rock slopes where measurements of groundwater exist. See chapter 5.5.6 for details
Joint strength	Converted Mohr-Coulomb strength from Barton-Bandis. Mean values are applied.	Based on field measurements presented in chapter 5.5.8. The historic slope failure might have failed along joints with lower strength values, but for the forward analysis the mean values reflect the current conditions.
Material and joint model	Plastic – strain softening	Strain softening is applied as the behaviour of rock masses is often seen to be strain softening or brittle (Manfredini et al., 1975). Additionally, the performed back-analysis showed that some amount of strain softening was necessary to cause failure, and is therefore assumed to reflect the rock mass at Kassen.
Rock mass strength	Converted Mohr-Coulomb strength from Hoek-Brown.	Based on field and laboratory work, presented in chapter 5.5.7.

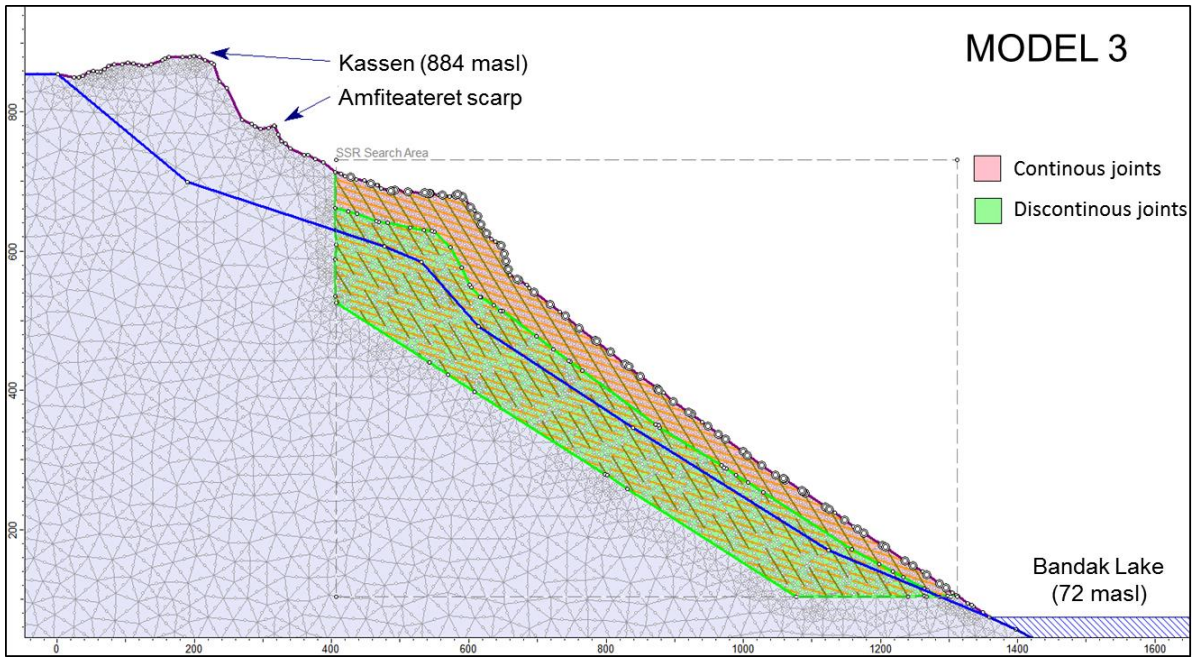


Figure 71: The geometry of Model 3 is the actual ground surface. The joints are added in two joint networks, the upper with continuous joints towards the surface and the lower with discontinuous joints.

The computed model gives an CSRF of 1.78, meaning that the slope is stable under present conditions (Figure 72). The displacement plot shows maximum local displacement of 9 cm, concentrated in the upper part of the slope. As for the back-analysis, the displacement follows J2 and J3 in the continuous joint layer, indicating biplanar failure as most likely failure mode. Potential sliding mass is defined after where the highest displacement occur in the model, and gives an area of 7872 m² in the modeled cross-section of the slope.

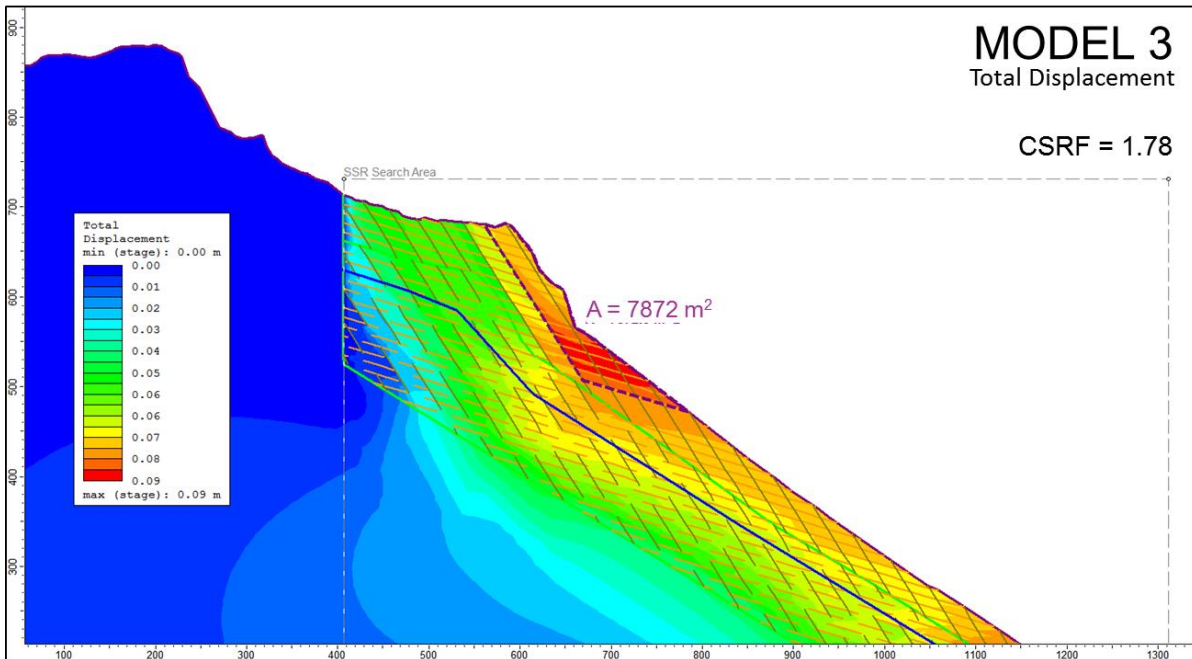


Figure 72: Total displacement plot of Model 3. Maximum displacement is 9 cm, and concentrated in the upper part of the slope. Potential sliding mass has an area of 7872.6 m² at this cross-section. The resulting CSRF of 1.78 shows that the slope is stable today.

5.8 Results from stability assessment of Skipet

Toppling

The two potential unstable blocks at Skipet were first tested for toppling. For Block 1, the block shape test given by Equation 16, introduced in chapter 5.6, was applied. Results from this test is presented in Table 31 below, which show that the block is stable against toppling.

Table 31: Block shape test of Block 1 shows that the block is stable against toppling since $\Delta x/y > \tan \psi_p$.

	Width (Δx)	Height (y)	$\Delta x/y$	$\tan \psi_p$
Block 1	14.1	10.0	1.41	0.75

As the geometry of Block 2 is rather irregular, a simplified sketch dividing the block into familiar shapes was performed in order to check if the centre of gravity fell outside the base of the block. The calculations of centroids for Block 2 is given in Appendix 8.8, and the result show that the centre of gravity falls inside the base of the block, i.e. Block 2 is stable against toppling.

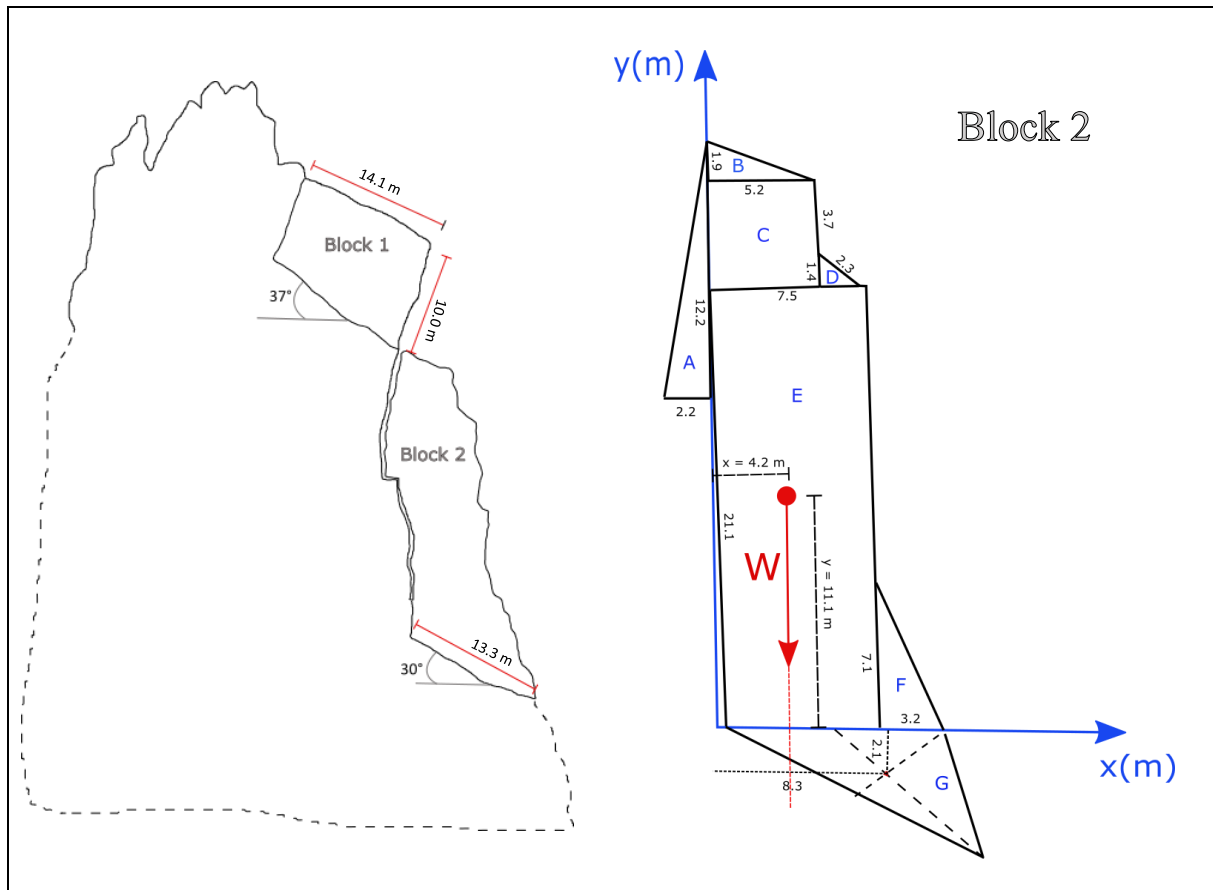


Figure 73: Both potential unstable blocks at Skipet is stable against toppling. For Block 2, the geometry was simplified in order to calculate the centroids of known figures such as triangles and squares.

Planar sliding

To check whether the blocks are stable against planar sliding a calculation of the FS is performed using the LEM method where driving forces are compared against resisting forces. Table 32 show that both blocks are stable under dry conditions as the calculated Factors of Safety for Block 1 and Block 2 are respectively 1.57 and 1.74.

Figure 74 shows the calculated FS for different water heights in the tension crack of Block 2, by applying Equation 22 and 23, introduced in chapter 5.6. Even when water pressure acts over the entire length of the tension crack (28 m), the block is stable with a FS of 1.55.

Table 32: Results from the calculations of FS for planar sliding fro Block 1 and 2 under dry conditions.

Parameter	Symbol	Unit	Block 1	Block 2	Comments
Joint Compressive Strength	JCS	Mpa	125	125	Measured at a J2 surface located at the southeastern side of Skipet.
Joint Rougness Coefficient	JRC	-	15	15	See column above.
Residual friction angle	ϕ_r	°	23.9	23.9	Tilt test from laboratory and fieldwork. r is measured at the same surface as JRC/JCS. R is taken from Amfiteateret, as no fresh joint surfaces were found near Skipet.
Inclination of sliding plane	ψ_p	°	37	30	Measured on sketch. Corresponds well to J2 dip in this area ranging from 25 – 45 ° (field notes).
Weight of block	W	MN	40.89	73.47	Assuming one unit length, as the analysis is in 2D. Unit weight found from laboratory of the rock sample collected in Amfiteateret. As the rock type is the same at Skipet and in Amfiteateret (Amphibolite), this is assumed satisfactory.
Area of sliding plane	A	m ²	14.1	13.3	Measured on the sketch. Assuming one unit length.
Normal stress acting on the sliding plane	σ_n	Mpa	2.32	4.78	See Equation 20, chapter 5.6.
Factor of Safety	FS	-	1.57	1.74	See Equation 22, chapter 5.6.

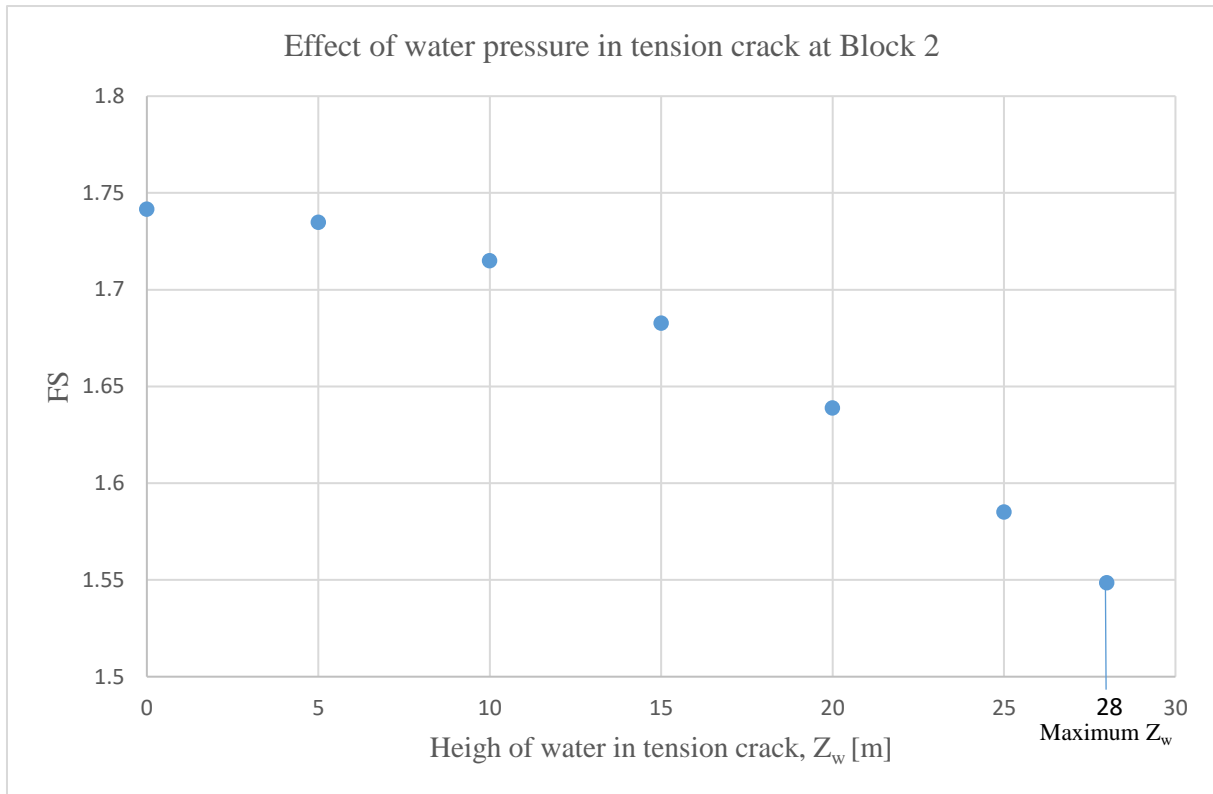


Figure 74: Diagram showing how the FS decreases with increasing water in the tension crack at Block 2. The block is still stable, even if water pressure acts over the entire length of the crack (maximum Z_w).

6 Discussion

6.1 Hazard and future risk at Kassen

Results from the hazard classification showed that four scenarios are in the medium hazard class and three scenarios in the low hazard class. This discussion will be based on the medium class scenarios, as they oppose the highest hazard and consequently the highest risk at the Kassen site.

Scenario A, B and F are the smallest scenarios with estimated volumes ranging from 110 000 – 210 000 m³, and fall into the medium hazard class. These scenarios differ from the other scenarios, since potential sliding structures penetrate the whole size of the potential sliding blocks. This increases the hazard score in criterion 2 (potential sliding structures) and criterion 4 (kinematic feasibility test). Scenario A and B are both fully isolated blocks, meaning that the back scarp and the lateral release surfaces are fully developed. Scenario F has an open back scarp and fully developed eastern flank, but the western flank is only partly developed consisting of discontinuous cracks. These clear structures, increases the certainty of the volume estimations as the delimitation of the scenarios are set with confidence.

The run-out assessment show that scenario A and B have run-out lengths reaching Bandak Lake with a relative high susceptibility. This is verified in the field, as the terrain downslopes of these scenarios consist of talus with an average dip angle in the range 30 – 40 ° (measured in ArcGIS 10.4). For scenario F, the run-out assessment show that some material will reach the lake. The susceptibility for this is somewhat lower, as flat terrain exist at the toe of this scenario.

Scenario G also fall into the medium hazard class, and is the scenario with the highest maximum hazard score (10.0) and highest estimated volume of 2.09 million m³. The potential sliding structures were not identified as persistent in the field. However, the rock mass is highly fractured and consists of multiple, closely spaced structures which means that there are no continuous bedrock left. In such cases, the potential sliding structures shall be evaluated in the same way as for clearly, persistent structures, as the rock bridges that would have to fail are small (Hermanns, Oppikofer, et al., 2012). The depth of this fractured rock mass is however unknown, and cannot be determined with certainty without applying more sophisticated methods such as core drilling. Coring would also reduce the uncertainty of the estimated volume found by the SLBL technique, as it could reveal the most likely sliding plane. The assumed toe-line of the event is determined based on hillshade maps, and should be investigated in more detail in field where geomorphological features such as bulging, or daylighting structures at the toe shall be in focus.

The displacement measurements for scenario E, F and G are not yet available, and to reflect the uncertainty in criterion 6 (displacement rates) and criterion 7 (acceleration), several outcomes are weighted with the strongest weight towards small displacement rates. Consequently, the hazard assessments for these scenarios will have to be re-evaluated after NGUs field campaign in 2017. Based on geomorphology, it is believed that the resulting displacement rates for scenario E and F will show no significant movement similar to the other dGNSS rover points. The deformation in this area is similar, and even less than the deformation where rover points have been measured over several years. For scenario G, the situation is different as the rock mass in this area is much more deformed than in the adjacent areas, and therefore it cannot be assumed if the future displacement rates will increase or decrease the hazard score.

Preliminary risk and follow-up activities

In NGUS system, risk classification combines the hazard score and the potential life losses in a risk matrix which defines the unstable slope in question as either low risk (green), moderate risk (yellow) or high risk (red) as shown in Figure 75. Only scenario B and G are plotted the figure as they scored highest in the hazard assessment. Scenario B fall into the medium-risk category while scenario G is approaching the transition zone between medium and high risk.

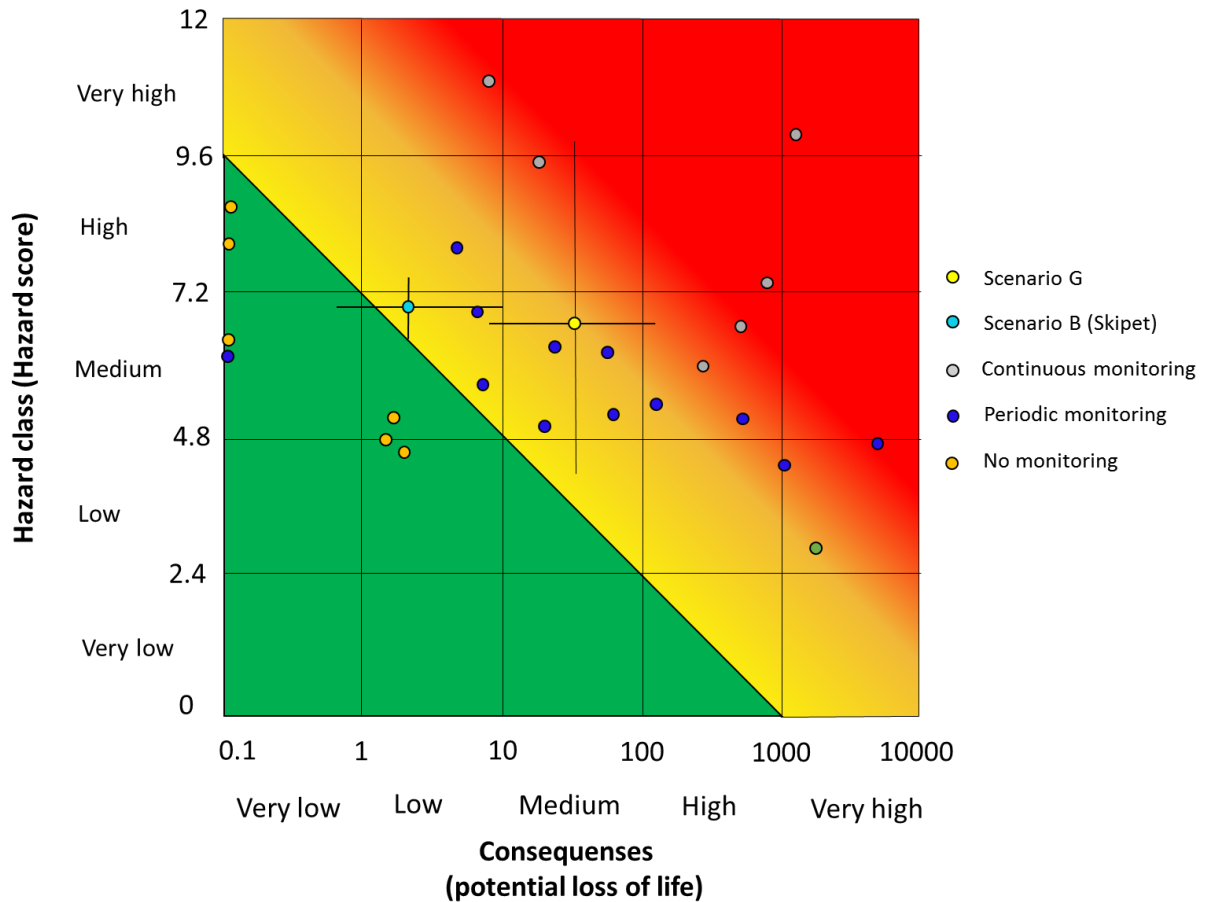


Figure 75: Potential risk matrix for scenario B and G at Kassen. The figure is modified from NVE, showing other risk classified sites, with different type of monitoring.

The consequences cannot be determined without a detailed run-out modelling and displacement wave assessment. Consequently, the risk matrix presented is only a preliminary risk matrix for the scenarios at Kassen. Potential loss of life is based on map studies (The Norwegian Mapping Authority, 2016) of residences located at the shoreline around Bandak Lake that could be hit by displacement waves from the two scenarios. This map study is only a first rough estimate, and should be re-evaluated after the displacement wave assessment is performed by NGU.

The empirical run-up heights for respectively scenario B and G were found to be 3.8 and 14 meters in Roeid, located 2.5 km away from Kassen. At Roeid, only a few residences are located at the shoreline, and some of these might also be cabins. To be conservative, potential loss of life at this location is set to 10. In Dalen and Lårdal the run-up heights from scenario G are respectively 2.7 and 4.2 meters, which can be hazardous for the houses located right at the shoreline. A conservative approach of potential loss of lives in these areas are set to 100. Run-

up heights from scenario B at Dalen and Lårdal are in the dimension of storm waves, and is believed to not cause loss of life.

The aim of the risk matrix is to decide on follow-up activities of unstable rock slopes which can be type of monitoring, further investigations and/or eventual mitigation measures (Hermanns, Oppikofer, et al., 2012). In Figure 75, other completed risk-classified sites in Norway are plotted and labeled with the type of monitoring performed at these sites. As seen in the figure, the scenarios at Kassen plot in the same area as other sites which are monitored periodically. It is therefore suggested to continue with yearly dGNSS measurements at Kassen.

As a supplement to the dGNSS measurements, GB - InSAR (Ground Based Interferometric Synthetic Aperture Radar) can help to understand potential deformation in the slope better. This monitoring technique provides measurements of ground displacement through remote sensing, and is able to detect a continuous two-dimensional deformation field of the measured area without any physical contact with the slope through positioning targets (Ferrigno, Gigli, Fanti, & Casagli, 2015). The technique can independently measure the atmospheric conditions and provide a dense measurement coverage of the observed area, which is a key advantage with respect to point-like measurement techniques like dGNSS (Monserrat, Crosetto, & Luzi, 2014). Applying periodic monitoring with GB-InSAR would be especially useful for Amfiteateret, where scenario G is located. One punctual deformation measurement (BAN-7) might not reveal the areas with highest deformation rates due to the great extent of the scenario and the many various and potential sliding structures within the rock mass. At Skipet on the other hand, one dGNSS measurement point is believed to be sufficient as this scenario is an isolated block with few, penetrative sliding structures. Therefore, the displacement is assumed to be uniform within scenario B.

6.2 Evaluation of the numerical modeling

Numerical modeling requires idealization and simplification of a real problem. It is impossible to include all features and details of rock mass response in to one model. Rock masses are unpredictable compared to man-made materials in other branches of mechanics, and their behaviour is a result of many unknown and uncertain details (Wyllie & Mah, 2004). Consequently, numerical programs are not black boxes that give the solution, but they help to narrow down uncertainties and to test the influence of different geological parameters.

6.2.1 Model settings and input parameters

Manfredini et al. (1975) concludes that in it is necessary to know at least the parameters listed in Table 33 and their relative importance, when analyzing the stability of a jointed rock mass. These parameters and others are discussed in the next sections, where the uncertainties of the parameters are in focus.

Table 33: Important parameters related to stability assessments of jointed rock masses, after (Manfredini et al., 1975)

Characteristics	Parameters	Importance
Joint peak strength	Cohesion and friction angle	Basic
Joint brittleness	Residual cohesion and friction angle	Basic
Original state of stress	Horizontal and vertical stress	Considerable
Joint deformability prior to failure	Joint normal and shear stiffness	Moderate
Elastic parameters of the rock mass	Young's modulus and Poisson's ratio	Small

Field stress

The potential influences of changes regarding *field* stresses should be assessed and be a part of the model evaluation (Eberhardt, 2003). The field stress is an essential parameter that plays a considerable role regarding design and stability of rock slopes. This parameter is however expensive and difficult to measure in field because applied methods are originally developed for ideal materials (Myrvang, 2001). Since no direct or indirect measurements of the field stress at Kassen exist, stress measurements were obtained from the borehole located 21 km away from the study site for the first evaluation. As concluded in 5.5.6, this field stress configuration gave an inappropriate response from the model, evaluated by the maximum shear strain plot. A possible explanation for this outcome is that the borehole is located in the lower parts of the slope, and therefore strongly influenced by topography. Input of in situ stresses should not be local, but rather regional since the computed model adjust the magnitude and orientation of field stresses after the defined model geometry (Nilsen, 2016).

Several field stress set-ups are tested and evaluated for the model at Kassen using a gravitational stress field. For the Kassen site, assuming pure gravitational stress field, gave an in plane and out-of-plane horizontal to vertical total stress ratio of 0.37 which was tested in analysis 6 in Step 1 of the numerical modeling. However, the best field stress configuration of the six analyses was obtained with an in plane and out-of-plane horizontal to vertical total stress ratio of respectively 2 and 3, indicating that the horizontal stress components are not pure gravitational. In fact, measured horizontal stresses in the Western Fennoscandia are often higher than gravitational stresses would suggest (Hanssen, 1998). Myrvang (2001) show several examples of rock masses of different ages with high, anisotropic horizontal stresses in Norway, which can indicate that these are tectonic stresses caused by Norway's tectonic history.

Based on the discussion above the chosen field stress set up might be appropriate for the rock mass at Kassen. However, this is difficult to verify in any more detail and remains as one of the major uncertainties regarding the numerical modeling.

Rock mass shear strength

The Generalized Hoek-Brown failure criterion was chosen to calculate the strength of the highly dissected rock mass in Amfiteateret. This is in accordance with recommendations from several authors (Hammah et al., 2004; Hoek, 2000; Wyllie & Mah, 2004) as a linear failure criterion is inappropriate for such rock masses.

As discussed earlier, to apply the SSR technique in order to determine a CSR, the Hoek-Brown strength properties are converted to equivalent Mohr-Coulomb parameters for the numerical

analysis in this master thesis. This approach is proposed by Hammah et al. (2004) and described as simple, practical, and accurate. However, it is sensitive to the range of normal stresses over which the linear Mohr-Coulomb strength envelope is determined (Hammah, Yacoub, Corkum, & Curran, 2005). Therefore, Hammah et al. (2005) describes a method that allows direct use of the Generalized Hoek-Brown criterion in Finite Element SSR analysis of rock slopes. This method can be implemented in RS², but due to increased computation time, conversion to equivalent Mohr-Coulomb parameters were preferred for this study. A normal stress level defined by the depth to the rupture surface of the Bandak rock avalanche, was used to overcome the sensitivity of the Mohr-Coulomb fitting regarding the range of normal stresses. As previously discussed, this depth is depending on the accuracy of the reconstructed topography which was done in a very simple manner. Consequently, uncertainties are related to the final instantaneous, equivalent Mohr-Coulomb strengths cohesion and friction angle applied in the model.

The resulting instantaneous, equivalent cohesion and friction angle of the rock mass was calculated to be respectively 65.9° and 2.2 Mpa. As seen in Figure 76, these values differ significantly from other strength values for different rock masses. The other rock masses plotted in the figure are mainly weaker material than amphibolite, such as shales, slates, sedimentary series, chalk and strongly weathered volcanics. The rock mass labeled with 4, is however a granite which also differs remarkably from the amphibolite from Kassen. Still, comparing the amphibolite to only one similar rock type might be inadequate. The unexpected high strength values can be connected to the high stiffness and high strength found in laboratory for the Amphibolite sample.

On the other hand, some errors might have occurred when deriving the equivalent, instantaneous Mohr-Coulomb strength parameters. For future analyses, it would be recommended to use the Generalized Hoek-Brown strength parameters directly to limit the steps of uncertainties.

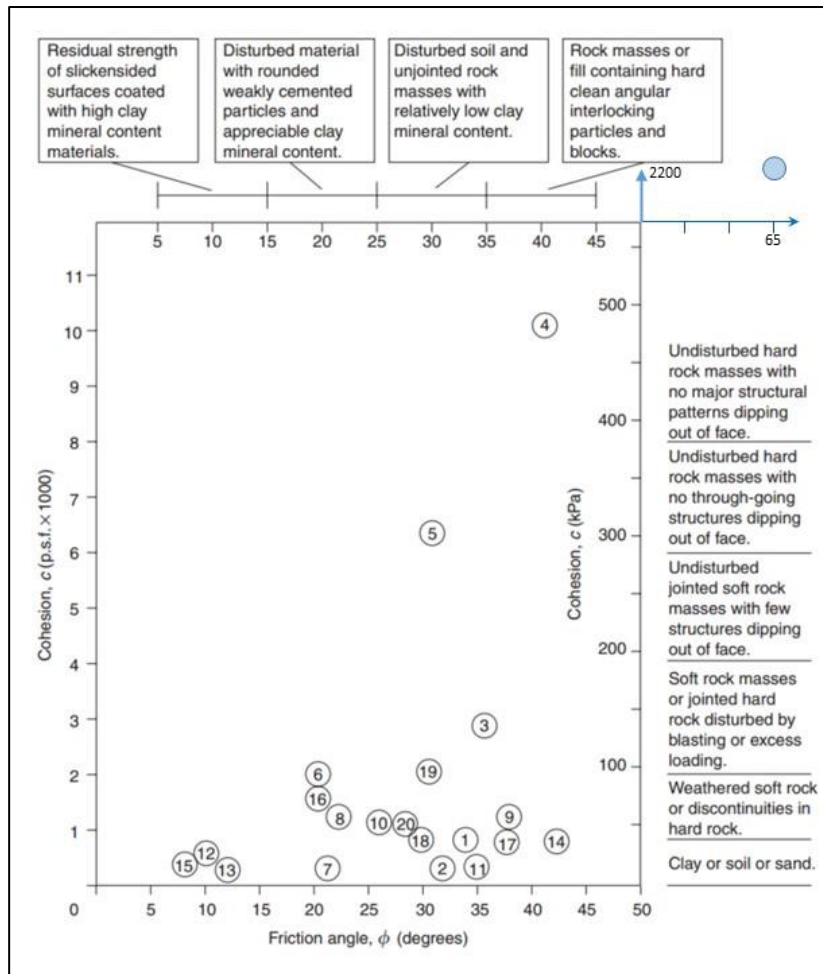


Figure 76: Chart showing friction angles and cohesive strengths for different rock masses found by back-analyses (Wyllie & Mah, 2004). The rock mass of amphibolite from Kassen is marked with a blue circle and show very high shear strength.

Joint shear strength

The Barton-Bandis shear strength model for joints were applied in this study, which include the determination of the JCS, JRC and the residual friction angle (α_r). Determination of these parameters are done following the procedures presented by Grøneng and Nilsen (2008).

JCS values were obtained through Schmidt hammer rebound values. The measurement of JCS is of high importance since the overall strength and deformation properties of the rock mass is dependent on the thin layers of rock adjacent to joint walls (Barton & Choubey, 1977). Barton (1973) suggests to use a conservative lower boundary for the JCS value equal to $\frac{1}{4}$ of UCS in studies lacking Schmidt hammer measurements. A conservative lower value for JCS following this recommendation is 60.25 Mpa for the joints at Kassen. As Table 34 shows, even the lowest values obtained through fieldwork exceed this value.

In a later study by Barton and Choubey (1977) the *relative alteration* (UCS/JCS) was investigated for different rock types and ranged from 5.2 to 1.0. The highest value was from calcite coated joints in a hornfels while the lowest value was for joint in a coarse-grained, slightly weathered granite. A relative alteration as high as 5.2 is not applicable for the Kassen

site, as no coating was observed on the amphibolite joints. However, most relative alteration values laid between 1.4 and 1.9 in the study from 1977, which gives JCS estimations from 127 to 172 for the amphibolite at Kassen. This is in correspondence with the mean JCS values obtained with the Schmidt hammer.

Table 34: JCS values for J2 and J3.

Joint set	Mean JCS	Lowest JCS
J2	149.7	90
J3	152	87

The residual friction angle (α_r) was calculated using equation 15, where rebound values from respectively fresh, dry rock surfaces (R) and weathered, wet joint surfaces (r) and the basic friction angle (α_b) are parameters in the equation.

As only one fresh, dry joint surface was found during field work, some uncertainties arise regarding the reliability in R of 58.2. A correlation between R and UCS can be obtained by using the diagram in Appendix 8.5 (originally after Deere and Miller (1966)). Converting the UCS from laboratory (241 Mpa) gives a corresponding R value of 59.5 which is a marginal increase of 2.2 %. Even though only one measurement of R was done with the Schmidt hammer, it is representative for the rock mass in Amfiteateret.

Figure 77 shows that the parameters α_b , α_r , R and r for the amphibolite at Kassen clusters fairly good together with other common rock types tested by Richards (1975). This observation supports that field and laboratory work done in order to determine α_r is of satisfactory quality.

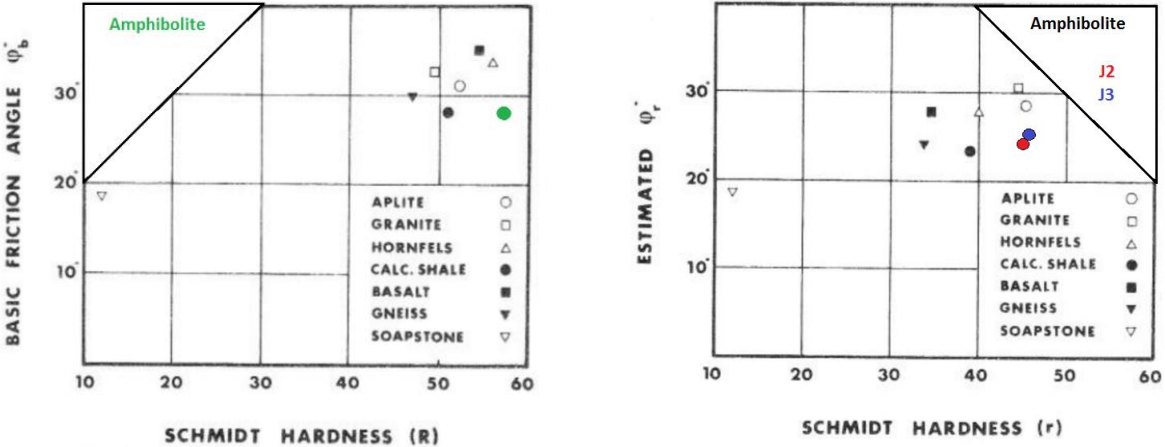


Figure 77: Comparison of Amphibolite properties (α_b , α_r , R and r) to other rock types. The left figure show mean results of tilt tests to determine α_b plotted against Schmidt rebound tests on dry, fresh rock surfaces. The right figure shows estimations of α_r from equation 15 using the data in the left figure and Schmidt rebound tests on wet, weathered surfaces. The figures are modified from Barton and Choubey (1977).

As for the Generalized Hoek-Brown criteria, the Barton-Bandis parameters (JCS, JRC and α_r) are converted to equivalent, instantaneous Mohr-Coulomb shear strength defined by the same normal stress level as the rock mass. Table 35 reviews the estimated cohesion and friction values:

Table 35: Review of the mean and lowest shear strength properties estimated for J2 and J3 by converting Barton-Bandis parameters to equivalent Mohr-Coulomb parameters for a certain normal stress.

	Cohesion		Friction angle	
	Mean	Lowest	Mean	Lowest
J2	0.43	0.09	44.5	29
J3	0.33	0.05	42.6	26.1

It can be discussed if it is realistic to perform analyses with the lowest strength values, as they are far from the average joint strength values. On the other hand, failure could have initiated at particular locations where the joint strength is low. Generally the joints observed in field had no joint infilling and shear strength was directly related to the joint wall strength and roughness of the surfaces. However, at one location in Amfiteateret, a filled joint was observed consisting of around 50 cm of soft, schistose, gouge material with a high mica content (Figure 78). The shear strength can be reduced drastically when part of the joints surface is not in intimate contact, but covered with soft filling material (Hoek, 2000). The observed location of the filled joint is close to the scar of the rockslide event. If failure took place at similar, filled joint surfaces, the assigned lowest strength values could be realistic to assume as they lay in the range of common values (Table 36).

Table 36: Shear strength of filled discontinuities and filling materials (modified from Hoek (2000)).

Rock	Description	Cohesion [Mpa]	Friction angle [°]
Clay shale	Triaxial tests Stratification surfaces	0.06	32
Dolomite	Altered shale bed	0.012	16
Granite	Clay filled faults	0-0.1	24-45
Granite	Tectonic shear zone	0.24	42
Schists, quartzites and siliceous schists	Thick clay filling	0.03 – 0.08	32
Slates	Finely laminated and altered	0.05	33

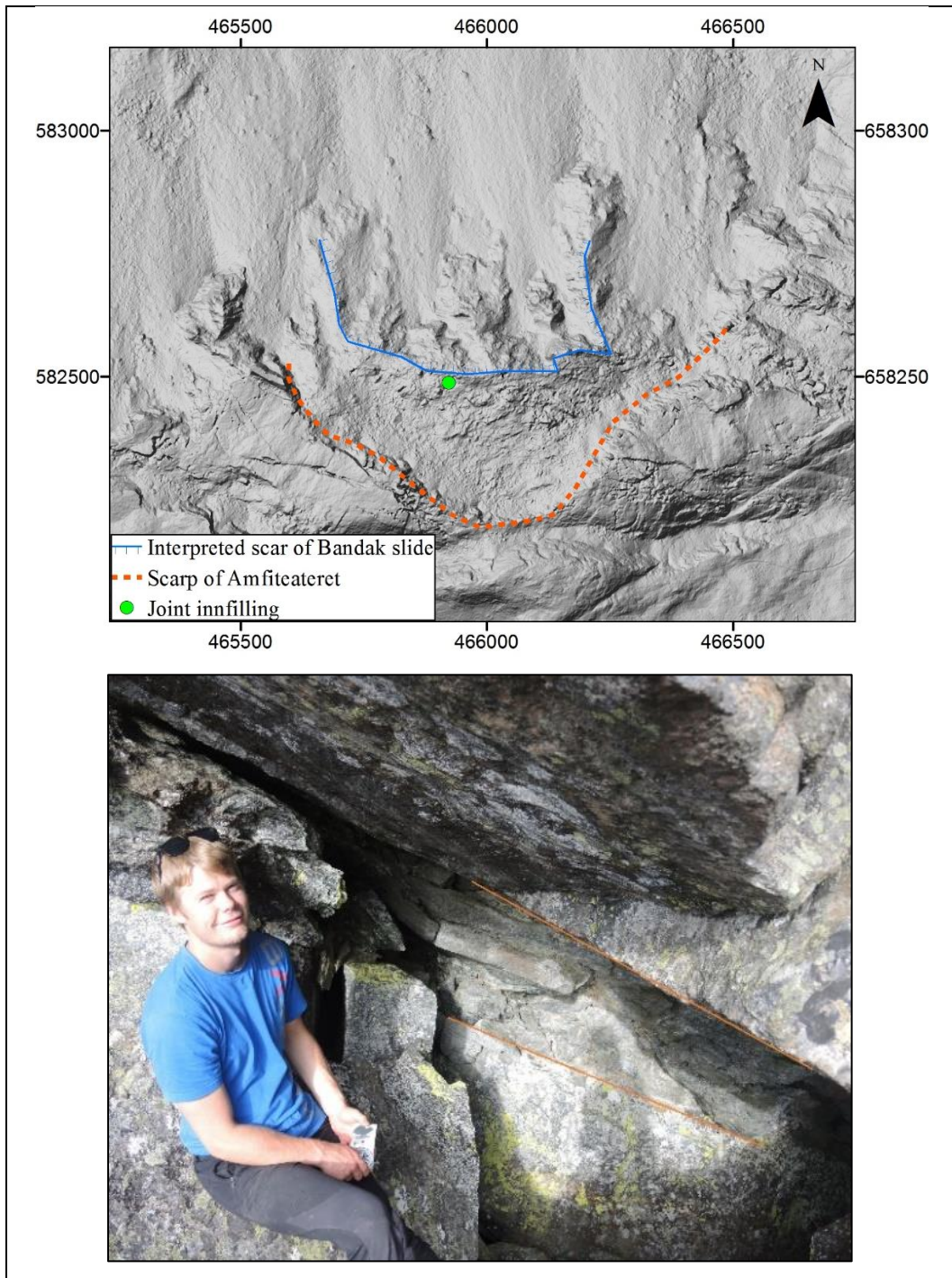


Figure 78: The upper figure shows the location of where the filled joint were observed. The lower picture shows the infilling consisting of disintegrated, schistose material with a high mica content.

Joint Stiffness

Stiffness parameters for the joints in amphibolite were calculated as recommended by Rocscience (2016c). There are more precise methods for estimating the joint stiffness such as triaxial testing, direct shear testing and *in situ* measurements (Rosso, 1976). The calculations in this master thesis are based on the deformation modulus of the intact rock (Young's modulus), the deformation modulus of the rock mass, the mean joint spacing and Poisson's ratio (see

Appendix 8.6 for details). Even though the joints are modeled with an exaggerated mean spacing, the spacing estimated in field was used for the calculations of stiffness in order to reflect real conditions.

The resulting calculated normal and shear stiffness for the joint sets are very high compared to values reviewed in literature for different rock types. However, these values differ a lot, and are found by different methods which made comparison incomprehensible. As the stiffness parameters are directly dependent on Young’s Modulus for the intact rock, this parameter is compared with other common rock types. As Table 37 shows, the amphibolite has the highest value of all rock types, indicating that the tested rock from Kassen is very stiff. This observation supports the high-calculated joint stiffness.

Further on, the performed parameter study in step 4 showed that the model is less sensitive to changes in the joint stiffness than other parameters related to the joints. Decreasing both normal and shear stiffness with 80 % only gave a 15 % reduction in the CSRf. A similar reduction of the friction angle reduced the CSRf with 36 %.

Table 37: Representative values of Young’s modulus for common rock types after (Johnson & DeGraff, 1988)

	Granite	Basalt	Gneiss	Schist	Quartzite	Marble	Limestone	Sandstone	Shale	Amphibolite at Kassen
Average Young’s Modulus [Gpa]	59.3	62.6	58.6	42.4	70.9	46.3	50.4	15.3	13.7	74.5

6.2.2 Deformation history

Numerical modeling performed in Step 2 did not support the presented deformation theory. Either, the model set up is incorrect or the deformation theory is different from the real history of Amfiteateret.

As discussed, uncertainties are related to both the reconstruction of topography and the chosen field stress, and can be the reason for why the model did not respond as expected. On the other hand, if the model set-up is assumed to be correct, deformation of the slope could have occurred in another order. Perhaps, the collapse in the lower part was the first event. This would remove the lower support in the slope, and eventually lead to low velocity displacement in the upper part.

Further analyses of the deformation sequence at Amfiteateret has not been conducted, and remains as one of the uncertainties at the Kassen site.

6.2.3 SSR analyses

The numerical modeling is done with the shear strength reduction (SSR) technique. A SSR search area was added to the model in order to decrease computation time and to analyze the area of interest, as the location of the historic failure surface is known. The effect of different triggering mechanisms have been analyzed through the CSRf.

Effect of groundwater

Groundwater pressure acts as a driving force in slope stability. The effect of adding groundwater to the model has been investigated in several steps of the numerical modeling where three different configurations have been tested (dry slope, present groundwater conditions and fully saturated slope). The results all show that the CSRFB decreases when lowering the groundwater table from high to present (Figure 79).

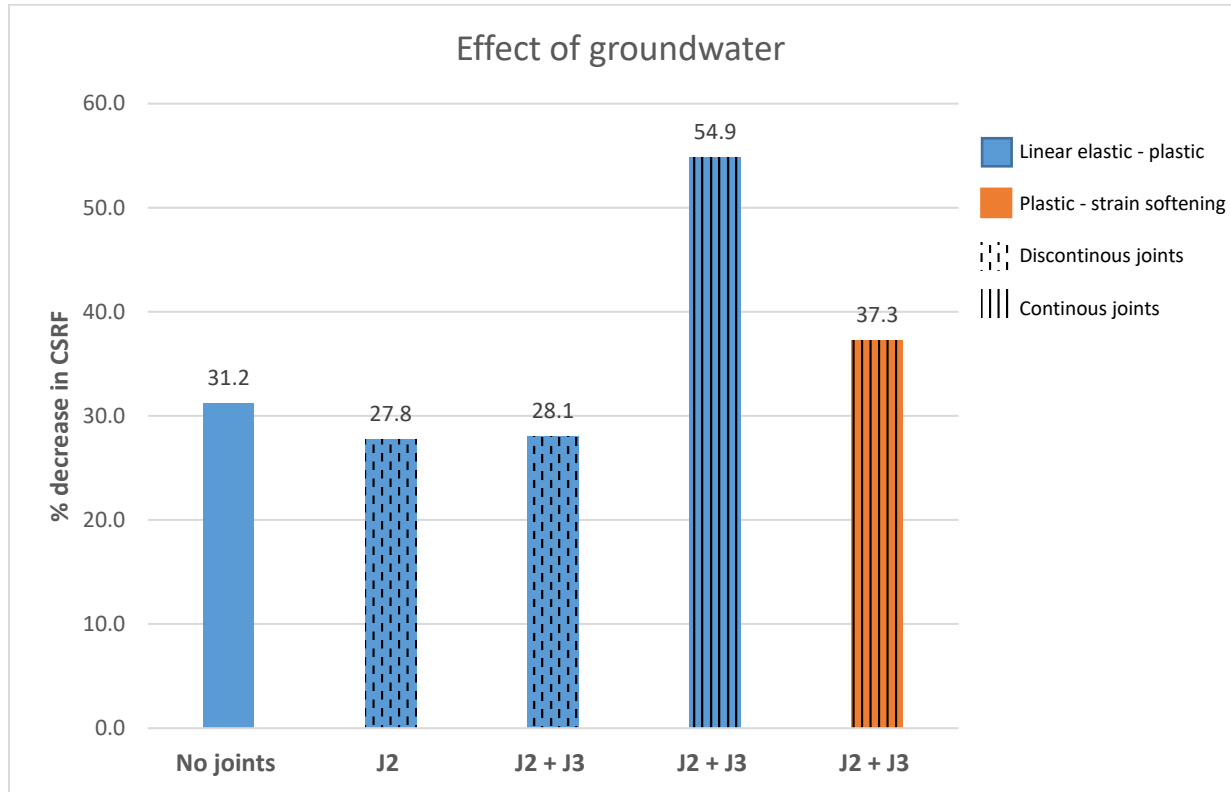


Figure 79: Comparison of the effect of lowering the groundwater table from high to present for different model set-ups. Dry slope conditions are not included in this comparison. All joints are assigned with their mean strength values.

For all analyses including joints the groundwater pore pressure is added as an additional pressure inside joints. Therefore, it is expected that the CSRFB would decrease the most when lowering the groundwater from high to present for the models including joints. However, this is not the situation when modeling the joints as discontinuous (Figure 79), where the percentage decrease in CSRFB actually is lower than for the model without joints. There is no geological or hydrogeological reason for this result, and the explanation might be connected to software details beyond the aim of this master thesis. A significant effect of lowering the groundwater is first seen when the joints are modeled as continuous as the CSRFB decreases with 54.9 % for the linear elastic – perfectly plastic model. It is therefore clear that the groundwater have the greatest effect when the water pressure acts over the entire length of the joints, leading to a high resultant force.

For the strain softening model, with continuous joints, the decrease in CSRFB is lower than for the linear elastic – plastic model. The lack of sensitivity in the modeling for this situation can be justified by the dominance of rock mass and joint strength due to strain softening.

Effect of joints

Even though several joint sets and several random joints were observed in Amfiteateret, only J2 and J3 were included in the numerical modeling. As previously discussed, most JRC and JCS measurements existed on these joints and kinematic stability tests showed that they were critical joint sets for the stability. Numerical models are simplifications of real conditions, for this study the effect of joints is assumed to be investigated with an acceptable uncertainty through J2 and J3.

Adding joints to the model decreases the stability of the slope (Figure 80).

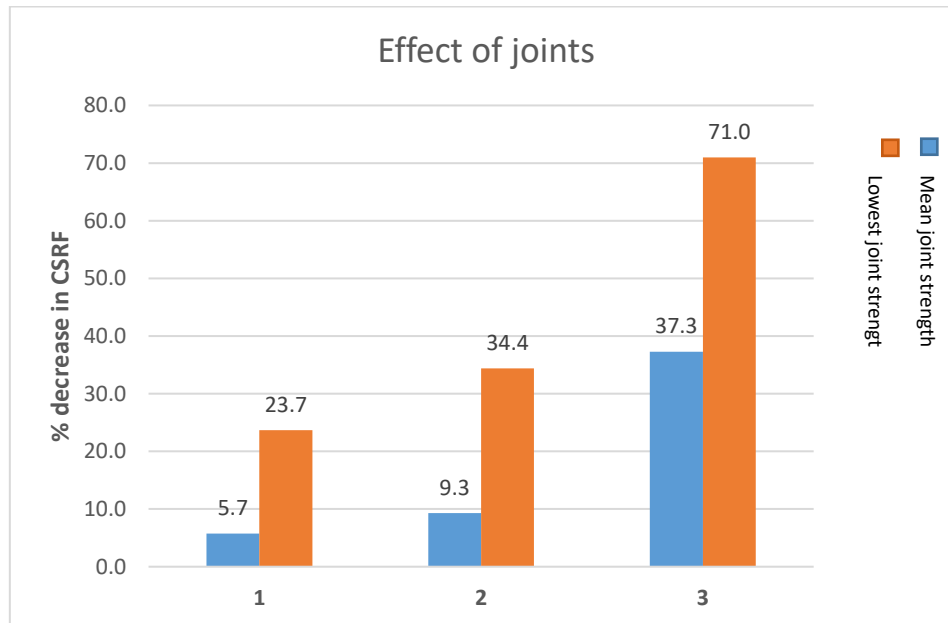


Figure 80: The effect of adding joints to the model analyzed through the percentage decrease in CSRF compared to a model without joints. In all analyses, the groundwater is high and the material and joint models are linear elastic – perfectly plastic.

When joints are added as discontinuous, failure of intact rock (rock bridges) is necessary to develop a failure surface. As a result, discontinuous joints increases the CSRF compared to continuous joints as seen in Figure 80. For the situation where both J2 and J3 is added to the model with infinite lengths, the slope is close to unstable conditions for the mean value (CSRF = 1.1) and unstable for the lowest strength values (CSRF = 0.81).

A significant slope stability reduction is seen when the joint shear strengths are assigned with the lowest recorded values from fieldwork. This result show that the joint strength is a crucial parameter for the stability, and were therefore systematically analyzed through the parameter study of cohesion and friction angle of J2. The results showed that the friction angle is the parameter influencing the stability the most; a 80 % decrease in friction angle gave a 36.1 % decrease in CSRF, while the same decrease of cohesion caused a decrease in CSRF of 16.7 %.

The term cohesion is originally a soil mechanics term, where the physical meaning of cohesion is the adhesion of soil particles. True cohesion for discontinuities occur when cemented surfaces are sheared (Hoek, 2000). For natural rock joints (which are not cemented) the term cohesion is related to surface roughness; for the case of planar, smooth surfaces the cohesion is consequently zero. For rough rock surfaces, apparent cohesion is developed as the asperities (irregularities on the surface) are teared off during movement and will increase with increasing

normal stress. If the normal stresses are low compared to the strength of intact rock, apparent cohesion might not develop along sliding surfaces, and the shear strength is then dominated by the friction angle. The amphibolite at Kassen has a high uniaxial compressive strength (241 Mpa) and a relatively low normal stress level (1.6 Mpa) which can explain why the model is most sensitive to the friction parameter.

Effect of strain-softening

In Step 5 of the modeling, several analyses were performed with residual strength values equal to 2/3 of peak values to reflect strain softening of both the rock mass and joint material. Results presented in chapter 5.7 revealed that the slope stability is highly sensitive for changes in type of material model. Keeping all other parameters constant, except the value of residual strength lead to a decrease in CSRF of up to 44.3 %.

None of the analyses without strain softening material models lead to a CSRF below 1. For the present modeling, it is therefore clear that some amount of strain softening is required to cause failure.

The magnitude of the residual values for both the rock mass and joints were determined after recommendations from Trinh (2016). Table 38 shows that this recommendation is a slightly overestimated value compared to residual friction angle values for the joints derived from field and laboratory work. The influence of soft straining could therefore be even higher and lead to even smaller CSRF, which supports the importance of brittle joint behaviour in relation to slope failure. A similar comparison for the rock mass friction angle, is not possible to obtain, and the recommendations from Trinh, is therefore assumed satisfactory for the rock mass and joint material in total.

Table 38: Comparison of residual friction angles of joints.

Friction angle	J2		J3		Comments
Peak	44.5		42.6		Instantaneous friction and cohesion after conversion of Barton-Bandis parameters in RocData.
	Value	% of peak	Value	% of peak	
Residual 1	29.7	67	28.4	67	Recommended by Trinh (2016).
Residual 2	24.3	55	24.6	58	Field and laboratory work: $\varphi_r = (\varphi_b - 20) + 20 \frac{r}{R}$

6.2.4 Unstable slope conditions

Several factors are observed to decrease the slope stability at Amfiteateret. Slope failures are generally not caused by a single factor, but a combination of various factors which eventually can bring a slope to a critical damage threshold where failure occurs (Stead & Eberhardt, 2013). The effect of groundwater for instance was shown to be much more dominating for slope stability when continuous joints were added to the model than for the model without joints.

In step 5 of the numerical modeling, the last analyses were performed in order to create unstable slope conditions (CSRF < 1). All these analyses were run with continuous joints, as this is assumed to reflect the situation in Amfiteateret most precisely. Four of the tested model configurations show unstable conditions as shown in Table 39. The different parameters are

coloured after uncertainty level, i.e. which conditions were most likely to cause the Bandak rock avalanche, and will be discussed in the following.

Table 39: Analyses which led to unstable or close to unstable slope conditions. The different parameters in each case are coloured after uncertainty level. Green is likely, yellow is possible and red is not likely.

Groundwater level	Joint Strength	Material model	CSRF
Dry slope	Low	Plastic – strain softening	1.04
Present	Low	Plastic – strain softening	0.99
High	Mean	Plastic – strain softening	0.81
High	Low	Linear elastic – perfectly plastic	1.10

All analyses have been highly sensitive to changes in groundwater level, and a drastic decrease in the CSRF is seen for models when the groundwater level is changed from present to high. Therefore, it is believed that groundwater pressure were one of the main factors causing unstable conditions.

A high groundwater level, or fully saturated slope, is not the case for the present hydrological situation at Kassen, but could be likely at an earlier stage. The only certain information regarding the time of the event is that the failure took place some time after the last glaciation in Younger Dryas, 12.7 – 11.5 ka (Hughes, Gyllencreutz, Lohne, Mangerud, & Svendsen, 2016), since rock avalanche deposits still are located beneath the slope. If the slope failed relatively short time after ice-retreat, a high water table is likely to assume. There are several reasons for this. During the cold Younger Dryas, permafrost probably existed down to sea level in southern and western parts of Norway (Blikra et al., 2006). After and during deglaciation, melting of permafrost could thus influence the stability of the slope. Permafrost located at some depth in the ground would additionally block for water drainage through the slope which in turn builds up water pressure (Hermanns, 2016b). After Younger Dryas the climate was so warm that the glacier covering Norway melted away in around 1000 years. At the lower parts of the glacier about 10-15 meters of ice melted away each summer which corresponds to 10 000 – 15 000 mm of rain (Ramberg et al., 2007). These conditions would result in a high groundwater table in the slope.

The lowest measured joint strength are realistic for filled joints. Since the majority of observed joints during fieldwork show rock to rock contact, it is assumed that rather the mean joint strength is most representable based on the present available information.

Several authors conclude that the behaviour of rock masses is often seen to be strain softening or brittle (Bieniawski, 1967; Bishop, 1967; Manfredini et al., 1975) leading to a progressive failure. As shown, plastic – strain softening material models gave a significant response from the rock mass, evaluated by the CSRF. It is therefore reasonable to assume that a certain amount of soft straining of the rock mass was a contributing factor for the failure.

Presumably, increased water pressure was not the only de-stabilizing process caused by the glacial retreat. Debuttressing after melt down might have caused failure of the slope, especially in parts that long has been unstable, but just froze in during glacial times. It is actually not

certain that the deformation at Kassen is purely post-glacial. Behind Amfiteateret there is a 100 m high scarp, defined as the back scarp of the whole unstable area, which seem to have been inactive since deglaciation. If this scarp was active prior to LGM (last Glacial Maximum) than the slope might have been at a critical stability condition already prior to LGM. Imagine if a new glaciation started in Norway today with more than 300 unstable slopes. These slopes would unlikely collapse during glacial time, but would reactivate immediately after deglaciation and could fail catastrophically soon after.

To summarize, several trigger mechanisms contributed to the Bandak rock avalanche. The groundwater table in the slope was most likely high considering the climatic situation after the glacier-retreat, and consequently water pressure in the slope contributed to failure. Additionally Debuttressing of a frozen instability is believed to have reactivated the slope, and contributed to the rapid collapse at the frontal part of Amfiteateret. Due to the significant model sensitivity for the strain softening material and joint models, some amount of strain softening of the rock mass is likely. When the two above factors are included in the numerical modeling, unstable slope conditions are reached for the mean strength value of the joints. However, as one observation of joint infilling is seen at the site, it cannot be excluded that the joint strength of the failed rock mass was even lower and maybe approaching the lowest measured values from fieldwork.

6.2.5 Forward analysis of present slope conditions

A forward analysis was performed in Step 6 of the modeling in order to analyse the present stability of the slope. Based on the numerical analysis, the slope is stable under the assumed present conditions with a CSRF of 1.78.

A potential sliding plane was defined based on maximum displacement in the model and the calculated area of the potential sliding mass (seen in the cross-section of the modeling) is 7872.6 m². Using the length of the back scarp of scenario G, the resulting potential sliding volume would be 3.17 million m³, which is 1.08 million m³ more than the calculated volume using the SLBL-technique. The main reason for this difference in volume is due to the limitations occurring when analyzing a slope in 2D. The slope geometry varies along the width of scenario G, and consequently a volume assessment where a constant slope geometry is assumed over the entire width of the scenario leads to errors.

On the other hand, the SLBL technique could have given a wrong volume as the technique does not account for sliding along discontinuities in the same way as with numerical modeling. It is however believed, that for this case, the errors occurring when a 2D problem is transferred to a 3D problem is of higher degree. The most likely volume of scenario G is therefore believed to be 2.09 million m³, found by the SLBL technique. However, based on the numerical analysis, it can be suggested that this volume is the minimum volume of the scenario. As previously discussed, further field investigations of scenario G is required to limit uncertainties related to the delimitation of the scenario.

6.2.6 Limitations with the numerical analysis

As numerical models require simplifications of real problems, every single parameter cannot be included or analyzed.

The effect of earthquakes as a triggering mechanism at Kassen was not included in order to limit the analysis. Hermanns, Hansen, et al. (2012) showed examples of 32 historic catastrophic

rock slope failures from Norway and around the world, and suggested that aseismic failure does not occur without the existence of pre-failure slope deformation. It is suggested that the offshore Storegga slide (approximately 8200 year ago) was seismically triggered, but beside this event there are no sure examples of avalanches triggered by earthquakes in Norway (Blikra et al., 2006). The seismicity rates over the 20th century in Norway suggests that there typically occurs one magnitude 5 or larger earthquake every 8-9 years and one magnitude 6 or larger earthquake every 90-100 years (Olesen et al., 2013). As seen in Figure 81, there are clear regional differences with most seismic activity located at near-shore or off shore areas. Earthquake magnitudes of 6 is considered to be the lower boundary to cause rock avalanches (Jibson, 1996; Keefer, 1984). Smaller rockslides and rock falls can however be triggered by lower magnitude earthquakes.

The clustering of earthquakes shown in Figure 81 are not in the vicinity of Telemark county. However, the registration of earthquakes presented in the figure started first in 1980, and it is assumed that Norway had a higher degree of seismicity 10 000-6000 years ago (Olesen et al., 2013). It can therefore not be excluded that an earthquake triggered the Bandak rock avalanche.

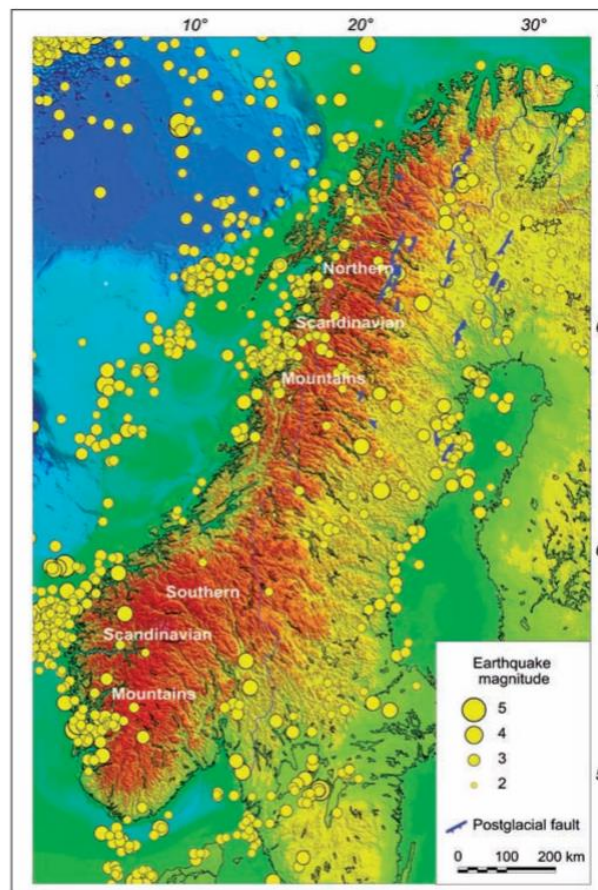


Figure 81: Earthquakes in Norway during the period 1980-2011. A concentration of earthquakes is seen at the western and northern coast areas and off shore. After (Olesen et al., 2013)

6.3 Stability of blocks at Skipet

The stability assessment for toppling and planar failure using LEM methods for the two potential unstable blocks at Skipet showed that the blocks are stable under dry conditions. Block 2 is stable even with a water pressure acting over the entire length of the open tension crack. The effect of incorporating water pressure decreased the FS with 11 % for the case where water filled the whole tension crack. Such a situation is rather unlikely, as the present groundwater is located at a deeper level. Water in the tension crack could have come from a heavy rainstorm, but still the tension crack is open and drainage to the sides would prevent build up of water in the crack. However, motivated by the historic event recorded from Skipet in 1985, a potential rockslide cannot be excluded to occur in the future.

In contrast to the numerical analysis, the strength of the discontinuities delimitating the blocks are determined with a higher degree of certainty. There are two main reasons for this. First, the measured JRC and JCS were performed at a surface with the same orientation as the sliding planes, very close to the studied stability problem. Secondly, the Barton-Bandis shear strength was applied directly in the calculations of FS, and not converted to equivalent Mohr-Coulomb parameters.

In order to relate potential failure to future consequences at the Kassen site, some estimations of volume of the blocks can be made. The LEM is a two-dimensional method, where the blocks are assigned with one unit length. The real length of the blocks were not possible to observe in field. In the worst-case, the maximum possible length of the blocks are 60 meters, which is the length of Skipet (determined by measuring tool in ArcGIS 10.4). The resulting maximum volumes of the two blocks is 8460 and 15202 m³ for respectively Block 1 and Block 2. These volumes are much less than the volumes of the previously defined scenarios, where the smallest scenario (Scenario B) has a volume of 110 000 m³. Applying the empirical relation to estimate potential run-up heights introduced in chapter 6.1 by T. Oppikofer et al. (2016) gives the following run-up heights for the locations Roeid, Lårdal, Dalen and Hogga Lock:

Table 40: Empirical estimation of run-up heights from potential failure of Block 1, Block 2 and of both blocks simultaneously.

	Estimated volume [Mm ³]	R [cm]			
		Roeid x = 2.5 km	Lårdal x = 12.5 km	Dalen x = 23 km	Hogga Lock x = 45
Block 1	8.46 * 10 ⁻⁶	0.6	0.18	0.12	0.07
Block 2	15.2 * 10 ⁻⁶	0.83	0.25	0.16	0.10
Block 1 + 2	23.66 * 10 ⁻⁶	1.08	0.33	0.21	0.13

Even if both blocks failed simultaneously, the resulting run-up heights are only in the dimensions of storm waves.

7 Conclusions and further investigations

Several tools have been applied to investigate the unstable area at Kassen. A hazard and preliminary consequence assessment is performed for seven minor, potential unstable scenarios, where the main findings and suggestions for future investigations are;

- Scenario A, B, F and G fall into the medium hazard class, while the other three scenarios fall into the low hazard class. The medium hazard class scenarios, except scenario F, have a high susceptibility to run out all the way to Bandak Lake. Scenario G have the highest score of 10.0, however this hazard should be re-evaluated after displacement measurements from dGNSS point BAN 7 are available.
- The volumes of the different scenarios are found by the SLBL technique, and range from 0.11 – 2.09 million m³. The greatest volume (scenario G) is uncertain due to the highly dissected rock mass which made it difficult to define the location of the delimiting structures and the persistence of potential sliding surfaces. This area should be investigated more throughout in field, especially at the toe-line of the scenario. In addition, core drilling could be used to measure the depth of the fracture rock mass and determine the location of the most likely sliding plane for scenario G. At the same time, the groundwater level in the slope could be found.
- Based on the estimated volumes of the scenarios, run-up heights from displacement waves are roughly estimated around the shoreline of Bandak by applying empirical relations. Only displacement waves from scenario G can cause devastating run-up heights in Dalen and Lårdal where most residences are located.
- Scenario B and G are plotted in a preliminary risk matrix, based on their hazard score and potential loss of life. Both scenarios classify as medium risk sites. By comparing with other risk-classified scenarios in Norway, it is suggested to follow up the unstable area with periodic monitoring, continuing with annual dGNSS measurements. To understand and limit the uncertainties of scenario G, GB-InSAR is suggested as a supplement to the dGNSS measurements.
- To complete the hazard and consequence assessment at the Kassen site, a detailed displacement wave analysis should be performed such that potential loss of life can be determined with higher certainty. When this work is completed the site can be risk classified and enter the database of unstable rock slopes in Norway.

The stability is further investigated at two sites, Amfiteateret and Skipet, which differ in scale, potential failure mode and rock mass conditions. Consequently two different analyse techniques are applied in order to achieve the most reliable results for each site. Numerical modeling was applied for the analysis at Amfiteateret, where the main findings are listed below.

- It is believed that the slope have failed catastrophically at the location of Scenario G some time after the last ice retreat in Younger Dryas. This is evident from the rock avalanche deposits in Bandak Lake, identified through bathymetric data. Due to the highly dissected character of the rock mass in the source area, a back-analysis of the Bandak rock avalanche was modeled as a continuum with the Finite Element Method with the software RS².

- The back-analysis show that it is very unlikely that the failure took place without the presence of a high groundwater table.
- It is clear that some amount of strain softening has to be associated with the failure, as none of the analyses with linear elastic – perfectly plastic material models lead to a CSRF below one.
- The models are highly sensitive to changes in joint strength from the mean values to the lowest values derived from fieldwork. A parameter study of the joint strength showed that the friction angle influences the CSRF the most, which is expected when the normal stress level is low compared to the strength of the intact rock.
- The most likely failure mode for the Bandak rock avalanche is seen to be translational, biplanar with J3 structures as the rear release surface, and J2 as the sliding structure. The persistence of these joint sets are uncertain, so the failure might have been partly irregular involving failure of intact rock bridges.
- Under present geological and hydrogeological conditions, the slope is stable at this location with a CSRF of 1.78.
- Numerical modelling is associated with uncertainties regarding the input parameters and the individual geological interpretations. In the numerical modeling at Amfiteateret, the highest uncertainties are related to the field stress, the equivalent, instantaneous Mohr-Coulomb strength of rock mass and joints, and the present level of the groundwater. These uncertainties can be limited by applying more comprehensive ground investigations such as stress measurements in the slope and drilling for determination of the groundwater level. The rock mass can in further analyses be modeled directly with Hoek-Brown strength to avoid uncertainties in the Mohr-Coulomb conversion. Still, the performed modeling is useful to understand the relative importance of different triggering mechanisms related to the Bandak rock avalanche.

Two unstable blocks were detected at Skipet. As these blocks were limited by clear structures, the stability of these blocks were investigated by applying Limit Equilibrium Methods, which revealed the following;

- The two potential unstable blocks at Skipet are most likely to slide, as the centre of gravity for both blocks fall inside their base which makes toppling not kinematic feasible.
- The respective FS for Block 1 and Block 2 are 1.57 and 1.74 under dry conditions. If the tension crack at the scarp of Block 2 were filled with water, the block would still be stable with a FS of 1.55. Based on this LEM analysis, the blocks at Skipet are assumed stable.

References

- Agliardi, F., Crosta, G., & Zanchi, A. (2001). Structural constraints on deep-seated slope deformation kinematics. *Engineering Geology*, 59(1), 83-102. doi: 10.1016/S0013-7952(00)00066-1
- Aubertin, M., Gill, D. E., & Simon, R. (1994). *On the use of the brittleness index modified (BIM) to estimate the post-peak behavior of rocks*. Paper presented at the 1st North American Rock Mechanics Symposium.
- Augustinus, P. (1996). *Rock mass strength and the stability of some glacial valley slopes*. Paper presented at the International Journal of Rock Mechanics and Mining Sciences and Geomechanics Abstracts.
- Ballantyne, C. K. (2002). Paraglacial geomorphology. *Quaternary Science Reviews*, 21(18), 1935-2017.
- Bandis, S. (1993). Engineering properties and characterization of rock discontinuities. *Comprehensive rock engineering*, 1, 155-183.
- Barton, N. (1973). Review of a new shear-strength criterion for rock joints. *Engineering Geology*, 7(4), 287-332.
- Barton, N. (1976). *The shear strength of rock and rock joints*. Paper presented at the International Journal of rock mechanics and mining sciences & Geomechanics abstracts.
- Barton, N., & Bandis, S. (1991). Review of predictive capabilities of JRC-JCS model in engineering practice. *Publikasjon-Norges Geotekniske Institutt*, 182, 1-8.
- Barton, N., & Choubey, V. (1977). The shear strength of rock joints in theory and practice. *Rock mechanics*, 10(1-2), 1-54.
- Bieniawski, Z. T. (1967). *Mechanism of brittle fracture of rock: part I—theory of the fracture process*. Paper presented at the International Journal of Rock Mechanics and Mining Sciences & Geomechanics Abstracts.
- Bishop, A. (1967). *Progressive failure with special reference to the mechanism causing it*. Paper presented at the Proc. Geotech. Conf., Oslo.
- Blikra, L., Longva, O., Braathen, A., Anda, E., Dehls, J., & Stalsberg, K. (2006). Rock slope failures in Norwegian fjord areas: examples, spatial distribution and temporal pattern *Landslides from massive rock slope failure* (pp. 475-496): Springer.
- Braathen, A., Blikra, L. H., Berg, S. S., & Karlsen, F. (2004). Rock-slope failures in Norway; type, geometry, deformation mechanisms and stability. *Norwegian Journal of Geology*, 84(1), 67-88.
- Brady, B. H., & Brown, E. T. (2013). *Rock mechanics: for underground mining*: Springer Science & Business Media.
- Chugh, A. K. (2003). On the boundary conditions in slope stability analysis. *International journal for numerical and analytical methods in geomechanics*, 27(11), 905-926.
- Corominas, J. (1996). The angle of reach as a mobility index for small and large landslides. *Canadian Geotechnical Journal*, 33(2), 260-271.
- Dahlgren, S. (1993). Litt om geologien i det sentrale Telemark.
- Dalsegg, E., & Rønning, J. S. (2012). Geofysiske målinger på Mannen i Rauma kommune, Møre og Romsdal: NGU.
- Deere, D. U., & Miller, R. (1966). Engineering classification and index properties for intact rock: DTIC Document.
- Eberhardt, E. (2003). Rock slope stability analysis—utilization of advanced numerical techniques. *Earth and Ocean sciences at UBC*.
- Eberhardt, E. (2006). From cause to effect: using numerical modelling to understand rock slope instability mechanisms *Landslides from Massive Rock Slope Failure* (pp. 85-101): Springer.
- Eiken, T. (2013). Førebels Rapport om Deformasjonsmålinger i potensielle fjellskred, Telemark 2013.
- Farsund, T. Ø. (2011). *Geological and numerical stability modelling of Mannen, Romsdalen*. (Master degree), NTNU, Trondheim.

- Ferrigno, F., Gigli, G., Fanti, R., & Casagli, N. (2015). GB-InSAR monitoring and observational method for landslide emergency management: the Montaguto earthflow (AV, Italy). *Natural Hazards and Earth System Sciences Discussions*, 3, 7247-7273.
- Fredin, O., Bergstrom, B., Eilertsen, R., Hansen, L., Longva, O., Nesje, A., & Sveian, H. (2013). Glacial landforms and Quaternary landscape development in Norway. *Quaternary Geology of Norway*, edited by: Olsen, L., Fredin, O., and Olesen, O., Geological Survey of Norway Special Publication, Geological Survey of Norway, Trondheim, 525.
- Grøneng, G. (2010). Stability analyses of the Åknes rock slope, Western Norway.
- Grøneng, G., & Nilsen, B. (2008). Procedure for determining input parameters for Barton–Bandis joint shear strength formulation: Technical Report, Department of Geology and Mineral Resources Engineering, Norwegian University of Science and Technology.
- Hammah, R. (2005). *A comparison of finite element slope stability analysis with conventional limit-equilibrium investigation*. Paper presented at the Proceedings of the 58th Canadian Geotechnical and 6th Joint IAH-CNC and CGS Groundwater Specialty Conferences–GeoSask 2005.
- Hammah, R., Yacoub, T., Corkum, B., & Curran, J. (2005). *The shear strength reduction method for the generalized Hoek-Brown criterion*. Paper presented at the Alaska Rocks 2005, The 40th US Symposium on Rock Mechanics (USRMS).
- Hammah, R. E., Curran, J. H., Yacoub, T., & Corkum, B. (2004). *Stability analysis of rock slopes using the finite element method*. Paper presented at the Proceedings of the ISRM regional symposium EUROCK.
- Hanssen, T. (1998). *Rock stresses and tectonic activity*. Paper presented at the Proceedings of the Norwegian National Rock Mechanics Conference. Oslo.
- Hermanns, R., Oppikofer, T., Molina, F. X. Y., Dehls, J. F., & Böhme, M. (2014). Approach for systematic rockslide mapping of unstable rock slopes in Norway *Landslide Science for a Safer Geoenvironment* (pp. 129-134): Springer.
- Hermanns, R. L. (2016a). *Landslide*. Springer International Publishing AG 2016.
- Hermanns, R. L. (2016b). Personal Communication.
- Hermanns, R. L., Blikra, L. H., Anda, E., Saintot, A., Dahle, H., Oppikofer, T., . . . Eiken, T. (2013). *Systematic mapping of large unstable rock slopes in Norway*. Paper presented at the 2nd World Landslide Forum, WLF 2011, Rome.
- Hermanns, R. L., Hansen, L., Sletten, K., Böhme, M., Bunkholt, H., Dehls, J., . . . Høgaas, F. (2012). Systematic geological mapping for landslide understanding in the Norwegian context. *Landslide and engineered slopes: protecting society through improved understanding*. Taylor & Francis Group, London, 265-271.
- Hermanns, R. L., Oppikofer, T., Anda, E., Blikra, L., Böhme, M., Bunkholt, H., . . . Yugsy Molina, F. (2012). Recommended hazard and risk classification system for large unstable rock slopes in Norway. (NGU).
- Hermanns, R. L., Oppikofer, T., Anda, E., Blikra, L. H., Böhme, M., Bunkholt, H., . . . Molina, F. X. Y. (2013). Hazard and risk classification for large unstable rock slopes in Norway. *Italian Journal of Engineering Geology and Environment*, 2013(TOPIC2), 245-254. doi: 10.4408/IJEGE.2013-06.B-22
- Highland, L., & Bobrowsky, P. T. (2008). *The landslide handbook: a guide to understanding landslides*: US Geological Survey Reston.
- Hoek, E. (1983). Strength of jointed rock masses. *Geotechnique*, 33(3), 187-223.
- Hoek, E. (1994). Strength of rock and rock masses. *ISRM News Journal*, 2(2), 4-16.
- Hoek, E. (2000). Practical rock engineering: Rocscience.
- Hoek, E. (2007). Practical rock engineering. 2007. *Online. ed. Rocscience*.
- Hoek, E., & Bray, J. D. (1981). *Rock slope engineering*: CRC Press.
- Hoek, E., Brown, E. T., Institution of, M., & Metallurgy. (1980). *Underground excavations in rock*. London: Institution of Mining and Metallurgy.

- Hoek, E., Carranza-Torres, C., & Corkum, B. (2002). Hoek-Brown failure criterion-2002 edition. *Proceedings of NARMS-Tac*, 1, 267-273.
- Horton, P., Jaboyedoff, M., Rudaz, B., & Zimmermann, M. (2013). Flow-R, a model for susceptibility mapping of debris flows and other gravitational hazards at a regional scale. *Natural Hazards and Earth System Sciences*, 13(4), 869-885.
- Hughes, A. L., Gyllencreutz, R., Lohne, Ø. S., Mangerud, J., & Svendsen, J. I. (2016). The last Eurasian ice sheets—a chronological database and time-slice reconstruction, DATED-1. *Boreas*, 45(1), 1-45.
- Hungr, O., & Evans, S. (2004). Entrainment of debris in rock avalanches: an analysis of a long run-out mechanism. *Geological Society of America Bulletin*, 116(9-10), 1240-1252.
- Hungr, O., Leroueil, S., & Picarelli, L. (2014). The Varnes classification of landslide types, an update. *Journal of the International Consortium on Landslides*, 11(2), 167-194. doi: 10.1007/s10346-013-0436-y
- ISRM. (1978). Suggested methods for determining hardness and abrasiveness of rocks.
- ISRM. (1979). Suggested methods for determining the uniaxial compressive strength and deformability of rock materials. .
- Jaboyedoff, M., Baillifard, F., Couture, R., Locat, J., & Locat, P. (2004). Toward preliminary hazard assessment using DEM topographic analysis and simple mechanical modeling by means of sloping local base level. *Landslides: evaluation and stabilization*. Balkema, Taylor & Francis Group, London, 199-206.
- Jaboyedoff, M., & Labiouse, V. (2011). Technical Note: Preliminary estimation of rockfall runout zones. *Natural Hazards and Earth System Sciences*, 11(3), 819-828.
- Jansen, I. J. (1986). *Kvartærgeologi, Jord og landskap i Telemark gjennom 11 000 år.*: Institutt for naturanalyse.
- Jibson, R. W. (1996). Use of landslides for paleoseismic analysis. *Engineering Geology*, 43(4), 291-323.
- Johnson, R. B., & DeGraff, J. V. (1988). *Principles of engineering geology*: Wiley.
- Keefer, D. K. (1984). Landslides caused by earthquakes. *Geological Society of America Bulletin*, 95(4), 406-421.
- Kveldsvik, V., Einstein, H. H., Nilsen, B., & Blikra, L. H. (2009). Numerical analysis of the 650,000 m² Åknes rock slope based on measured displacements and geotechnical data. *Rock Mechanics and Rock Engineering*, 42(5), 689-728.
- Longva, O., Blikra, L. H., & Dehls, J. (2009). Rock avalanches: distribution and frequencies in the inner part of Storfjorden, Møre og Romsdal County, Norway. *Geological Survey of Norway*, 32.
- Manfredini, G., Martinetti, S., & Ribacchi, R. (1975). *Inadequacy of limiting equilibrium methods for rock slopes design*. Paper presented at the The 16th US Symposium on Rock Mechanics (USRMS).
- Marinos, V., Marinos, P., & Hoek, E. (2005). The geological strength index: Applications and limitations. *Bulletin of Engineering Geology and the Environment*, 64(1), 55-65. doi: 10.1007/s10064-004-0270-5
- Monserrat, O., Crosetto, M., & Luzi, G. (2014). A review of ground-based SAR interferometry for deformation measurement. *ISPRS Journal of Photogrammetry and Remote Sensing*, 93, 40-48.
- Myrvang, A. (2001). *Bergmekanikk (Rock Mechanics)*. Trondheim: Department of Geology and Mineral Resources Engineering, NTNU.
- NGU. (2016). Bedrock N250. 2016, from <https://www.ngu.no/en/topic/datasets>
- Nilsen, B. (2000). New trends in rock slope stability analyses. *Bulletin of Engineering Geology and the Environment*, 58(3), 173-178.
- Nilsen, B. (2016). Personal Communication.
- Nilsen, B., & Broch, E. (2013). *Ingeniørgeologi-berg Grunnkurskompendium*. (NTNU).
- Nilsen, K. S., Dons J.A., & Gyøry, E. (Cartographer). (2013). Bergrunnskart (Bedrock map) BANDAK 1513 I, M 1:50 000.
- Norrish, N. I., & Wyllie, D. C. (1996). Rock slope stability analysis. *Landslides: Investigation and Mitigation: Transportation Research Board Special Report*, 247, 391-425.

- Norwegian Water Resources and Energy Directorate. (2016). National database of landslides. from The Norwegian Water Resources and Energy Directorate
<http://skredatlas.nve.no/html5Viewer/?viewer=nveatlas>
- Olesen, O., Bungum, H., Dehls, J., Lindholm, C., Pascal, C., & Roberts, D. (2013). Neotectonics, seismicity and contemporary stress field in Norway—mechanisms and implications. *NGU Special Publication, 13*, 145-174.
- Oppikofer, T., Böhme, M., Nicolet, P., Penna, I., & Hermanns, R. L. (2016). Metodikk for konsekvensanalyse av fjellskred. (Vol. 47, pp. 67): Geological Survey of Norway.
- Oppikofer, T., Hermanns, R., Sandøy, G., Böhme, M., Jaboyedoff, M., Horton, P., . . . Fuchs, H. (2016). Quantification of casualties from potential rock-slope failures in Norway. *Landslides and Engineered Slopes. Experience, Theory and Practice - Proceedings of the 12th International Symposium on Landslides, 3*, 1537-1544.
- Oppikofer, T., Nordahl, B., Bunkholt, H., Nicolaisen, M., Jarna, A., Iversen, S., . . . Molina, F. X. Y. (2015). Database and online map service on unstable rock slopes in Norway—From data perpetuation to public information. *Geomorphology, 249*, 69-81.
- Panthi, K. K., & Nilsen, B. (2006). Numerical analysis of stresses and displacements for the Tafjord slide, Norway. *Bulletin of Engineering Geology and the Environment, 65*(1), 57-63.
- Patton, F. D. (1966). *Multiple modes of shear failure in rock*. Paper presented at the 1st ISRM Congress.
- Popescu, M. E. (2002). *Landslide causal factors and landslide remedial options*. Paper presented at the Third International Conference on Landslides, Slope Stability & The Safety of Infrastructures.
- Ramberg, I. B., Bryhni, I., & Nøttvedt, A. (2007). *Landet blir til: Norges geologi*: Norsk geologisk forening.
- Richards, L. R. (1975). *The shear strength of joints in weathered rock*. University of London.
- Rocscience. (2016a). DIPS 7.0. Retrieved 10.09.16, 2016, from
<https://www.rocscience.com/rocscience/products/dips>
- Rocscience. (2016b). RS2. Retrieved 09.11.2016, from
<https://www.rocscience.com/rocscience/products/rs2>
- Rocscience. (2016c). RS2: Webhelp 9, Rocscience Inc. Retrieved 25.10.16, from
<https://www.rocscience.com/help/phase2/webhelp9/phase2.htm>
- Rosso, R. (1976). *A comparison of joint stiffness measurements in direct shear, triaxial compression, and in situ*. Paper presented at the International Journal of Rock Mechanics and Mining Sciences & Geomechanics Abstracts.
- Sandersen, F., Bakkehøi, S., Hestnes, E., & Lied, K. (1997). The influence of meteorological factors on the initiation of debris flows, rockfalls, rockslides and rockmass stability. *Publikasjon-Norges Geotekniske Institutt, 201*, 97-114.
- Sandøy, G. (2012). *Back-analysis of the 1756 Tjellefonna rockslide, Langfjorden*. (Master thesis), NTNU, Trondheim.
- Scheidegger, A. E. (1973). On the prediction of the reach and velocity of catastrophic landslides. *Rock Mechanics and Rock Engineering, 5*(4), 231-236.
- Schleier, M., Hermanns, R. L., Rohn, J., & Gosse, J. C. (2015). Diagnostic characteristics and paleodynamics of supraglacial rock avalanches, Innerdalen, Western Norway. *Geomorphology, 245*, 23-39.
- Statistics Norway. (2016). Tettsteder. Folkemengde og areal, etter kommune. (Communities. Population and area after municipality). Oslo.
- Stead, D., & Eberhardt, E. (2013). Understanding the mechanics of large landslides. *Ital. J. Eng. Geol. Environ. Book Ser, 6*, 85-112.
- Stead, D., Eberhardt, E., & Coggan, J. (2006). Developments in the characterization of complex rock slope deformation and failure using numerical modelling techniques. *Engineering Geology, 83*(1), 217-235.
- Strahler, A. H., & Strahler, A. N. (2000). *Introducing physical geography*: Wiley.

- The Norwegian Mapping Authority. (2016). Norgeskart (Map of Norway). Retrieved 25.12.16, from http://www.norgeskart.no/?_ga=1.93680413.1274485604.1461699745#5/378604/7226208
- Travelletti, J., Demand, J., Jaboyedoff, M., & Marillier, F. (2010). Mass movement characterization using a reflexion and refraction seismic survey with the sloping local base level concept. *Geomorphology*, 116(1), 1-10.
- Trinh, N. Q. (2016). Personal communication.
- Turner, A. K., & Schuster, R. L. (1996). *Landslides : investigation and mitigation* (Vol. 247). Washington: National Academy Press.
- Ureel, S., & Momayez, M. (2014). *An investigation of the limit equilibrium method and numerical modeling for rock slope stability analysis*. Paper presented at the Rock Mechanics and Its Applications in Civil, Mining, and Petroleum Engineering.
- Varnes, D. J. (1978). Slope movement types and processes. *Transportation Research Board Special Report*(176).
- Wyllie, D. C., & Mah, C. (2004). *Rock slope engineering*: CRC Press.
- Wyrwoll, K.-H. (1977). Causes of rock-slope failure in a cold area: Labrador-Ungava. *Geological Society of America Reviews in Engineering Geology*, 3, 59-67.

8 Appendix

8.1 Hazard assessments scenarios A-G

Hazard assessment of large unstable rock slopes in Norway							
Site name:	Kassen	Scenario:	A	Made by:	Kaja Krogh	Date:	19.10.2016
Hazard classes	Probability	Cumulative prob.	Hazard score		Fitted normal distribution		
Very low	0.0 %	0.0 %	Minimum	3.8	Mean μ	4.8	
Low	42.5 %	42.5 %	Maximum	6.0	St. dev. σ	0.6	
Medium	57.5 %	100.0 %	Mode	5.3	$\mu - 2\sigma$	3.7	
High	0.0 %	100.0 %	Mean	4.9	$\mu + 2\sigma$	6.0	
Very high	0.0 %	100.0 %	5% percentile	3.8	Corr. Coeff..	0.9995	
			95% percentile	5.6	K-S-test	5.8 %	
1. Backscarp						Score	Norm. prob.
Not developed						0	0.0 %
Partly open over width of slide body (few cm to m)						0.5	0.0 %
Fully open over width of slide body (few cm to m)						1	100.0 %
Comment: Backscarp fully developed. Potetial unstable block is fully isolated.							
2.Potential sliding structures						Score	Norm. prob.
No penetrative structures dip out of the slope						0	0.0 %
Penetrative structures dip on average < 20 degree or steeper than the slope						0.5	80.0 %
Penetrative structures dip on average > 20 degree and daylight with the slope						1	20.0 %
Comment: Dip angle = 17° of potential sliding plane (J2) at the nearest measurement point. The average dip of this joint set in the structural domain is however 21°.							
3. Lateral release surfaces						Score	Norm. prob.
Not developed						0	0.0 %
Partly developed on 1 side						0.25	0.0 %
Fully developed or free slope on 1 side or partly developed on 2 sides						0.5	0.0 %
Fully developed or free slope on 1 side and partly developed on 1 side						0.75	0.0 %
Fully developed or free slope on 2 sides						1	100.0 %
Comment: Both lateral surfaces are free							
4. Kinematic feasibility test						Score	Norm. prob.
Kinematic feasibility test does not allow for planar sliding, wedge sliding or toppling						0	0.0 %
Failure is partly kinematically possible (movement direction is more than $\pm 30^\circ$ to slope orientation)						0.5	0.0 %
Failure is kinematically possible (movement direction is less than $\pm 30^\circ$ to slope orientation)						0.75	50.0 %
Failure is partly kinematically possible on persistent discontinuities (movement direction is more than $\pm 30^\circ$ to slope orientation)						0.75	0.0 %
Failure is kinematically possible on persistent discontinuities (movement direction is less than $\pm 30^\circ$ to slope orientation)						1	50.0 %
Comment: Planar and toppling failure is possible along respectively J2 and J1. Wedge failure is partly possible along the intersection of J2 and J3.							
5. Morphologic expression of the rupture surface						Score	Norm. prob.
No indication on slope morphology						0	100.0 %
Slope morphology suggests formation of a rupture surface (bulging, concavity -convexity, springs)						0.5	0.0 %
Continuous rupture surface is suggested by slope morphology and can be mapped out						1	0.0 %
Comment: Possible rupture surface covered by debris. No morphologic expressions of rupture surface recognized on hillshade maps.							
6. Displacement rates						Score	Norm. prob.
No significant movement						0	100.0 %
0.2- 0.5 cm/year						1	0.0 %
0.5 - 1 cm/year						2	0.0 %
1 - 4 cm/year						3	0.0 %
4 - 10 cm/year						4	0.0 %
> 10 cm/year						5	0.0 %
Comment: dGNSS measurements from 2012 - 2016 (BAN-1) show average movement < 0.2 cm/y.							
7. Acceleration (if velocity is >0.5 cm/yr and <10 cm/yr)						Score	Norm. prob.
No acceleration or change in displacement rates						0	100.0 %
Increase in displacement rates						1	0.0 %
Comment: Movement < 0.5 cm/y.							
8. Increase of rock fall activity						Score	Norm. prob.
No increase of rock fall activity						0	30.0 %
Increase of rock fall activity						1	70.0 %
Comment: Ortophoto and field observations show some fresh rock falls beneath the toe-line. Which is a relatively increase in rock fall activity compared to adjacent slopes both inside and outside of the whole unstable area.							
9. Past events						Score	Norm. prob.
No post-glacial events of similar size						0	0.0 %
One or several events older than 5000 years of similar size						0.5	50.0 %
One or several events younger than 5000 years of similar size						1	50.0 %
Comment: Bathymetric model show rockslide or rockfall deposits in Bandak lake, beneath scenario A. Age is uncertain.							

Hazard assessment of large unstable rock slopes in Norway							
Site name:	Kassen	Scenario:	B (Skipet)	Made by:	Kaja Krogh	Date:	04.12.2016
Hazard classes	Probability	Cumulative prob.	Hazard score		Fitted normal distribution		
Very low	0.0 %	0.0 %	Minimum	6.5	Mean μ	6.9	
Low	0.0 %	0.0 %	Maximum	7.5	St. dev. σ	0.1	
Medium	84.0 %	84.0 %	Mode	7.0	$\mu - 2\sigma$	6.6	
High	16.0 %	100.0 %	Mean	7.0	$\mu + 2\sigma$	7.1	
Very high	0.0 %	100.0 %	5% percentile	6.5	Corr. Coeff..	0.9979	
			95% percentile	7.5	K-S-test	15.8 %	
1. Backscarp							
					Score	Norm. prob.	
Not developed					0	0.0 %	
Partly open over width of slide body (few cm to m)					0.5	0.0 %	
Fully open over width of slide body (few cm to m)					1	100.0 %	
Comment: "Skipet" is an isolated rock cliff.							
2. Potential sliding structures							
					Score	Norm. prob.	
No penetrative structures dip out of the slope					0	0.0 %	
Penetrative structures dip on average < 20 degree or steeper than the slope					0.5	20.0 %	
Penetrative structures dip on average > 20 degree and daylight with the slope					1	80.0 %	
Comment: Mean values of J1 dips into the slope, but can act as release surface for biplanar failure. J2 varies from 5° to 21°, measured at opposite sites of Skipet. J1 and J2 are penetrative.							
3. Lateral release surfaces							
					Score	Norm. prob.	
Not developed					0	0.0 %	
Partly developed on 1 side					0.25	0.0 %	
Fully developed or free slope on 1 side or partly developed on 2 sides					0.5	0.0 %	
Fully developed or free slope on 1 side and partly developed on 1 side					0.75	0.0 %	
Fully developed or free slope on 2 sides					1	100.0 %	
Comment: See criterion 1.							
4. Kinematic feasibility test							
					Score	Norm. prob.	
Kinematic feasibility test does not allow for planar sliding, wedge sliding or toppling					0	0.0 %	
Failure is partly kinematically possible (movement direction is more than $\pm 30^\circ$ to slope orientation)					0.5	0.0 %	
Failure is kinematically possible (movement direction is less than $\pm 30^\circ$ to slope orientation)					0.75	0.0 %	
Failure is partly kinematically possible on persistent discontinuities (movement direction is more than $\pm 30^\circ$ to slope orientation)					0.75	0.0 %	
Failure is kinematically possible on persistent discontinuities (movement direction is less than $\pm 30^\circ$ to slope orientation)					1	100.0 %	
Comment: "Skipet" is located in the LW domain, where planar sliding and toppling is possible along respectively J2 and J1. Wedge sliding is partly possible along the intersection of J2 and J3. J2 and J1 are persistent through Skipet.							
5. Morphologic expression of the rupture surface							
					Score	Norm. prob.	
No indication on slope morphology					0	80.0 %	
Slope morphology suggests formation of a rupture surface (bulging, concavity -convexity, springs)					0.5	20.0 %	
Continuous rupture surface is suggested by slope morphology and can be mapped out					1	0.0 %	
Comment: Foot of "Skipet" is covered by rockfall debris. Hillshade maps and field observations might indicate some minor bulging at the toe.							
6. Displacement rates							
					Score	Norm. prob.	
No significant movement					0	0.0 %	
0.2 - 0.5 cm/year					1	100.0 %	
0.5 - 1 cm/year					2	0.0 %	
1 - 4 cm/year					3	0.0 %	
4 - 10 cm/year					4	0.0 %	
> 10 cm/year					5	0.0 %	
Comment: dGNNS measurements from 2013-2016 show average movement of 2.65 mm/year. Note that this is not statistically significant, but still given full score to be conservative.							
7. Acceleration (if velocity is >0.5 cm/yr and <10 cm/yr)							
					Score	Norm. prob.	
No acceleration or change in displacement rates					0	100.0 %	
Increase in displacement rates					1	0.0 %	
Comment: Movement < 0.5 cm/y.							
8. Increase of rock fall activity							
					Score	Norm. prob.	
No increase of rock fall activity					0	0.0 %	
Increase of rock fall activity					1	100.0 %	
Comment: Orthophoto and field observations indicate increase in rockfall activity compared to adjacent slopes - both inside and outside of the defined unstable area.							
9. Past events							
					Score	Norm. prob.	
No post-glacial events of similar size					0	0.0 %	
One or several events older than 5000 years of similar size					0.5	0.0 %	
One or several events younger than 5000 years of similar size					1	100.0 %	
Comment: Rock slide event recorded from "Skipet" around 1985, resulting in displacement waves in Bandak lake of minor size (www.skrednett.no).							

Hazard assessment of large unstable rock slopes in Norway							
Site name:	Kassen	Scenario:	C	Made by:	Kaja Krogh	Date:	03.10.2016
Hazard classes	Probability	Cumulative prob.	Hazard score		Fitted normal distribution		
Very low	1.5 %	1.5 %	Minimum	2.0	Mean μ	3.5	
Low	98.5 %	100.0 %	Maximum	4.5	St. dev. σ	0.7	
Medium	0.0 %	100.0 %	Mode	3.5	$\mu - 2\sigma$	2.1	
High	0.0 %	100.0 %	Mean	3.7	$\mu + 2\sigma$	5.0	
Very high	0.0 %	100.0 %	5% percentile	2.3	Corr. Coeff..	0.9945	
			95% percentile	4.5	K-S-test	17.4 %	
1. Backscarp							
Not developed					Score	Norm. prob.	
Partly open over width of slide body (few cm to m)					0	0.0 %	
Fully open over width of slide body (few cm to m)					0.5	10.0 %	
Fully open over width of slide body (few cm to m)					1	90.0 %	
Comment: Not verified in field, but looks fully open on Hillshade.							
2. Potential sliding structures							
No penetrative structures dip out of the slope					Score	Norm. prob.	
Penetrative structures dip on average < 20 degree or steeper than the slope					0	100.0 %	
Penetrative structures dip on average > 20 degree and daylight with the slope					0.5	0.0 %	
Penetrative structures dip on average > 20 degree and daylight with the slope					1	0.0 %	
Comment: No penetrative structures relative to the size of the potential sliding body.							
3. Lateral release surfaces							
Not developed					Score	Norm. prob.	
Partly developed on 1 side					0	0.0 %	
Fully developed or free slope on 1 side or partly developed on 2 sides					0.25	0.0 %	
Fully developed or free slope on 1 side and partly developed on 1 side					0.5	0.0 %	
Fully developed or free slope on 2 sides					0.75	100.0 %	
Fully developed or free slope on 2 sides					1	0.0 %	
Comment: Western flank is partly developed. Degree of displacement on eastern flank is uncertain, but is assumed to be either partly developed or fully developed.							
4. Kinematic feasibility test							
Kinematic feasibility test does not allow for planar sliding, wedge sliding or toppling					Score	Norm. prob.	
Failure is partly kinematically possible (movement direction is more than $\pm 30^\circ$ to slope orientation)					0	0.0 %	
Failure is kinematically possible (movement direction is less than $\pm 30^\circ$ to slope orientation)					0.5	0.0 %	
Failure is partly kinematically possible on persistent discontinuities (movement direction is more than $\pm 30^\circ$ to slope orientation)					0.75	100.0 %	
Failure is kinematically possible on persistent discontinuities (movement direction is less than $\pm 30^\circ$ to slope orientation)					0.75	0.0 %	
Failure is kinematically possible on persistent discontinuities (movement direction is less than $\pm 30^\circ$ to slope orientation)					1	0.0 %	
Comment: Kinematic feasibility test for the LW domain states that planar sliding and toppling is possible along respectively J2 and J1. Wedge failure is partly possible along the intersection of J2 and J3. Discontinuities are not persistent through the whole potential sliding body.							
5. Morphologic expression of the rupture surface							
No indication on slope morphology					Score	Norm. prob.	
Slope morphology suggests formation of a rupture surface (bulging, concavity -convexity, springs)					0	100.0 %	
Continuous rupture surface is suggested by slope morphology and can be mapped out					0.5	0.0 %	
Continuous rupture surface is suggested by slope morphology and can be mapped out					1	0.0 %	
Comment: Potential rupture surface covered by debris.							
6. Displacement rates							
No significant movement					Score	Norm. prob.	
0.2 - 0.5 cm/year					0	100.0 %	
0.5 - 1 cm/year					1	0.0 %	
1 - 4 cm/year					2	0.0 %	
4 - 10 cm/year					3	0.0 %	
> 10 cm/year					4	0.0 %	
> 10 cm/year					5	0.0 %	
Comment: BAN-2 and BAN-3 show displacement < 2mm/year. They are either not statistically significant.							
7. Acceleration (if velocity is >0.5 cm/yr and <10 cm/yr)							
No acceleration or change in displacement rates					Score	Norm. prob.	
Increase in displacement rates					0	100.0 %	
Increase in displacement rates					1	0.0 %	
Comment: Movement < 0.5 cm/y.							
8. Increase of rock fall activity							
No increase of rock fall activity					Score	Norm. prob.	
Increase of rock fall activity					0	30.0 %	
Increase of rock fall activity					1	70.0 %	
Comment: Increase in rockfall activity compared to adjacent slopes outside the unstable area. However, there are slopes inside the unstable area with signs of higher activity and freshness of rockfalls. Verified by orthophoto studies and field observations.							
9. Past events							
No post-glacial events of similar size					Score	Norm. prob.	
One or several events older than 5000 years of similar size					0	50.0 %	
One or several events younger than 5000 years of similar size					0.5	0.0 %	
One or several events younger than 5000 years of similar size					1	50.0 %	
Comment: Rock slide recorded from Skipet from around 1985 is relevant for scenario C. However, this is not an event of similar size, which is why this outcome only gets half score.							

Hazard assessment of large unstable rock slopes in Norway								
Site name:	Kassen	Scenario:	D	Made by:	Kaja Krogh	Date:	03.10.2016	
Hazard classes	Probability	Cumulative prob.		Hazard score		Fitted normal distribution		
Very low	2.0 %	2.0 %		Minimum	2.0	Mean μ	3.9	
Low	82.0 %	84.0 %		Maximum	5.3	St. dev. σ	0.8	
Medium	16.0 %	100.0 %		Mode	4.0	$\mu - 2\sigma$	2.4	
High	0.0 %	100.0 %		Mean	4.0	$\mu + 2\sigma$	5.5	
Very high	0.0 %	100.0 %		5% percentile	2.6	Corr. Coeff..	0.9998	
				95% percentile	5.3	K-S-test	4.3 %	
1. Backscarp							Score	Norm. prob.
Not developed							0	0.0 %
Partly open over width of slide body (few cm to m)							0.5	100.0 %
Fully open over width of slide body (few cm to m)							1	0.0 %
Comment:	Deformation of backscarp varies in space. Fully open towards the north western part of the instability, while more juvenile displacement towards the east end.							
2. Potential sliding structures							Score	Norm. prob.
No penetrative structures dip out of the slope							0	50.0 %
Penetrative structures dip on average < 20 degree or steeper than the slope							0.5	0.0 %
Penetrative structures dip on average > 20 degree and daylight with the slope							1	50.0 %
Comment:	J2 dips from 14 to 23° out of the slope (mean values from two spatial relevant observation points). J1 varies in the two observation points by dipping into the slope/parallel to the slope/steeper than the slope. Degree of penetration of the structures is uncertain.							
3. Lateral release surfaces							Score	Norm. prob.
Not developed							0	0.0 %
Partly developed on 1 side							0.25	0.0 %
Fully developed or free slope on 1 side or partly developed on 2 sides							0.5	0.0 %
Fully developed or free slope on 1 side and partly developed on 1 side							0.75	100.0 %
Fully developed or free slope on 2 sides							1	0.0 %
Comment:	Free face on the north western flank and partly developed on the south eastern flank.							
4. Kinematic feasibility test							Score	Norm. prob.
Kinematic feasibility test does not allow for planar sliding, wedge sliding or toppling							0	0.0 %
Failure is partly kinematically possible (movement direction is more than $\pm 30^\circ$ to slope orientation)							0.5	0.0 %
Failure is kinematically possible (movement direction is less than $\pm 30^\circ$ to slope orientation)							0.75	50.0 %
Failure is partly kinematically possible on persistent discontinuities (movement direction is more than $\pm 30^\circ$ to slope orientation)							0.75	0.0 %
Failure is kinematically possible on persistent discontinuities (movement direction is less than $\pm 30^\circ$ to slope orientation)							1	50.0 %
Comment:	Planar sliding possible along J2 (where it exceeds the friction angle), and toppling is possible along J1. Wedge failure partly possible at intersection of J2 and J3. Persistence of discontinuities uncertain.							
5. Morphologic expression of the rupture surface							Score	Norm. prob.
No indication on slope morphology							0	100.0 %
Slope morphology suggests formation of a rupture surface (bulging, concavity -convexity, springs)							0.5	0.0 %
Continuous rupture surface is suggested by slope morphology and can be mapped out							1	0.0 %
Comment:	Potential rupture surface covered by rock deposits. No morphologic expressions of rupture surface observed on hillshade maps.							
6. Displacement rates							Score	Norm. prob.
No significant movement							0	100.0 %
0.2 - 0.5 cm/year							1	0.0 %
0.5 - 1 cm/year							2	0.0 %
1 - 4 cm/year							3	0.0 %
4 - 10 cm/year							4	0.0 %
> 10 cm/year							5	0.0 %
Comment:	BAN-3 and BAN-4 are installed close to the scenario, which both show movement < 0.2 cm/year. Movement is either not statistically significant.							
7. Acceleration (if velocity is >0.5 cm/yr and <10 cm/yr)							Score	Norm. prob.
No acceleration or change in displacement rates							0	100.0 %
Increase in displacement rates							1	0.0 %
Comment:	Movement < 0.5 cm/year.							
8. Increase of rock fall activity							Score	Norm. prob.
No increase of rock fall activity							0	20.0 %
Increase of rock fall activity							1	80.0 %
Comment:	Certainly increase in rockfall activity compared to adjacent slopes outside the unstable area. Full score is however not given, due to areas inside the unstable area with relatively higher activity.							
9. Past events							Score	Norm. prob.
No post-glacial events of similar size							0	20.0 %
One or several events older than 5000 years of similar size							0.5	40.0 %
One or several events younger than 5000 years of similar size							1	40.0 %
Comment:	Historic rock slide events in the unstable area is obvious due to deposits in Bandak lake. Age uncertain.							

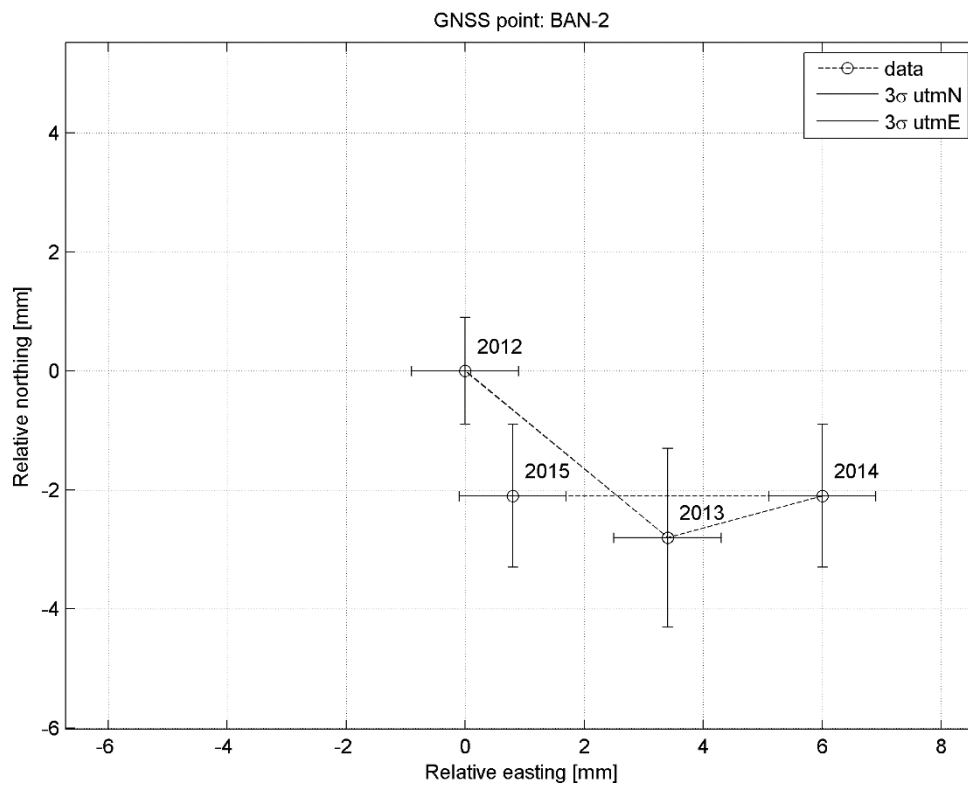
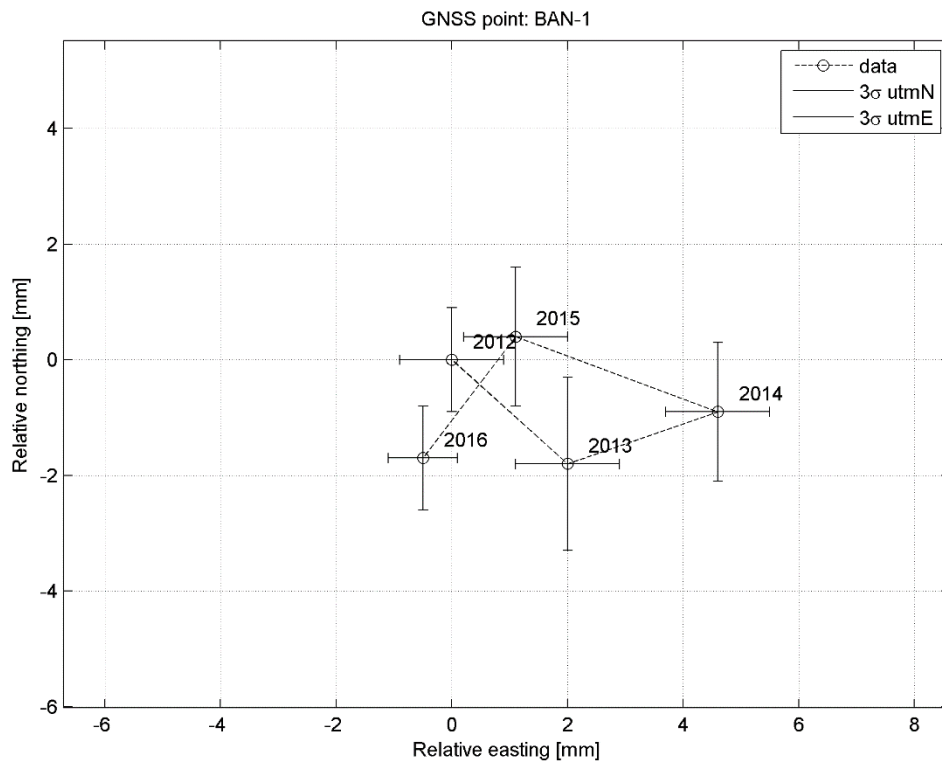
Hazard assessment of large unstable rock slopes in Norway							
Site name:	Kassen	Scenario:	E	Made by:	Kaja Krogh	Date:	20.12.2016
Hazard classes	Probability	Cumulative prob.	Hazard score		Fitted normal distribution		
Very low	1.8 %	1.8 %	Minimum	2.0	Mean μ	4.5	
Low	52.5 %	54.3 %	Maximum	8.0	St. dev. σ	1.5	
Medium	42.9 %	97.2 %	Mode	4.0	$\mu - 2\sigma$	1.5	
High	2.8 %	100.0 %	Mean	4.7	$\mu + 2\sigma$	7.5	
Very high	0.0 %	100.0 %	5% percentile	2.5	Corr. Coeff..	0.9984	
			95% percentile	7.0	K-S-test	7.1 %	
1. Backscarp							
					Score	Norm. prob.	
Not developed					0	0.0 %	
Partly open over width of slide body (few cm to m)					0.5	100.0 %	
Fully open over width of slide body (few cm to m)					1	0.0 %	
Comment: Disconnected cracks forms the backscarp							
2. Potential sliding structures							
					Score	Norm. prob.	
No penetrative structures dip out of the slope					0	100.0 %	
Penetrative structures dip on average < 20 degree or steeper than the slope					0.5	0.0 %	
Penetrative structures dip on average > 20 degree and daylight with the slope					1	0.0 %	
Comment: No structures are penetrative relative to the size of the scenario.							
3. Lateral release surfaces							
					Score	Norm. prob.	
Not developed					0	0.0 %	
Partly developed on 1 side					0.25	0.0 %	
Fully developed or free slope on 1 side or partly developed on 2 sides					0.5	0.0 %	
Fully developed or free slope on 1 side and partly developed on 1 side					0.75	100.0 %	
Fully developed or free slope on 2 sides					1	0.0 %	
Comment: Fully developed in the west, partly developed in the east.							
4. Kinematic feasibility test							
					Score	Norm. prob.	
Kinematic feasibility test does not allow for planar sliding, wedge sliding or toppling					0	0.0 %	
Failure is partly kinematically possible (movement direction is more than $\pm 30^\circ$ to slope orientation)					0.5	0.0 %	
Failure is kinematically possible (movement direction is less than $\pm 30^\circ$ to slope orientation)					0.75	0.0 %	
Failure is partly kinematically possible on persistent discontinuities (movement direction is more than $\pm 30^\circ$ to slope orientation)					0.75	100.0 %	
Failure is kinematically possible on persistent discontinuities (movement direction is less than $\pm 30^\circ$ to slope orientation)					1	0.0 %	
Comment: Planar sliding possible along J2, and shallow parts of J1. Toppling possible along overturned structures of J1. Wedge sliding partly possible along intersection of J4 and J2.							
5. Morphologic expression of the rupture surface							
					Score	Norm. prob.	
No indication on slope morphology					0	100.0 %	
Slope morphology suggests formation of a rupture surface (bulging, concavity -convexity, springs)					0.5	0.0 %	
Continuous rupture surface is suggested by slope morphology and can be mapped out					1	0.0 %	
Comment: Potential rupture surface covered by rock deposits. No morphologic expressions of rupture surface observed on hillshade maps.							
6. Displacement rates							
					Score	Norm. prob.	
No significant movement					0	30.0 %	
>0 - 0.5 cm/year					1	30.0 %	
0.5 - 1 cm/year					2	30.0 %	
1 - 4 cm/year					3	10.0 %	
4 - 10 cm/year					4	0.0 %	
> 10 cm/year					5	0.0 %	
Comment: dGNSS point (BAN-6) installed summer 2016, so displacement rates are not yet available. To account for this uncertainty, several outcomes are weighted, assumin that the unstable area moves less than 4cm/year.							
7. Acceleration (if velocity is >0.5 cm/yr and <10 cm/yr)							
					Score	Norm. prob.	
No acceleration or change in displacement rates					0	50.0 %	
Increase in displacement rates					1	50.0 %	
Comment: Equally weighted due to uncertainty of displacement rates.							
8. Increase of rock fall activity							
					Score	Norm. prob.	
No increase of rock fall activity					0	30.0 %	
Increase of rock fall activity					1	70.0 %	
Comment: Certainly increase in rockfall activity compared to adjacent slopes outside the unstable area. Full score is however not given, due to areas inside the unstable area with relatively higher activity.							
9. Past events							
					Score	Norm. prob.	
No post-glacial events of similar size					0	20.0 %	
One or several events older than 5000 years of similar size					0.5	40.0 %	
One or several events younger than 5000 years of similar size					1	40.0 %	
Comment: Bathymetric data show rockslide deposits in Bandak lake, but these do not origin from scenario E. Age is uncertain.							

Hazard assessment of large unstable rock slopes in Norway							
Site name:	Kassen	Scenario:	F	Made by:	Kaja Krogh	Date:	20.12.2016
Hazard classes	Probability	Cumulative prob.	Hazard score		Fitted normal distribution		
Very low	0.0 %	0.0 %	Minimum	2.5	Mean μ	5.7	
Low	26.6 %	26.6 %	Maximum	9.8	St. dev. σ	1.5	
Medium	50.9 %	77.5 %	Mode	5.5	$\mu - 2\sigma$	2.6	
High	22.0 %	99.6 %	Mean	5.9	$\mu + 2\sigma$	8.8	
Very high	0.4 %	100.0 %	5% percentile	3.5	Corr. Coeff..	0.9996	
			95% percentile	8.4	K-S-test	3.3 %	
1. Backscarp							
					Score	Norm. prob.	
Not developed					0	0.0 %	
Partly open over width of slide body (few cm to m)					0.5	0.0 %	
Fully open over width of slide body (few cm to m)					1	100.0 %	
Comment: Backscarp fully developed over entire width, clearly visible on hillshade and verified in field.							
2. Potential sliding structures							
					Score	Norm. prob.	
No penetrative structures dip out of the slope					0	40.0 %	
Penetrative structures dip on average < 20 degree or steeper than the slope					0.5	0.0 %	
Penetrative structures dip on average > 20 degree and daylight with the slope					1	60.0 %	
Comment: Based on two observation points, J2 dips from 15 - 35° and J1 has a dip angle approximately parallel the slope. Relative to the size of potential sliding body, these structures are partly penetrative.							
3. Lateral release surfaces							
					Score	Norm. prob.	
Not developed					0	0.0 %	
Partly developed on 1 side					0.25	0.0 %	
Fully developed or free slope on 1 side or partly developed on 2 sides					0.5	0.0 %	
Fully developed or free slope on 1 side and partly developed on 1 side					0.75	100.0 %	
Fully developed or free slope on 2 sides					1	0.0 %	
Comment: Eastern flank is a free slope, while the western flank is partly developed.							
4. Kinematic feasibility test							
					Score	Norm. prob.	
Kinematic feasibility test does not allow for planar sliding, wedge sliding or toppling					0	0.0 %	
Failure is partly kinematically possible (movement direction is more than $\pm 30^\circ$ to slope orientation)					0.5	0.0 %	
Failure is kinematically possible (movement direction is less than $\pm 30^\circ$ to slope orientation)					0.75	50.0 %	
Failure is partly kinematically possible on persistent discontinuities (movement direction is more than $\pm 30^\circ$ to slope orientation)					0.75	0.0 %	
Failure is kinematically possible on persistent discontinuities (movement direction is less than $\pm 30^\circ$ to slope orientation)					1	50.0 %	
Comment: Planar sliding is possible along J2 and shallow parts of J1. Toppling is possible along overturned structures of J1. Wedge sliding partly possible along the intersection of J2 and J4.							
5. Morphologic expression of the rupture surface							
					Score	Norm. prob.	
No indication on slope morphology					0	100.0 %	
Slope morphology suggests formation of a rupture surface (bulging, concavity -convexity, springs)					0.5	0.0 %	
Continuous rupture surface is suggested by slope morphology and can be mapped out					1	0.0 %	
Comment: Not identified in field. Rockfall deposits cover the foot of the instability.							
6. Displacement rates							
					Score	Norm. prob.	
No significant movement					0	30.0 %	
0.2 - 0.5 cm/year					1	30.0 %	
0.5 - 1 cm/year					2	30.0 %	
1 - 4 cm/year					3	10.0 %	
4 - 10 cm/year					4	0.0 %	
> 10 cm/year					5	0.0 %	
Comment: See discussion for scenario E.							
7. Acceleration (if velocity is >0.5 cm/yr and <10 cm/yr)							
					Score	Norm. prob.	
No acceleration or change in displacement rates					0	50.0 %	
Increase in displacement rates					1	50.0 %	
Comment: Displacement not expected to exceed 0.5 cm/year.							
8. Increase of rock fall activity							
					Score	Norm. prob.	
No increase of rock fall activity					0	30.0 %	
Increase of rock fall activity					1	70.0 %	
Comment: Certainly increase in rockfall activity compared to adjacent slopes outside the unstable area. Full score is however not given, due to areas inside the unstable area with relatively higher activity.							
9. Past events							
					Score	Norm. prob.	
No post-glacial events of similar size					0	20.0 %	
One or several events older than 5000 years of similar size					0.5	40.0 %	
One or several events younger than 5000 years of similar size					1	40.0 %	
Comment: Bathymetric data show rockslide deposits in Bandak lake of uncertain age, but these are not assumed to origin from scenario F.							

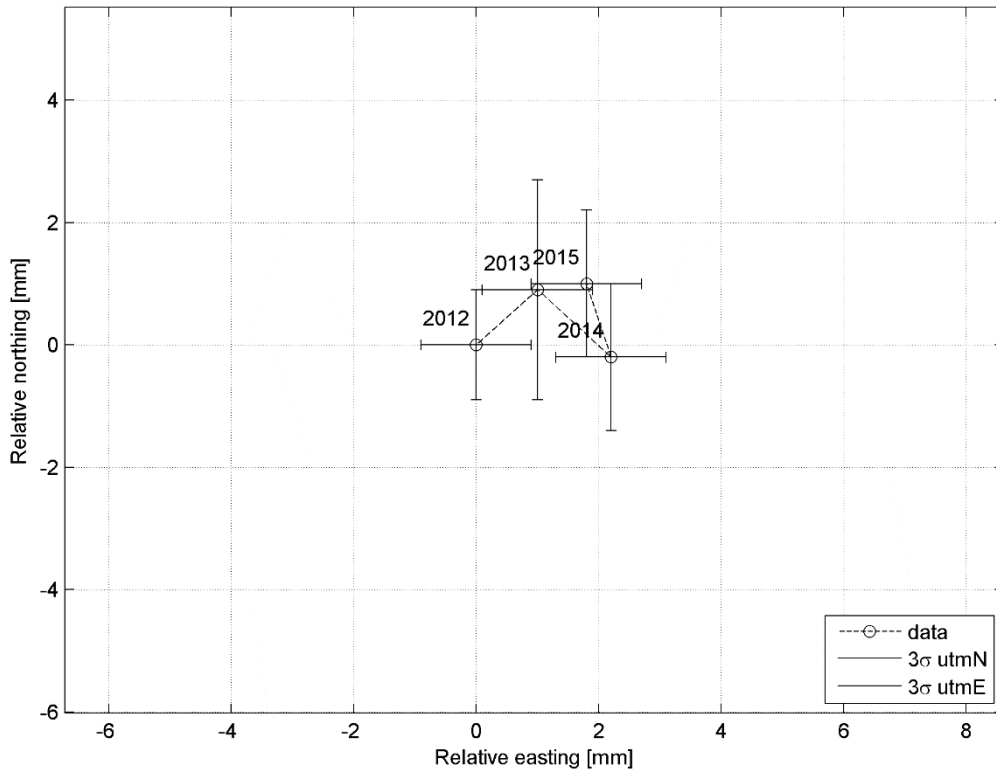
Hazard assessment of large unstable rock slopes in Norway							
Site name:	Kassen	Scenario:	G	Made by:	Kaja Krogh	Date:	20.12.2016
Hazard classes	Probability	Cumulative prob.	Hazard score		Fitted normal distribution		
Very low	0.0 %	0.0 %	Minimum	4.3	Mean μ	6.3	
Low	11.3 %	11.3 %	Maximum	10.0	St. dev. σ	1.5	
Medium	56.3 %	67.5 %	Mode	5.3	$\mu - 2\sigma$	3.4	
High	31.3 %	98.8 %	Mean	6.5	$\mu + 2\sigma$	9.2	
Very high	1.3 %	100.0 %	5% percentile	4.3	Corr. Coeff..	0.9992	
			95% percentile	8.8	K-S-test	5.7 %	
1. Backscarp					Score	Norm. prob.	
Not developed					0	0.0 %	
Partly open over width of slide body (few cm to m)					0.5	0.0 %	
Fully open over width of slide body (few cm to m)					1	100.0 %	
Comment: The rock mass is highly dissected in this area and consists mostly of blocks, consequently it is believed that there are no continuous bedrock left.							
2. Potential sliding structures					Score	Norm. prob.	
No penetrative structures dip out of the slope					0	50.0 %	
Penetrative structures dip on average < 20 degree or steeper than the slope					0.5	0.0 %	
Penetrative structures dip on average > 20 degree and daylight with the slope					1	50.0 %	
Comment: J2 is overturned in the area and dips around 50° in the nearest observation point. J1 dips parallel the slope/steeper than the slope. Due to the dissected character of the rock mass, it is uncertain if the structures daylight the slope or not and the outcomes are weighted equally.							
3. Lateral release surfaces					Score	Norm. prob.	
Not developed					0	0.0 %	
Partly developed on 1 side					0.25	0.0 %	
Fully developed or free slope on 1 side or partly developed on 2 sides					0.5	0.0 %	
Fully developed or free slope on 1 side and partly developed on 1 side					0.75	0.0 %	
Fully developed or free slope on 2 sides					1	100.0 %	
Comment: Same situation as for the backscarp; full score is given to both lateral release surfaces, as the rock mass is continuously destroyed.							
4. Kinematic feasibility test					Score	Norm. prob.	
Kinematic feasibility test does not allow for planar sliding, wedge sliding or toppling					0	0.0 %	
Failure is partly kinematically possible (movement direction is more than $\pm 30^\circ$ to slope orientation)					0.5	0.0 %	
Failure is kinematically possible (movement direction is less than $\pm 30^\circ$ to slope orientation)					0.75	50.0 %	
Failure is partly kinematically possible on persistent discontinuities (movement direction is more than $\pm 30^\circ$ to slope orientation)					0.75	0.0 %	
Failure is kinematically possible on persistent discontinuities (movement direction is less than $\pm 30^\circ$ to slope orientation)					1	50.0 %	
Comment: Kinematic feasibility test for the LW domain states that planar sliding and toppling is possible along respectively J2 and J1. Wedge failure is partly possible along the intersection of J2 and J3. The persistences of the discontinuities is unknown, and to account for this uncertainty, the outcomes are equally weighted.							
5. Morphologic expression of the rupture surface					Score	Norm. prob.	
No indication on slope morphology					0	100.0 %	
Slope morphology suggests formation of a rupture surface (bulging, concavity -convexity, springs)					0.5	0.0 %	
Continuous rupture surface is suggested by slope morphology and can be mapped out					1	0.0 %	
Comment: Possible rupture surface covered by debris. No evident morphological expression of rupture surface observed on hillshade map.							
6. Displacement rates					Score	Norm. prob.	
No significant movement					0	30.0 %	
>0 - 0.5 cm/year					1	30.0 %	
0.5 - 1 cm/year					2	30.0 %	
1 - 4 cm/year					3	10.0 %	
4 - 10 cm/year					4	0.0 %	
> 10 cm/year					5	0.0 %	
Comment: dGNNS point (BAN-7) installed summer 2016, so no results available for this point yet. To describe this uncertainty, several outcomes are given scores, assuming that the unstable area moves less than 4cm/year.							
7. Acceleration (if velocity is >0.5 cm/yr and <10 cm/yr)					Score	Norm. prob.	
No acceleration or change in displacement rates					0	50.0 %	
Increase in displacement rates					1	50.0 %	
Comment: Equally weighted due to uncertainty of displacement rates.							
8. Increase of rock fall activity					Score	Norm. prob.	
No increase of rock fall activity					0	0.0 %	
Increase of rock fall activity					1	100.0 %	
Comment: Clearly increase in rockfall activity relative to adjacent slopes both inside and outside the unstable area.							
9. Past events					Score	Norm. prob.	
No post-glacial events of similar size					0	0.0 %	
One or several events older than 5000 years of similar size					0.5	50.0 %	
One or several events younger than 5000 years of similar size					1	50.0 %	
Comment: Bathymetric model shows rock avalanche deposits in Bandak lake, right beneath scenario G. These deposits origin from a earlier collapse at the same location. The age of this event is uncertain.							

8.2 dGNSS movement

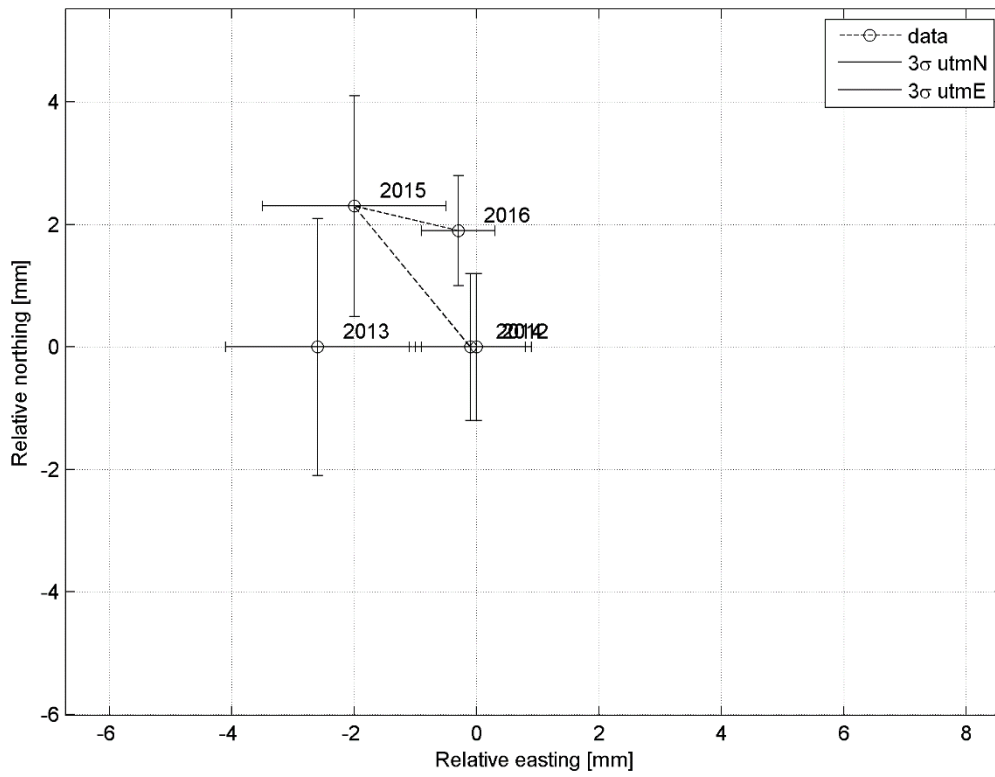
The following figures show the raw files for horizontal movement for the dGNSS points BAN 1 – BAN 5. Martina Bøhme (NGU) made the figures in MATLAB (MathWorks).

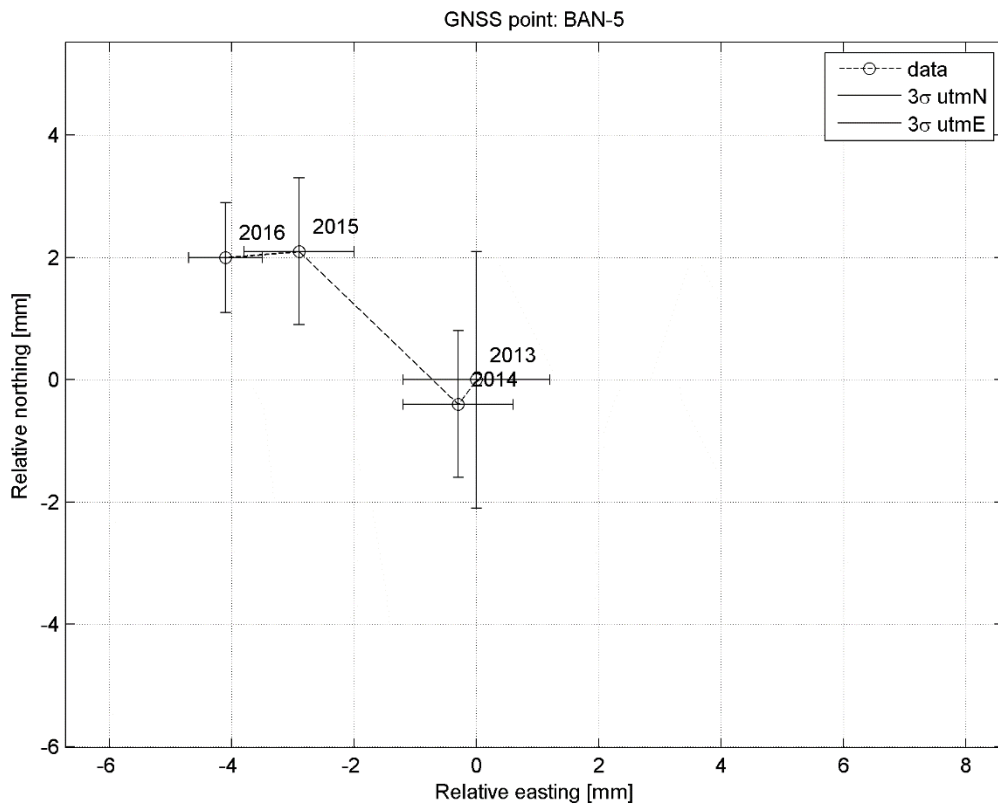


GNSS point: BAN-3



GNSS point: BAN-4





Results from tilt test. Values in the table show the basic friction

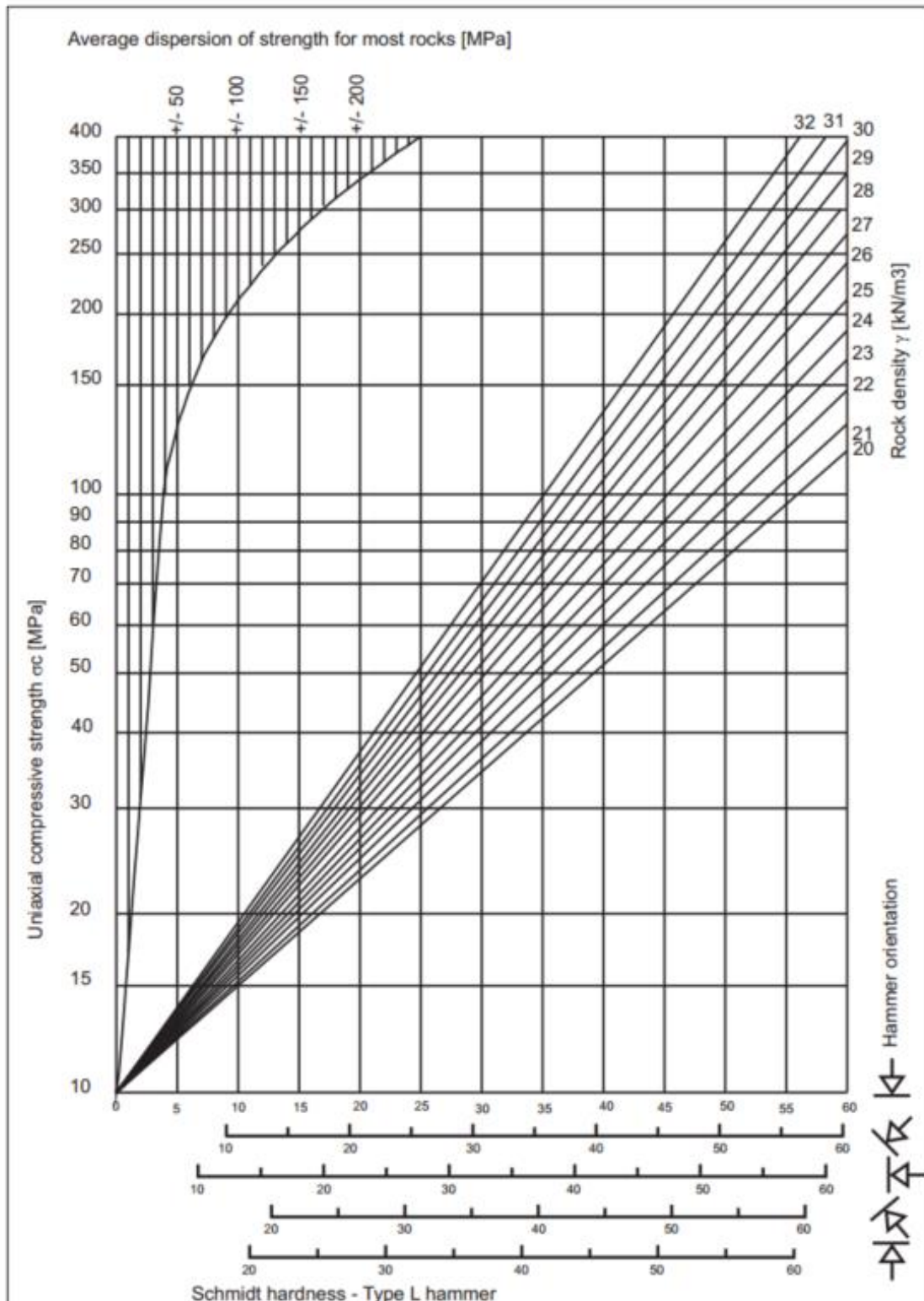
Sample #	Configuration 1 [°]	Configuration 2 [°]	Configuration 3 [°]	Configuration 4 [°]	Mean value [°]
1	27.9	24.8	28.6	28.6	27.6
2	28.7	25.2	27.7	28.6	29.3
3	31.8	27.6	27.9	29.1	29.5

Results from UCS test, sonic velocity test and deformability test (E-modulus and

Sample name	D1 [mm]	D2 [mm]	D3 [mm]	D4 [mm]	D5 [mm]	D6 [mm]	Mean diameter	Failure angle (measured on the sample)	Length [mm]	Weight [g]	Density (g/cm ³)	Unit weight (kN/m ³)	Sonic time [μs]	Sonic velocity [m/s]	UCS sample [Mpa]	UCS _{50D} [Mpa]	E-modul (GPa)	Poissons Ratio
Amfi 1	34.31	34.23	34.24	34.27	34.26	34.35	34.28	16°	90.35	247.64	2.97	29.1	14.9	6064	273	255.063	71.86	0.26
Amfi 2	34.21	34.27	34.33	34.28	34.36	34.39	34.31	28°	88.43	239.95	2.94	28.8	15.4	5742	202.7	189.412	71.83	0.25
Amfi 3	34.21	34.3	34.45	34.26	34.28	34.44	34.32	-	90.99	247.04	2.93	28.8	15.4	5908	246.4	230.267	74.43	0.26
Amfi 6	34.21	34.34	34.39	34.18	34.26	34.28	34.28	29°	90.4	247.46	2.97	29.1	15.4	5870	255.1	238.339	79.77	0.31
Mean values												29.0	15.275	5896	258.167	241.223	74.47	0.27

8.3 Laboratory results

8.5 Determination of JCS based on Schmidt hardness

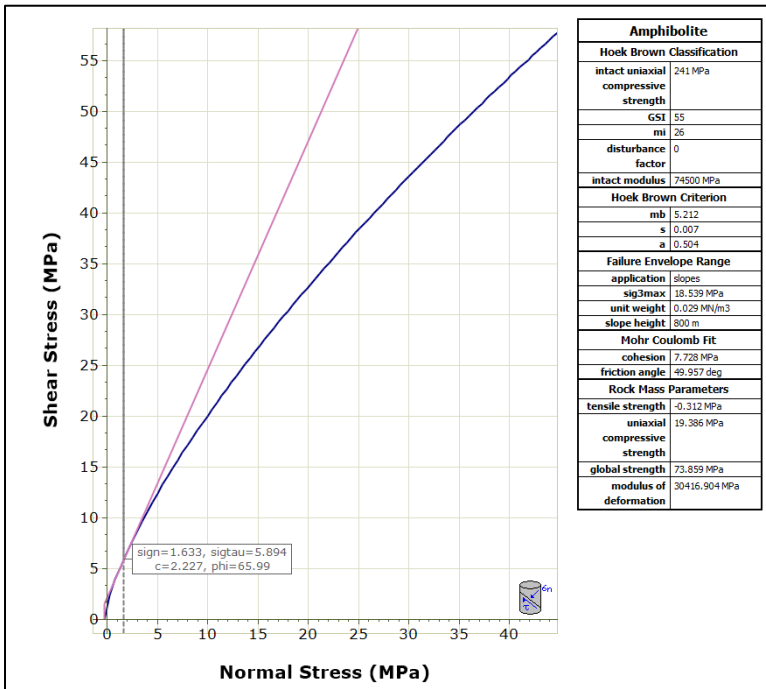


Relationship between Schmidt hardness (R) and UCS. If the Schmidt test is taken from wet, weathered surfaces, the JCS value can be determined by using the same diagram. Figure from Grøneng and Nilsen (2008).

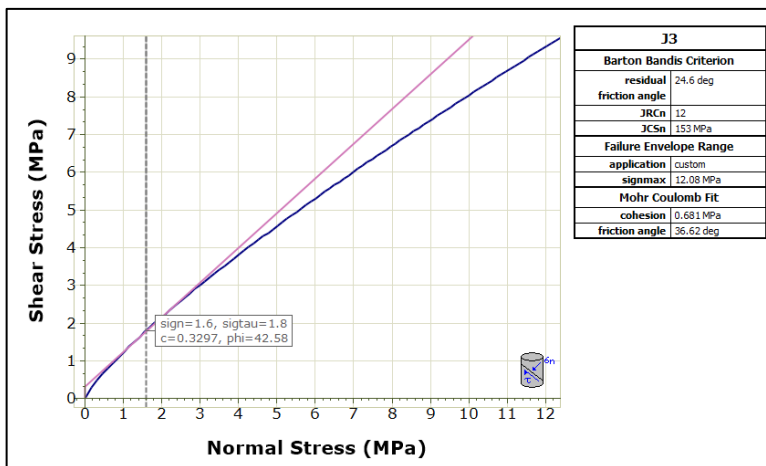
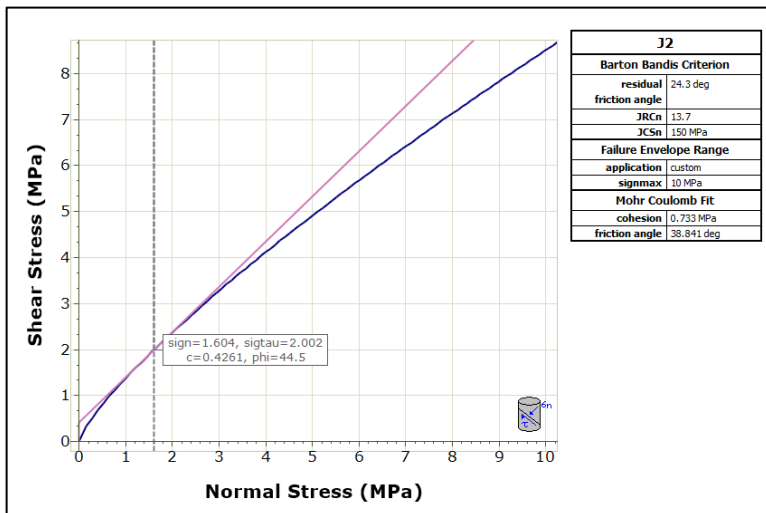
8.6 Calculation of Joint Stiffness

Parameter	Symbol	Value		Remarks
Rock mass modulus	E_m	30416.9 Mpa		Derived in RocLab from the Hoek-Brown failure classification
Intact rock modulus	E_i	74500.0 Mpa		Young's modulus. Determined in laboratory.
Rock mass shear modulus	G_m	11975.2 Mpa		(Myrvang (2001)): $G_m = \frac{E_m}{2(1 + \nu)}$
Intact rock shear modulus	G_i	29330.7 Mpa		Myrvang (2001): $G_i = \frac{E_i}{2(1 + \nu)}$
Mean joint spacing	L	J2	J3	Field estimates (results from specialization project)
		0.5 m	1 m	
Normal joint stiffness	K_n	J2	J3	Rocscience (2016b), Barton (1973): $K_n = \frac{E_i E_m}{L(E_i - E_m)}$
		102808.5 Mpa/m	51404.3 Mpa/m	
Shear joint stiffness	K_s	J2	J3	Rocscience (2016b), Barton (1973): $K_s = \frac{G_i G_m}{L(G_i - G_m)}$
		40476.0 Mpa/m	20238.0 Mpa/m	

8.7 RocLab conversions



Screenshots of the conversion from Hoek-Brown and Barton Bandis parameters for the rock mass (Amphibolite) and the joint sets. The graphs show how a non-linear relationship is fitted to instantaneous Mohr-Coulomb parameters at a certain level of normal stress.



8.8 Centroid of Block 2

Calculations of the centre of gravity of Block 2. The Block was simplified into familiar shapes (triangles and rectangles), and the centroid for each figure was found in order to place the final centroid in Block 2. The results show that the centre of gravity falls inside the base of Block 2, and it will not topple.

Figure	A [m ²]	x-coordinate of centroid [m]	y-coordinate of centroid [m]	x * A	y * A
A	13.42	-0.7	19.7	-9.394	264.374
B	9.88	2.6	27.1	25.688	267.748
C	26.52	2.6	23.6	68.952	625.872
D	1.61	5.9	21.56	9.499	34.7116
E	158.25	3.75	10.55	593.4375	1669.5375
F	11.36	8.56	2.36	97.2416	26.8096
G	32.33	8.26	-2.1	267.0458	-67.893
SUM	253.37			1052.4699	2821.1597
Centroid of Block 2			X - coordinate	$x * A / \sum A$	4.2 m
			Y - coordinate	$y * A / \sum A$	11.1 m

